VNiVERSiDAD
D SALAMANCA

FACULTAD DE CIENCIAS QUÍMICAS
DEPARTAMENTO DE INGENIERÍA QUÍMICA

ENGINEERING A DUAL STIMULI-RESPONSIVE PLATFORM FOR POST-SURGICAL BREAST CANCER TREATMENT

Marcos Blanco López

TESIS DOCTORAL

SALAMANCA, 2026

UNIVERSIDAD DE SALAMANCA

FACULTAD DE CIENCIAS QUÍMICAS

VNiVERSiDAD
D SALAMANCA

ENGINEERING A DUAL STIMULI-RESPONSIVE PLATFORM FOR POST-SURGICAL BREAST CANCER TREATMENT

Memoria que, para optar al grado de Doctor en Ingeniería Química (Ciencia y Tecnología Químicas) por la Universidad de Salamanca, presenta:

Marcos Blanco López

Fecha:
2026.05.27
12:33:38 +02'00'

La Dra. Dña. Eva Martín del Valle, Catedrática del área de Ingeniería Química de la Universidad de Salamanca, y el Dr. D. Antonio Tabernero de Paz, Profesor Titular, también adscrito al Departamento de Ingeniería Química de la Universidad de Salamanca,2

Certifican:

Que la presente memoria, titulada “Engineering a dual stimuli-responsive platform for post-surgical breast cancer treatment”, presentada por Marcos Blanco López para optar al grado de Doctor en Ciencia y Tecnología Químicas por la Universidad de Salamanca, ha sido realizada bajo su dirección en el grupo de investigación Aplicaciones Biomédicas de Ingeniería Química del organismo citado.

Considerando que esta tesis reúne los requisitos científicos necesarios, autorizan su depósito y defensa. Para que así conste, firman el presente informe, en Salamanca a 20 de mayo de 2026.

EVA MARÍA MARTÍN VALLE

Firmado digitalmente por EVA MARÍA MARTÍN VALLE
Fecha: 2026.05.25 17:50:28 +02'00'

TABERNERO DE PAZ, ANTONIO (FIRMA)

Firmado digitalmente por TABERNERO DE PAZ, ANTONIO (FIRMA)
Fecha: 2026.05.25 15:59:42 +02'00'

Dña. Eva Martín del Valle

D. Antonio Tabernero de Paz

A mi familia,

Por ser hogar allá donde yo esté.

Agradecimientos

En primer lugar, gracias a mi directora, Eva Martín del Valle, por su dedicación, orientación, y apoyo constante a lo largo de esta etapa. Asimismo, a mi codirector, Antonio Tabernero de Paz, gracias por toda la ayuda brindada, la constante guía, y los consejos para poder mejorar tanto personal como laboralmente. Gracias por la confianza depositada en mí para llevar a cabo esta tesis y por la oportunidad de poder dedicarme a un campo profesional por el que siempre tuve curiosidad.

En segundo lugar, quiero agradecer a todos los compañeros y compañeras de laboratorio que me han ayudado desde dentro o fuera de mi labor investigadora, ya sea con experimentos, clases, cafés de media mañana, charlas de descompresión, o momentos fuera del laboratorio. Gracias a Celia, Álvaro, Javi, Carlos, Ángel, Álex, Milena, Valentín, Belén, Jesús, Audelino, y al resto del departamento.

De igual manera, quiero agradecer al grupo de investigación del Healthcare Technologies Institute (HTI) de la Universidad de Birmingham y a CERU, por la inmejorable acogida que me pudieron dar en mi estancia en Reino Unido, breve pero fructífera. En especial, me gustaría agradecer a la Dra. Patricia Pérez Esteban por haberse preocupado tanto por mí, mi bienestar, y mi rendimiento. También a mi colaboradora Inma, que siempre me ha ayudado en todo lo que ha podido, y con la que disfruté y compartí especialmente esos tres meses.

Gracias a toda mi familia: Mis padres, mi hermano, mis tías y mis abuelas, por haber sido siempre refugio allá donde esté y allá donde vaya. Gracias por haberme ayudado a levantarme todas las veces que me he caído sin cansaros ni una sola. Y gracias a mi red de apoyo, a mis amigas y amigos: De Salamanca, de la carrera, del Erasmus, de deporte, o “de la vida”. Gracias por haber sabido entenderme y apoyarme a lo largo de estos años por muy duro que pudiera resultar. Gracias a todas estas personas por haber sido parte imprescindible del empujón que he necesitado a veces para salir adelante, quitarme las dudas, y avanzar.

Above all, do not fear difficult moments.
The best comes from them.

Rita Levi-Montalcini

General Index

List of figures.....I

List of tables.....V

Abstract.....VII

1. Introduction: Preventing post-surgical breast cancer recurrence through dual-responsive hydrogel systems....1

1.1. Conceptual framework of cancer and its treatments 3

1.1.1. Impact of cancer worldwide..... 3

1.1.2. The hallmarks of cancer..... 4

1.1.3. Evolution of cancer chemotherapy and its transition to targeted therapy..... 6

1.1.3.1. First conventional drugs for systemic chemotherapy ... 6

1.1.3.2. Adjuvant chemotherapies 7

1.2. Breast cancer as a clinical paradigm for targeted therapy 8

1.2.1. Stats on breast cancer 8

1.2.2. Molecular subtypes of breast cancer..... 9

1.2.3. Stages of breast cancer..... 9

1.2.4. Current treatments for breast cancer 10

1.2.5. Post-surgical therapeutic landscape and systemic limitations 13

1.2.5.1. Tumour recurrences..... 13

1.2.5.3. Breast irradiation drawbacks 14

1.2.5.3. Systemic administration drawbacks..... 15

1.3. Injectable hydrogels as thermo-responsive drug reservoirs 17

1.3.1. Precursor gels for local administration 17

1.3.2. *In situ* forming injectable hydrogels..... 18

1.3.3. Thermo-responsive injectable hydrogels for drug delivery in breast cancer 20

1.3.4. Comparison of thermo-sensitive polymers for injectable formulations 22

1.3.5. Additional tumour targeting strategy 24

1.4. pH-responsive strategies for tumour targeting 26

1.4.1. Mechanisms of pH-response 27

1.4.1.1. Ionisable functional groups 27

1.4.1.2. Acid labile linkage 28

1.4.1.3. Coating with pH-sensitive polymers 28

1.4.1.4. Combined strategies 28

1.4.2. pH-responsive hydrogels 29

1.5. Dual temperature and pH-responsive hydrogels 30

1.5.1. Reported dual-responsive hydrogel formulations for breast cancer therapies 31

1.5.2. Nanocarriers to incorporate into hydrogels matrices 33

1.5.3. Dual-responsive hybrid hydrogels with incorporated nanocarriers 35

1.5.3.1. pH-responsive liposomes 37

1.5.3.2. pH-responsive coacervates 38

1.5.4. Optimal dual-response approach 40

1.6. Conclusions 41

1.7. References 42

1.8. List of abbreviations 49

2.Thesis objectives 53

3. Materials and methods 59

3.1. Introduction 61

3.2. Materials 61

3.3. Experimental methodology 62

3.3.1. Synthesis of the dual-response system and its separate components 62
3.3.1.1. Alginate-Gelatin A coacervates synthesis 62
3.3.1.2. Conventional and EU coated liposomes synthesis 64
3.3.1.3. Synthesis of PF-127 based hydrogels with different polysaccharides 66
3.3.1.4. Dual-response injectable hydrogel synthesis 68
3.3.2. Characterizations of systems 69
3.3.2.1. Zetasizer for dynamic light scattering (DLS) technique 69
3.2.2.2. Static light scattering (SLS) 70
3.3.2.3. Optical microscopy 70
3.3.2.4. Turbidity 71
3.3.2.5. Rheology 71
3.3.2.6. Cryogenic Scanning Electron Microscopy (Cryo-SEM) 72
3.3.3. Drug encapsulation and drug release experiments 73
3.3.3.1. Liposomes encapsulation efficiency and loading capacity 73
3.3.3.2. Drug release from liposomal formulations 73
3.3.3.3. Drug releases from PF-127 based hydrogels 74
3.3.3.4. Hydrogels drug release fitting to a mathematical model 75
3.3.3.5. Drug release from liposomal hydrogels 77
3.3.3.6. Drug release fitting to theoretical models 77
3.3.4. *In vitro* assays for model validation 78
3.3.4.1. MTT assays of 5-FU, liposomes, and liposomal hydrogels 79
3.3.4.2. Liposomal cellular uptake 81

3.3.4.3. Viability assays on spheroids subjected to dual-responsive system 81
3.3.5. Statistical analysis 82
3.4. References 82
3.5. List of abbreviations 84

4. Study of Alginate-Gelatin A coacervates as potential drug delivery system..... 87
4.1. Introduction 89
4.2. Coacervation process 89
4.3. Alginate-gelatin coacervates 90
4.3.1. pH-sensitivity in alginate-gelatin coacervates 93
4.3.2. Temperature-sensitivity in gelatin structural conformation 93
4.4. Published article related to this chapter 94
4.5. Conclusions 118
4.6. References also cited 119
4.7. List of abbreviations 120

5. Expanding the pH window of liposomal drug delivery using Eudragit-based polymeric coatings..... 123
5.1. Introduction 125
5.2. Liposomes as drug delivery carriers 126
5.3. Liposomes targeting capacity 127
5.4. pH-sensitive liposomes 128
5.4.1. Eudragit® coated pH-responsive liposomes 130
5.4.1.1. Eudragit® S100 coated liposomes 130
5.4.1.2. Eudragit® EPO coated liposomes 131
5.5. Article related to this chapter 132
5.6. Conclusions 177

5.7. References also cited.....179
5.8. List of abbreviations 180

6. Innovative thermos-sensitive composite materials: Merging Poloxamer PF-127 and polysaccharides.....183
6.1. Introduction.....185
6.2. Polymers in thermo-sensitive hydrogel networks 186
6.2.1. Natural polymers 186
6.2.2. Synthetic polymers 187
6.2.2.1. Poly(N-Isopropylacrylamide) (PNIPAAM) 187
6.2.2.2. Poly(Ethylene Oxide) (PEO) and Poloxamers.....187
6.3. PF-127 hydrogels for breast cancer treatment 189
6.4. Rheological characterization of hydrogel thermo-response ...190
6.4.1. Oscillatory flow analysis 190
6.4.2. Static flow analysis 190
6.5. Article related to this chapter.....192
6.6. Conclusions 218
6.7. References also cited.....220
6.8. List of abbreviations 221

7. Developing a dual-responsive drug delivery system based on injectable thermos-sensitive PF-127 hydrogel.....225
7.1. Introduction.....227
7.2. Synthesis of liposomal hydrogels.....228
7.3. Stimuli-responsive liposomal hydrogels for breast cancer therapy.....230
7.4. Article related to this chapter.....231
7.6. Conclusions 278
7.7. References also cited.....280

7.8. List of abbreviations 281

8. Conclusions.....285

List of figures

Figure 1.1. Age-standardized incidence rates up to 2025 of all cancers globally in males (top) and females (bottom)

Figure 1.2. Hallmarks of cancer: Original hallmarks (black), emerging hallmarks (purple), and tumour enabling characteristics (green).

Figure 1.3. Scheme of first conventional anticancer drugs mechanisms of action

Figure 1.4. Breast cancer incidence (a) and mortality (b) worldwide in 2022.

Figure 1.5. Molecular subtypes of breast cancer.

Figure 1.6. Stages of breast cancer.

Figure 1.7. Types of tumour resection surgeries.

Figure 1.8. Decision diagram for breast cancer procedures in different diagnosis cases. Rectangles correspond to techniques or procedures, and rhombuses to intertwined decisions depending on the diagnosed tumour characteristics.

Figure 1.9. Passive targeting of tumour sites by EPR effect.

Figure 1.10. Biological barriers present in systemic therapies

Figure 1.11. *In situ* forming hydrogel strategy for breast cancer post-surgery therapies.

Figure 1.12. Main gelling mechanism of *in situ* forming hydrogels.

Figure 1.13. Endogenous and exogenous stimuli for responsive therapies

Figure 1.14. Cancer cell metabolic reprogramming leading to an acidic extracellular environment and acidic endolysosomal intracellular compartments.

Figure 1.15. pH-response mechanisms in systems presenting a) Ionisable functional groups, b) Acid labile linkages, or c) Either crosslinking or coating. The drug release is illustrated as either swelling (stable particle) or disassembly (disrupted particle).

Figure 1.16. Photographs of remaining hydrogels *in vivo* at different time points of one (DEA) and two (MP) tertiary amines formulations developed by Lin et al [65].

Figure 1.17. Main reported nanocarriers

Figure 1.18. Release pH-response mechanisms for loaded T-sensitive hydrogels. Top tier describes the basic hydrogel matrix [64-69], middle tier includes the NC formulation [72-74], and low tier incorporates the pH-response into the NC directly, which is the optimized mechanism [75].

Figure 1.19. Liposome structure and functionalizations

Figure 1.20. Coacervates formation via electrostatic interaction

Figure 2.1. Thesis objective summarized: The synthesis of a dual-responsive drug delivery system based on a thermo-sensitive injectable PF-127 hydrogel matrix with incorporated pH-responsive carrier for breast cancer post-surgical therapy preventing local recurrences. The doctoral thesis will be focused on the synthesis, optimization, characterization, functionalization and biological validation of the proposed novel strategy.

Figure 3.1. Coacervates synthesis process scheme

Figure 3.2. Scheme of conventional liposomes synthesis

Figure 3.3. Scheme of Eudragit® coated liposomes synthesis

Figure 3.4. Brief scheme of PF-127 based hydrogels synthesis processes.

Figure 3.5. Scheme of liposomal hydrogels synthesis

Figure 3.6. Gel support for drug release as: a) Illustration of design, b) Measurements of the device for a 100 mL beaker, and c) Drug release experiment setup.

Figure 3.7. Gel support device for 24-well plates in *in vitro* assays. a) Support device in well plates, b) Side view to assure the bottom is not reached, and c) Design of support device made in AutoCAD.

Figure 4.1. Coacervation process driven by the electrostatic interactions between the oppositely charged functional groups of alginate and gelatin A

Figure 4.2. Temperature influence on gelatin A structural conformation.

Figure 4.3. Conclusions of coacervates synthesis optimization and incompatibility with intended application.

Figure 5.1. Different liposomal structural organization depending on the different synthesis variables.

Figure 5.2. pH-responsive mechanism for liposomes with implemented DOPE and CHEMS, compromising their stability at physiological conditions.

Figure 5.3. Eudragit® coating formulations for synthesis of pH-responsive liposomes.

Figure 5.4. Summarized conclusions of the synthesis of conventional and EU coated liposomes, and the EU EPO coated liposomes tumour targeting evidence.

Figure 6.1. Thermo-sensitivity in PF-127 for injectable hydrogel design

Figure 6.2. Rheological analyses on thermo-sensitive PF-127 hydrogels showing compatible properties for the intended application.

Figure 6.3. General conclusions on development of PF-127 thermo-sensitive hydrogels formulations for sustained 5-FU release.

Figure 7.1. Arrangements of liposomal hydrogels: a) Liposomes incorporated into hydrogel matrix, b) Hydrogel formation due to liposomes gelation, and c) Lipid coated micro/nano hydrogels.

Figure 7.2. Proposed joint drug release mechanism scheme based on sustained release from strong gel (drug reservoir at 37ºC) with incorporated pH-response in acidic media

Figure 7.3. Main results obtained from the development of the dual-responsive platform for breast cancer post-surgical treatment.

Figure 8.1. Brief scheme of conclusions developed in this doctoral thesis about the synthesis and functioning mechanism of a dual temperature and pH-responsive injectable hydrogel for local recurrences prevention in post-surgery breast cancer treatment.

List of tables

Table 1.1. Representative mechanistic classes of classical chemotherapy

Table 1.2. Preferred therapies for molecular subtypes breast cancer.

Table 1.3. Reported thermo-sensitive injectable hydrogels for breast cancer therapy

Table 1.4. Thermo-sensitive polymers for injectable formulations comparison.

Table 1.5. Nanocarriers advantages and limitations for breast cancer.

Table 1.6. T and pH-dual responsive platforms

Table 3.1. Alginate-Gelatin A coacervates formulations

Table 3.2. Conventional liposomes formulations

Table 3.3. PF-127 based hydrogels formulations

Table 4.1. Alginate-gelatin coacervates reported lately

Table 5.1. Stimuli to respond for nanocarriers

Table 5.2. Reported pH-sensitive liposomal systems

Table 6.1. Reported PF-127 hydrogels for breast cancer therapy

Table 7.1. Benefits and limitations of hybrid and separate liposomes and hydrogels systems

Abstract

Nowadays, the procedure for an early stage non-metastatic diagnosed breast cancer is the breast-conserving therapy, consisting of tumour resection therapy by lumpectomy followed by breast irradiation to prevent local recurrences. Despite late advances, the radiotherapy off-targeting toxicity, as well as the alternative chemotherapies based on drug delivery systems systemically administered present major drawbacks. The poor therapeutic efficiency, resulting from limited drug accumulation at tumour site, together with systemic toxicity, constitute the main limitations of systemic administration. Since residual tumour cells responsible for recurrence are predominantly located within the surgical bed, the development of local therapies targeting these cells can help overcome the current limitations associated with tumour relapse.

Therefore, this doctoral thesis addresses this challenge through the design and development of a dual stimuli-responsive local drug delivery platform for post-surgical therapy which presents combined thermo-sensitivity by an injectable hydrogel matrix, and pH-sensitivity by an engineered nanocarrier. These responses exploit two basic features that can be found in the surgical bed: Physiological temperature to induce gelation after injection, providing a locally administered strong drug depot, and the acidic tumour microenvironment, providing a reproducible targeting strategy. The final drug delivery system is based on a PF-127 hydrogel network incorporating Eudragit® EPO coated liposomes encapsulating the anticancer drug 5-fluorouracil (5-FU) as a model chemotherapeutic agent.

However, the first approach consisted of developing alginate-gelatin A coacervates for pH-responsive strategy. Their synthesis optimization was accomplished by the study of process variables, including temperature and pH, obtaining nano sized coacervates systems of 500-750 nm with low polidispersity index (PDI <0.25). Nonetheless, their dependence on temperature and pH resulted in instability under physiological conditions, preventing their use for the intended application.

Consequently, new pH-responsive approaches were explored. In this case, liposomes were selected due to their current use in clinic, showing their high biocompatibility, efficiency, and versatility as vesicles resembling cellular membranes. Conventional liposomes were successfully synthesized and optimized via sonication and extrusion, obtaining a stable small unilamellar vesicle system (85 nm) with narrow size distribution (PDI < 0.1) for a 3-week period, able to encapsulate more than 90% of loaded 5-FU. Nevertheless, they exhibited fast drug release (under 8h) with no pH-response, evidencing a non-specific mechanism.

Therefore, strategies to introduce pH-responsive release were investigated. In order to preserve the liposomes stability at physiological conditions, a surface modification rather than the conventional method of composition alteration was preferred. Regarding this, an innovative coating procedure with Eudragit® family of polymers offered a promising alternative. Moreover, the broad range of Eudragit® formulations, providing opposite pH-responsive behaviours depending on the intended application, enabled the optimization of the coating process to obtain a versatile liposomal platform. Accordingly, two oppositely pH-responsive coatings (Eudragit® S100 and EPO) were implemented to evaluate drug release under contrasting conditions, thereby expanding the potential applicability of stable liposomes at physiological conditions for enhancing cancer therapy through different administration routes.

Eudragit® S100 (EU S100, designed for alkaline releases) coating procedure provided liposomal micron scale aggregates due to its high molecular weight and behaviour in aqueous solution. Meanwhile, Eudragit® EPO (EU EPO, designed for acidic releases) showed stable liposomal systems slightly larger (114 nm) but still monodisperse (PDI <0.15), presenting a promising formulation for the thesis objective. Moreover, both coatings showed higher encapsulation efficiencies than the conventional liposomes, and their releases were delayed until 24 h, preventing up to 50% of drug release in insoluble pH ranges for each coating. Mathematical modelling supported that insoluble coatings introduced a change in release mechanism, whilst supporting diffusion as the predominant one in Higuchi and first order fittings. This presented

potential applications for alkaline delivery in colon or intestine from oral formulations (EU S100), and more importantly, acidic tumour microenvironment targeting (EU EPO).

In fact, cell viability studies showed biocompatibility of all developed liposomal formulations. The pH-response of both coatings was validated through MTT assays in healthy fibroblast (HS-5) and breast cancer (BT-474) cell lines. Specifically, EU EPO coated liposomes enhanced cytotoxicity over 30% more than the rest of formulations in breast cancer cells after 72h, preserving fibroblasts viability. Therefore, tumour targeting was confirmed by *in vitro* studies.

In parallel, a thermo-responsive injectable PF-127 hydrogel platform was developed for the local drug delivery reservoir. Comprehensive rheological analyses were used to characterize the thermo-response and evaluate the gelation completion temperature, the viscoelasticity and viscosity of the system, and ultimately, the suitability for injection and sustained release. Since PF-127 hydrogel showed fast degradation, different polysaccharides were implemented in the hydrogel network and the effect of their concentrations as well as their structural conformations was studied. Implemented polysaccharides matrices presented improved rheological properties (G' from 8 to 11-18 kPa) and more resistance against flow (viscosities from 4.1 to 6.1-7.1 Pa·s), establishing final optimal formulations for local administration. These formulations provided a more prolonged 5-FU release, reaching up to four times (450 min) the release time that PF-127 hydrogel exhibited (90 min). Moreover, mathematical modelling confirmed that the polysaccharides implementation caused an additional diffusional resistance based on their concentration and structural complexity, decreasing the degradation rate and resisting water permeation through the matrix.

The final hybrid dual-responsive platform was synthesized by incorporating the pH-responsive Eudragit® EPO coated liposomes into the thermo-responsive injectable PF-127 hydrogel matrix. Characterization techniques showed the successful liposomal incorporation into the hydrogel matrix via scanning electron microscopy,

as well as improved viscoelastic properties (G' of 15 kPa, and viscosity of 6.8 Pa·s) of the system via rheology. Moreover, the pH-responsiveness was preserved, as demonstrated by drug release studies. In fact, hydrogel incorporation introduced an additional diffusion barrier, leading to a sustained 5-FU release for up to 48h, where up to 50% of drug release was prevented for coating insolubility range. This insolubility proved once again a change of release mechanism in one and two-stage models fitting, whilst the hydrogel matrix delayed release was supported by lower kinetic constants.

Finally, biological validation of the dual-responsive system was performed in 2D cell cultures and 3D breast tumour spheroids, for a better prediction of its *in vivo* behaviour. 2D cell assays replicated the results shown in liposomal systems, with the only exception that tumour cell mortality was slightly reduced (from 5% cell viability to 15% in 3 days) for the dual-responsive formulation, which was attributed to the delayed 5-FU release. However, the tumour targeting capacity was preserved. This was further supported by the results obtained in 3D tumour spheroids assays, where the dual-responsive hydrogel targeted successfully cancer cells promoting its therapeutic efficiency, showing disaggregated and disintegrated spheroids compared to off-targeting drug solution (from 40% cell viability in 5-FU solution to 28% in dual-responsive hydrogel after 3 days).

Overall, this thesis presents an engineered dual-responsive local drug delivery platform for post-surgical breast cancer treatment. The innovative strategy of combining two separately optimized stimuli-responses for local administration and tumour targeting presented improvements regarding the current therapies: High therapeutic efficiency, and decreased systemic toxicity.

1. Introduction: Preventing post-surgical breast cancer recurrence through dual-responsive hydrogel systems

1.1. Conceptual framework of cancer and its treatments

Cancer is a term used to define not one but a wide range of diseases where an uncontrolled cell division process is observed in different parts of the body. As defined by pathologist Rupert Allan Willis, a neoplasm is an anomalous tissue mass whose growth exceeds the one of healthy tissues, persisting even after the stimuli that gave rise to it ends. It may begin in a controlled manner and disseminate to other surrounding tissues. Generally, it can lead to death if it is not correctly treated in time. There are more than one hundred types documented currently in literature, being one of the biggest burdens in society nowadays [1].

1.1.1. Impact of cancer worldwide

In accordance with reports shared in 2025 by the Global Cancer Observatory (GCO), a web-based platform of the World Health Organization (WHO), the incidence of all cancers is close to reach 20M cases, causing almost 10M deaths. A total of 22% of incidence and 20% of mortality belongs to Europe. However, as illustrated in Figure 1.1, the heterogeneity of cancer prevails currently worldwide independently of age, sex, or residence [2].

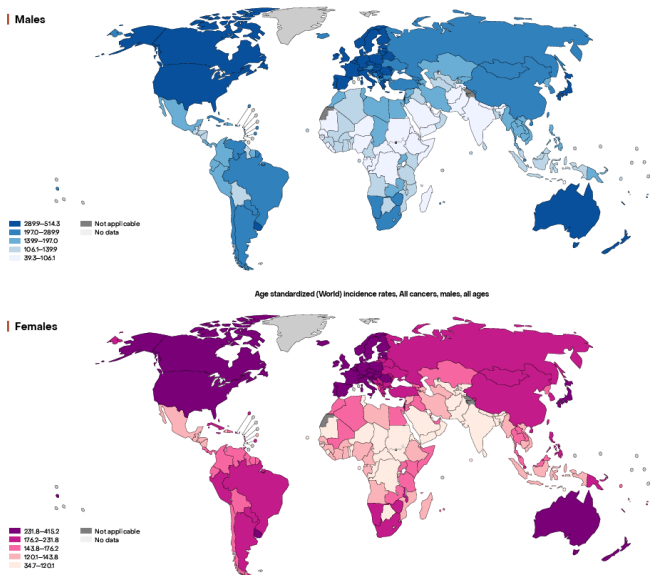

Figure 1.1. Age-standardized incidence rate up to 2025 of all cancers globally in males (top) and females (bottom)

1.1.2. The hallmarks of cancer

These deadly diseases present a big heterogeneity depending on the type of cancer that the patient has. At first, these could be interpreted as a group of diseases with great variety of different mechanisms and symptoms [1].

However, despite the apparent heterogeneity of tumours across tissues and patients, a unifying conceptual framework emerges when cancer is viewed through the lens of cell biology. As a matter of fact, Hanahan and Weinberg already described how all mammalian cells exhibit similar processes for regulating their proliferation, differentiation and ultimately, death based on mutation of oncogenes taking over healthy cells, resembling Darwinian evolution. These authors reported that there exist 6 shared alterations in cell physiology, accompanied by other two extended alterations, and two tumour enabling characteristics in further research. These alterations are more commonly known as the hallmarks of cancer, as observed in Figure 1.2 [3, 4].

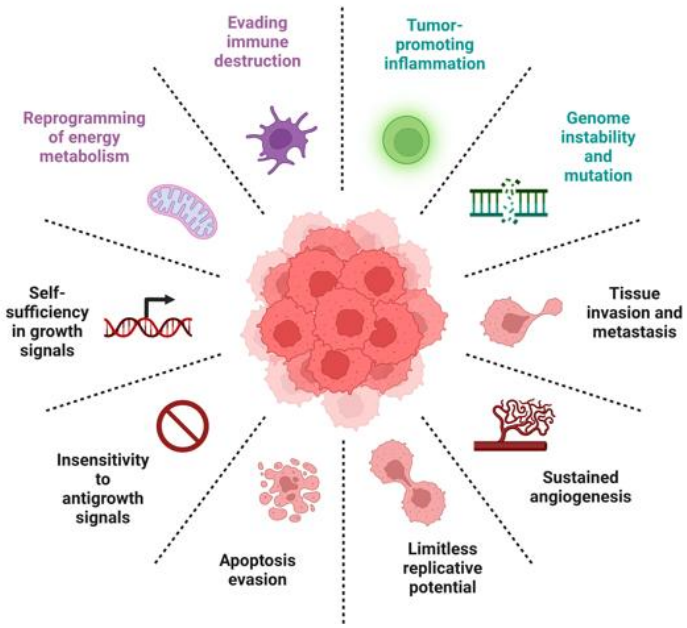

Figure 1.2. Hallmarks of cancer: Original hallmarks (black), emerging hallmarks (purple), and tumour enabling characteristics (green).

These hallmarks are briefly described below [3, 4]:

- Self-sufficiency in growth signals: Cancer cells show a greatly increased independence on exogenous growth simulation, suggesting they are able to generate their own growth signals.

- Insensitivity to antigrowth signals: Cancer cells are able to evade growth suppression signalling.

- Apoptosis evasion: Cancer cells can evade the execution of apoptosis program by alterations, or activation of survival pathways.

- Limitless replicative potential: Cancer cells are able to maintain telomeres length after many replications via telomerase activation.

- Sustained angiogenesis: Cancer cells can activate the "angiogenic switch", stimulating new blood vessels formation in their environment.

- Tissue invasion and metastasis: Cancer cells reach the capacity of leaving the primary tumour, enabling surrounding tissues invasion, entering the circulation, and even establishing secondary colonies at distant sites.

- Reprogramming of energy metabolism: Cancer cells are able to change metabolic pathways in their cells in order to meet the tumour proliferation energy necessities. The most interesting finding is the preference for glycolysis over mitochondrial oxidative phosphorylation in cell metabolism, even in aerobic conditions. This is more commonly known as the Warburg effect, which causes the acidification of tumour microenvironment.

- Evading immune destruction: Cancer cells present mechanisms to evade immune detection, or even resist the attacks mediated by the immune system, by processes such as immunoediting.

- Genome instability and mutation: Tumour cells act interfering in the DNA repair mechanisms or in the cell-cycle checkpoints, accumulating DNA mutations and enabling the tumourigenesis.

- Tumour-promoting inflammation: Cancer cells have the ability to turn inflammation by immune cells infiltration from suppressor to promoter of tumour growth, releasing bioactive molecules from inflammatory cells, which stimulate their proliferation.

All of these hallmarks and enabling characteristics define precisely common cancer survival and promotion cellular mechanisms, as well as the tumour microenvironment conditions. This exhaustive profiling enabled the design of therapies which could be used to treat systemically these diseases throughout history.

1.1.3. Evolution of cancer chemotherapy and its transition to targeted therapy

At first, cancer treatment relied almost exclusively on surgery or radiotherapy, targeting the visible tumour. However, a different and more ambitious idea started changing the therapeutic perspective: Addressing the disease systemically by synthesizing drugs capable of circulating throughout the body, and attacking cancer cells at their site, originating systemic chemotherapy [5, 6].

1.1.3.1. First conventional drugs for systemic chemotherapy

Throughout the years and many research starting since the 1940s, different conventional anti-tumour drugs were designed in order to act on different mechanisms of cancer cells inducing cell death and suppressing tumour growth. Examples of the first most essential drugs can be seen in Table 1.1. and Figure 1.3.

Table 1.1. Representative mechanistic classes of classical chemotherapy

Class	Example	Mechanism
Alkylating agents	Cyclophosphamide	DNA crosslinking
Anti-metabolites	MTX	DHFR inhibition
Purine analogues	6-MP	Nucleotide synthesis inhibition
Fluoropyrimidines	5-FU	Thymidylate synthesis inhibition
Microtubule drugs	Vinca alkaloids, taxanes	Mitotic spindle disruption
Topoisomerase inhibitors	Camptothecin derivates	DNA unwinding inhibition

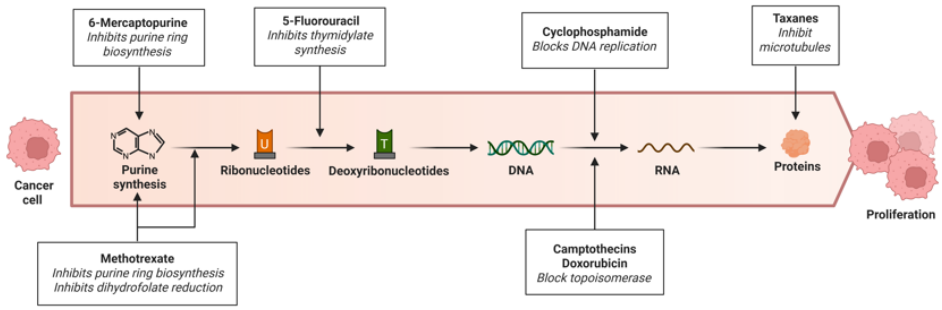

Figure 1.3. Scheme of first conventional anticancer drugs mechanisms of action

1.1.3.2. Adjuvant chemotherapies

Further advances led to adjuvant chemotherapy, where drug administration took place after primary tumour resection surgery. For the first time, residual cells after tumour resection were considered target of an adjuvant therapy, in order to prevent recurrences [7]. Nonetheless, at the end of 20th century, consensus was made that systemic cytotoxic chemotherapy presented relevant limitations, mainly damaging healthy tissues [5, 6].

Subsequent developments in molecular biology and cancer genetics (1980s-1990s), helped understand the DNA alterations that cancer cells could induce. This knowledge opened the possibility of targeted therapies, designed for each cancer molecular powerhouses, marking a shift from drug synthesis to guided deliveries targeting mechanisms [8]. Nowadays, novel biomaterials designed to improve drug delivery in alternative therapeutic strategies have been developed, referred to as

nanocarriers (NCs). The ensemble of these platforms intended to transport antioneoplastic agents to the tumour site and release them efficiently is known as drug delivery systems (DDS)[8].

Drug delivery systems can be broadly chosen, optimized, functionalized, tuned, or designed for specific characteristics of the treatment they are intended for [8]. This field is still being profoundly studied and exponentially expanded nowadays, designing more precise and personalized anti-cancer strategies each time, mainly dependent on the type of cancer treatment they are designed for.

1.2. Breast cancer as a clinical paradigm for targeted therapy

1.2.1. Stats on breast cancer

Breast cancer is currently ranked as the second most incidental and fourth deadliest cancer globally as shown in Figure 1.4, referencing previous WHO statistics. This cancer accumulates 2.3M incidence and 0.67M mortality cases, being women almost all of the affected patients in these data. These facts set it as one of the most invested in oncology research [9]. The mortality of breast cancer is mainly related to the molecular subtype aggressiveness, and the stage at which it is diagnosed. These two variables will define the treatment to follow in each patient [10, 11].

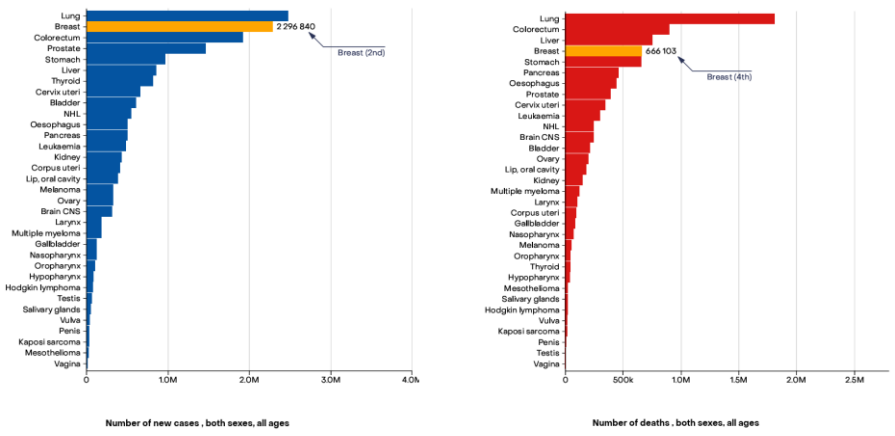

a) b)

Figure 1.4. Breast cancer a) incidence, and b)mortality worldwide in 2022.

1.2.2. Molecular subtypes of breast cancer

Breast cancer is also a complex and biologically heterogeneous disease. There exist many different subtypes of diseases and behaviours within breast tumour invasion. Currently, the main classification of these diseases is based on the expression or absence of hormonal receptors: Estrogen receptor (ER), progesterone receptor (PR), or human epidermic growth factor receptor 2 (HER2) [10, 11].

Besides, tumours with positive receptor expressions can be defined as luminal A for ER+ and/or PR+ expression, whilst luminal B presents higher proliferation and could combine ER+ and/or PR+ with HER2+ receptor overexpression. Finally, the absence of all receptors expressions constitutes the triple negative breast cancer (TNBC). Molecular subtypes are illustrated in Figure 1.5. Receptors overexpressions can guide more efficient treatment decisions by being targeted [10, 11]. However, treatment decisions are also dependent on the stage of breast cancer when it is diagnosed.

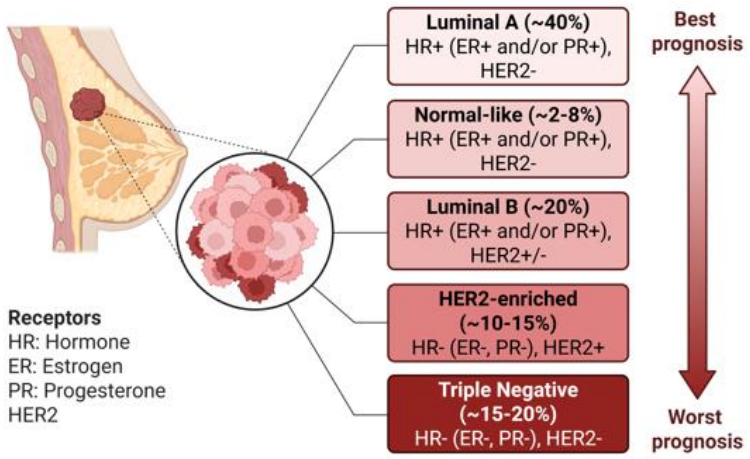

Figure 1.5. Molecular subtypes of breast cancer.

1.2.3. Stages of breast cancer

As stated previously, prognosis and decisions of treatments to cure breast cancer do not only depend on the molecular subtype of cancer, but also its behaviour and the stage at which it is diagnosed. Different

stages can be found in breast cancer classified from 0 to stage IV, briefly summarized in Figure 1.6 [10, 11].

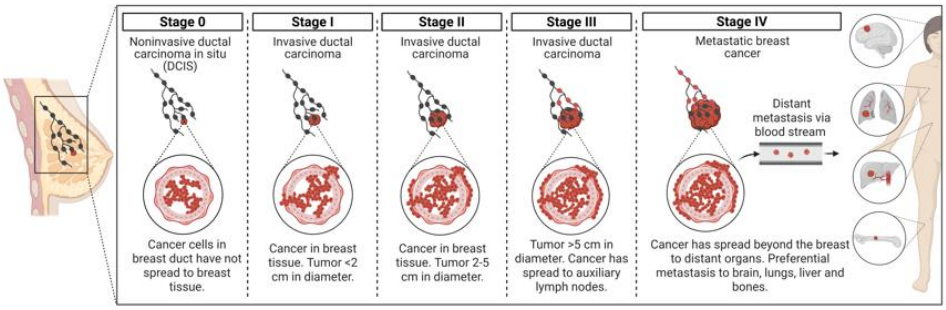

Figure 1.6. Stages of breast cancer.

Breast cancer usually starts with mutations in epithelial cells found in breast ducts, starting carcinomas *in situ* (stage 0). Proliferation disrupts the basal membrane and invasion of stroma happens as tumour grows (stage I-II), and spreads to auxiliary lymph nodes (stage III). Finally, tumour cells are able to penetrate in blood vessels and invade distant organs, most likely to be brain, lungs, liver, and bones for metastatic breast cancer (stage IV) [10].

1.2.4. Current treatments for breast cancer

Taking into account the heterogeneity of breast cancer in each molecular subtype and stage when diagnosed, multiple treatment approaches can be developed for its cure. Besides, regarding previous approaches, it is clearly stated that novel therapies must be focused on the biological particularities or hallmarks of cancer disease, rather than general clinic characteristics. Molecular profiling and targeted therapy are the main outcomes of this paradigm, implementing active targeting mechanisms, for instance: Antibody, small molecule, vaccine, or gene-based therapies, including immunotherapy as well [12]. Depending on molecular subtypes, Table 1.2. displays the current preferred approaches.

Table 1.2. Preferred therapies for molecular subtypes breast cancer.

Molecular subtype	Receptors expresion	Therapies	Ref
Luminal A / B	HR+, HER2-	Endocrine therapy, using tamoxifen or aromatase inhibitors	13
HER2+	HER2+	Monoclonal antibody therapies: Trastuzumab or Pertuzumab	14
TNBC	HR-, HER2-	Chemotherapy	15

However, as research keeps prospering, novel strategies for combined therapies are the current way of action, including surgery, systemic treatments, and radiotherapy. Treatment for patients diagnosed in an early stage of the tumour with no metastatic condition usually follow the protocol: Optional pre-operative therapy (systemic therapies), primary tumour resection surgery (main stage of treatment), and finally, systemic therapies in post-operative stage to avoid recurrence risks [16].

The primary tumour resection surgery is conceived by two main options: Breast-conserving therapy (BCT) by lumpectomy (or least preferred wide excision, or quadrantectomy), where only tumour and safety margins are removed and breast is preserved, or total mastectomy, where the full breast is removed [16]. Differences in these procedures can be appreciated in Figure 1.7.

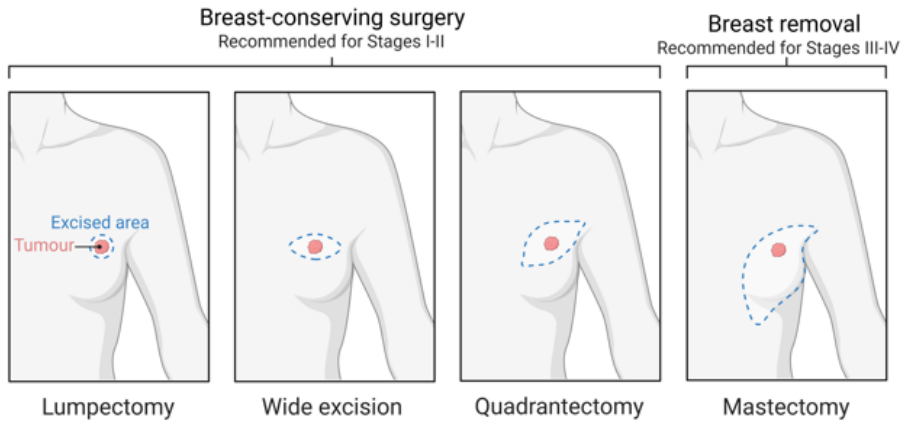

Figure 1.7. Types of tumour resection surgeries.

Late clinical assays keeping track up to 20 years after surgery, showed that BCT followed by radiotherapy survival rate is similar to the mastectomy procedure for early stages (I and II). These results preference the BCT over mastectomy when conditions allow it, maintaining a conservative surgical perspective, followed by irradiation of the entire breast. Radiotherapy is used in order to eliminate any possible tumour residue that stays in the breast tissue after surgery [17-20].

However, decisions regarding treatments based on the time of diagnosis require a multifactorial study in order to decide the ultimate therapies. Sentinel lymph node biopsy (SLNB) must be performed in order to determine whether the tumour has disseminated through the lymphatic system. If more than 2 nodes have been affected, usually an axillary lymph node dissection (ALND) is also needed. Breast radiation (XRT) is frequently performed after lumpectomy, or in post-mastectomy radiation (PMRT). The basic decision diagram is displayed in Figure 1.8 [16].

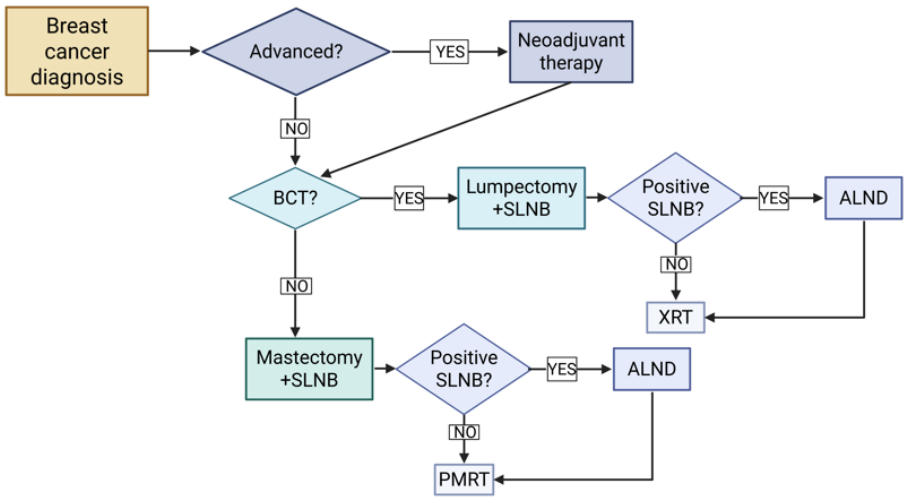

Figure 1.8. Decision diagram for breast cancer procedures in different diagnosis cases. Rectangles correspond to techniques or procedures, and rhombuses to intertwined decisions depending on the diagnosed tumour characteristics.

In this decision diagram, the surgery treatment option has been optimized to perform breast conserving therapy whilst maintaining the

same survival rates than mastectomy [18]. However, the radiation as post-surgery treatment still lacks efficiency and specificity for a more secure recovery of the patient without damaging their quality of life due to targeting inability [16]. This leaves a current landscape for post-surgical approaches with a wide margin to improve.

1.2.5. Post-surgical therapeutic landscape and systemic limitations

When studying post-surgical alternative treatments, outbreak pathologic studies in mastectomy samples showed that up to 63% of cases presented small tumour residues located in primary tumour site, or displaced in a 2cm perimeter around it. These data highlights the need for adjuvant therapies in post-operative stage in order to avoid recurrences [21]. Currently, adjuvant radiotherapy role is, to ensure durable control of disease eradication. After lumpectomy, breast irradiation can reduce local recurrence up to 50%, and also 10-year recurrence risk from 35% to 19% [17-20]. Moreover, long term survival rate statistics have improved because of this adjuvant therapy [22].

However, radiotherapy is a procedure which causes many harm to patients and affects negatively in their quality of life. Therefore, systemic adjuvant therapies are also taken into account for eliminating disseminated cancer cells after tumour-resection. Modern tools like genomic trials or molecular profiling have helped to adjust better personalised treatments regarding the specific biological characteristics of each tumour. [23] The main challenges of post-operative breast cancer treatment and its therapies to address recurrences are described in the subsequent sections.

1.2.5.1. Tumour recurrences

Tumour recurrence still prevails as one of the most challenging inconveniences in breast cancer therapy. Recurrence can happen in the same surgical bed as primary tumour, or slightly disseminated from it, in the chest wall, regionally displaced in lymph nodes, or as metastasis in other organs, mostly in bones, lungs, liver, or brain [24]. Recurrences may happen in the long term after resection, since residual cancer cells left in surgical bed have demonstrated abilities to wait in quiescence

state or surviving the stromal surroundings until their relapse, positioning recurrence eradication as one of the main current focus in modern oncology [25]. The possibility of suffering from tumour recurrences also depends on the aggressiveness of the molecular subtype [10]. The most aggressive subtypes, HER2+ and TNBC show significantly higher ratios of recurrences than luminal subtypes, up to 6-8 times higher [26].

Currently, BCT supported by post-operative adjuvant therapies have successfully reduced recurrence risk down to 5-15%, but this still implies a great number of patients, overall women, still suffering from this. Additionally, in case of local recurrence, the clinical management has to be set back at a surgery to remove the secondary tumour, complicating many aspects of the patients' health and quality of life. On this occasion, many times full mastectomy will be compulsory, and adjuvant therapies may follow this procedure as well [27]. It should be noted that up to 95% of relapses occur at the primary tumour site or the surgical bed, highlighting this region as a key target for the development of novel therapeutic approaches [28]. This is the reason why current treatments rely on breast irradiation, which treats directly the affected area. However, off-target toxicity remains one of its major limitations [16].

1.2.5.3. Breast irradiation drawbacks

In order to solve the off-target toxicity of breast irradiation, new alternative therapies focus on the implementation of nanocarriers, exploiting drug delivery systems for active targeting of tumour cells, taking advantage of their hallmarks [4, 8]. Moreover, many carriers can also passively accumulate at tumour site by the Enhanced Permeability and Retention (EPR) effect, due to leaky permeable vasculature of angiogenesis, and poor lymphatic drainage, taking more time to remove the nanocarriers from it. This effect is illustrated in Figure 1.9.[8]

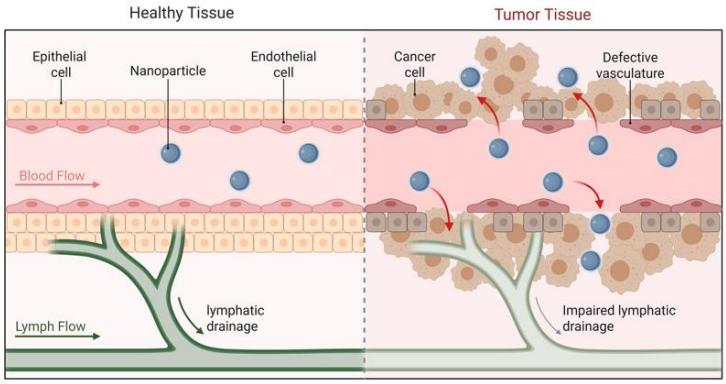

Figure 1.9. Passive targeting of tumour sites by EPR effect.

Although the use of drug delivery systems can put an end to off-targeting breast irradiation, new problems arise with their systemic administration, predominating intravenous injection [13-15]. This systemic administration causes the drug to circulate around the body until reaching tumour site. Thereby, more locations are exposed to its cytotoxic effects, affecting healthy cells and tissues, and greatly limiting the maximum tolerable dose for the patient, reducing the treatment efficiency [8].

1.2.5.3. Systemic administration drawbacks

Despite the advances that anti-cancer therapies and current drug delivery systems present, their systemic administration is still one of the biggest hurdle, due to systemic toxicity and great decrease of their therapeutic efficiency. In fact, analyses conclude that less than 1% of the administered drug dose (an estimated average of 0.7%) is able to reach the tumour site [29]. This extremely low bioavailability is the consequence of biological barriers that act sequentially since the administration.

Firstly, during its circulation in the bloodstream after intravenous injection, the nano-sized drugs or DDS with payloads experience a rapid interaction with plasma proteins, causing the so-called protein corona formation, changing their physicochemical properties and promoting their recognition by the immune system via opsonization, where

antibodies and complement components are implemented in the protein coating [29].

In parallel, the mononuclear phagocytic system plays the role of biological filter ruled by Kupffer cells located in the liver, and splenic macrophages. This filter is so strict it can cause more accumulation of delivery systems in kidney or spleen than in the tumour site. Thus, biologically suppressed drug taken by the immune system can affect maliciously to the kidney and the spleen, presenting systemic toxicity [29]. Furthermore, solid tumours characteristics, including irregular vasculature or interstitial pressure, complicate drug penetration in its microenvironment [30]. These biological barriers are illustrated in Figure 1.10.

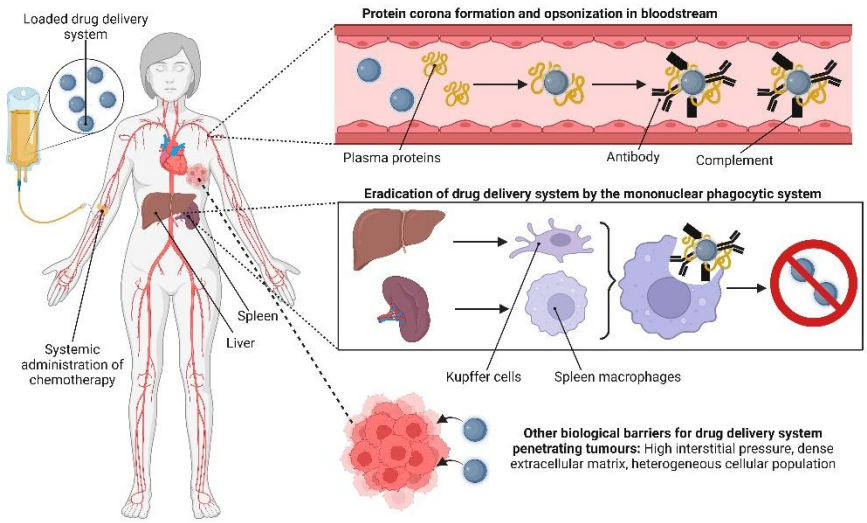

Figure 1.10. Biological barriers present in systemic therapies

In order to solve these limitations, new approaches are focused on alternative administration routes. Specifically, in breast cancer, since the majority of residual cancer cells are found in the surgical bed, or in its margins, a local administration of drugs represents a direct accumulation at desired site evading systemic toxicity in the rest of the body [29]. Moreover, since these therapies always require a previous surgical intervention which leaves a cavity behind, the local

administration can be designed to fill in the cavity, without adding any side problems [31].

These filling matrices are usually based on macroscopic hydrogels, which can act as drug reservoirs, accumulating higher drug doses at tumour site and prolonging its release *in situ* [31]. Furthermore, these hydrogels can be designed in order to be injectable so that they adapt to the cavity of the patient and gel *in situ*, using the increase from room to physiological temperature, making this a thermo-sensitive matrix [32].

1.3. Injectable hydrogels as thermo-responsive drug reservoirs

As stated previously, since breast cancer relapses occur in the primary tumour site or surgical scar in 95% of possibilities, local administration presents a promising strategy [28]. This administration is yet to be achieved given that the latest approved drug delivery systems by FDA, EMA, or in clinical trials for breast cancer treatment and prevention of breast cancer recurrences all use intravenous administration [33]. This demonstrates the potential in developing an adaptable drug depot into the cavity.

1.3.1. Precursor gels for local administration

At first, this approach placed rigid drug depots administered in tumour sites directly. Biodegradability of their materials enabled their implantation during surgery, without the need of additional processes for their withdrawal. First formats came in shape of polymeric films, wafers, or rods. These macrostructures encapsulated many different compounds independently of their nature. Polymers conforming gels can come from natural (alginate, chitosan, dextran, hyaluronic acid) or synthetic origins (polyesters)[34].

Although these formats presented high promising results, there were still inconveniences associated with these therapies, like drug penetration in the tumour tissue, or reducing the homogeneous distribution of the therapeutic agent. Moreover, the surgical implantation

also limited the clinical applicability [34]. Engineering wise, materials must be designed towards prolonged times.

1.3.2. *In situ* forming injectable hydrogels

New generations of hydrogel-based DDS have been promoted trying to solve their forerunner limitations. The solutions require materials of gelling *in situ* after the local administration as their liquid precursor (injectable), normally responding to a physicochemical transformation induced by physiological stimuli or controlled crosslinking reactions. This way, the local administration is kept minimally invasive, with platforms improved adaptability to the tumour tissue geometry, as shown in Figure 1.11. [31]. Injectable hydrogels make more efficient the localized drug delivery, controlling space and time, and adapting themselves to irregular surgical cavities. Rigid implants or pre-formed gels, on the other hand, lack all of these advantages [34].

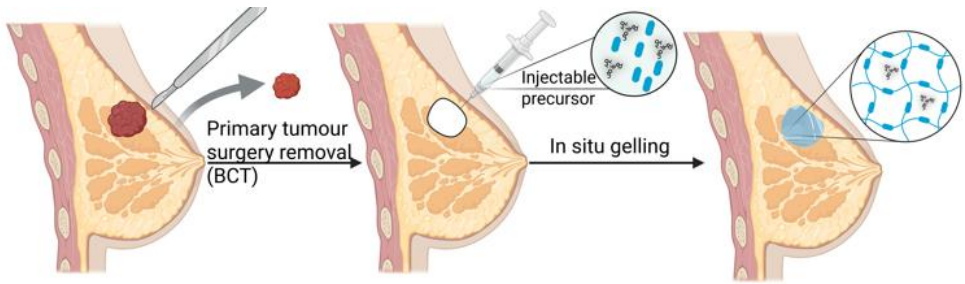

Figure 1.11. *In situ* forming hydrogel strategy for breast cancer post-surgery therapies.

As stated, polymers conforming hydrogels can come from natural or synthetic origins [34]. Alginate, chitosan, dextran, or hyaluronic acid outstand as natural polymers in gels, added to collagen or gelatin as structural proteins. These compounds mainly form networks out of crosslinking or self-assembly processes. For instance, alginate gels were used for wound dressings before studying their potential as DDS [35]. Synthetic polymers also control the hydrogel degradation, drug delivery or mechanical resistance. In fact, polyesters like PLA, PGA, or PLGA constitute the majority of the hydrogels in biomedicine [33].

When studying their impact in breast cancer treatments, hydrogels can take action as interface between pharmacologic intervention and the

local tissue biology [32]. For instance, Mi et al. [36] developed photopolymerizable hydrogels based of PEG dimethacrylate, and sericin methacryloyl, able to gel inside the surgical breast cavities in murine models. The physical hurdle added to delayed drug delivery achieved direct contact with residual tissue, achieving a 50% survival rate with mice remaining disease free for more than six months.

Besides, injectable hydrogels have reported to fulfil other functions within the breast cancer treatment [37]. The main side roles are tissue engineering and tumour modelling, also presenting combined progresses with drug delivery. For instance, Balahura et al. [38] synthesized cellulose nanofiber (CNF) based hydrogels loaded with 5-FU and alginate/pectin. This formulation improved biocompatibility, and suppressed breast cancer growth, as well as supported the growth of adipose-derive stem cells, a promising result for soft tissue reconstruction.

Different gelling mechanisms might take action *in situ*. These are illustrated in Figure 1.12 [31]. Physical ones usually are preferred, since they do not need toxic solvent or catalysis, do not generate heat, and usually evade harmful irradiation processes for the encapsulated molecules or cells [31]. An approved example, OncoGel™, is made from copolymers of PLGA and PEG, loaded with PTX, used for local administration in solid tumours, undergoing gelation after temperature increase [39].

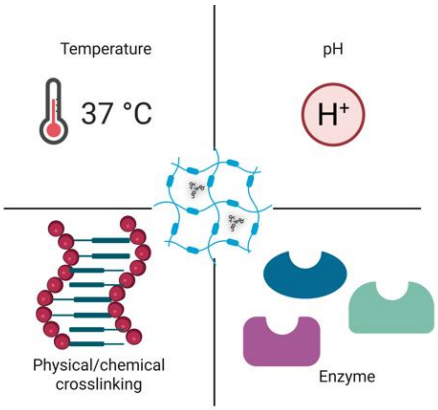

Figure 1.12. Main gelling mechanism of *in situ* forming hydrogels.

1.3.3. Thermo-responsive injectable hydrogels for drug delivery in breast cancer

Thermo-sensitive hydrogels are the most studied. Polymers that constitute them present LCST (lower critical solution temperature), defined as the temperature below which a material remains soluble (sol), and above which polymer aggregation (gel) occurs. Thus, it stablishes a turning point between the liquid injectable precursor and the gel form. Therefore, many systems developed for thermo-response are constituted by synthetic polymers designed for desired values of LCST lower than the physiological one, so that the gelation process occurs as soon as it stablishes contact with the tissue [31].

In this matter, there have been numerous studies in breast cancer treatments for thermo-responsive injectable hydrogels used as antineoplastic agents delivery platforms. For instance, a hydrogel based of poly(organe-phosphazene) (PPZ) loaded with DOX enabled 40 times higher solubility of DOX encapsulated. However, the inhibitory concentration 50 (IC_{50}) of the system was similar to the free drug in cell line MCF-7, proving no decrease in therapeutic efficiency [40, 41]. Table 1.3. collects different reported formulations for this application.

Table 1.3. Reported thermo-sensitive injectable hydrogels for breast cancer therapy

Hydrogel formulation	Drug	Target	Highlights	Ref
CS/β-GP	Cis	MCF-7	Hydrogel showed 2.05 fold more antitumour activity than DDP solution in MCF-7 cell line.	42
PPZ	2-ME	MDA-MB-231	Release from hydrogel by diffusion and surface erosion of matrix, enhanced antitumour activity in MDA-MB-231 cell line.	43
PEGylated (hydro/fluoro)carbon NPs	PTX DOX	MCF-7	Hydrogel formed because of incompatible assembly of hydro and fluorocarbon NP cores	44
PECE@mPEG-PCL NPs	PTX	4T1	Reduced local recurrence to 9.1% and increased survival to 67 days after tumour resection in mouse model	45

PF-127	PTX-NCR	4T1 MCF-7	Enhanced antitumour efficacy in cell lines and mouse retained up to 10% PTX 20 days after injection	46
HDI-PF-127/HA	DOX	MCF-7	Obtained a more biocompatible formulation and increased hydrophilicity	47
PLA-coupled Poloxamer/PEI-alt-PEG	PTX (shRNA Akt1)	MCF-7 MDA-MB-231	Effective combination of therapies induced apoptosis and prevented angiogenesis	48
PCNA@AuNRs	DOX	4T1	Recurrence reduction to 16.7% in 4T1 cell line	49
PF127/P188@ niosomes	TMC	*In vivo* mice model	Ehrlich solid tumour growth inhibition of 97.4% and tumour retention 14 times higher	50
CINPs	17-AAG	4T1	Reduced tumour inhibition in 98% and lung metastasis in 89% in 4T1 murine model	51
PLGA-PEG-PLGA	Tmab	SKBR-3	Sustained release of 80 days and better tumour growth inhibition with total suppression of recurrence for 4 weeks	52
HA-CS-g-PNIPAm @ GOFA	DOX	MCF-7	Reduced 52% of tumour volume in 3 weeks	53
CS-β-GP+PF-127	5-FU	MCF-7	Reduced cell viability to 20% and relative tumour volume to 8% in less than 2 weeks	54

Hydrogels may also be used for other kinds of deliveries, like gene therapy, immunotherapy or chemo immunotherapy, which also have earned great interest in localized anticancer strategies. For instance, immunotherapy benefits also from hydrogel formulations, being new immunoadjuvants or monoclonal antibodies depots in tumour microenvironment. Additionally, synergic therapies can also be mediated with hydrogels. In this context, combined administration of niclosamide and PTX and their prolonged release from PLGA-PEG-PLGA hydrogels allowed breast cancer proliferation and growth inhibition up to 69% in TNBC murine models and cellular migration [55].

To recapitulate, as it can be seen in Table 1.3, there is a wide range of different strategies to develop thermo-sensitive injectable platforms. In order to optimize the injectability and mechanical properties within the body for intended application, it is essential to choose a suitable polymers base for the hydrogel network.

1.3.4. Comparison of thermo-sensitive polymers for injectable formulations

As it has been stated, hydrogel materials must be selected and designed for the physicochemical and the desired drug release properties. Therefore, thermo-responsive polymer choice to base hydrogel formulation is crucial for the application, and the main options reported are displayed in Table 1.4 [31, 32, 37, 56].

Table 1.4. Thermo-sensitive polymers for injectable formulations comparison.

Hydrogel base	Gelling mechanism	Benefits	Limitations
PNIPAM copolymers	Hydrophobic structural collapse	LCST well defined and easily modified Well studied systems	Potential toxicity Non biodegradable Restricted clinical use
Biodegradable PEG-polyester copolymers	Self-assembly of hydrophobic blocks	Biodegradable and highly biocompatible Good mechanic stability and sustained releases	Complex synthesis Reproducibility variabilities (sol-gel transition) Acidic degradation More expensive
Poloxamer Pluronics	Micellar aggregation capacity	High biocompatibility Reversible gelation *in situ* Good injectability Easy combination with other NCs Non-toxic synthesis More economic	Low mechanical resistance Fast erosion in physiological media Faster drug release
Modified natural polymers	Physical interactions by induced thermal transition	High biocompatibility Possibility of biologic targeting	Less reproducible Transition not well defined
Hybrid polyesters	Hydrophobic aggregations	Controlled degradation High stability	Complex synthesis Less standarized

As observed in Table 1.4, the polymers presenting best thermal control are PNIPAM family, however their toxicity restrains them for biological applications, unless modifications are made to improve their biocompatibility. On the contrary, natural polymers, which present this biocompatibility, need to be functionalized to present systems with LCST (Chitosan with β-GP, HA or gelatin modifications), making their design or synthesis much more complex to control or optimize. Similar weakness is shared with hybrid polyesters, where modifications from conventional ones and their intricate gelling mechanisms makes them a less preferred option for this strategy.

Then, biodegradable PEG copolymers show the best stability and degradation conditions, but still compromises future clinical translations due to complex synthesis and potential variability in sol-gel transition. Meanwhile, poloxamers stability under *in vivo* conditions are not as promising due to faster degradation, but their affordability, biocompatibility, injectability, and reproducibility position them as the preferred base of the hydrogel. Moreover, they can be easily tuneable or functionalized in order to overcome their weaknesses, without the need of complex solvents or methodologies difficult to reproduce.

Specifically, Pluronic F127 (PF-127) presents substantial interesting characteristics compared to the other thermo-responsive poloxamers. Firstly, it has already been approved and regulated by FDA, used in biomedical and pharmaceutical formulations. It gels without the need of chemical reactions, initiators, catalysts, and never produces toxic residues. Its self-assembly micelles organization is convenient for drug hydrophilicity, and it presents an easy synthesis by cold method. Furthermore, great compatibility with embedded NPs, or NCs to form hybrid systems highlights it for synergic therapies [55].

In fact, PF-127 formulations combined with polymeric excipients (PEG-400 or hydroxipropylmethylcellulose) have been approved for low-grade urothelial carcinoma of upper urinary tract. However, specifically for breast cancer, therapeutic hydrogels are still in preclinical stages. The only clinical studies currently available are based on formulations intended for secondary effects of radiotherapy, presenting high

molecular weight polysaccharides derived from aloe vera [57]. This highlights the oportunity to keep developing new platforms as antineoplastic drug delivery in a safer, more efficient and reproducible way, as the thermo-sensitive strategy of the local administration approach.

However, thermo-sensitive hydrogels providing solely sustained drug release remain insufficient for efficient cancer therapy. Despite the favourable gelling behaviour and prolonged release achieved, the drug released from the local depot would still be non-selectively distributed within the surrounding environment, potentially affecting healthy tissues in addition to cancer cells. Therefore, the incorporation of an additional tumour-targeting strategy becomes necessary to obtain a selective release within tumour microenvironment.

1.3.5. Additional tumour targeting strategy

Tumour targeting can be done passively, by the EPR effect maintaining nano-sized particles at tumour site, actively, by designing systems with specific characteristics towards cancer cell characteristics, or stimuli-responsive, by targeting tumour microenvironment features. Since the strategy is designed for a local administration, the most efficient approach is to target the specific tumour microenvironment which has been confirmed to be reproducible despite heterogeneity, as the aforementioned hallmarks described. In this sense, stimuli that can selectively trigger drug release response can be classified in two main categories: Endogenous, for the ones that are originated within the tumour microenvironment, and exogenous, for the ones that come from external sources of the microenvironment, or the organism. A brief scheme of these stimuli can be seen in Figure 1.13 [33, 58].

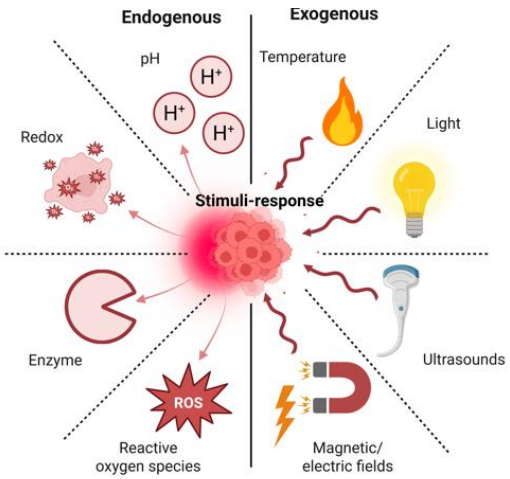

Figure 1.13. Endogenous and exogenous stimuli for responsive therapies

Although some stimuli-responsive systems consider the option of exogenous stimuli exploitation, the need of an external source to trigger the response mechanism is viewed as an important limitation. Therefore, the endogenous stimuli are preferred. Briefly, these are:

- pH: It is the most exploited in nanomedicine. This is due to the difference found in the physio-pathological pH in tumour microenvironments. As part of cancer hallmarks, the Warburg effect produces high concentrations of lactic acid [3, 4]. Ultimately, pH of tumour environment acidifies, reaching values of 6.8-6.5 in the extracellular region compared to 7.4 in healthy tissues. Moreover, tumour pH reaches acidic values down to 5.5 and 4.5 in endosomal or lysosomal stages, respectively [58]. This difference is highly exploited as stimuli-response since it enables a wide range to work efficiently.

- Redox-responsive: They exploit the intracellular high glutathione (GSH) concentration. Cancer cells overstimulate GSH production, in order to compensate the increased ROS preventing cell death by oxidative stress, and promote proliferation and metastasis. Redox-responsive NCs present disulfide bonds (-S-S-) in their structure, which are bound to break under the high reducing activity inside cancer cells once penetrated, releasing therapeutic agent [58].

- Enzyme-responsive: There is a highly altered enzymatic activity in tumours microenvironment, overexpressing some of them. DDS used in this scope present peptide sequences, or specific chemical bonds that are cleaved under tumour enzymes activity. Eventually, bond is hydrolysed when the compounds come into contact with enzymes, producing drug release [58].

- ROS and H_2O_2-reponsive: They focus on the elevated presence of ROS in the tumour microenvironment. Systems incorporating chemical bonds that are susceptible to oxidation are chosen for this stimulus trigger. Therefore, usually NCs with thioethers or peroxalate groups are used, causing structural changes when they are exposed to ROS or H_2O_2, ultimately releasing the drug [58].

After studying the different stimuli surrounding cancer cells, pH represents the most efficient one. This is due to the reprogrammed metabolism causing Warburg effect and accumulating protons in the extracellular microenvironment, as well as intracellular compartments. Therefore, it is the most reliable and reproducible endogenous stimulus to exploit in an additional tumour targeting approach for injectable hydrogels.

1.4. pH-responsive strategies for tumour targeting

As it has been concluded, pH is the most exploited and often efficient stimulus when targeting tumour microenvironment. Its acidity compared to healthy tissues is the consequence of its hallmarks, as explained in previous section, specifically reprogramming the metabolic energy. The preference of many metabolic routes in cancer cells for glycolysis instead of oxidative phosphorylation, even in aerobic conditions, causes the accumulation of lactate and protons. This is defined as the Warburg effect [4, 5].

The overproduction of these protons included to abnormal vascularization and inefficient perfusion, which hinders their elimination, is what acidifies the inner and outer environment of the cancer cells compared to healthy ones. pH gradients stablished are around 6.5-6.8 for extracellular environment, going down to 6.0-4.5 for inner

compartments like endosomes or lysosomes [5]. These mechanisms are illustrated in Figure 1.14.

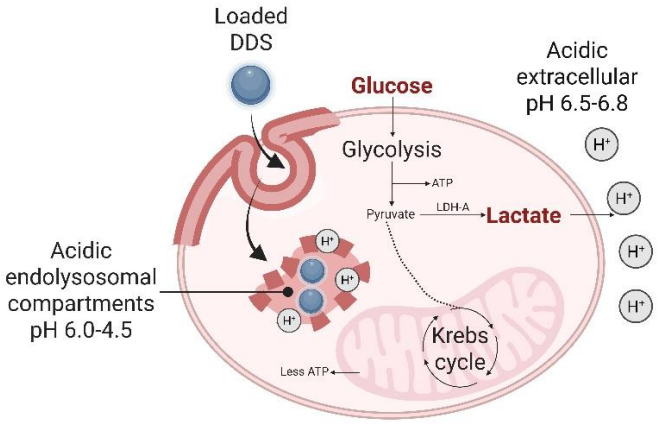

Figure 1.14. Cancer cell metabolic reprogramming leading to an acidic extracellular environment and acidic endolysosomal intracellular compartments.

This pH gradient establishes an endogenous stimulus for potential exploitation, due to its difference with healthy physiological environments, around 7.4. The fact that this broad difference can promote drug release without the need of an external source of energy is what makes it a preferred strategy for tumour targeting. Focusing on this, pH-sensitive systems do not only release drug at tumour site, but also prevent its release in healthy pH ranges, decreasing systemic toxicity. pH-responsiveness in DDS can be achieved by different mechanisms [59,60].

1.4.1. Mechanisms of pH-response

1.4.1.1. Ionisable functional groups

Systems presenting polymers with ionisable groups usually are based on amines, carboxylates, sulfonates, or imidazoles. When pH decreases, these groups change their charge, altering the system stability. Specifically, cationic polymers present hydrophobicity at physiological pH and are protonated when it decreases, hydrophilizing themselves and inducing electrostatic repulsion for the system instability. On the other hand, anionic polymers are ionised and hydrophilic at physiological pH,

losing their charged status when it decreases, and turning them into hydrophobic compounds which causes a structural reorganization, and consequent drug release [60].

1.4.1.2. Acid labile linkage

These chemical bonds are selectively disrupted under acidic environments, inducing their hydrolisis. The main ones are the hydrazine, imine, acetal, ketal, orthoester or oxime bonds [61].

1.4.1.3. Coating with pH-sensitive polymers

Although not as common, another strategy to achieve pH-response to systems that do not present susceptible ionisable groups or labile bonds is coating them with a system that does. This way the nature of the linking does not have to be acid labile, and the encapsulated system does not lose or alter any other physicochemical properties than the surface ones (increasing size, or change in surface charge) [60].

1.4.1.4. Combined strategies

Platforms combining protonation, acid labile linkages, and crosslinking mechanisms use the synergy of multiple pH-responses. These systems usually undergo a swelling process under acidic pH values, which can modulate drug release kinetics. In other cases, the proper crosslinking systems are acid labile, inducing a complete disassembly of the carrier. The different mechanisms are illustrated in Figure 1.15 [59, 60].

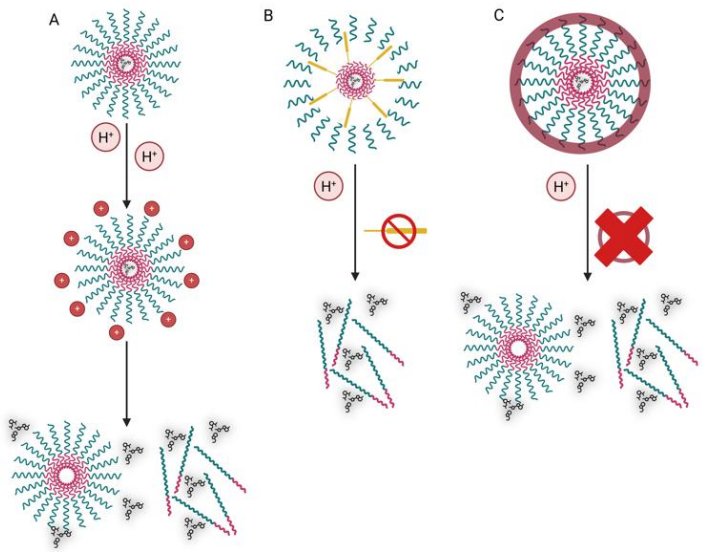

Figure 1.15. pH-response mechanisms in systems presenting a) Ionisable functional groups, b) Acid labile linkages, or c) Either crosslinking or coating. The drug release is illustrated as either swelling (stable particle) or disassembly (disrupted particle).

In the case of hydrogels, several systems have already been reported to be designed for pH-response, targeting acidic tumours for a faster drug release.

1.4.2. pH-responsive hydrogels

Although they have only been mentioned as thermo-sensitive injectable drug depots, hydrogels can also present pH-response as drug release mechanism [31]. For instance, in one study, DOX was conjugated to succinated chitosan via Schiff base between the ketone group of the drug and the amine group of the chitosan. The resulting hydrogel presented pH-response [31]. Oxidized alginate was also used as a crosslinker to synthesize a pH-responsive system by coupling reactions between its aldehyde groups with amine groups of the modified chitosan. DOX release showed a 65% release at pH 5.0 compared to 5% at 7.4. Moreover, tumour growth inhibitory capacity was confirmed on breast cancer cell line MCF-7 (*in vitro*) and MDA-MB-231 human xenograft breast tumours in mice [62].

Since hydrogels have proven to be thermo-sensitive (injectable) and pH-responsive (tumour targeting) networks, then it is also possible to

combine both responses in a dual-sensitive drug delivery system which presents benefits from both strategies simultaneously.

1.5. Dual temperature and pH-responsive hydrogels

As it has been stated, although the *in situ* forming hydrogels for local administration enable effective concentrations of drugs and sustained release at tumour site, this release lacks the active recognition of tumour characteristic features. Implemented pH-response compensates this limitation by strategically targeting acidic environments [63]. After analysing both stimuli-response strategies, authors have reported dual-response hydrogels as drug delivery systems with intended cancer applications.

For instance, in 2018 Jommanee et al. [64] developed hydrogels based on diblock copolymers mPEG and ε-caprolactone (PCL), grafted onto pH-sensitive biopolymer chitosan. The solution-gel (sol-gel) transition temperature was dependent on pH, PCL composition, and diblock copolymer and grafting content concentration. Although the transition temperature was highly tuneable, only few formulations could present gel state at acidic tumour conditions, and rheological assays confirmed elastic modulus increase past 37ºC, which could imply slow gelation *in vivo* conditions. This system encapsulated a hydrophilic (DOX) and hydrophobic (Cur) drug proving sustained releases reaching 40% and 60% during 15 days period of time, respectively. However, pH-sensitivity was not tested on drug delivery, and cell assays were not performed.

Later in 2023, Lin et al. [65] studied different tertiary amines polypeptides inclusions in mPEG hydrogels. The structure of these amines changed from α-helix to β-sheets when pH was increased from 4.0 to 7.4. High polymer concentrations were needed to stablish sol-gel transition, which was also dependant on the pH. Conformation change in its structure showed pH-responsive release of DOX, reaching 100% in two days at pH 4.0, whilst releasing only 50% in 14 days for pH range 6.5-7.0. Moreover, high biocompatibility of the hydrogel formulations was proven on NIH 3T3 cells and *in vivo*, showing gel degradation during 14

days after injection without inflammation, as shown in Figure 1.16. However, loaded formulations were not proven on any cell or animal model, lacking the release behaviour or pH-sensitivity in these conditions.

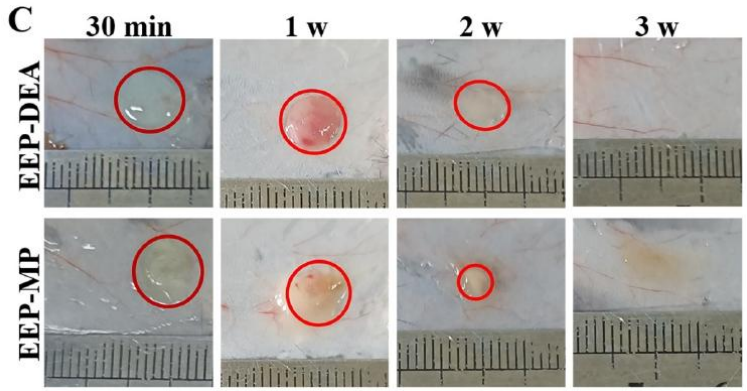

Figure 1.16. Photographs of remaining hydrogels *in vivo* at different time points of one (DEA) and two (MP) tertiary amines formulations developed by Lin et al [65].

Therefore, reported systems in the last decade have been able to synthesize a hydrogel matrix which exhibited dual-response release and was biocompatible with cell cultures and animal models. However, these studies were in many cases underdeveloped and did not target specific diseases. Regarding this, some authors have designed dual-response hydrogels for intended breast cancer treatment.

1.5.1. Reported dual-responsive hydrogel formulations for breast cancer therapies

Focusing on breast cancer treatments and prevention of local recurrences, the latest studies from 2019 until nowadays report dual-response hydrogels as one of the most promising strategies for localized therapies. For this purpose, the most exploited hydrogel base is modified PNIPAAm polymers, which gel transition temperature can be tuned, with chitosan (CS) to increase its biocompatibility, using β-glycerophosphate (β-GP) as crosslinking agent.

For instance, Fathi et al. [66] formulated dual response hydrogels based on PNIAAm-co-IA and CS/ β-GP. LCST was defined at 39ºC, and

DOX releases were promoted at 37ºC and acidic conditions (pH 5.5), where 100% of release was achieved in 2 days for low loading concentrations (0.1 mg/mL), compared to 40% at pH 7.4 sustained release for 8 days. Furthermore, MTT on MCF-7 cell line proved biocompatibility, and their proliferation on the loaded hydrogels showed their potential for local therapy of breast cancer.

More recently, in 2024, Mohan et al. [67] developed a network hydrogel with melamine functionalized PNIPAM derivate copolymerized using glycidyl methacrylate (pNIPAm-co-pGMA-Mela) to study the release of hydrophilic (5-FU) and hydrophobic (Ibu) drugs separately. Since the gel state was confirmed at 45ºC with transition starting past 37ºC, their releases presented dual-response, being faster at higher temperatures (45ºC) and lower pHs (4.0), releasing the whole drug loaded in 10h (Ibu) and 8h (5-FU), compared to sustained 40% of both drugs during 12h at 25ºC and pH 7.4. TNBC cell line MDA-MB-231 was used to confirm its biocompatibility, presenting a promising drug carrier system regardless of hydrophilicity of the desired drug. Moreover, drug loaded hydrogels presented more cell death than drug solutions at all concentrations studied.

Next, in 2025, Ahmadi et al. [68] proved successful synergy of treatments co-delivering MTX and Cur with a NIPAAm-co-MA formulation, with a transition temperature of 38.5ºC. This caused dual-sensitive release of drugs, where pH played an essential role. Separately loaded hydrogels presented MTX release of 80% at pH 5.5, compared to 70% at 7.4 for a week period of time, whilst 60% against 40% for Cur release in the same conditions. However, pH-sensitivity decreased in dual-loaded hydrogels for releases at 37ºC (reaching 60% of cumulative release), whilst maintaining a 20% of difference at 40ºC, demonstrating a stronger gel state. However, the synergy of both drugs proved cytotoxicity effect increase in breast cancer cell lines MCF-7 and MDA-MB-241 by over 27% and 42% above individual MTX and Cur treatments, respectively.

Luo and Hu [69] also developed a dual-response platform for 5-FU delivery, this time based on pNIAAm-co-IA, modifying its LCST from 32

to 37ºC. The injectable hydrogel presented swelling mechanism dependent on temperature and pH, sustaining releases until 6 days of until 50% (40ºC, pH 5.8), and preventing them at lower temperatures (25% at 37ºC) or higher pH values (20% at pH 7.4). Moreover, TNBC growth cells *in vitro* and *in vivo* were tested, where loaded hydrogel showed more effect than free drug against it. Additionally, non-systemic toxicity was detected in mice.

These formulations proved efficient gelation *in situ* and sustained thermo and pH dual-responsive drug releases, but both stimuli-responses relied on the hydrogel network, making it a simple DDS. Among other limitations, like complex synthesis due to making PNIPAAM hydrogels biocompatible and chitosan thermo-responsive, or gel transition temperatures higher than the physiological one, the main drawback was lacking a proper drug delivery to tumour cells. This was due to hydrogels presenting weak problems of penetration as a consequence of their matrices size. Therefore, despite their dual thermo- and pH-responsive behaviour, these hydrogel matrices still released the encapsulated drug into the extracellular environment without selective intracellular delivery towards tumour cells. In order to overcome this limitation and introduce an additional level of control over drug delivery, previously described DDS can be incorporated within the local hydrogel reservoir. In this context, the hydrogel matrix enables the localized administration of nanocarriers, thereby overcoming the systemic administration drawbacks while promoting sustained intracellular delivery [70].

1.5.2. Nanocarriers to incorporate into hydrogels matrices

As previously stated, tumour targeting is needed for improving protection against toxicity affecting healthy surrounding tissues. For this issue, dual-responsive hydrogels present the promoted pH-responsive drug release from their matrices when subjected to tumour microenvironmental characteristics, but lack an active delivery reaching cancer cells. Additionally, hydrogels also present multi-component synthesis for improved mechanical, physicochemical properties, and

ultimately, their drug delivery function (degradation, drug release sustainability, biocompatibility, etc.)

Regarding this, DDS in localized administration based on nanocarriers present the best option for drug delivery targeting cells and tissues once they are released from the hydrogel matrix, instead of unspecified drug release into the extracellular environment. The principal nanocarriers can be seen in Figure 1.17. and further discussed in Table 1.5. [8].

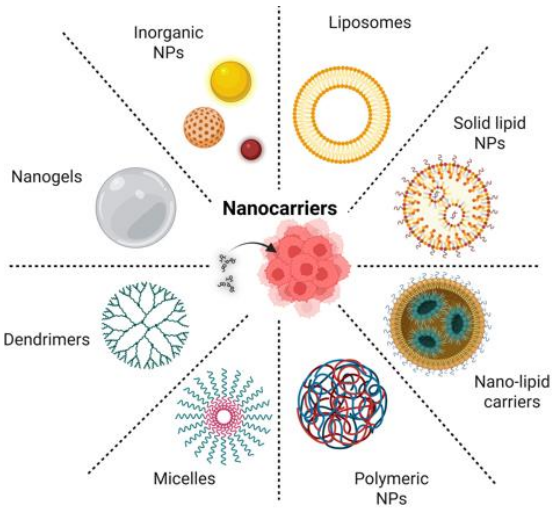

Figure 1.17. Main reported nanocarriers

Table 1.5. Nanocarriers advantages and limitations for breast cancer.

Nanocarrier	Benefits	Limitations
Liposomes	Enhances wide range of drugs encapsulation preventing drug undesired effects, ability for functionalization	Rapid mononuclear phagocytosis and carrier degradation
SLN	Biodegradable and biocompatible protection of drug against degradation, sustained release	Low drug loading capacities and may present other colloidal structures
NLC	Overcomes SLN limitations, better physical stability remaining sustained drug release, and abity for functionalization	Polymorphic transition altering physical properties due to lipid gelation
PNPs	Longer blood circulation times, biocompatible and biodegradable, lower reactivity to enzymatic degradation	Potential polymer degradation or cytotoxicity, complex synthesis

Micelles	Reduced toxicity and other undesired effects	Low drug loading capacity, initial drug burst release, long-term toxicity
Dendrimers	Higher loading capacity for its multifunctional surface groups, high bioavailability	Synthesis variability, organ accumulation, fast clearance
Inorganic carriers	High fluorescence stability for imaging, and enhance tumour penetration	Potential metal toxicity, long-term biocompatibility, oxidative stress and DNA damage

Out of all the common reported nano-sized carriers, only liposomes and SLNPs formulations are efficient enough to be marketed and clinically used as DDS. Liposomes constitute one of the most studied and advanced DDS in oncology. They are defined structurally as phospholipid bilayers, generally stabilized with cholesterol, that surround an inner aqueous core. Their amphiphilic nature enables them to encapsulate drugs of different solubility natures (hydrophilic and hydrophobic), and even genetic material. Their principal benefits include high biocompatibility and tuneable surface capacity. More recently, fusogenic liposomes are studied due to their capacity of merging directly with the cellular membrane and releasing the drug in the cytoplasm [33]. Even some formulations are approved and commercialized, used clinically for some types of cancer [71]. Besides, incorporation into a hydrogel matrix compensate their drawbacks, mainly brought by systemic administration [70]. Additionally, they present an additional control barrier for drug delivery in dual-responsive hydrogel matrices, improving their performance.

1.5.3. Dual-responsive hybrid hydrogels with incorporated nanocarriers

As stated previously, an incorporated nanocarrier within the dual-responsive hydrogel matrix represents an improved version of these platforms towards sustained drug delivery. For instance, microgels can be embedded in greater hydrogel networks, as developed by Singh et al. [72] delaying moxifloxacin (MFX) release from 20h to 70h in dual-response PNIPAM-co-MAA microgels in CS hydrogels. However, pH-responsiveness only prevented 15% of release in a wide range (5.0 against 9.2).

Nonetheless, liposomes have already been presented as preferred nanocarriers improving drug delivery in many formulations for cancer treatment [8]. Since they are the most exploited nanocarrier, some authors have reported their use in dual-responsive T-pH thiolated chitosan (CSSH) hydrogels for different cancer treatments.

Firstly, Li et al. [73] developed a CSSH with Cur loaded liposomes hydrogel for treating breast cancer recurrence in 2020. Hydrogel showed gelation at 37ºC, sustaining Cur release for 3 days at 80-20% depending on loaded concentration. Although no pH-sensitive release tests were performed, cell viability assays showed great mortality of loaded hydrogels in MCF-7 cell line. Moreover, *in vivo* assays confirmed these hydrogels could deliver high concentrations of drug whilst the tissue could also be repaired by them.

Later in 2022, Li et al. [74] used the same formulation to study the co-delivery of Cur loaded liposomes and DOX loaded CSSH hydrogel. Although gelation time for these composites was stablished between 8 and 12 minutes, the hydrogels exhibited sustained pH-responsive drug release for up to 6 days. Separately, Cur showed 30% release at 5.5, whilst 20% at 7.4, whereas DOX showed 60% against 40% for same conditions. In co-loaded hydrogels there was a 40% release of both drugs at 5.5 whilst 20% at 7.4. In MCF-7 cell viability assays the dual loaded hydrogel showed synergy of 20% more than single loaded formulations.

These formulations presented the benefits of a hybrid system, using its hydrogel network as drug reservoir, whilst the incorporated nanocarrier presented improved drug delivery. However, they still lack a more efficient performance, since the stimuli-responses still rely exclusively on the hydrogel matrix, rather than the nanocarrier. As it has been described, making a hydrogel network dual-responsive causes its thermo-sensitivity to be dependent on the pH-responsiveness, and viceversa, showing higher transition temperatures than the physiological one or low pH-responsive releases.

Accordingly, since dual-responsive hydrogels incorporating non-responsive nanocarriers have already showed promising results, the

development of a pH-responsive nanocarrier embedded within a thermo-sensitive injectable hydrogel emerges as a highly suitable dual-response strategy for the intended application. A brief scheme of these release mechanisms can be seen in Figure 1.18.

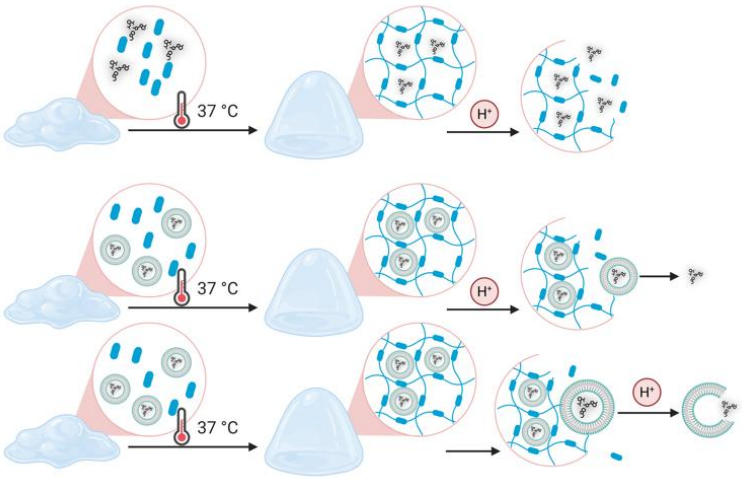

Figure 1.18. Release pH-response mechanisms for loaded T-sensitive hydrogels. Top tier describes the basic hydrogel matrices [64-69], middle tier includes the NC formulation [72-74], and low tier incorporates the pH-response into the NC directly, which is the optimized mechanism [75].

Therefore, specific pH-responsive nanocarriers must be studied. Specifically, liposomes which are the most exploited ones and also have been described in hydrogel formulations can easily be tuned into pH-sensitive nanocarriers. Moreover, among other pH-responsive nanocarriers, novel alternatives have earned increasing interest in the last years due to their versatility and stimuli-response, such as coacervates.

1.5.3.1. pH-responsive liposomes

pH-sensitive liposomes stand out among the rest of NCs due to their versatility, and their action mechanism combining structural changes, molecular interactions and membrane dynamics for acidic environments response. Besides, their surface can be easily and widely functionalized [71]. All of these options are illustrated in Figure 1.19.

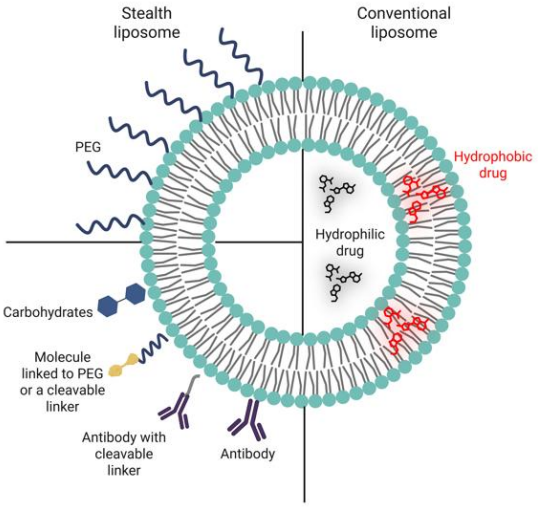

Figure 1.19. Liposome structure and functionalizations

pH-responsive liposomes are usually based on neutral lipids (phosphatidylamine derivative, DOPE) and weakly amphiphiles like CHEMS. Under physiological conditions, DOPE adopts an inverted hexagonal (HII) configuration, which is non-stable, needing the CHEMS as stabilizer. Once the pH is acidified, the carboxyl group of CHEMS is protonated, inducing a structural transition that promotes drug release [76, 77].

Concerning breast cancer therapies, many studies collect the current advances. Zhai et al. [77] developed pH-responsive liposomes encapsulating DOX with the acid-sensitive peptive DVar7, developing a release 5 times faster at pH 5.3 compared to 7.4. This formulation was also efficient when tested on cervical carcinoma and breast cancer cell lines, as well as mice with inoculated breast carcinoma. Additionally, Zarrabi et al. [78] attached citraconic anhydride (CA) to DSPE/PEG liposomes loaded with curcumin. Sustained releases showed initial burst at pH 6.6 due to disruptiveness of pH-sensitive bond and disassembly of CA-PEG layer.

1.5.3.2. pH-responsive coacervates

Coacervates are not mentioned as conventional nanocarriers since they do not strictly fall under any category. The most similar definition

would be polymeric nanoparticles (partially), since they can be nanospheres or capsules, and be formed by controlled assembly.

Coacervates are indeed a very wide concept including multiple compounds and structures which have lately emerged as versatile platforms for biomolecules encapsulation and transport. They are based on the liquid-liquid separation phases (LLSP) phenomenon, where a homogeneous molecule solution is splitted spontaneously in a diluted and a concentrated (coacervated) phase [79].

LLSP phenomenon may partake in different structure ensembles like liquid microdrops, films, or even reaching 3D hydrogel networks when physical or chemical crosslinking is involved among coacervates. Moreover, the range of compounds able to form coacervates is representatively wide: Proteins, polysaccharides, synthetic polyelectrolytes, NPs, or small therapeutic molecules can be found in these carriers. Their stabilization is reached overall by electrostatic interactions, or hydrogen bonds, often influenced by external conditions like pH, temperature or ionic strength, depending on the physicochemical properties of the compounds involved [79]. Figure 1.20. schemes the process via electrostatic interactions.

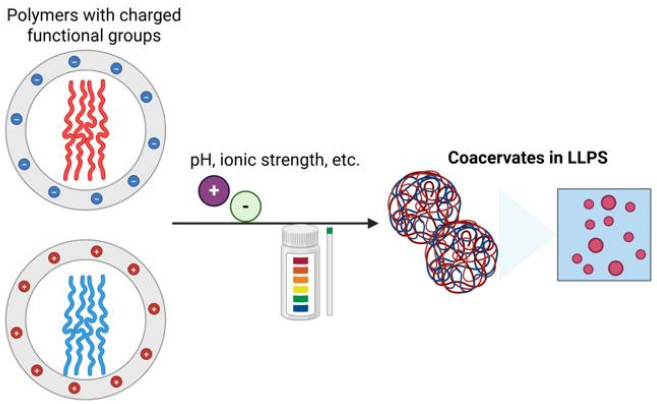

Figure 1.20. Coacervates formation via electrostatic interaction

These characteristics have placed coacervate systems in applications such as tissue engineering, gene therapy, regenerative medicine, and drug delivery. The presence of ionisable groups and

electrostatic interactions handling their stability positions them as strong potential pH-responsive delivery system [79]. Regarding breast cancer applications, Chen et al. [80] developed a pH-responsive coacervate system based of poly-L-lysine and poly-aspartic acid in 1:1 ratio loaded with propranolol showing more release under acidic media due to its promoted instability. This system also improved bioavailability, showed biocompatibility in 4T1 cell lines and in *in vivo* TNBC model, inhibiting metastasis and tumour growth.

Coacervates have also been incorporated in hydrogels for cancer therapies. Lee et al. [81] formed an injectable hydrogel from triblock copolymers PEG-polycarbonate with PBA and cationic copolymers, with micelles embedded loaded with bortezomib (BTZ) linked via pH-sensitive boronate bond. This bond cleavage under acidic conditions (pH 4.5-6.0) triggered drug release to 85%, compared to 7% at 7.4. In the xenograft model of multiple myeloma (MM.1S) the system could successfully delay the tumour growth, whilst free micelles did not reach this result.

To recapitulate, DDS can be designed in order to obtain a pH-response for tumour targeting. However, when this nanocarrier is incorporated in the previously described hydrogel matrix, both strategies (thermo and pH-sensitivity) are combined in the same dual-response optimized system.

1.5.4. Optimal dual-response approach

Regarding this optimal mechanism, only Chen et al. [75] reported the formulation of a pH-sensitive liposomal system targeting acidic vaginal conditions, based on cleavable mPEG-Hz-CHEMS, incorporated into an injectable hydrogel (P407 and P188) for vaginal deliveries. The formulation presented great pH-response of arctigenin (AC) release due to pH-sensitive liposomes, accumulating 65% for pH 5.0 whilst only 5% at pH 7.4 during 2 days. Although injectability and gelation of the system was not deeply studied or optimized, the sustained release and biocompatibility positioned this formulation as a promising platform for vaginal deliveries.

Therefore, it was proven that this last described approach presents significant benefits over the rest of reported dual-response systems. Concluding, the proposed strategy for breast cancer treatment will be: Synthesis of a dual-sensitive drug delivery system based on a thermo-sensitive injectable hydrogel incorporating pH-responsive nanocarriers targeting acidic tumour microenvironment. This way, the developed strategy would present improvements over the limitations in previous reported formulations, summarized in Table 1.6.

Table 1.6. T and pH-dual responsive platforms

System (hydrogel) formulation	Drug	Mechanism	*In vitro/ In vivo*	Limitation of mechanism	Ref
CS-g-(mPEG-b-PCL)	DOX Cur	Hydrogel degradation	None	Only hydrogel matrix as release barrier for sustained delivery	64
mPEG/EEP-TAs	DOX	Conformational structure shift	NIH 3T3 Mice		65
PNIAAm-co-IA/CS/β-GP	DOX	Swelling/deswelling	MCF-7		66
PNIPAM-co-GMA-Mela	5-FU Ibu	Structure collapse and protonation	MDA-MB-231		67
PNIPAAm-co-MA/CS/β-GP	MTX Cur	Swelling/deswelling	MCF-7 MDA-MB-241		68
PNIPAM-co-IA/CS/β-GP	5-FU	Swelling/deswelling	TNBC *(in vitro* and *in vivo*)		69
PNIPAM-co-MAA MG/ CS HG	MFX	Diffusive double barrier	HeLa HEK-293	Both thermo and pH-response depend only on hydrogel	72
CSSH/Lip	Cur	Hydrogel degradation Liposomal release	MCF-7 Mice		73
CSSH/Lip	DOX Cur		MCF-7		74
(*)mPEG-Hz-CHEMS	AC	Cleavage and liposomes pH response	HEK 293	Not oriented towards breast cancer	75

(*) Not intended for breast cancer therapies.

1.6. Conclusions

As it has been described, the actual status of post-surgery breast cancer therapies to eradicate recurrences is currently one of the most

relevant oncologic challenges. Recent status in the approval of formulations, and the latest studies reported in literature, demonstrate there is still room for improvement regarding systemic toxicity and low therapeutic efficiency. Thus, taking into account the current limitations of the therapeutic landscape, a novel platform is proposed: The synthesis of a local administration therapy able to fill in the cavity after tumour resection acting as drug reservoir. The best fit for these characteristics are macroscopic hydrogels, which can be designed for injectability, presenting thermo-response to enable *in situ* gelling at physiological conditions, after the administration.

However, drug delivery is still not selectively targeting cancer cells in the implantation site. Therefore, an additional design for targeting tumour cells is essential. For instance, targeting acidic tumour microenvironment implies a reproducible and reliable strategy despite its heterogeneity, described by the hallmarks of cancer. Specifically, a pH-response strategy targeting acidic extracellular environment or intracellular acidic compartments due to Warburg effect is proposed, forming a dual-response hydrogel system. In this context, a dual-response hydrogel matrix does not provide the best results since the drug cannot be properly delivered in tumour cells due to hydrogel weak penetration drawback. Therefore, the incorporation of a pH-responsive nanocarrier, such as coacervates or liposomes, in the thermo-sensitive hydrogel matrix confirms an optimal pH/T dual-responsive drug delivery system adequate for the intended post-surgical breast cancer recurrence prevention therapy.

1.7. References

[1] National Cancer Institute. What is cancer? Bethesda(MD):National Cancer Institute;2007. [Last accessed on April 6th 2026. Available in: https://www.cancer.gov/about-cancer/understanding/what-is-cancer]

[2] International Agency for Research on Cancer. Global Cancer Observatory: All cancers fact sheet. Lyon:IARC;2024.

[3] Hanahan D, Weinberg RA. The hallmarks of cancer. Cell. 2000;100:57-70.

[4] Hanahan D, Weinberg RA. Hallmarks of cancer: The next generation. Cell. 2011;144:646-674.

[5] DeVita VT, Chu E. A History of Cancer Chemotherapy. Cancer Res.2008;68:8643-53.

[6] Chabner BA, Roberts TG. Chemotherapy and the war on cancer. Nat Rev Cancer. 2005;5:65-72.

[7] Salmon SE. Kinetic rationale for adjuvant chemotherapy for cancer. In: Salmon SE, Jones SE, editors. Adjuvant therapy of cancer. Amsterdam: Elsevier/North Holland Biomedical Press; 1977.

[8] Cho K, Wang X, Nie S, Chen Z (Georgia), Shin DM. Therapeutic Nanoparticles for Drug Delivery in Cancer. Clin Cancer Res. 2008;14:1310-6.

[9] International Agency for Research on Cancer. Global Cancer Observatory: Breast cancer fact sheet. Lyon:IARC;2024.

[10] Trayes KP, Cokenakes SEH. Breast cancer treatment. Am Fam Physician. 2021;104:171-178.

[11] Jallah JK, Dweh TJ, Anjankar A, Palma O. A Review of the Advancements in Targeted Therapies for Breast Cancer. Cureus. 2023:47847.

[12] Simsek BI, Halici H, Cadirci E. Molecularly targeted therapies in breast cancer:A traditional review. FABAD J Pharm Sci. 2024;49:435-448.

[13] Jordan VC. Tamoxifen (ICI46,474) as a targeted therapy to treat and prevent breast cancer. Br J Pharmacol. 2006;147.

[14] Jiang H, Rugo HS. Human epidermal growth factor receptor 2 positive (HER2+) metastatic breast cancer: how the latest results are improving therapeutic options. Ther Adv Med Oncol. 2015;7:321-39.

[15] O'Sullivan CC, Loprinzi CL, Haddad TC. Updates in the Evaluation and Management of Breast Cancer. Mayo Clin Proc. 2018;93:794-807.

[16] Moo TA, Sanford R, Dang C, Morrow M. Overview of Breast Cancer Therapy. PET Clin. julio de 2018;13:339-54.

[17] Fisher B, Deutsch M. Twenty-Year Follow-up of a Randomized Trial Comparing Total Mastectomy, Lumpectomy, and Lumpectomy plus Irradiation for the Treatment of Invasive Breast Cancer. N Engl J Med. 2002;347:1233-1242.

[18] Veronesi U, Cascinelli N, Mariani L, Greco M, Saccozzi R, Luini A, et al. Twenty-Year Follow-up of a Randomized Study Comparing Breast-Conserving Surgery with Radical Mastectomy for Early Breast Cancer. N Engl J Med. 2002;347:1227-32.

[19] Poggi MM, Danforth DN, Sciuto LC, Smith SL, Steinberg SM, Liewehr DJ, et al. Eighteen-year results in the treatment of early breast carcinoma with mastectomy versus breast conservation therapy: The National Cancer Institute randomized trial. Cancer. 2003;98(4):697-702.

[20] Voogd AC, Nielsen M, Peterse JL, Blichert-Toft M, Bartelink H, Overgaard M, et al. Differences in risk factors for local and distant recurrence after breast-conserving therapy or mastectomy for stage I and II breast cancer: Pooled results of two large European randomized trials. J Clin Oncol. 2001;19:1688–1697.

[21] Holland R, Veling SHJ, Mravunac M, Hendriks JHCL. Histologic multifocality of tis, T1–2 breast carcinomas implications for clinical trials of breast-conserving surgery. Cancer. 1985;56:979-90.

[22] Effect of radiotherapy after breast-conserving surgery on 10-year recurrence and 15-year breast cancer death: meta-analysis of individual patient data for 10 801 women in 17 randomised trials. The Lancet. 2011;378:1707-16.

[23] Marino N, Woditschka S, Reed LT, Nakayama J, Mayer M, Wetzel M, et al. Breast Cancer Metastasis. Am J Pathol. 2013;183:1084-95.

[24] Moody SE, Sarkisian CJ, Hahn KT, Gunther EJ, Pickup S, Dugan KD, et al. Conditional activation of Neu in the mammary epithelium of transgenic mice results in reversible pulmonary metastasis. Cancer Cell. 2002;2:451-61.

[25] Belkacemi Y, Hanna NE, Besnard C, Majdoul S, Gligorov J. Local and Regional Breast Cancer Recurrences: Salvage Therapy Options in the New Era of Molecular Subtypes. Front Oncol. 2018;8:112.

[26] Voduc KD, Cheang MC, Tyldesley S, Gelmon K, Nielsen TO, Kennecke H. Breast cancer subtypes and the risk of local and regional relapse. J Clin Oncol. 2010;28:1684–1691.

[27] Gradishar WJ, Anderson BO, Balassanian R, Blair SL, Burstein HJ, Cyr A, et al. Invasive Breast Cancer Version 1.2016, NCCN Clinical Practice Guidelines in Oncology. J Natl Compr Canc Netw. 2016;14:324-54.

[28] Wahl AO, Rademaker A, Kiel KD, Jones EL, Marks LB, Croog V, et al. Multi-Institutional Review of Repeat Irradiation of Chest Wall and Breast for Recurrent Breast Cancer. Int J Radiat Oncol. 2008;70:477-84.

[29] Cheng Y-H, He C, Riviere JE, Monteiro-Riviere NA, Lin Z. Meta-analysis of nanoparticle delivery to tumours using a physiologically based pharmacokinetic modelling and simulation approach. ACS Nano. 2020;14:3075-3095.

[30] Danhier F, Feron O, Préat V. To exploit the tumor microenvironment: Passive and active tumor targeting of nanocarriers for anti-cancer drug delivery. J Controlled Release. 2010;148:135-46.

[31] Norouzi M, Nazari B, Miller DW. Injectable hydrogel-based drug delivery systems for local cancer therapy. Drug Discov Today. 2016;21:1835-49.

[32] Yan Y, Chen Y, Huang L, Cai M, Yin X, Zhu YZ, et al. Bioengineered *In Situ*-Forming Hydrogels as Smart Drug Delivery Systems for Postoperative Breast Cancer Immunotherapy: From Material Innovation to Clinical Translation. J Funct Biomater. 2025;16:381.

[33] Samad MA, Ahmad I, Zughaibi TA, Suhail M, Zaidi SK, Al-Abbasi FA, et al. Nanotechnology-based drug delivery for breast cancer treatment: Current applications and future directions. Eur J Med Chem Rep. 2025;14:100268.

[34] Wolinsky JB, Colson YL, Grinstaff MW. Local drug delivery strategies for cancer treatment: Gels, nanoparticles, polymeric films, rods and wafers. J Control Release. 2012;159:14-26.

[35] Li J, Mooney DJ. Designing hydrogels for controlled drug delivery. Nat Rev Mater. 2016;1:16071.

[36] Mi D, Li J, Wang R, Li Y, Zou L, Sun C, et al. Postsurgical wound management and prevention of triple-negative breast cancer recurrence with a pryoptosis-inducing, photopolymerizable hydrogel. J Controlled Release. 2023;356:205-18.

[37] Gao X, Caruso BR, Li W. Advanced Hydrogels in Breast Cancer Therapy. Gels. 2024;10:479.

[38] Balahura LR, Dinescu S, Balaș M, Cernencu A, Lungu A, Vlăsceanu GM, et al. Cellulose Nanofiber-Based Hydrogels Embedding 5-FU Promote Pyroptosis Activation in Breast Cancer Cells and Support Human Adipose-Derived Stem Cell Proliferation, Opening New Perspectives for Breast Tissue Engineering. Pharmaceutics. 2021;13:1189.

[39] DuVall GA, Tarabar D, Seidel RH, Elstad NL, Fowers KD. Phase 2: A dose-escalation study of OncoGel (ReGel/paclitaxel), a controlled-release formulation of paclitaxel, as adjunctive local therapy to external-beam radiation in patients with inoperable esophageal cancer. Anti-Cancer Drugs. 2009;20:89–95.

[40] Kang G, Cheon S, Song S. Controlled release of doxorubicin from thermosensitive poly(organophosphazene) hydrogels. Int J Pharm. 2006;319:29-36.

[41] Chun C, Lee SM, Kim CW, Hong KY, Kim SY, Yang HK, et al. Doxorubicin–polyphosphazene conjugate hydrogels for locally controlled delivery of cancer therapeutics. Biomaterials. 2009;30:4752-62.

[42] Abdel-Bar HM, Abdel-Reheem AY, Osman R, Awad GAS, Mortada N. Defining cisplatin incorporation properties in thermosensitive injectable biodegradable hydrogel for sustained delivery and enhanced cytotoxicity. Int J Pharm. 2014;477:623-30.

[43] Cho J,Hong K-Y, Park JW, Yang H-K, Son S-C. Injectable delivery system of 2-methoxyestradiol for breast cancer therapy using biodegradable thermosensitive poly (organophosphazene) hydrogel. J Drug Target. 2011;19:270–280.

[44] Wang W, Song H, Zhang J, Li P, Li C, Wang C, et al. An injectable, thermosensitive and multicompartment hydrogel for simultaneous encapsulation and independent release of a drug cocktail as an effective combination therapy platform. J Controlled Release. 2015;203:57-66.

[45] Lei N, Gong CY, Qian ZY, Luo F, Wang C, Wang HL et al. Therapeutic application of injectable thermosensitive hydrogel in preventing local breast cancer recurrence and improving incision wound healing in a mouse model. Nanoscale. 2012;4:5686–5693.

[46] Lin Z, Gao W, Hu H, Ma K, He B, Dai W, et al. Novel thermo-sensitive hydrogel system with paclitaxel nanocrystals: High drug-loading, sustained drug release and extended local retention guaranteeing better efficacy and lower toxicity. J Controlled Release. 2014;174:161-70.

[47] Chen YY, Wu HC, Sun JS, Dong GC, Wang TW. Injectable and Thermoresponsive Self-Assembled Nanocomposite Hydrogel for Long-Term Anticancer Drug Delivery. Langmuir. 2013;29:3721-9.

[48] Guo DD, Hong SH, Jiang HL, Kim JH, Minai-Tehrani A, Kim JE, et al. Synergistic effects of Akt1 shRNA and paclitaxel-incorporated conjugated linoleic acid-coupled poloxamer thermosensitive hydrogel on breast cancer. Biomaterials. 2012;33:2272-81.

[49] Qu Y, Chu BY, Peng JR, Liao JF, Qi TT, Shi K, et al. A biodegradable thermo-responsive hybrid hydrogel: therapeutic applications in preventing the post-operative recurrence of breast cancer. NPG Asia Mater. 2015;7:e207-e207.

[50] Shaker DS, Shaker MA, Klingner A, Hanafy MS. *In situ* thermosensitive Tamoxifen citrate loaded hydrogels: An effective tool in breast cancer loco-regional therapy. J Drug Deliv Sci Technol. 2016;35:155-64.

[51] Zhai L, Li L, Liao T, Zhu Y, Li C, Xu Z, et al. In-situ injectable hydrogel for near-infrared-regulated hyperthermic perfusion therapy of triple-negative breast cancer. J Colloid Interface Sci. 2025;690:137228.

[52] Chen X, Wang M, Yang X, Wang Y, Yu L, Sun J, et al. Injectable hydrogels for the sustained delivery of a HER2-targeted antibody for preventing local relapse of HER2+ breast cancer after breast-conserving surgery. Theranostics. 2019;9:6080-98.

[53] Fong Y, Chen CH, Chen JP. Intratumoral Delivery of Doxorubicin on Folate-Conjugated Graphene Oxide by In-Situ Forming Thermo-Sensitive Hydrogel for Breast Cancer Therapy. Nanomaterials. 2017;7:388.

[54] Abdellatif AAH, Mohammed AM, Saleem I, Alsharidah M, Al Rugaie O, Ahmed F, et al. Smart Injectable Chitosan Hydrogels Loaded with 5-Fluorouracil for the Treatment of Breast Cancer. Pharmaceutics. 2022;14:661.

[55] Zhao D, Hu C, Fu Q, Lv H. Combined chemotherapy for triple negative breast cancer treatment by paclitaxel and niclosamide nanocrystals loaded thermosensitive hydrogel. Eur J Pharm Sci. 2021;167:105992.

[56] Bagheri E, Ramezani M, Mohammadi M, Alibolandi M. Injectable Hydrogels for Intratumoral Administration Against Breast Cancer. J Polym Environ. 2024;32:5468-98.

[57] Clegg JR, Adebowale K, Zhao Z, Mitragotri S. Hydrogels in the clinic: An update. Bioeng Transl Med. 2024;9:e10680.

[58] Qiao Y, Wan J, Zhou L, Ma W, Yang Y, Luo W, et al. Stimuli-responsive nanotherapeutics for precision drug delivery and cancer therapy. WIREs Nanomedicine Nanobiotechnology. 2019;11:e1527.

[59] AlSawaftah NM, Awad NS, Pitt WG, Husseini GA. pH-Responsive Nanocarriers in Cancer Therapy. Polymers. 26 de febrero de 2022;14(5):936. doi:10.3390/polym14050936

[60] Kanamala M, Wilson WR, Yang M, Palmer BD, Wu Z. Mechanisms and biomaterials in pH-responsive tumour targeted drug delivery: A review. Biomaterials. 2016;85:152-67.

[61] Liu J, Huang Y, Kumar A, Tan A, Jin S, Mozhi A, et al. pH-Sensitive nano-systems for drug delivery in cancer therapy. Biotechnol Adv. 2014;32:693-710.

[62] Shi J, Guobao W, Chen H, Zhong W, Qiu X, Xing M. Schiff based injectable hydrogel for *in situ* pH-triggered delivery of doxorubicin for breast tumor treatment. Polym Chem. 2014;5:6180–6189

[63] Zuo H, Jiao Y, Chen J, Tong S, Li Y, Zhao W. Recent Advances in Smart Stimulus-Responsive Hydrogels for Precision Drug Delivery in Tumours. Gels. 2026;12:98.

[64] Jommanee N, Chanthad C, Manokruang K. Preparation of injectable hydrogels from temperature and pH responsive grafted chitosan with tuned gelation temperature suitable for tumor acidic environment. Carbohydr Polym. 2018;198:486-94.

[65] Lin Z, Ding J, Chen X, He C. pH- and Temperature-responsive Hydrogels Based on Tertiary Amine-modified Polypeptides for Stimuli-responsive Drug Delivery. Chem – Asian J. 2023;18:e202300021.

[66] Fathi M, Alami-Milani M, Geranmayeh MH, Barar J, Erfan-Niya H, Omidi Y. Dual thermo-and pH-sensitive injectable hydrogels of chitosan/(poly(N-

isopropylacrylamide-co-itaconic acid)) for doxorubicin delivery in breast cancer. Int J Biol Macromol. 2019;128:957-64.

[67] Mohan A, Santhamoorthy M, Phan TTV, Kim SC. pNIPAm-Based pH and Thermoresponsive Copolymer Hydrogel for Hydrophobic and Hydrophilic Drug Delivery. Gels. 2024;10:184.

[68] Ahmadi S, Olad A, Fathi M, Molavi O. An injectable chitosan based dual thermo/pH-responsive fast gelling hydrogel loaded by methotrexate/curcumin as local drug delivery system of breast cancer. J Drug Deliv Sci Technol. 2025;104:106540.

[69] Luo K, Hu W. A dual thermo/pH-sensitive hydrogel as 5-Fluorouracil carrier for breast cancer treatment. Anticancer Drugs. 2025;36:220-31.

[70] Mou Y, Zhang P,Lai W-F, Zhang D. Design and applications of liposome-in-gel as carriers for cancer therapy. Drug Deliv. 2022;29:3245-3255.

[71] Allen TM, Cullis PR. Liposomal drug delivery systems: From concept to clinical applications. Adv Drug Deliv Rev. 2013;65:36-48.

[72] Singh N, Aery S, Juneja S, Kumari L, Lone MS, Dar AA, et al. Chitosan Hydrogels with Embedded Thermo- and pH-Responsive Microgels as a Potential Carrier for Controlled Release of Drugs. ACS Appl Bio Mater. 2022;5:3487-99.

[73] Li R, Lin Z, Zhang Q, Zhang Y, Liu Y, Lyu Y, et al. Injectable and *In Situ* -Formable Thiolated Chitosan-Coated Liposomal Hydrogels as Curcumin Carriers for Prevention of *In Vivo* Breast Cancer Recurrence. ACS Appl Mater Interfaces. 2020;12:17936-48.

[74] Li N, Lin J, Liu C, Zhang Q, Li R, Wang C, et al. Temperature- and pH-responsive injectable chitosan hydrogels loaded with doxorubicin and curcumin as long-lasting release platforms for the treatment of solid tumors. Front Bioeng Biotechnol. 2022;10:1043939.

[75] Chen D. pH and temperature dual-sensitive liposome gel based on novel cleavable mPEG-Hz-CHEMS polymeric vaginal delivery system. Int J Nanomedicine. 2012;2621.

[76] Hafez IM, Ansell S, Cullis PR. Tunable pH-Sensitive Liposomes Composed of Mixtures of Cationic and Anionic Lipids. Biophys J. 2000;79:1438-46.

[77] Zhai L, Luo C, Gao H, Du S, Shi J, Wang F. A Dual pH-Responsive DOX-Encapsulated Liposome Combined with Glucose Administration Enhanced Therapeutic Efficacy of Chemotherapy for Cancer. Int J Nanomedicine. 2021;16:3185-99.

[78] Zarrabi A, Zarepour A, Khosravi A, Alimohammadi Z, Thakur VK. Synthesis of Curcumin Loaded Smart pH-Responsive Stealth Liposome as a Novel Nanocarrier for Cancer Treatment. Fibers. 2021;9:19.

[79] Souri M, Yim W, Halder M, Jin Z, Jokerst JV. Coacervate-Based Delivery Systems: Bridging Fundamentals and Applications. ACS Appl Mater Interfaces. 2025;17:41513-53.

[80] Chen J, Mei C, Tan Y, Yang F, Yang S, Wen X, et al. pH-responsive coacervate with adrenergic nerve blockade function inhibits triple-negative breast cancer metastasis by blocking nerve-tumor-immune loop. Chem Eng J. 2024;494:152997.

[81] Lee ALZ, Voo ZX, Chin W, Ono RJ, Yang C, Gao S, et al. Injectable Coacervate Hydrogel for Delivery of Anticancer Drug-Loaded Nanoparticles *in vivo*. ACS Appl Mater Interfaces. 2018;10:13274-82.

1.8. List of abbreviations

17-AAG — 17-Allylamino-17-Demethoxygeldanamycin
2-ME — 2-Methoxyestradiol
4T — Tumour Line 4
5-FU — 5-Fluorouracyl
6-MP — 6-Mercaptopurine
ALND — Axillary Lymph Node Disection
alt — Alternating
AC— Arctigenin
AuNRs — Gold Nanorods
b — Block
BCT — Breast Conserving Therapy
BTZ — Bortezomib
BxPC — Pancreatic Carcinoma Cell Line
CA — Citraconic Anhydride
CEC — N-Carboxyethyl Chitosan
CHEMS — Cholesterol Hemysuccinate
CINPs — Cuttlefish Ink Nanoparticles
Cis — Cisplatin
CLA — Conjugated Linoleic Acid
CNF — Cellulose Nanofiber
co — Copolymer
CS — Chitosan
CSSH—Thiolated Chitosan
Cur— Curcumine
DDS — Drug Delivery System
DEA — Diethylamine
DHFR — Dihydrofolate Reductase
DMO — Drug-loaded Mesoporous Organosilica
DNA — Deoxyribonucleic Acid
DOPE — 1,2-Dioleoyl-sn-Glycero-3-Phosphoethanolamine
DOX — Doxorubicin
DSPE —1,2-Distearoyl-sn-Glycero-3-phosphoethanolamine
EEP — mPEG-b-P(ELG-co-PLG)

EMA — European Medical Association
EPR — Enhanced Permeability and Retention
ER — Estrogen receptor
FDA — Food and Drug Association
g — Graft
GCO — Global Cancer Observatory
GMA — Glycidyl Methacrylate
GOFA — Graphene Oxide Folic Acid
GSH —Glutathione
GTE — Green Teat Extract
HA — Hyaluronic Acid
HDI — Hexamethylene Diisocyanate
HEK — Human Embryonic Kidney Cell Line
HeLa — Henrietta Lacks
HepG2 — Human Hepatocellular Carcinoma Cell Line
HER2 — Human Epidermal Growth Factor Receptor 2
HG — Hydrogel
HII — Inverted Hexagonal
HL-60 — Human Laukemia Cell Line
HR — Hormonal receptor
Hz — Hydrazone
IA — Itaconic Acid
Ibu — Ibuprofen
IC_{50} — Inhibitory Concentration 50
IR — Infrared
LCST — Lower Critical Solution Temperature
Lip— Liposome
LLSP — Liquid-Liquid Separation Phase
MA — Maleic Anhydride
MAA — Methacrylic Acid
MCF — Michigan Cancer Foundation Breast Cancer Cell Line
MDA-MB — MD Anderson Mammary Breass Cancer Cell Line
Mela — Melamine
MFX — Moxifloxacin
MG — Microgel
MM — Multiple Myeloma Cell Line
MP — Methylpiperazine
mPEG — Methoxy-Poly(Ethylene Glycol)
MTT— 3-(4,5-dimethylthiazol-2-yl)-2,5-diphenyltetrazolium Bromide
MTX — Methrotrexate
NCs — Nanocarriers
NCR — Nanocrystals
NIH — National Institute of Health
NIPAAm — N-Isopropylacrylamide
NLCs — Nanolipid Carriers
NPs —Nanoparticles
ODPDC — OXCS/DOX/PTX/DMO-PTX-FA/CEC
OXCS — Oxidized Chrondroitin Sulfate

P — Poloxamer / Pluronic
PBA — Phenylboronic Acid
PCL — Poly(ε-Caprolactone)
PCNA — PECA/COS-GMA/NIPAm/AAm
PECE — PEG-PCL-PEG
PEG — Poly(Ethylene Glycol)
PEI —Poly(Ethylenimine)
PEOz — Poly(2-Ethyl-2-Oxazoline)
PF — Pluronic in Flakes
PGA —Poly(L-Glutamic Acid)
PGMA — Poly(Glycidyl Methacrylate)
PLA —Poly(Lactic Acid)
PLGA — Poly(Lactic-co-Glycolic Acid)
PMRT — Post-mastectomy Radiation Therapy
PNIPAM — Poly(N-Isopropylacrylamide)
PNPs — Polymeric Nanoparticles
PPZ — Poly(organe-phosphazene)
PR — Progesterone receptor
PTX — Paclitaxel
ROS — Reactive Oxygen Species
shRNA — Short Hairpin Ribonucleic Acid
SKBR — Sloan-Kettering Breast Cancer Cell Line
SLNB — Sentinel Lymph Node Biopsy
SLNPs — Solid Lipid Nanoparticles
TAs — Tertiary Amines
Tmab — Trastuzumab
TMC — Tamoxifen Citrate
TNBC — Triple Negative Breast Cancer
WHO — World Health Organization
XRT — External Beam Radiation Therapy
β-GP — β-Glycerophosphate

2. Thesis Objectives

Breast cancer represents the second most incidental and fourth deadliest cancer type, affecting overall women worldwide. Despite current advances in its treatment, the therapeutic landscape lacks better strategies in post-surgical therapies in order to eradicate residual cancer cells after tumour resection, preventing recurrences. Regarding this, the current approach, breast irradiation, presents off-target toxicity, whilst alternative therapies based on drug delivery systems present systemic administration, which implies low therapeutic efficiency and systemic toxicity. In this context, local administration of novel therapies has emerged as a promising solution to major drawbacks of systemic administration, providing a more efficient recovery with a better quality of life.

Therefore, the main objective of this doctoral thesis is the development of a dual-responsive drug delivery system based on a thermo-sensitive injectable hydrogel matrix incorporating a pH-responsive drug delivery system. This hybrid system combines the benefits of two features that can be exploited during this treatment: Physiological temperature, enabling local administration whilst forming a resistant drug reservoir filling the cavity left after the tumour resection, and acidic pH microenvironment, enabling tumour targeting and selective drug delivery in cancer cells, preventing the exposure in healthy surrounding tissues. Thus, this system simultaneously achieves high drug concentrations accumulated directly at tumour site, evading systemic toxicity, and targeting delivery to cancer cells, increasing its therapeutic efficiency.

To achieve this goal, two different pH-responsive nanocarriers, namely alginate-gelatin coacervates, and liposomal formulations will be developed and evaluated for future incorporation into a hydrogel network. Their evaluation will determine their efficiency as strategy in terms of stability, drug encapsulation, release kinetics, dual-responsiveness, and biocompatibility.

The coacervate system will be optimized by studying the influence of formulation and process variables on their physicochemical, rheological properties, and stability. In parallel, conventional liposomal formulations

will be developed for 5-FU encapsulation and controlled release. Moreover, electrostatic coating with a pH-responsive polymer (Eudragit®) will be investigated as an improved strategy to achieve pH-sensitive behaviour and tumour targeting capacity. Furthermore, different Eudragit® coatings will be used to develop a liposomal versatile platform for extended pH-responsive behaviours and applications.

Another important objective of this thesis is the development of a thermo-sensitive hydrogel network based on PF-127 for injectable administration and local drug retention. The gelation mechanism will be optimized and characterized by rheological analyses, and hydrogels drug release performance will be evaluated in accordance with implemented polysaccharides into the polymer matrix.

Finally, the selected pH-sensitive liposomal system will be incorporated into the thermo-sensitive hydrogel, forming the proposed dual-responsive platform capable of responding to both stimuli, as illustrated in Figure 2.1.

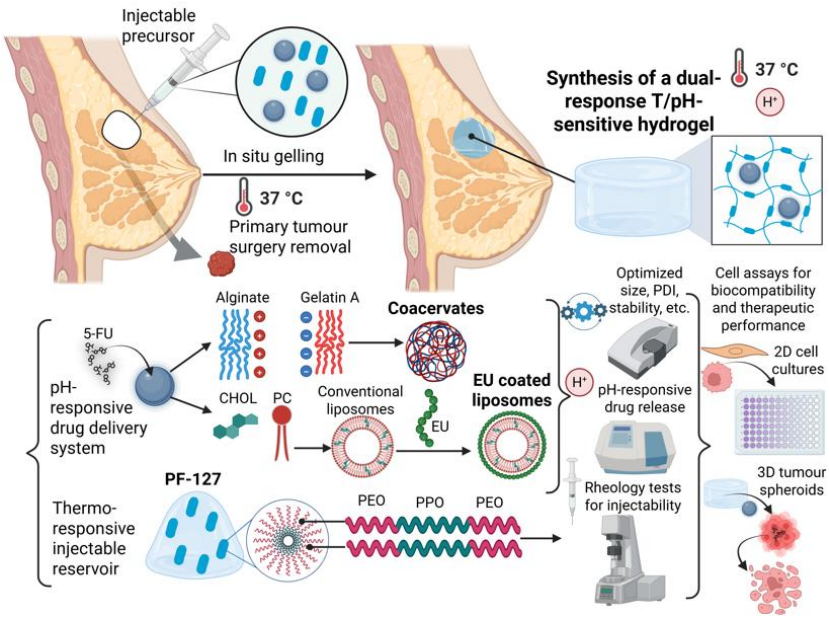

Figure 2.1. Thesis objective summarized: The synthesis of a dual-responsive drug delivery system based on a thermo-sensitive injectable PF-127 hydrogel matrix with incorporated pH-responsive carrier for breast cancer post-surgical therapy preventing local recurrences. The doctoral thesis will be focused on the synthesis, optimization, characterization, functionalization and biological validation of the proposed novel strategy.

The final systems will be characterized and biologically validated in breast cancer and healthy fibroblasts cell lines to evaluate their biocompatibility and therapeutic potential. Furthermore, the dual-response system will also be tested on breast tumour spheroids to better predict its behaviour under *in vivo* conditions.

Overall, this thesis aims to provide a comprehensive strategy for the development of localized drug delivery systems combining smart pH-responsive nanocarriers and injectable synthetic thermo-responsive copolymers for safer and more effective post-surgical breast cancer treatment.

3. Materials and methods

3.1. Introduction

The purpose of this chapter is to describe comprehensively the materials and experimental methodologies that have been used during the development of the thesis objectives. Therefore, the procedures for synthesis, functionalization, and characterization of the developed dual-response drug delivery system have been collected and detailed, including pH-responsive nanocarriers, thermo-sensitive hydrogel matrix and the hybrid formulations intended for the sustained and localized drug release in post-surgical breast cancer treatment.

Firstly, the different reagents used for the material synthesis and characterizations will be presented. Following this section, the experimental methodologies developed for the synthesized and optimized stimuli-responsive platforms, like alginate-gelatin coacervates, Eudragit® coated liposomes, and PF-127 hydrogel networks with implemented polysaccharides, will be described. After presenting the procedure to obtain the dual-responsive platform intended for the post-surgical breast cancer treatment, the characterization techniques used to describe the systems physicochemical and viscoelastic properties will be explained. Finally, their functionalization determining drug encapsulation efficiency of model drug 5-FU, drug release tests for pH-sensitive and sustained deliveries, mathematical modelling of the release mechanisms, and biological validations in 2D and 3D models assays will also be described.

3.2. Materials

The following materials were purchased from Sigma Aldrich: Alginic acid sodium salt from brown algae (ref. A2033, MW 150 kDa), with mannuronic to guluronic acid ratio 1.56, and gelatin from porcine skin powder type A (ref. G1890), with 300g Bloom gel strength, to synthesize coacervates. Poloxamer PF-127 (ref. P2443, MW 12.6 kDa), 5-FU (ref. F6627, MW 130 Da) and polysaccharides xanthan gum (XG, ref. G1253, MW 1,000 kDa), gellan gum (GG, Gelzan™ low acyl, ref. G1910, MW 1,000 kDa), for hydrogel synthesis with polysaccharides. Egg L-α-phosphatidylcholine with a 60% of yield determined by TLC (PC, ref.

61755, MW 758 Da), cholesterol (CHOL, ref. C8667, MW 386 Da) and cholesterol hemysuccinate (CHEMS, ref. C6512, MW 487Da) for liposomes synthesis, and Thiazolyl Blue Tetrazolium Bromide (MTT reagent, ref. M5655) for *in vitro* MTT assays.

The following materials were purchased from ThermoFisher, or Fisher Scientific: Acetic acid glacial ACS (99.7%+, ref. 423220100, MW 60 Da) for coacervation process, and Dulbecco's Modified Eagle Medium (DMEM from Gibco™, ref. 41966052), Foetal Bovine serum (FBS from Gibco™, ref. 10500064), penicillin-streptomycin (PS from Corning™, ref. 30-002-CI), trypsin 0.05% EDTA (from Gibco™, ref. 11590626), rhodamine B (ref. 11470084), CellTracker® Green CMFDA (ThermoFisher Scientific, ref. C7025) and Phosphate Buffer Saline (PBS, ref. 10728775) for *in vitro* assays.

Additionally, levan (LEV) was synthesized using D(+)-sucrose pure (ref. 141621.1211), and ethanol pure (ref. 131086) purchased from PanReacc AppliChem, and levan-sucrase enzyme (fructosyltransferase 68A), purchased from Creative Enzymes (ref. NATE-1384). Moreover, chloroform for liposomes synthesis (99.0% w/v) was purchased from PanReacc AppliChem ITW Reagents (ref. 131252-1612).

Pure PC with a 99% yield was purchased from Avanti Polar Lipids (ref. 840051P) for liposomes synthesis. Eudragit® S100 (EU S100, MW 135,000 g/mol) and Eudragit® EPO (EU EPO, MW 47,000 g/mol) for their coating were kindly donated by Evonik OnCare.

3.3. Experimental methodology

3.3.1. Synthesis of the dual-response system and its separate components

3.3.1.1. Alginate-Gelatin A coacervates synthesis

Gelatin and alginate coacervates were synthesized by mixing two previously separately done aqueous solutions of alginate and gelatin. Both solutions were left in constant stirring at 0.5-1% w/v concentration overnight at room temperature [1]. Gelatin A solution temperature was

changed to 37ºC when studying the temperature effect in coacervation process and its partial unravelling through heat [2].

The mixture of both aqueous solutions was done at different volume ratios (1:4-1:6 in alginate:gelatin A) and pHs 4-5 controlled by pH-meter (BASIC 20+ from Crison, Barcelona, Spain) , due to the isoelectric point of gelatin A and the alginate pKa value. pH was acidified with acetic acid solution [2]. The mixture process was controlled with continuous orbital stirring during 30 min at 25ºC and 37ºC inside an incubator and orbital shaker (ES20 from Biosan, Madrid, Spain.). Moreover, the hysteresis cycle was evaluated by measuring coacervates daily after heating them up at 37ºC for 30 min, and left at room temperature overnight. Coacervates synthesis and formulations can be seen in Table 3.1. and Figure 3.1.

Table 3.1. Alginate-Gelatin A coacervates formulations

ALG/GEL (% w/v)	Volume ratio (ALG:GEL)	pH	T (ºC)	ALG/GEL (% w/v)	Volume ratio (ALG:GEL)	pH	T (ºC)
0.5	1:4	4	25	0.5	1:6	4	25
			37				37
		5	25			5	25
			37				37
	1:5	4	25	1.0	1:5	5	25
			37				37
		5	25	2.0	1:5	5	25
			37				37

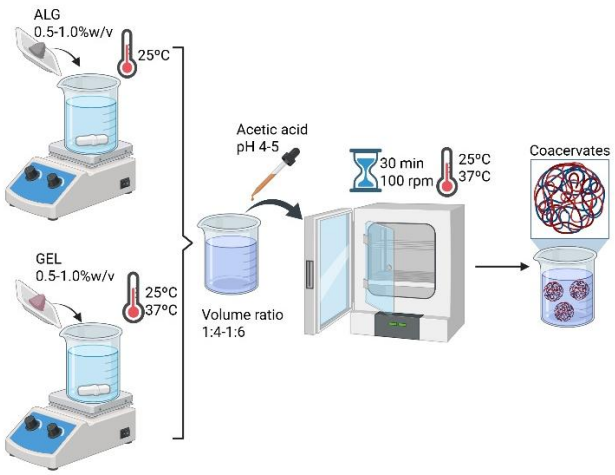

Figure 3.1. Coacervates synthesis process scheme

3.3.1.2. Conventional and EU coated liposomes synthesis

Conventional liposomes were synthesized using thin film hydration methodology [3]. Firstly, reagents (PC (60% or pure), CHOL) were weighed and mixed at set molar ratio (MR, 50:50-100:0, respectively) in chloroform for 30 min under magnetic stirring. The mixture was then taken to a rotary evaporator (Büchi Rotavapor R-114 from Büchi, Newmarket, U.K.) set at 50ºC (Büchi waterbath B-480) for 10 mins, where a thin film was left in the round-bottomed flask wall. This organic film was resuspended in buffered aqueous solutions at different pHs (7.4, or 4.5) depending on the desired final formulation. This buffered aqueous suspension contained the 50 ppm of 5-FU for loaded liposomes. The re-suspended mixture is taken to a sonicator (Starsonic 90 from Liarre) for 1h at set temperatures (25-65ºC), where the film was detached from the flask walls and a multilamellar vesicle system was synthesized in the flask. In order to obtain SUV, an extrusion process was added afterwards [4]. The extrusion set (Avanti Polar Lipids mini-extruder, Alabama, U.S.A.) was assembled using PC hydrophilic membrane discs of 0.1 µm pore diameter as filter and filter supports (Cytvia Nuclepore, Fisher Scientific), and heated upon set temperature (25-65ºC). The liposomal suspension was passed from syringe to syringe through the mini-extruder a set number of even passes, following references (1, 5, 9, 13, or 17). Conventional liposomes (L) synthesis and formulations are summarized in Table 3.2 and Figure 3.2.

Table 3.2. Conventional liposomes formulations

Passes of extrusion	Temperature (ºC)	MR	Passes of extrusion	Temperature (ºC)	MR
1	65	50:50	13	65	60:40
5					70:30
9					80:20
13					90:10
17					100:00
13	55		9(*)	65	50:50
	45		13(*)		
	35		17(*)		
	25		(*)Synthesized with pure PC		

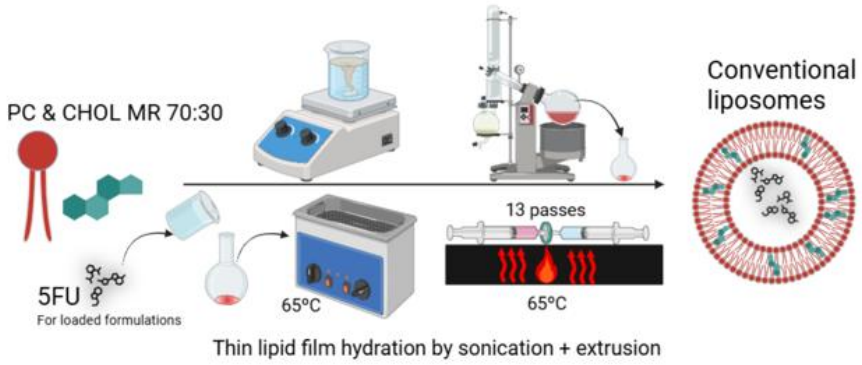

Figure 3.2. Scheme of conventional liposomes synthesis

For pH-responsive coated formulations, conventional loaded or unloaded liposomes were mixed in 1:1 volume ratios with the EU diluted solutions. For EU S100 coating, conventional liposomes had to implement stearylamine (SA) in their bilipid layer by addition with PC and CHOL at the start of the synthesis. EU S100 concentrations were ranged from 0.01 to 0.25% w/v in PBS at 7.4 [5], whilst EU EPO were ranged from 0.1 to 0.5% w/v in sodium acetate buffer at 4.5 [6]. Liposomes were poured onto EU solutions stirring at 1,000 rpm. Coating processes are illustrated in Figure 3.3.

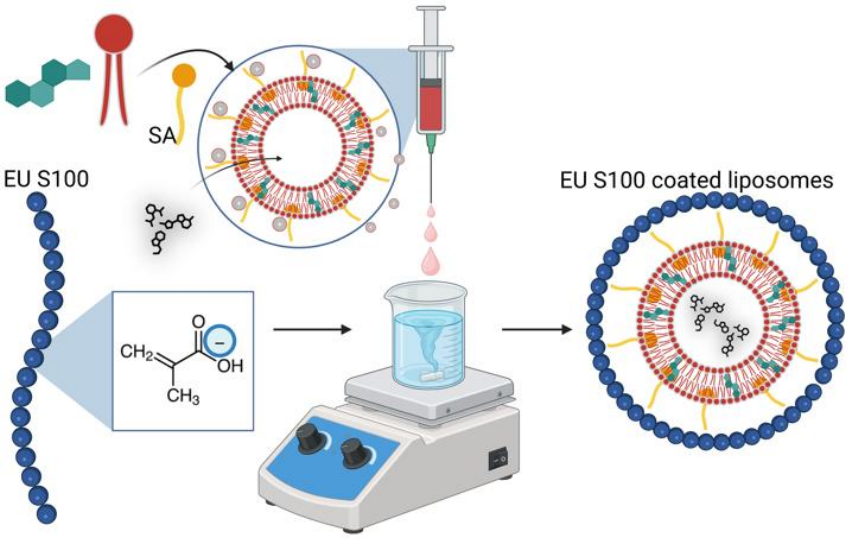

a)

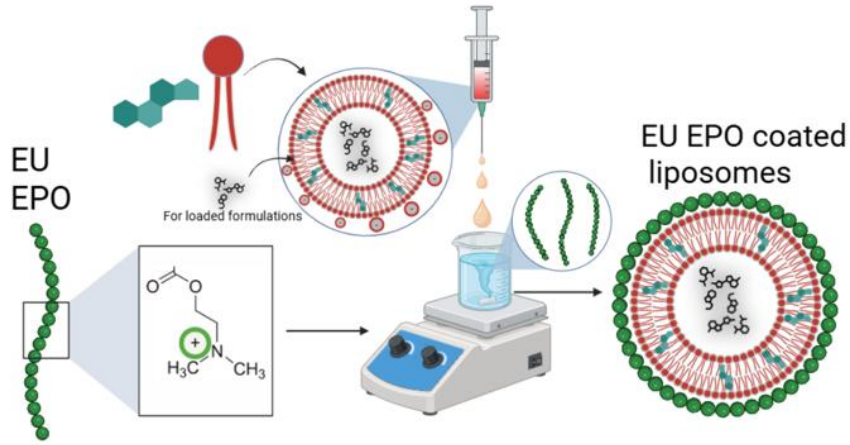

b)

Figure 3.3. Scheme of Eudragit® coated liposomes synthesis

3.3.1.3. Synthesis of PF-127 based hydrogels with different polysaccharides

PF-127 alone hydrogel was synthesized by cold method, adding weighed PF-127 flakes to aqueous solutions in 10, 20, and 30% w/v concentrations and left stirring overnight at 4ºC in a cold chamber or fridge [7].

For LEV-incorporated hydrogels, LEV was synthesized by cell-free methodology reported elsewhere, obtaining LEV around 2,000 kDa [8]. Firstly, a water solution of sucrose (90 g/L) was done, and levan-sucrase enzyme was added onto it, at 0.2 mg/L concentration. The reaction then took place in an AFORA reactor (Barcelona, Spain) of 250 mL with temperature set at 37ºC during 3 days. Afterwards, the reaction was stopped and the polymer was isolated by addition of ethanol in a ratio of three times the volume of polysaccharide solution. The solution with ethanol was left at -20ºC for another day, inducing LEV precipitation. Once the polymer precipitated, which could be clearly seen by a Tyndall effect, the mixture was taken to centrifugation (Falcon centrifuge 5804 from Eppendorf, Madrid, Spain) during 10 mins at 10,000 rpm. LEV was then separated in the pellet, and supernatant was thrown away. Finally, the LEV pellet was frozen at -80ºC (Ultralow Temperature Freezer U570 from New Brunswick Scientific, Hertfordshire, U.K.) for 5 min and

lyophylized for another day (Telstar LyoQuest, Barcelona, Spain) at -55ºC and 5 mbar.

When adding polysaccharides (XG, ALG, GG, or LEV), firstly the weighed polysaccharide at 0.5 or 1% w/v concentrations were added to the aqueous solution and left stirring at room temperature for 1h. GG was the only polysaccharide solution that needed to be heated up to 85ºC previous to addition and after for 1h, in order to correctly dissolve GG [9]. Afterwards, it was allowed to cool down to room temperature. Once the polysaccharides solutions were mixed and homogeneous, they were taken to a cold chamber under magnetic stirring conditions. Finally, PF-127 was added over these polysaccharides solutions and left stirring overnight.

For 5-FU loaded formulations, 50ppm of 5-FU were loaded due to IC_{50} found in references [10], once the aqueous solutions or polysaccharides solutions were at 4ºC and stirring, previous PF-127 addition. All the formulations studied and a brief scheme of their synthesis can be seen in Table 3.3. and Figure 3.4.

Table 3.3. PF-127 based hydrogels formulations

Formulation (% w/v)	Formulation (% w/v)	Formulation (% w/v)
10% PF	0.5% ALG+10% PF	1.0% GG+10% PF
20% PF	0.5% ALG+20% PF	1.0% GG+20% PF
30% PF	0.5% ALG+30% PF	1.0% GG+30% PF
0.5% XG+10% PF	1.0% ALG+10% PF	0.5% LEV+10% PF
0.5% XG+20% PF	1.0% ALG+20% PF	0.5% LEV+20% PF
0.5% XG+30% PF	1.0% ALG+30% PF	0.5% LEV+30% PF
1.0% XG+10% PF	0.5% GG+10% PF	1.0% LEV+10% PF
1.0% XG+20% PF	0.5% GG+20% PF	1.0% LEV+20% PF
1.0% XG+30% PF	0.5% GG+30% PF	1.0% LEV+30% PF

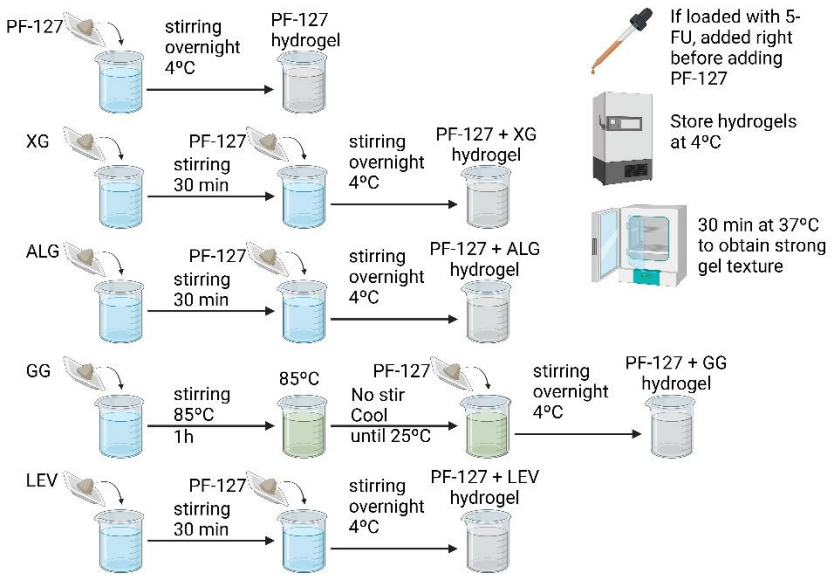

Figure 3.4. Brief scheme of PF-127 based hydrogels synthesis processes.

3.3.1.4. Dual-response injectable hydrogel synthesis

For liposomal formulations implemented PF-127 hydrogel synthesis, liposomal formulations were taken to 4ºC and PF-127 at 20% w/v concentration was added afterwards under stirring, and left overnight [7].

It must be noted for these systems, the conventional liposomes were synthesized with the optimized process: 70:30 MR, 65ºC in sonication and extrusion, and 13 passes of extrusion. Coated liposomes used 0.1% w/v of EU S100 or 0.5% w/v of EU EPO. For loaded formulations, loaded liposomes were directly embedded into the hydrogel matrix. The final concentration of the systems was 50 ppm of 5-FU, or 2.5 µM for *in vitro* assays after preliminary results. Liposomal hydrogels synthesis is illustrated in Figure 3.5.

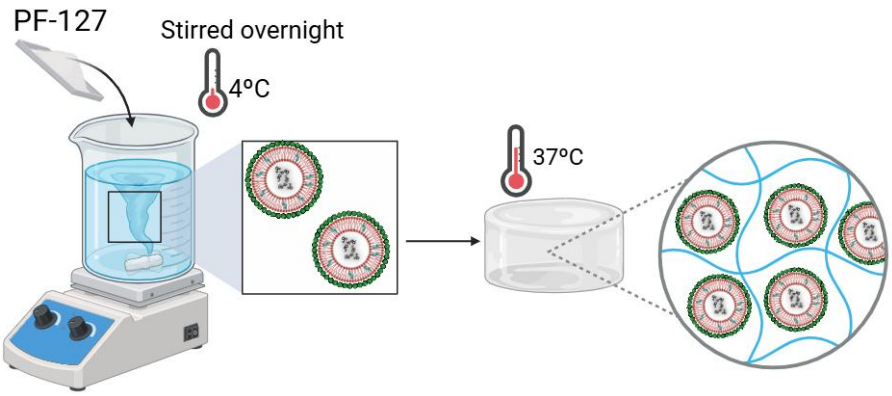

Figure 3.5. Scheme of liposomal hydrogels synthesis

3.3.2. Characterizations of systems

3.3.2.1. Zetasizer for dynamic light scattering (DLS) technique

Particle size and polydispersity index (PDI) of colloidal solutions, such as coacervates or liposomes, were measured in a Zetasizer Nano (Malvern Instruments, Worcestershire, UK) by the technique of dynamic light scattering (DLS). Automatic attenuation was selected and the results presented were interpreted by number of particles. The measurement angle was set at 173º and the peak integration method was the standard one. Size, polidispersity index, and zeta potential results were expressed as the mean average of 3 measurements.

Stability of particles was also followed by Zetasizer measurements. Coacervates hysteresis cycle was measured daily after re-heating at 37ºC for 30 min the samples, kept at 25ºC at any other time. Liposomes and coated liposomes used the Zetasizer and DLS to measure the mean particle size and PDI for at least 15 days.

Zeta potential was also measured in the Zetasizer in special cuvettes which allow the application of electric fields that induce the movement of charged particles, determining the surface charge of the colloids in the sample.

3.2.2.2. Static light scattering (SLS)

Zetasizer also has methods for static light scattering (SLS) for interactions among particles and medium and molecular weight determination. For coacervates, the second virial coefficient was calculated (A2), which describes colloids stability as a balance between attraction and repulsion forces between particles and the solvent. For this calculus, the Debye equation is used, as follows in Eq.1 [11]:

$$\frac{K \cdot C}{R_\theta} = \frac{1}{MW} + 2 \cdot A2 \cdot C \qquad \text{(Eq. 1)}$$

Being K the Debye constant (mol·cm^3/g^2), C the sample concentration (mg/mL), R_θ the Rayleigh ratio (cm^{-1}), MW the average molecular weight (kDa), and $A2$ the second virial coefficient (mL·mol/g). This test was performed on both coacervates synthesized at 25ºC and 37ºC, 1:5 in alginate:gelatin A ratio, and pH 5. The concentrations used for these experiments ranged from 1.5-6.5 mg/mL, which enabled characterization of the electrostatic interactions between the compounds with increasing concentrations until macroscopic precipitates were formed.

3.3.2.3. Optical microscopy

Optical microscopy was also used to characterize coacervates 1:5 ratio and pH 5 at synthesis temperature 25ºC and 37ºC. Optical microscope (Leica Optical compound light microscope DM1000, Barcelona, Spain) was used with objective 100X and immersion oil. Single drops of samples were poured on slides and firstly adjusted with 40X objective. Afterwards, a drop of immersion oil was placed on the slide, and the 100X objective was moved in order to create an oil film between it and the sample. Samples could be visualized by software IC Capture 2.4 and measured by IC Measure, using a DFK MKU130 camera of 13 MPX (from IVS Imaging, Texas, U.S.A.) attached to the microscope.

3.3.2.4. Turbidity

Turbidity was also performed to measure stability of coacervates, as reference supported. TurbiScan MA Classic model (Formulaction Scientific Instruments, France) was the instrument used for 7.0 mL samples in the specific transparent lab tube for this matter with lid on. Turbidity was measured on coacervates synthesized of 25ºC and 37ºC at different pH (4, 5) of 1:5 volume ratio. Also, it was used to determine salt concentration effect with NaCl added in a range of concentrations: 50-200 mM increasing 50mM each step [12].

3.3.2.5. Rheology

Rheology was also used to characterize the alginate-gelatin interactions with concentration and temperature effect. A rheometer AR 1500ex (TA Instruments, Madrid, Spain) equipped with an aluminium plate of 4 cm diameter and 1 mm gap set was used for this purpose. Frequency sweep oscillatory flow analyses were performed on samples of alginate and gelatin 0.5% w/v at 25ºC and 37ºC, as well as coacervates at pH 4, 5, 1.0% and 2.0% w/v at both set of temperatures once again [5]. The desired temperature was set at the Peltier surface and samples were loaded and tested from 0.5 to 500 rad/s with strain percentage fixed at 2.0% to ensure the solutions viscoelastic region, obtaining storage or elastic (G') and loss or viscous (G'') moduli values. These determined whether the material was more elastic-like (solid) or viscous-like (liquid).

Moreover, static flow analysis was performed on alginate and gelatin solutions (same formulations as oscillatory tests) and coacervates at 1:5 volume ratio, 37ºC and pH 4 and 5. Shear rate ramp tests were performed from 0.1 to 200 s^{-1}, obtaining viscosity values. Strain sweep was fixed at 1 Hz. Data from these experimental measurements were further fitted to Cross equation in Eq.2 [13]:

$$\eta = \eta_\infty + \frac{\eta_0 - \eta_\infty}{1+(K\cdot\dot{\gamma})^m} \qquad \text{(Eq. 2)}$$

Being η_0 and η_∞ the zero and infinity shear-rate viscosity, respectively (Pa·s), K the consistency (s), $\dot{\gamma}$ the strain rate (s^{-1}), and m the rate

constant. Rate constant is related to the power law relation between shear rate and shear stress in the shear-thinning region, being 0 for Newtonian formuations, and consistency indicates relaxation times, the inverse of critical strain rates [13].

Rheology was also used for characterizing the thermo-sensitivity of PF-127 based hydrogels. Samples were loaded on the Peltier and 1mm gap was set [14, 15]. Also, a solvent trap was used to prevent water evaporation. Oscillatory and static flow analyses were performed.

Temperature and frequency sweep tests were done with oscillatory flow. G' and G'' were obtained against a temperature sweep (5-40ºC with 1ºC/min rate [16]) and a frequency sweep (0.5-500 rad/s). Strain percentage was fixed (0.2%) in order to work within the viscoelastic region of hydrogels, and temperature sweep tests fixed the frequency (10 Hz) whilst frequency sweep tests fixed the temperature at 37ºC to study hydrogels properties in physiological conditions. On the contrary, temperature ramp tests were performed with static flow. Viscosities of hydrogels were provided as temperature increased (15-45ºC). Shear rate was fixed at 50 s^{-1} for proper MAC observation in results as references [14]. Moreover, all of these analyses were reproduced for all the gel formulations containing liposomes.

3.3.2.6. Cryogenic Scanning Electron Microscopy (Cryo-SEM)

Cryo-SEM (Cryogenic Scanning Electron Microscopy, SEM-FEI FIB Quanta 3D, Brno, Czech Republic) was used to take pictures of coated and conventional liposomes solutions and hydrogels. A drop of the formulation (3 µL) was placed in the grid, which was carefully placed in liquid nitrogen for a couple of seconds until freezing was visualized, which protected the native structure. Afterwards, the grid was inserted in the attached cryo-chamber (Quorum PP3010 Prepdek, California, U.S.A.) to the microscope. Samples were cut by the use of a blade, sublimated at -100ºC during 5 min and then sputtered using Ar gas to coat the surface metallically (Au). Afterwards, the grid was transferred to the microscope chamber where the temperature was kept at -140ºC and the distance to the lens was 5mm with a maximum voltage of 5 kV.

3.3.3. Drug encapsulation and drug release experiments

3.3.3.1. Liposomes encapsulation efficiency and loading capacity

For liposomal formulations entrapment efficiency, loaded and non-loaded liposomal samples were taken to an ultracentrifuge (Optima L-80K Ultracentrifuge, Beckman Coulter, Barcelona, Spain). The ultracentrifuge used a 70-TI rotor at 39,000 rpm (60,000 G) at 4ºC for 1 h. After centrifugation, pellets were visible in each sample. The non-encapsulated 5-FU in the supernanant was taken to spectrophotometry (Shimadzu UV-1800), and quantified there as specified before, taking into account the non-loaded liposomes solutions were used as blank [17]. The encapsulation efficiency was calculated as follows in Eq.3:

$$\%EE = \frac{C_{50ppm\ pattern} - C_{supernanant}}{C_{50ppm\ pattern}} \times 100 \quad \text{(Eq. 3)}$$

Being $C_{supernanant}$ the concentration of non-encapsulated 5FU determined from the absorbance difference between loaded and unloaded liposomal supernatants after centrifugation, and $C_{50ppm\ pattern}$ the concentration of the standardized 5FU solution (50 ppm).

3.3.3.2. Drug release from liposomal formulations

For liposomal drug release tests, 5 mL of liposomes solutions loaded with 50 ppm of 5-FU and non-loaded were introduced in a dialysis membranes (SpectraPor® 7 MWCO 1,000 Da 18 mm,Carl Roth, Karlsruhe, Germany) [18]. The releases were in 100 mL buffered aqueous solutions at different pH values (7.4, 6.5, 5.5, and 4.5), set at 37ºC and 50 rpm in orbital shaking within the incubator. Aliquots of 0.5 mL were collected at stated times: 0, 0.5, 1, 2, 4, 8, 12, and 24 h, substituting with 0.5 mL of fresh buffer. The 5-FU released quantification was determined as explained before, using non-loaded liposomes as blank for each time. Drug release profile at each time point was calculated according to Eq. 4:

$$\frac{C}{C_{max}} = \frac{C_{aliquot\ at\ time\ t}}{C_{aliquot\ at\ time\ t=24h}} \quad \text{(Eq. 4)}$$

Being $\frac{C}{C_{max}}$ the normalized cumulative drug release at each time point; $C_{aliquot\ at\ time\ t}$ the concentration of 5FU released at time *t* (determined from the absorbance difference between loaded and unloaded liposomal formulations), and $C_{aliquot\ at\ time\ t=24h}$ the maximum concentration of 5FU released, corresponding to the final sampling time (24 hours), at which release plateau was observed.

In addition, the cumulative release of 5FU relative to the initial loading concentration in each experiment was calculated according to Eq. 5:

$$\%5FU\ released = \frac{C_{aliquot\ at\ time\ t=24h}}{C_{50ppm\ pattern}} \quad \text{(Eq. 5)}$$

3.3.3.3. Drug releases from PF-127 based hydrogels

Drug releases from PF-127 based hydrogels were done with 5mL of formulations loaded with 50 ppm of 5-FU previously gelled in a 35 mm diameter Petri dish in the incubator (EN025, Nuve Incubator, Ankara, Turkey) at 37ºC for 30 min. These gels were put on a 3D printed support aided by a double bottom which enabled transfer and placement of the gel in final release system, and assembled better physiological conditions since only one gel surface was covered. The release system consisted on: A beaker containing 100 mL of distilled water at 37ºC controlled by thermometric probe, 50 rpm magnetic stirring (Isotemp from Fisher Scientific, Pennsylvania, U.S.A.) to ensure media homogenization under laminar flow, and connection to a probe attached to a spectrophotometer (Cary 60 UV-Vis from Agilent Technologies, Santa Clara, California, U.S.A.). This probe collected automatically measurements of absorbance at a wavelength of 260 nm (peak for 5-FU detection) for more than 8 hours [10]. Quantification of drug released was performed using a previously established 5-FU calibration curve obtaining Eq.6:

$$Abs = 0.049 \cdot C + 0.0063 \quad \text{(Eq. 6)}$$

Being Abs the absorbance measured, and C the 5-FU concentration (ppm). Figure 3.6. illustrates the drug release device and gel support 3D printed and designed for these experiments [9].

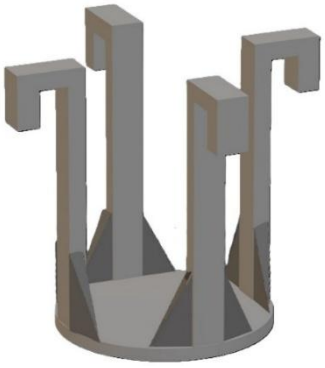

a)

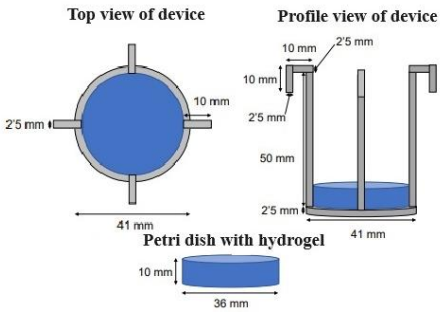

b)

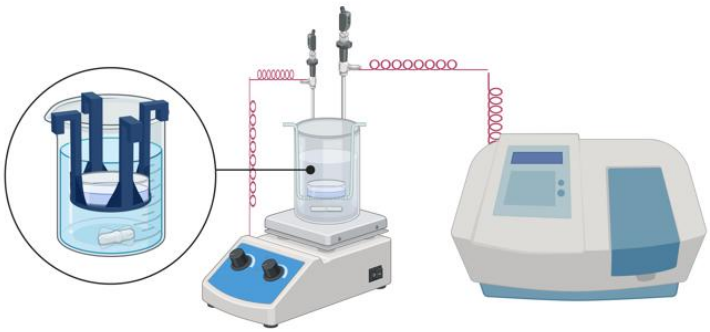

c)

Figure 3.6. Gel support for drug release as: a) Illustration of design, b) Measurements of the device for a 100 mL beaker, and c) Drug release experiment setup.

3.3.3.4. Hydrogels drug release fitting to a mathematical model

Moreover, 5-FU release results were fitted to a mathematical model which determined the contribution of the polysaccharides implemented (when incorporated) and the PF-127. This model stated that the released mass of 5-FU was directly proportional to the degradation rate of the hydrogel, which is a function of relative loss of mass of polymers (W) and the fraction of released chains from the hydrogel matrix (F) [19]. This is expressed in the kinetic equation Eq.7:

$$M^{rel}{}_{5-FU} = K_r \cdot (W_{PF} \cdot F_{PF} + W_X \cdot F_X) \qquad \text{(Eq. 7)}$$

Being $M^{rel}{}_{5-FU}$ the percentage of mass of 5-FU released, K_r the release constant, including all the resistances in transport phenomena, and PF and X the contributions of the poloxamer and the

polysaccharides, respectively. Then, in order to estimate F value, a new parameter P was described as a variable function of time according to previous equation. This is expressed in the following equation Eq.8:

$$P = 1 - exp(k_d \cdot t) \quad \text{(Eq. 8)}$$

Being P the unitary fraction of degradation, k_d the degradation rate of hydrogel chains (s^{-1}), and t the time (s). When the unitary fraction of degradation is defined, then the release chains of polymers can be determined following equations Eq.9 and Eq.10:

$$F_X = (1 - (1 - P)^2)^N \quad \text{(Eq. 9)}$$

$$F_{PF} = P^2 + P \cdot (1 - P) \cdot F_X \quad \text{(Eq. 10)}$$

Being N the erosion paramenter, ranging from 0 to 1. Therefore, the determined constants of this fitting will be the degradation rate, the erosion factor, and the release constant. Parameter estimation was carried out by the Solver complement of Excel, where relative error was the function to be minimized. The relative error is defined as Eq.11:

$$E_r = \frac{E_{abs}}{n} = \left|\frac{V_{th} - V_{exp}}{V_{th}}\right| \cdot \frac{100}{n} \quad \text{(Eq. 11)}$$

Being E_r and E_{abs} the relative and absolute errors, V_{th} and V_{exp} the theoretical and experimental values, respectively, and n the total number of experimental values that were collected in data. Additionally, Stokes-Einstein equation was used to discuss the diffusion coefficient in bulk and the hydrogels viscosity. This equation is as follows in Eq.12:

$$D = \frac{k_B \cdot T}{6\pi\mu R_0} \quad \text{(Eq. 12)}$$

Being D the diffusion coefficient ($m^2\ s^{-1}$), k_B the Boltzmann constant ($5.67 \cdot 10^{-8}\ W \cdot m^{-2} \cdot K^{-4}$), T the temperature (K), μ the viscosity of the solvent (Pa·s), and R_0 the solute radius (m).

3.3.3.5. Drug release from liposomal hydrogels

For hydrogel formulations with liposomes, same methodology was reproduced without dialysis membrane, taking additional aliquots at 36 and 48h, gelling formulations, and using the 3D printed gel support within the beaker, just as section 3.2.3.1. explained. Also non-loaded formulations were used as blanks. All drug release experiments are presented as the mean average data of three experiments.

3.3.3.6. Drug release fitting to theoretical models

For release data in liposomal solutions and hydrogels, theoretical model fitting was also used. It must be noted that representations of drug release (C/Cmax) were defined with respect to Cmax being the maximum concentration released in each system, rather than the initial loading 5-FU concentration. Models used for liposomal formulations were zero and first order kinetics, Higuchi and Korsmeyer-Peppas. For the latter two, only the range of points until 60% of Cmax released were fitted, according to recommendations [20]. The equations for the different models are as follows in Eq.13-Eq.16:

Zero order kinetics: $\frac{C}{C_{max}} = k_0 \cdot t$ (Eq. 13)

Being $\frac{C}{C_{max}}$ the fraction of drug released, k_0 the kinetic constant for zero order kinetics (h^{-1}), and t the time (h).

First order kinetics: $\frac{C}{C_{max}} = 1 - e^{-k_1 \cdot t}$ (Eq. 14)

Being k_1 the first order kinetic constant (h^{-1})

Higuchi model: $\frac{C}{C_{max}} = k_H \cdot \sqrt{t}$ (Eq. 15)

Being k_H the Higuchi kinetic constant ($h^{-0.5}$)

Korsmeyer-Peppas model: $\frac{C}{C_{max}} = k_{KP} \cdot t^n$ (Eq. 16)

Being k_{KP} the Korsmeyer-Peppas kinetic constant (h^{-n}), and n the exponent that associates the release with the type of transport of drug. Briefly, for values of n around 0.43 or lower, the transport is considered purely based on Fickian diffusion, between 0.43 and 0.85 it is considered abnormal, and for values higher than 0.85 it is considered a transport II case [20].

Moreover, for hydrogels containing liposomes formulations, it is important to also take into account two-stage release models. Therefore, two new models were added to the analysis: Peppas-Sahlin, and Weibull as a contrast model, which equations are Eq.17 and Eq.18 [21, 22]:

Peppas-Sahlin model: $\frac{C}{C_{max}} = k_1 \cdot t^m + k_2 \cdot t^{2m}$ (Eq. 17)

Being k_1 the kinetic constant due to diffusion term (h^{-m}), k_2 the kinetic constant due to relaxation term (h^{-2m}), and m the exponent that describes system geometry and the temporal form of transport. For this case $m \approx 0.4 - 0.5$ is used for spherical systems (liposomes) which experience Fickian diffusion dominance.

Weibull model: $\frac{C}{C_{max}} = 1 - e^{\left[-\left(\frac{t}{\alpha}\right)^{\beta}\right]}$ (Eq. 18)

Being α the parameter of temporal scale (h), and β the shape parameter of the release curve.

3.3.4. *In vitro* assays for model validation

In order to validate the proposed systems and their drug release towards the application, cell viability assays were performed on two different cell lines: Fibroblast normal HS-5 (ATCC® CRL11882™), and breast carcinoma BT-474 (ATCC® HTB20™), obtained from the American Tissue Collection (Manassas, VA, U.S.A.). Maintenance of cells were by cultivation in DMEM supplemented with 10% FBS and 1% P-S (DMEM+). They were kept at 37ºC in a humidified incubator with 5% CO_2 atmosphere. Upon reaching 80-90% confluence, cells were subcultured using 0.05% trypsin/EDTA 1X.

3.3.4.1. MTT assays of 5-FU, liposomes, and liposomal hydrogels

To determine biocompatibility, cell viability was evaluated by MTT assays. Cells were seeded in triplicate in flat-bottomed 24-well-plates (Costar) at an initial concentration of 16,000 cells per well. Later, they were exposed to different treatments for 24, 48, and 72h. Untreated cells and DMEM+ were also evaluated as cell and medium control, respectively.

Briefly, MTT assays work as a colorimetric test to determine cytotoxicity of treatments on cell lines, as referenced [23]. MTT reagent was dissolved in PBS in 5mg/mL concentration and later added to the wells in 10% of the volume measurement. MTT reacts with living cells, producing violet formazan crystals via mitochondrial metabolism during incubation. After 1h, DMEM+ with MTT solution was removed from the well, leaving formazan crystals attached to the bottom. These crystals were dissolved in 0.5 mL of DMSO per well. The absorbance in each well was measured using UV light (550 nm) in a Microplate reader (Techan Spark, Viena, Austria), and cell viability can be calculated as follows Eq.19:

$$Cell\ viability\ (\%) = \frac{Avg\ OD\ sample\ wells - Avg\ OD\ medium\ control\ wells}{Avg\ OD\ cell\ control\ wells - Avg\ OD\ medium\ control\ wells} \quad \text{(Eq. 19)}$$

Firstly, MTT assays of 5-FU at different concentrations were done in order to determine the current IC_{50} for our system and compare to the referenced one used before.

Aferwards, liposomes formulations were tested unloaded and loaded with previously determined IC_{50}. These were: L and L+5-FU (unloaded and loaded conventional liposomes), L+S100 and L+S100+5-FU (unloaded and loaded EU S100 coated liposomes), and L+EPO and L+EPO+5-FU (unloaded and loaded EU EPO coated liposomes).

Finally, hydrogels with liposomes were tested *in vitro* as well. In order to obtain the gel effect and compare results to previous release in buffered solutions, new 3D printed gel supports were designed for the hydrogel formulations in wells, resembling transwell inserts [24]. Gel supports were 3D printed (Creality, Shenzen Creality 3D Technology Co.,

China) using Panchroma Translucent Natural Filament. 0.5 mL of formulations of hydrogel could successfully gel and be submerged in 1 mL of DMEM+ for MTT assays without touching the cells attached at the bottom. Lateral slits favoured the transfer to the media bulk. Gel support for *in vitro* assays is shown in Figure 3.7. Treatments designed for this assay were: G, G+5-FU (unloaded and loaded PF-127 hydrogel alone), G+L and G+L+5-FU (unloaded and loaded conventional liposomes hydrogel), G+L+EPO and G+L+EPO+5-FU (unloaded and loaded EU EPO coated liposomes hydrogel, or final dual-responsive system).

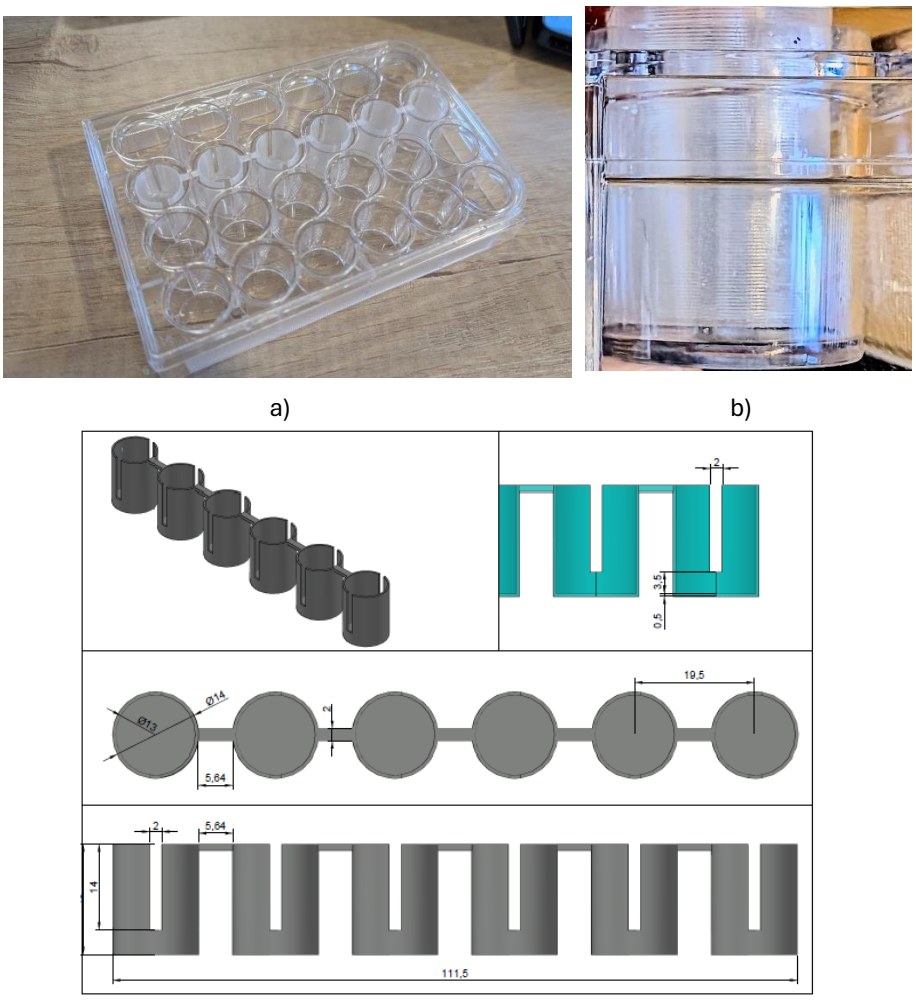

Figure 3.7. Gel support device for 24-well plates for *in vitro* assays. a) Support device in well plates, b) Side view to assure the bottom is not reached, and c) Design of support device made in AutoCAD.

It must be noted that all liquid formulations were sterilized via filtration of 0.2 µm in sterile conditions, and solid PF-127 flakes and gel supports were irradiated with UV light prior to use. Also, gel supports were immersed in an IMS solution for further cleaning and sterilization.

3.3.4.2. Liposomal cellular uptake

To complement the results obtained from the cell viability assays, the cellular uptake of the different liposomal formulations was evaluated in the BT-474 breast carcinoma cell line. For this purpose, cells were stained with CellTracker® Green CMFA (0.7 µM) according to the manufacturer's instructions and seeded in glass-bottom dishes at a density of 20,000 cells/mL. Then, cells were incubated at 37°C with the different liposomal formulations, in which rhodamine B had been previously encapsulated following the same procedure described for 5FU loading, reaching a final rhodamine concentration of 2 µg/ml. Cellular uptake was studied after incubation periods of 0,5, 1, 4, and 24 hours. Following each incubation period, cells were washed with PBS to remove non-internalized liposomes and imaged using confocal laser scanning microscopy (CLSM) (Leica SP8, Leica Camera, Wetzlar, Germany).

3.3.4.3. Viability assays on spheroids subjected to dual-responsive system

Multicellular Tumour Spheroids (MCTS) were obtained culturing BT-474 cells in Nuclon™ Sphera™ 96-well U-shaped bottom microplates (Thermo Fisher Scientific, Eugene, OR, USA) with a concentration of 2,000 cells /mL for 4 days to allow growth, as referenced [25]. Once the spheroids were grown, they were treated with 5-FU solution (5-FU), EU EPO coated liposomal gel (G+L+EPO) and its loaded version (G+L+EPO+5-FU). Results were evaluated using Trypan Blue cell-counting using Trypan Blue and Live/Death fluorescence imaging by CLSM at 24h, 48h, and 72h.

Cell-counting assay was performed in the same wells where the MCTS were developed. In order to keep resemblance with previous *in vitro* assays, 1/3 of media volume was replaced with the formulations in

each well, keeping a final concentration of 5-FU of 2.5 μM per well for loaded formulations. Control wells remained untouched and each treatment was applied to 4 wells per day and treatment. After treatment exposure the spheroids were collected, separated by centrifugation at 1,400rpm for 4 minutes (Centronic-BL II from JP Selecta, Barcelona, Spain), disaggregated, and resuspended in 75 μL of DMEM+. Afterwards, the percentage of alive and dead cells was quantified (InvitrogenCountess II FL Automated Cell Counter, ThermoFisher Scientific) with Trypan Blue.

Furthermore, cell viability was double assayed with Live/Death fluorescence staining. For this assay, the same procedure as mentioned before was reproduced in flat-glass bottom dishes after spheroids growth. At 48h and 72h, the spheroids were incubated with calcein AM (0.1 μM) and propidium iodide (0.94 μM) fluorescent dyes for 30 min. The stained samples were then imaged by Confocal Laser Scanning Microscopy (CLSM) (Leica TCS SP5, Leica Microsystems, L'Hospitalet de Llobregat, Barcelona, Spain) with an excitation / detection of 494/517 and 535/617 respectively.

3.3.5. Statistical analysis

Data measurements were accompanied by statistical analysis of experimental results reported as mean value ± standard deviations of at least 3 experiences. Specific comparison between groups was done by unpaired Student's t-tests. Meanwhile, multiple groups comparisons were done by one-way or two-way ANOVA. When statistically significant differences were confirmed, Tukey test was used as a post-hoc analysis.

3.4. References

[1] Saravanan M, Rao KP. Preparation and characterization of microcapsules based on biodegradable polymers: Pectin/casein complex for controlled drug release systems. Carbohydr Polym. 2010;80:808-816.

[2] Lau HC, Jeong S, Kim A. Gelatin-alginate coacervates for circumventing proteolysis and probing intermolecular interactions by SPR. Int J Biol Macromol. 2018;117:427-434.

[3] Zhang H. Thin-film hydration followed by extrusion method for liposome preparation. Methods Mol Biol. 2017;1522:17-22.

[4] Avanti® Research. How to use the Avanti® Mini-Extruder. Available online: https://www.sigmaaldrich.com/ES/es/technical-documents/protocol/materials-science-and-engineering/drug-delivery/avanti-mini-extruder. (Accesed on 19th March 2026)

[5] Caddeo C, Gabriele M, Fernández-Busquets X, Valenti D, Fadda AM, Pucci L, Manconi M. Antioxidant activity of quercetin in Eudragit-coated liposomes for intestinal delivery. Int J Pharm. 2019;565:64-69.

[6] Hasanovi A, Hollick C, Fischinger K, Valenta C. Improvement in physicochemical parameters of DPPC liposomes and increase in skin permeation of acyclovir and minoxidil by the addition of cationic polymers. Eur J Pharm Biopharm. 2010;75:148-153.

[7] Shriky B, Kelly A, Isreb M, Babenko M, Mahmoudi N, Rogers S et al. Pluronic F127 thermosensitive injectable smart hydrogels for controlled drug delivery system development. J Colloid Interface Sci. 2020;565:119-130.

[8] González-Garcinuño A, Tabernero A, Marcelo G, Sebastián V, Arruebo M, Santamaría J, Martín del Valle E. Differences in levan nanoparticles depending on their synthesis route: Microbial vs cell-free systems. Int J Biol Macromol. 2019;137:62-68.

[9] de Dios-Pérez I, González-Garcinuño A, Tabernero A, Blanco-López M, García-Esteban JA, Moreno-Rodilla V et al. Development of a thermosensitive hidrogel based on Poloxamer 407 and gellan gum with inclusion complexes (sulfobutylated-β-cyclodextrin-Farnesol) as a local drug delivery system. Eur J Pharm Sci. 2023;191:106618.

[10] Karthika C, Sureshkumar R, Sajini DV, Ashraf G, Rahman H. 5-fluorouracil and curcumin with pectin coating as a treatment regimen for titanium dioxide with dimethylhydrazine-induced colon cancer model. Environ Sci Pollut Res. 2022;29:63202-63215.

[11] Winzor DJ,Deszczynski M, Harding SE, Wills PR. Nonequivalence of second virial coefficients from sedimentation equilibrium and static light scattering studies of protein solutions. Biophys Chem. 2007;128:46-55.

[12] Derkach SR, Voron'ko NG, Kuchina YA. Intermolecular interactions in the formation of polysaccharide-gelatin compleces: A spectroscopic study. Polymers. 2022;14:2777.

[13] Cross MM. Rheology of non-Newtonian fluids: A new flow equation for pseudoplastic systems. J Colloid Sci. 1965;20:417-437.

[14] Chung Y-I, Lee S-Y, Tae G. The effect of heparin on the gelation of Pluronic F-127 hydrogel. Colloids Surf A. 2006;284:480-484.

[15] Newby GE, Hamley IW, King SM, Martin CM, Terrill NJ. Structure, rheology and shear alignment of Pluronic block copolymer mixtures. J Colloid Interface Sci. 2009;329:54.

[16] Constantinou AP, Nele V, Doutch JJ, Correia JS, Moiseev RV, Cihova M et al. Investigation of the thermogelation of a promising biocompatible ABC triblock terpolymer and its comparison with Pluronic F127. Macromolecules. 2022;55:1783-1799.

[17] da Costa CAM, Moraes AM. Encapsulation of 5-fluoroacil in liposomes for topical administration. Acta Sci Technol. 2003;25:53-61.

[18] Jayachandran P, Ilango S, Suseela V, Nirmaladevi R, Shaik MR, Khan M et al. Green synthesized silver nanoparticle-loaded liposome-based nanoarchitectonics for cancer management: *In vitro* drug release analysis. Biomedicines. 2023;11:217.

[19] Xu J, Feng E, Song J. Bioorthogonally cross-linked hydrogel network with precisely controlled disintegration time over a broad range. J Am Chem Soc. 2014;136:4105.

[20] Jain A, Jain SK. *In vitro* release kinetics model fitting of liposomes: An insight. Chem Phys Lipids. 2016;201:40-58.

[21] Peppas NA, Sahlin JJ. A simple equation for the description of solute release: Coupling of diffusion and relaxation. Int J Pharm. 1989;57:169-172.

[22] Barzegar-Jalali M, Adibkia K, Valizadeh H, Shadbad MRS, Nokhodchi A, Omidi Y et al. Kinetic analysis of drug release from nanoparticles. J Pharm Pharmaceut Sci. 2008;11:167-177.

[23] Duncan RE, Archer MC. Farnesol induces thyroid hormone receptor (THR) beta1 but inhibits THR-mediated signalling in MCF-7 human breast cancer cells. Biochem Ciophys Res Commun. 2006;343:239-243.

[24] Peng S, Lin J-Y, Cheng M-H, Wu C-W, Chu I-M. A cell-compatible PEO-PPO-PEO (Pluronic®) –based hydrogel stabilized through secondary structures. Mater Sci Eng. 2016;69:421-428.

[25] Nieto C, Vega MA, Martín del Valle E. Nature-inspired nanoparticles as paclitaxel targeted carrier for the treatment of HER2-positive breast cancer. Cancers. 2021;13:2526.

3.5. List of abbreviations

5-FU — 5-Fluorouracyl
A2 — Second Virial Coefficient
BT-474 — Breast Tumour Cell Line
CHOL — Cholesterol
CLSM — Confocal Laser Scanning Microscopy
DLS — Dynamic Light Scattering

DMEM — Dulbecco's Modified Eagle Medium
DMSO — Dimethyl Sulfoxide
EDTA — Ethylenediaminetetraacetic Acid
EU — Eudragit
FBS — Foetal Bovine Serum
G — Gel (PF-127)
GEL — Gelatin
GG — Gellan Gum
HS-5 — Human Bone Marrow Stromal Cell Line
IC_{50} — Inhibitory Concentration 50
IMS — Industrial Methylated Spirits
LEV — Levan
MAC — Micellar Aggregation Capacity
MCTS — Multicellular Tumour Spheroid
MPX — Megapixel
MR — Molar Ratio
MTT — 3-(4,5-dimethylthiazol-2-yl)-2,5-diphenyltetrazolium Bromide
MW — Molecular Weight
MWCO — Molecular Weight Cut Off
PBS — Phosphate Buffer Saline
PC — 1,2-Diacyl-sn-Glycero-3-Phosphocholine (Phosphatidylcholine)
PDI — Polidispersity Index
PF — Pluronic in Flakes
PS — Penicillin-Streptomycin
SA — Stearylamine
SEM — Scanning Electron Microscopy
SLS — Static Light Scattering
SUV — Small Unilamellar Vesicle
TLC — Thin Layer Chromatography
UV — Ultraviolet
XG — Xanthan Gum

4. Study of Alginate-Gelatin A Coacervates as Potential Drug Delivery System

4.1. Introduction

As it has been described in the thesis introduction, one of the main challenges in oncology is the prevention of tumour recurrence in post-surgical breast cancer treatment. Despite recent advances, current therapies still present limitations such as low therapeutic efficiency and systemic toxicity. In this context, the development of alternative strategies enabling local drug delivery has emerged as a promising approach to overcome these limitations. However, the proposed locally administered therapy based on an injectable thermo-responsive hydrogel matrix requires the incorporation of a nanocarrier capable of providing pH-responsive targeting towards tumour microenvironment. Accordingly, nanocarrier DDS have experienced a remarkable increase in recent years [1].

Among all of the drug delivery systems proposed for this strategy, coacervates have recently increased interest in research due to their high sensitivity to physiological stimuli, particularly pH changes, temperature, or ionic strength. These systems are mainly formed by electrostatic interactions highly adaptable to modify its synthesis and stability in different environments. Moreover, they present high encapsulation efficiency for payloads, positioning them as promising platforms for biomedical applications [2].

Thus, this chapter is focused on the development of a pH-responsive coacervate system based on alginate and gelatin A, and its optimization taking into account different process variables and how they affect the coacervation process. Finally, the compatibility of this system with the intended application will also be evaluated.

4.2. Coacervation process

Coacervation is defined as a liquid-liquid separation process (LLSP) occurring in a homogeneous aqueous polymer solution which spontaneously separates into a dilute phase with low polymer concentration and a coacervate phase enriched in polymer content. The LLSP is driven by the interactions established among molecules forming the coacervated phase, which are influenced by environmental factors,

such as pH, polymer ratios and concentrations, temperature, or ionic strength [3].

Specifically, complex coacervation requires at least two different polymers to interact for the LLSP. For this cases, electrostatic interactions between the oppositely charged functional groups of the polymers is usually the predominant force for the phase separation. This causes the assembly of hydrated high polymer concentration domains, known as the coacervate phase, as illustrated in Figure 1.19 in the introduction.

The resulting physicochemical properties of the coacervates, such as size, stability, viscoelasticity or sensitivity to environmental stimuli, are strongly dependent on the strength on the interactions between the polymers, which are subsequently influenced by the synthesis conditions and process variables. Therefore, with an optimized synthesis design, the coacervate properties can be modified on demand, taking into account the application they are intended for. Moreover, the high polymer density within the coacervate phase provides promising properties for the encapsulation of different therapeutic payloads. Together with their diffusion-controlled release behavior and adaptability to biological environments, these abilities position coacervates systems as promising platforms for drug delivery applications [3].

Nonetheless, the component selection must be carefully selected according to their designed application. Parameters such as biocompatibility, biodegradability, charge density, molecular weight, environmental responsiveness, and colloidal stability must be precisely balanced to achieve the desired encapsulation performance, structural integrity, and release behaviour [3].

4.3. Alginate-gelatin coacervates

Protein–polysaccharide combinations represent one of the most widely explored classes of coacervate systems for biomedical and drug delivery applications due to their ability to integrate the complementary properties of both biopolymer families. Proteins present a wide structural versatility, which conformation can be stimuli-responsive due

to the abundant functional groups and its complex organization. On the other hand, polysaccharides exhibit enhanced stability in aqueous solutions, easily tunable behavior, and biocompatibility. This synergistic combination causes the structurally versatile and adaptable platform to exploit in a wide range of applications, like drug delivery [4].

Specifically, alginate-gelatin coacervates constitute an interesting combination, since they present high biocompatibility and tunable characteristics depending on environmental stimuli. Alginate is a highly biocompatible and biodegradable polysaccharide exploited in bioapplications, which presents anionic behavior. Its linear structure is based on β-D-mannuronic and α-L-guluronic residues, which contain a high amount of carboxylate groups that determine a net negative charge under physiological conditions, which is promoted with acidic environments. This enhanced negative charge promoted electrostatic interactions with oppositely charged functional groups from other compounds.

In this sense, gelatin A presents the cationic behavior required for complex coacervation, due to the presence of protonable amino groups in its complex structure which conformation is temperature dependent. Moreover, its protein nature and its amphiphilic structure enables the interaction with hydrophilic and moderately hydrophobic compounds, which can enhance their encapsulation efficiency and biocompatibility. Thus, the alginate-gelatin combination offers a designed coacervate platform where strong electrostatic interactions are highly promoted, presenting promising adaptable, biocompatible and functionalized properties regarding drug encapsulation and delivery. In fact, some studies have reported higher drug encapsulation from this coacervate base than similar protein and polysaccharides systems [5]. The synthesis process via electrostatic interactions and reported drug delivery studies are schemed in Figure 4.1, and Table 4.1.

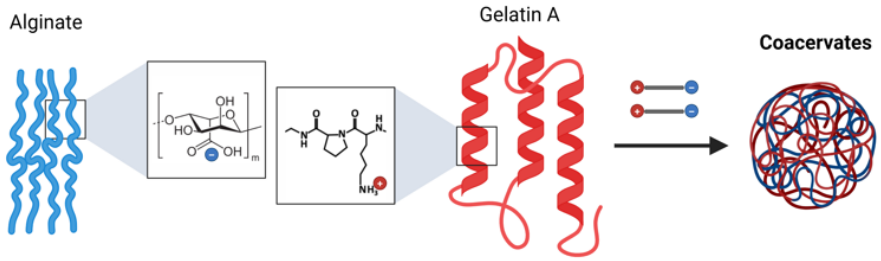

Figure 4.1. Coacervation process driven by the electrostatic interactions between the oppositely charged functional groups of alginate and gelatin A

This system has already been reported in several studies mentioned in Table 4.1.

Table 4.1. Alginate-gelatin coacervates reported lately

Coacervate formulation	Encapsulated molecule	Application	Reported results	Ref
Alginate and gelatin	BSA/EGF	Chronic wounds	BSA encapsulated and protected against trypsin	6
	bFGF	Diabetic foot ulcers	Sustained release and increase in HDF viability	7
	EGF	Diabetic ulcers	EGF protected and improved scarring activity	8
	EGF	Chronic woulds	Accelerated wound closure in mice and reduced inflammation	9
	IM	Drug oral formulations	Sustained release for 14h for gastrointestinal effects reduction	10
	MH, DS,IM	Drug oral formulations	Low releases in gastric fluids while sustained in intestinal.	5

As it can be seen in Table 4.1, some formulations have already been studied, but their stimuli-response is never exploited to design desired drug releases. Regarding this, the combination of alginate and gelatin via electrostatic interactions, as well as their stimuli-sensitive structures and interactions, can be used to design responses towards pH and temperature.

4.3.1. pH-sensitivity in alginate-gelatin coacervates

pH is usually one of the most influential factors for coacervation when electrostatic interactions predominate, since pH controls the ionization degree of polyelectrolites, and thereby, their charge modulation and interaction. In protein-polysaccharides systems, pH tends to show critic points in coacervation process defining their stability in aqueous solutions [11]. Specifically, in gelatin A, which isoelectric point is found for pH 7.0-9.0 range it is possible to positively charge its amine functional groups in acidic environments. Meanwhile, alginate maintains its carboxylic groups with anionic behaviour, promoting the charge difference, and consequently establishing more electrostatic interactions [12].

This presents an opportunity to design a pH-responsive drug delivery system. Since alginate-gelatin coacervates stability depends on the pH, then the drug release can also respond to this stimulus, targeting the acidic extracellular matrix of the tumour microenvironment, as well as acidic intracellular compartments such as endosomes, or lysosomes.

Moreover, the electrostatic interactions between alginate and gelatin are also dependent on the amount of available protonated functional groups they present. This characteristic can be changed with pH but also with a structure conformation shift of the gelatin. In this sense, its protein domains and its structural organization also presents dependence on the temperature [5].

4.3.2. Temperature-sensitivity in gelatin structural conformation

Temperature can add another stimulus sensitivity to certain polymers structure conformation involved in coacervation. In this case, gelatin A shows a partial unravelling of its helicoidally arranged structure with increasing temperatures, causing a higher availability of more functional groups and therefore promoting more electrostatic interactions with alginate anionic functional groups, illustrated in Figure 4.2 [5]. This phenomenon can redefine properties of the coacervates, such as their density or viscosity. Importantly, this variable has still not been included

in the reported systems studying coacervation between alginate and gelatin A.

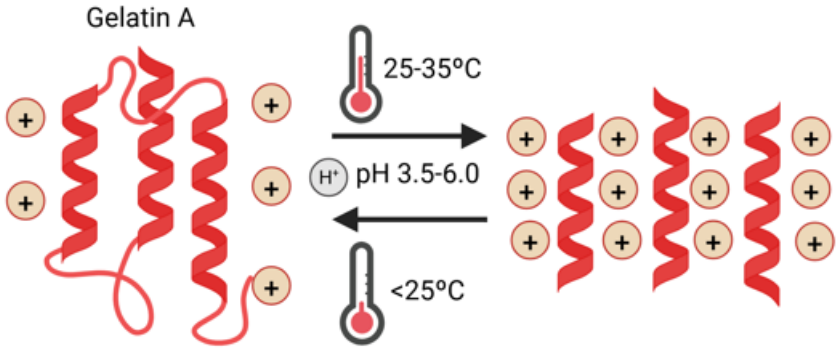

Figure 4.2. Temperature influence on gelatin A structural conformation.

Furthermore, the temperature-response of this system, depending on the polymeric concentration, could form a more packed structure among the compounds, producing a partial gelation [13]. Accordingly, coacervates can be designed in order to gel under certain temperature ranges, presenting cohesive structures which are more likely to provide a sustained drug release. For this system, this could provide complementary structural reinforcement to the thermo-responsive behaviour.

4.4. Published article related to this chapter

Following this section, the published article “Exploring the effect of experimental conditions on the synthesis and stability of alginate-gelatin coacervates” is presented as the results and discussions obtained within the framework of this experimental phase. The objective of this article was to evaluate how the alginate-gelatin A coacervate system could be useful for the designed approach of post-surgical breast cancer treatment, regarding optimal synthesis, stability, and stimuli-response.

In order to do this, the synthesis process of the coacervation in this system was deeply studied and all the process variables were analysed in order to understand the coacervation process and how different conditions influenced the electrostatic interactions between the

biopolymers and its stability. Importantly, the temperature was also added to this study, determining how the gelatin structural conformation affected the coacervates size and polidispersity, as well as polymer ratio, salt concentration, and pH.

Coacervates were also deeply characterized by different techniques including dynamic and static light scattering, turbidity, and rheology. pH and overall temperature demonstrated a key role in coacervates synthesis and stability denoting a change in their electrostatic interactions and viscoelastic properties.

• Blanco-López M, Marcos-García A, González-Garcinuño A, Tabernero A, Martín del Valle EM. Exploring the effect of experimental conditions on the synthesis and stability of alginate-gelatin coacervates. Polym Adv Technol. 2024;35:e6554.

Received: 27 May 2024 | Revised: 24 July 2024 | Accepted: 3 August 2024
DOI: 10.1002/pat.6554

RESEARCH ARTICLE

polymers advanced technologies WILEY

Exploring the effect of experimental conditions on the synthesis and stability of alginate–gelatin coacervates

Marcos Blanco-López | Alejandro Marcos-García | Álvaro González-Garcinuño | Antonio Tabernero | Eva M. Martín del Valle

Department of Chemical Engineering, University of Salamanca, Salamanca, Spain

Correspondence
Antonio Tabernero, Department of Chemical Engineering, University of Salamanca, Plaza de los Caídos s/n, 37008, Salamanca, Spain.
Email: antaber@usal.es

Funding information
University of Salamanca - Banco Santander, Grant/Award Number: Ayudaspara Contratos Predoctorales

Abstract

Alginate–gelatin coacervation has been studied by considering different experimental parameters, such as gelatin preheating, pH, alginate–gelatin ratio and their respective concentrations, and salt effect. Results were assessed in terms of size and polydispersion via dynamic light scattering, electrostatic charge in the surface by zeta potential measurements, electrostatic interaction forces by static light scattering, stability by turbidimetry and viscoelastic and pseudoplastic behavior by rheology (oscillatory and statistical analysis). According to the results, gelatin structure has to be previously modified to induce the proper interactions with a subsequent pH reduction. Specifically, stable coacervates (according to turbidimetry and dynamic light scattering) with a size of 300–600 nm and a polydispersion lower than 0.25 were obtained after preheating the gelatin at 37°C and with a subsequent pH reduction until 4–5 for an alginate–gelatin ratio between 1:4 and 1:6. However, different experimental conditions promote an unsuccessful coacervation, obtaining always precipitates and/or coacervates with a wider particle size distribution. Furthermore, in order to study the effect of the temperature on the coacervates, different cooling–heating cycles were applied on them over a week, showing the stability of the thermo-reversible coacervates for almost 5 days. Also, the interactions were characterized via static light scattering, analyzing the second virial coefficient. Moreover, rheological oscillatory results can be used to identify a proper coacervation due to the increase of the storage modulus. However, no significant changes were observed with statistical analysis due to the highly diluted character of the precursor solutions. These results highlighted how a proper combination of different experimental conditions, mainly temperature to promote a partial gelatin unraveling as well as pH reduction, is required to successfully produce coacervates. Finally, salt effect was proven to induce precipitation when NaCl was increasingly added to solutions of stable coacervates.

KEYWORDS
alginate, coacervates, gelatin, rheology

This is an open access article under the terms of the Creative Commons Attribution-NonCommercial License, which permits use, distribution and reproduction in any medium, provided the original work is properly cited and is not used for commercial purposes.
© 2024 The Author(s). *Polymers for Advanced Technologies* published by John Wiley & Sons Ltd.

1 | INTRODUCTION

Complex coacervates are liquid–liquid separation systems held together mainly by electrostatic interactions between polyelectrolytes. They present as spherical droplets and resemble the form of dispersant emulsion with a size range from nanometers to micrometers.[1–4] The formation of these structures consists of a fundamental physico-chemical phenomenon, presented in many biological processes like protein transcription, antigen–antibody reactions, or enzymatic channeling.[5,6] In fact, this phenomenon has different mechanisms to assemble the condensed polymeric molecules into a liquid. The first processes observed occurred in solutions of oppositely charged biopolymers and solutions of proteins with polyphenols.[7,8] This coacervation mechanism is complex coacervation, which consists of the complexation of oppositely charged molecules. Alternative mechanisms of complexation include the simple coacervation, which involves single self-associating molecule, and the autocomplex coacervation, which associates groups of ampholytic polymers.[9,10]

Coacervates have a potential use in biomedicine, concerning stimuli-responsive drug delivery systems (mainly pH and temperature) because its formation is strongly dependent on the different protein conformations, polymer networks, modifications in its surface charge, etc.[11–14] As an example, they were used in tests of insulin release for diabetes treatment with pH-response (stable coacervates between pH 7.4 and 9.5) of histidine-rich beak proteins (DgHBP-s peptide). Coacervates were synthesized to encapsulate insulin and glucose oxidase.[15] The glucose oxidase reacts with glucose to produce gluconic acid, so the pH will decrease and will trigger the insulin release. Another work proposed a temperature-responsive coacervate system between elastin-like polypeptides and hyaluronic acid. According to the results, a successful coacervation was produced at different temperatures (ranging from 32 to 42°C) depending on the ratio polypeptide/hyaluronic acid, forming particles between 400 and 600 nm.[16] In this context, several reviews have been published concerning the potential of the coacervates for similar biomedical applications.[17–24]

One of the most promising coacervate is the one formed between the protein gelatin A and the polysaccharide alginate. Gelatin A is a collagen derivative, which properties are defined by its extraction source. Its peculiar conformation can be modified with the temperature.[25–27] If a gelatin solution is made at ambient temperature (25°C), the protein coils assemble into triple helices.[28] Alginate, additionally, is an anionic polysaccharide, constituted by β-D-mannuronate and α-L-guluronate residues.[29] Alginate is usually obtained from brown algae and due to its biocompatibility, it is proposed as a polymer for biomedical applications.[30–35] Therefore, coacervates alginate/gelatin A have different advantages, such as biocompatibility, biodegradability, as well as the use of economic and accessible polymers that do not require previous chemical modifications. This is prevented because the coacervation is performed by changing pH, volume ratio, or concentrations to modify gelatin A structure and alginate density charge.[36,37] All of these physicochemical properties enable this system to be used in proteins and factors delivery and release for different chronic wound treatments.[38]

As a consequence, several works have studied the coacervation between alginate and gelatin A. This system also shows different bioapplications suitable for tissue engineering or drug delivery systems, as gelatin A and alginate can form hydrogel matrices. Several studies shown in references comment on this issues. For instance, Serafin et al.[39] characterize these hydrogel matrices combined with hyaluronic acid (HA) as well. The combination of gelatin and HA resulted to provide the longest term swelling properties with a minimal swelling after 168 h, with controlled morphology and mechanical properties, potentially useful for tissue engineering treatments.

Zamboni et al.,[40] on the other hand, used a gelatin–alginate hydrogel to implement polylactic acid loaded with curcumin. This caused an improvement to the compressive strength and mechanical performance of the hydrogels, without influencing the swellability or degradation capacities of these. Also, these gels showed a positive effect on cell growth of fibroblast as well as preserving the viability of monocytes.

Lau et al.[38] reported, based in turbidity and dynamic light scattering (DLS) studies, that the best experimental conditions for this coacervation were a gelatin A/alginate volume ratio of 4:1 at ambient temperature, a pH around 5, and concentrations of 0.5% w/w for both polymers. This means the coacervation was performed with a gelatin A structure in form of coils, without its partially unraveling. Therefore, the coacervation was mainly based on the interactions between the coils and the alginate chains due to the change of pH.

The results reported particle size always around 1 micron, and with high values of polydispersity index (PDI). Nevertheless, that work was focused on the encapsulation of bovine serum albumin in the coacervates, which was performed successfully with a great encapsulation yield and a proper release. Also, Kim and co-workers[41] encapsulated fibroblast growth factor in this coacervate. They studied different parameters, such as gelatin molecular weight, different ratios gelatin/alginate (from 0.5 to 2.0% w/w) and pH, on the coacervates formations and encapsulation yield. Again, in spite of the high encapsulation yield and the positive results of in vitro assays for a potential wound healing application, the particles obtained reported size of around 1 micron and with a wide range of PDI (higher than 0.4).

Finally, Saravanan and Rao[42] encapsulated three different drugs in alginate–gelatin and pectin–gelatin coacervates, modifying the pH with different acids. They obtained proper values of encapsulation for diclofenac sodium and indomethacin, but both systems were not adequate to encapsulate metronidazole hydrochloride. This might be caused from the escape of drug molecules from the coacervation phase, since this drug is highly soluble in water. Supporting previous results, pH values higher than 5 were most likely to induce precipitation, and the ones lower promoted the electrostatic interactions between the polymers to form the coacervates.[38]

Moreover, when reducing pH to optimize coacervates synthesis, authors found that some acids, such as chlorhydric acid, do not only induce coacervation, but also cause partial precipitation of free alginic acid from sodium alginate solution when adding such strong acid. In this context, acetic acid is the preferred compound for this purpose.[42] Besides, this article highlighted that alginate–gelatin coacervates are

RIGHTSLINK

10991581, 2014, 8, Downloaded from https://onlinelibrary.wiley.com/doi/10.1002/pat.3134 by Universidad De Salamanca, Wiley Online Library on [05/11/2024]. See the Terms and Conditions (https://onlinelibrary.wiley.com/terms-and-conditions) on Wiley Online Library for rules of use; OA articles are governed by the applicable Creative Commons License

10991581, 2014, 8, Downloaded from https://onlinelibrary.wiley.com/doi/10.1002/pat.3134 by Universidad De Salamanca, Wiley Online Library on [05/11/2024]. See the Terms and Conditions (https://onlinelibrary.wiley.com/terms-and-conditions) on Wiley Online Library for rules of use; OA articles are governed by the applicable Creative Commons License

smaller and form less aggregates than the pectin–gelatin. However, the size was always higher than 50 microns and with a high value of PDI.[42]

Previous articles were mainly focused in the potential of the coacervation to encapsulate different compounds, without performing a comprehensive study of the interactions alginate–gelatin A. These interactions in aqueous solutions were studied in more detail for alginate with fish gelatin,[43] and the results confirmed that the pH is a key parameter to set a boundary (pH around 5.4) between the proper interactions to induce coacervation and to form insoluble complexes. Moreover, these interactions between these compounds are pH-reversible and can be modified with the addition of NaCl.[43] Salt concentration is also another important parameter to take into account when studying this electrostatic interaction between gelatin A and alginate.

Based on the previous results, it can be concluded that it is difficult to control the alginate–gelatin interactions to promote the formation of stable and monomodal distributed coacervates with a low value of PDI, as well as to obtain particles smaller than 800 nm. Moreover, previous studies did not consider the effect of the temperature, and all the coacervates were synthesized at 25°C. At this temperature, gelatin is organized in a coiled structure with triple helices in fibrous form. But, after increasing the temperature, this conformation changes[44] and therefore, the available charges to promote interactions with alginate are different. In fact, this strategy has been used in several occasions to obtain thermo-reversible and thermo-responsive nanogels for different applications.[43-45] It is these thermo-sensitive and thermo-reversible property of the gelatin A that can contribute to optimize the coacervate synthesis.[46,47] This study of the gelatin A structure, and its modification by temperature, has not been used yet to obtain a monodisperse and smaller coacervates system.

Besides, to the best of our knowledge, no rheological studies have been performed for this system in aqueous solutions. This study might be useful to elucidate if the interactions are strong to form a solution with solid-like behavior, or even to change its pseudoplasticity. This rheological study has been previously performed for different systems of mixtures of polysaccharide-gelatin.[48–52] As an example, rheology measurements of a mixture gelatin/HA indicated that, although gelatin can produce an entanglement effect and increases viscoelasticity, the behavior of HA predominates in a solution of both components.[48]

Additionally, the interactions between gelatin A and alginate can be further characterized through a static light scattering (SLS) measurement. This technique has not been used in references to report the characterization of coacervates, or the experimental condition effects on their synthesis. This might be due to the broad distribution and polydispersion index they have in particle size for the referenced results. This is another approach to understand coacervation mechanism in this study.

Therefore, the aim of this work is to perform a comprehensive study of the complex coacervation of alginate–gelatin A, based on DLS, SLS, optical microscopy turbidity, and rheology to identify the best conditions in terms of particle size, PDI, stability, salt concentration effect, viscoelastic behavior, and force in electrostatic interactions. Gelatin A is the chosen gelatin due to its isoelectrical point (IEP), which is affected by the acid pH to have a positive net charge.[53] This positive charge interacts better with the anionic polymer in order to create stronger electrostatic interactions and therefore more stable coacervates. Parameters, such as pH between 4 and 6[38,40] (not lower than 4 to avoid alginate dissociation), modified with acetic acid, gelatin–alginate volume ratio, and concentration will be studied.

Moreover, it is proposed that the gelatin A conformation in the coacervation process determines the coacervate stability and size. Since its conformation is inherently related to temperature, it is important to study how this process variable affects the coacervation mechanism. Also, the influence of a cooling–heating cycle is considered to determine the thermo-reversibility of these interactions. Finally, rheology measurements, oscillatory, and steady are performed to elucidate if the coacervates behavior is mainly solid, viscous, or if there is crossover between both regimes.

2 | EXPERIMENTAL

2.1 | Materials

Alginic acid sodium salt from brown algae (CAS 9005-38-3) with an average molecular weight around 150 kDa and a mannuronic acid to guluronic acid ratio of approximately 1.56, and gelatin from porcine skin powder type A (CAS 9000-70-8) with an average molecular weight of 163 kDa, with a gel strength of approximately 300 g Bloom were purchased from Sigma–Aldrich, Madrid, Spain. Also, acetic acid, glacial, ACS, 99.7+% was purchased from Thermo Fisher Scientific, Kandel, Germany. Moreover, a heating and stirring plate purchased from Fisher, Madrid, Spain, and an orbital shaker incubator ES20 from Biosan, Madrid, Spain, were used in order to keep coacervates at 37°C when necessary. Finally, a pH-Meter BASIC 20+ model purchased from Crison, Barcelona, Spain.

2.2 | Coacervates formation

Coacervates were synthesized by mixing two different aqueous solutions of gelatin A and alginate stirred overnight. Two temperatures (25 and 37°C) were used to produce the coacervation phenomenon. In this context, when the temperature was 37°C (this temperature was chosen because it is the physiological temperature), the gelatin solution was previously heated at 37°C to partially unravel its structure, using the heating stirring plate and controlling the temperature with a thermometric probe. After that, this temperature was kept constant during the mixing process. In this context, Figure 1 illustrates the different gelatin conformations depending on the pH and temperature. In this case, the selected experimental conditions indicated that the gelatin was found in fibers or partially unraveled.

Once alginate and gelatin A solutions were mixed following the proposed volume ratio (1:4–1:6), the pH was adjusted to

RIGHTSLINK

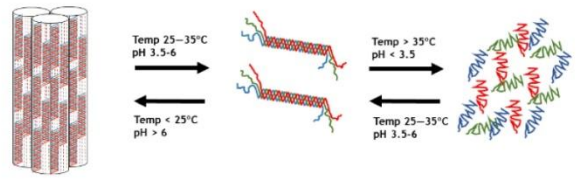

FIGURE 1 Gelatin structure configuration changes when controlling the temperature and pH-medium (adapted[42]).

TABLE 1 Dynamic light scattering results.

Run	Alginate conc. (% w/w)	Ratio alg–gel	pH	T (°C)	Z aver. (nm)	PDI
1	0.5	1:4	4	25	PF(*)	-
2				37	612 ± 205	0.21
3			5	25	402 ± 215	0.68
4				37	553 ± 182	0.17
5		1:5	4	25	PF(*)	-
6				37	750 ± 175	0.24
7			5	25	797 ± 224	0.63
8				37	561 ± 159	0.14
9		1:6	4	25	565 ± 214	0.69
10				37	685 ± 187	0.25
11			5	25	642 ± 234	0.59
12				37	360 ± 154	0.25
13	1.0	1:5	5	25	PF(*)	-
14				37	PF(*)	-
15	2.0	1:5	5	25	PF(*)	-
16				37	PF(*)	-

Note: (*) being PF precipitate formation.

the desired value with 0.5, 0.1, and 0.01 M solutions of acetic acid in order to prevent dilution problems while adjusting the desired pH values. This pH was selected between 4 and 6 due to the isoelectric point of the gelatin A, and the alginate pKa value, as stated previously. Coacervates samples were put under stirring with continuous pH measurement mode on pH-meter probe (previously calibrated with tampon solutions). Using this continuous measurement mode, it was possible to slowly add drops of the acetic acid solutions until the desired pH value was reached. Once it was adjusted, the coacervates samples were left under orbital shaking for 30 min at 25 or 37°C using an incubator.

In this context, the concentration of the gelatin A was always 0.5% w/w because a higher concentration of the gelatin did not produce a successful coacervation according to references.[38–40] Also, for a higher concentration of alginate (1.0% w/w and 2.0% w/w), only an alginate–gelatin A ratio of 1:5, since it was the optimal, as shown in Section 3. Finally, in order to study the thermo-reversibility of the heated coacervates at 37°C, the solution was cooled until 25°C, and then heated again until 37°C, keeping the pH constant. Table 1 (in results and discussion section) summarizes the experimental conditions of coacervation.

2.3 | Characterization in terms of optical microscopy, dynamic and SLS, and zeta potential measurements

Particle size and the aggregation of the coacervates are determined by DLS technique with a Zetasizer Nano (Malvern Instruments). Automatic attenuation was selected, and results were interpreted by number of particles per measurement. The peak integration method used by the equipment was the standard one. Moreover, the measurement angle was set at 173°. This same equipment was used to measure the zeta potential of the coacervates.

Moreover, coacervate samples synthesized at both temperatures (25 and 37°C) were taken to an optical microscope (Leica Optical compound light microscope DM1000) and were observed using the objective 100× and immersion oil. Single drops were poured in slides and adjusted first with the 40× objective. Afterwards, this objective

RIGHTSLINK

10991581, 2014, 8, Downloaded from https://onlinelibrary.wiley.com/doi/10.1002/pat.3134 by Universidad De Salamanca, Wiley Online Library on [05/11/2025]. See the Terms and Conditions (https://onlinelibrary.wiley.com/terms-and-conditions) on Wiley Online Library for rules of use; OA articles are governed by the applicable Creative Commons License

10991581, 2014, 8, Downloaded from https://onlinelibrary.wiley.com/doi/10.1002/pat.3134 by Universidad De Salamanca, Wiley Online Library on [05/11/2024]. See the Terms and Conditions (https://onlinelibrary.wiley.com/terms-and-conditions) on Wiley Online Library for rules of use; OA articles are governed by the applicable Creative Commons License

was removed and a drop of immersion oil was poured on the slide in order to create a film between it and the 100× objective that enables the extended zoom of the sample due to the change of the refractive index of the light in the medium (1.33 in oil and 1.00 in air). Once light and lenses were re-adjusted for the new objective, pictures were taken in IC Capture 2.4 software and further measured by IC Measure software, using a DFK MKU130 microscope camera of 13 megapixel.

SLS experiments were performed with the same Zetasizer Nano mentioned previously. This time the second virial coefficient (A2) was calculated. This parameter will characterize the electrostatic interactions that hold the coacervate system.

A2 is a thermodynamic parameter, which describes colloids stability as a balance between attraction and repulsion forces between the particles chains and the solvent. It is determined by the slope in the Debye equation, shown below:

$$\frac{K \cdot C}{R_\theta} = \frac{1}{MW} + 2 \cdot A2 \cdot C, \quad (1)$$

where K the Debye constant, C the sample concentration (mg/mL), R_θ the Rayleigh ratio (cm^{-1}), MW the average molecular weight (kDa), and $A2$ the second virial coefficient (mL mol/g).

Two series of coacervates were synthesized: One of them at 25°C while the other one was synthesized at 37°C, with pre-heated (partially unraveled) gelatin A. Experiments were done with coacervate solutions (1:5 and pH 5, for being optimal parameters) with the following concentration range: 1.5–6.5 mg/mL. This range allows to characterize the promotion of electrostatic interaction between gelatin A and alginate with increasing concentrations, until visible precipitation (higher than 6.5 mg/mL). The solutions were made following the previous procedure.

2.4 | Turbidity

Coacervates turbidity was measured by transmittance using a TurbiScan MA Classic model (Formulaction Scientific Instruments, France). The TurbiScan measures a 7.0 mL sample in the specific transparent lab tube inserted with its lid on. The backscatter sweep was also taken with every analysis of simple turbidity, determining whether the measurement was accurate or unstable with noisy signals.

This instrument was also used to characterize the salt concentration effect on coacervates synthesis. Coacervates at both synthesis temperatures (25 and 37°C) were added a small concentration of salt NaCl (50, 100, 150, and 200 mM) and their turbidity was measured to characterize the salt addition effect.

2.5 | Rheological analysis

The rheological properties of the coacervate samples were studied with a Rheometer AR 1500ex (TA Instruments, Madrid, Spain), equipped with an aluminum plate of 4-cm diameter and 1-mm gap. Both statistical and oscillatory flow analysis were performed. Coacervates were loaded on the Peltier and the temperature was set to the desired value, depending on the cold or heated formulation, at 25 and 37°C, respectively.

Statistical flow analysis consisted of a shear rate ramp from 0.1 to 200 s^{-1}. The controlled variable was the strain percentage at 2.0%, that was previously determined with a strain sweep at a frequency of 1 Hz. Afterwards, the results were fitted with the Cross model (Equation 1) obtaining as a result the different parameters of the equation.

$$\eta = \eta_\infty + \frac{\eta_0 - \eta_\infty}{1 + (K \times \dot{\gamma})^m}, \quad (2)$$

where η_0 the zero-shear-rate viscosity (Pa·s), η_∞ the infinity shear viscosity (Pa·s), K the consistency (s), and m the rate constant (dimensionless). All of these terms in the equation provide information about the rheological behavior of the solution, and therefore, the interactions within the system and its physico-chemical properties. Specifically, m is related to the power law relation between shear rate and shear stress in the shear thinning region, being $m = 0$ characteristic of Newtonian solutions, and K indicating the relaxation times, being its reverse the critical strain rate ($\dot{\gamma}_c$).

Oscillatory analysis was also performed on the samples with frequency sweeps, determining the evolution of the storage/elastic modulus (G'), and the loss/viscous modulus (G'') throughout the range of angular frequency from 0.5 to 500 s^{-1}. This evolution will indicate if the behavior of the coacervates is elastic- or viscous-like.

3 | RESULTS AND DISCUSSION

3.1 | Dynamic and SLS results

First results are concerning the effect of the different parameters on particle size, PDI, and stability of the coacervates and their electrostatic interactions. In this case, although not included in Table 1 (experimental conditions and DLS results), first experiments were performed with different ratios alginate–gelatin at 25°C with a pH of 7.

As was expected, precipitates were observed (Figure S1) due to the lack of required interactions alginate–gelatin A.

The coacervation was only produced after reducing the pH until acidic values (4–6) at 25°C, obtaining Tyndall effect (Figure S2). However, the PDI was always higher than 0.6 (as shown in Table 1), indicating the existence of at least a bimodal distribution (and sometimes even precipitates were observed). This is illustrated in Figure 2A,B for runs 7 and 11, respectively. This PDI, in spite of the successful coacervation, was always very high and strongly independent of the pH values (ranging from 4 to 5) and of the alginate–gelatin volume ratio. This phenomenon indicates an incomplete coacervation.

These results agree with the literature, since it is required an acidic pH around 4–6 to obtain coacervates.[42] The existence of a

RIGHTSLINK

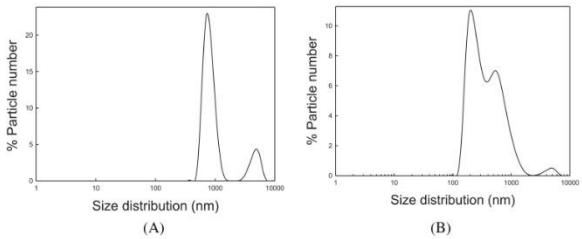

FIGURE 2 Bimodal particle distribution of (a) 1:5 and (b) 1:6 alginate: Gelatin ratio at pH 5 and 25°C.

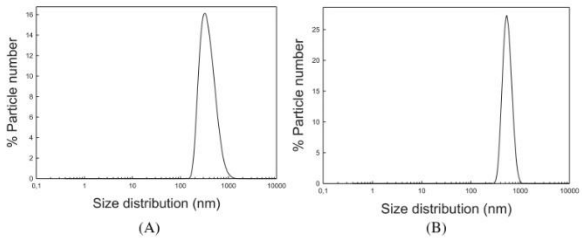

FIGURE 3 Unimodal size distribution for (a) 1:5 and (b) 1:6 alginate: Gelatin ratio at pH 5 and temperature 37°C with pre-heated gelatin at 37°C.

multimodal particle size distribution is explained due to the structure of the gelatin A at 25°C (fibers), which can partially prevent the interactions between all the available charges.

In order to test if the cause of the high PDI is the gelatin structure, same experiments were performed after heating the gelatin A solution until 37°C. This promotes its conformation change from fibers to a more unraveled structure, and a better mixing with the alginate, stablishing interactions at 37°C and pH reduction, with more functional groups available. This change induced the coacervation with reduced PDI values until 0.25 and lower (also shown in Table 1). This indicated the existence of a monodisperse particle size distribution, as illustrated in Figure 3A,B for the runs 8 and 12, respectively. In fact, the obtained size and PDIs were reduced in comparison with other results in literature.[38–40]

Moreover, the effect of the temperature was also proven to give better results when studying the autocorrelation function of the zeta sizer measurements (Figure S3).

Therefore, controlling the temperature is crucial to promote a monomodal coacervate system. In fact, some changes observed were also macroscopically visible, due to the correct synthesis in certain coacervates runs from precipitation at 25°C to a homogeneous sample at 37°C showing Tyndall effect (Figure S4).

Also, reaching a pH lower than 6 is a key parameter due to the isoelectric point (IEP) of the gelatin A. Values of pH under the IEP make the net charge of the protein (gelatin A) positive. In contrast with the negatively charged behavior of the alginate functional groups in aqueous solutions, this promotes the electrostatic interaction between both components, inducing coacervation.

Consequently, the higher the pH value is, the less coacervates will be formed, and the more unstable the system will be. Although the best results were obtained at a pH 5, there is not a clear effect of the pH in the particle size detected by DLS, since particle sizes are always between 400 and 700 nm in number measurements. Let it be noted that intensity and volume measurements did show similar results that the ones in number, and therefore, no added commentary on these measurements is made (see Figure S5). These particle distributions are explained by the gelatin A structure mentioned in the introduction. A solution with a homogeneous distribution of unraveled gelatin with more functional groups available for electrostatic interactions promotes the formation of similar size coacervates with the alginate.

A similar phenomenon was observed for the alginate–gelatin A ratio as long as the ratios are from 1:4 to 1:6 (particles always between 400 and 700 nm). Results indicated that ratios alginate–gelatin A below 1:4 and higher than 1:6 are not suitable to induce coacervation (Figure S3). On the one hand, high values of PDI were obtained for a ratio lower than 1:4 because there are not enough gelatin A functional groups available to interact with the alginate, and this allows the water to interfere with the coacervation phenomenon.[38]

On the other hand, due to the opposite effect, aggregates were found for a ratio higher than 1:6. The concentration of gelatin A at

RIGHTSLINK

10991581, 2014, 8, Downloaded from https://onlinelibrary.wiley.com/doi/10.1002/pat.3154 by Universidad De Salamanca, Wiley Online Library on [05/11/2024]. See the Terms and Conditions (https://onlinelibrary.wiley.com/terms-and-conditions) on Wiley Online Library for rules of use; OA articles are governed by the applicable Creative Commons License

this point is high, inducting these gelatin structures to bond amongst them, reorganizing the configuration to a more complex, non-soluble structure.[38] This phenomenon can be observed in the Figure S6.

Furthermore, additional experiments were performed to induce the coacervation with higher concentrations of alginate and gelatin A. Runs 13–16 indicate the formation of precipitates at these experimental conditions. This was attributed to the number of electrostatic interactions between both polymer–protein and protein–protein, promoting the formation of a high number of coacervates with a great difference in size.

Observing the improvements in results when pH and temperature act separately, it is clear that both parameters must be considered to induce a monomodal and stable coacervate system, heating up the solutions to partially unravel the gelatin structure, and lowering the pH values. These conditions will promote the electrostatic interactions between the functional groups of the partially unraveled protein and the alginate. Therefore, it can be concluded that it is possible to synthesize coacervates in a size range between 350 and 700 nm approximately with low PDI values, as long as temperature and pH are both controlled simultaneously.

Concluding, the best volume ratios are 1:4 or 1:5, due to the lower PDI values. Heating should be always applied (37°C), and pH values should be lowered to a value that ranges from 4 to 6 to start the coacervation. In order to further prove this point and study the temperature effect, optical microscopy was used to characterize two samples of the coacervates: 1:5 volume ratio, pH 5 and both synthesis temperatures (25 and 37°C).

Both of these samples were taken to an optical microscope and clear differences between their structures were observed. These images can be found in the Figures S7 and S8. Coacervates at 25°C showed a more polydisperse conformation in Figure S7a, with various size ranges of particles and even aggregates in certain zones, which are part of the gelatin A structure that has not been unraveled and therefore has not been able of stablish electrostatic interactions with alginate groups.

However, 37°C sample showed a more monodisperse particle distribution in Figure S7b, pointing that temperature effect is, once again, essential in order to obtain a homogeneous particle distribution due to a more complete coacervation process between the partially unraveled gelatin A structure and alginate. Nevertheless, it can also be observed that the image of coacervates synthesized at 25°C shows a higher definition of the particles than the 37°C synthesized coacervates sample. This is due to the difference in particle size slightly interfering with the detection limit of the optical microscope, and it is further proven in Figure S8. This figure shows the particles detected in both samples at 25°C (Figure S8a) and 37°C (Figure S8b) measured by the software mentioned previously. In this, image is verified that the samples do have the same size particle distribution detected by the DLS, and also further proves the monodispersity of those coacervates synthesized at 37°C, with a high percentage of the measurements entering the particle size 400–600 nm.

All of these results also confirm that we have achieved smaller coacervates droplets that the ones reported in literature by the same technique.[54] However, it was observed that after cooling, PDI and size of the coacervates were wider. Therefore, the effect of the temperature on the coacervates was also tested by carrying out daily repetitive cooling–heating cycles from 25 to 37°C during 7 days at a constant pH 5. The results showed that PDI values were kept still throughout the days after the heating stage. The size, however, slowly increased until approximately 1 μm. This size was constant for 5–7 days.

This can be explained due to the hysteresis cycle of the gelatin A structure that can be the reason why new interactions occur when heating the solution. Consequently, this transition between the different gelatin conformations (from helices fibers to a more disentangled linear structure) applies to the aggregation of the coacervates.

Results shown below, in Figure 4A,B, determine 5 days as a stability cycle for coacervates. Results for the sixth day showed particles determined at both too low and high size distribution (less than 100 nm and more than 5 μm, respectively), and a great PDI increase.

SLS experiments were also performed to characterize the electrostatic interactions between gelatin A and alginate. Following the methodology procedure, a Debye plot was made to show the results on two coacervates series.

Both series were synthesized coacervates at 1:5 volume ratio and pH 5, for the concentration range proposed, due to previous results that show these as optimal values for stability and particle distribution. Let it also be noted that the concentration reported in references is 5.0 mg/mL.[38–40] The Debye plot obtained for these experiments is shown in Figure 5 below:

The Debye plot represents the term $K \cdot C/R_\theta$ (1/kDa) versus C (mg/mL) from Equation 1. Therefore, the inverse of the intercept is the molecular weight (MW) of the coacervates and the slope will determine the second virial coefficient ($A2$).

Interactions particle–particle will be stronger than particle-solvent if this virial coefficient is negative. However, the interactions particle-solvent will prevail if the coefficient is positive. The tendency line equations provide this information.

First, both tendency lines show a coefficient of determination (R^2) of 0.85, which implies a good and valid correlation of the mathematical adjustment. These equation adjustments include the concentration range of our experimental values tested with DLS, confirming once again interactions in the concentration of 0.5% w/w.

The second virial coefficient is positive for the 25°C synthesized coacervates ($4.16 \times 10^{-4} \pm 6.62 \times 10^{-5}$ mL mol/g^2) meanwhile the run for 37°C synthesized coacervates shows a negative one ($-1.69 \times 10^{-4} \pm 2.88 \times 10^{-5}$ mL mol/g^2). This implies a change in the interaction forces between particles when the temperature increases. The heated coacervates have stronger electrostatic interactions between the compounds, meanwhile the cold ones have a stronger interaction with the solvent. This change contributes to a more stable coacervate system provided by the only difference of the pre-heated gelatin A and coacervation temperature rise to 37°C. Therefore, the temperature effect is proven once again. To conclude, another technique characterizes the electrostatic interactions that hold the coacervate system, and proves the benefits of the heated synthesis.

RIGHTSLINK

10991581, 2014, 8, Downloaded from https://onlinelibrary.wiley.com/doi/10.1002/pat.3514 by Universidad De Salamanca, Wiley Online Library on [05/11/2024]. See the Terms and Conditions (https://onlinelibrary.wiley.com/terms-and-conditions) on Wiley Online Library for rules of use; OA articles are governed by the applicable Creative Commons License

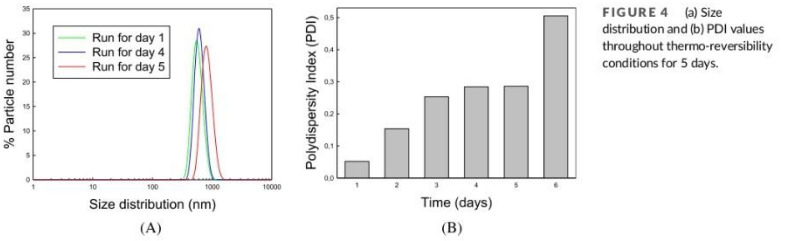

FIGURE 4 (a) Size distribution and (b) PDI values throughout thermo-reversibility conditions for 5 days.

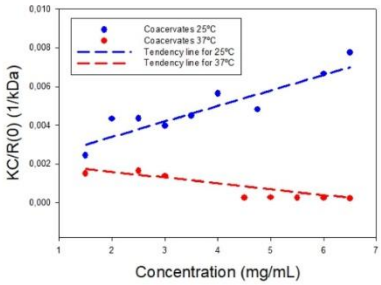

FIGURE 5 Debye plot performed by static light scattering on coacervates 1:5 and pH 5 at 25°C (blue) and 37°C (red), and their line tendencies.

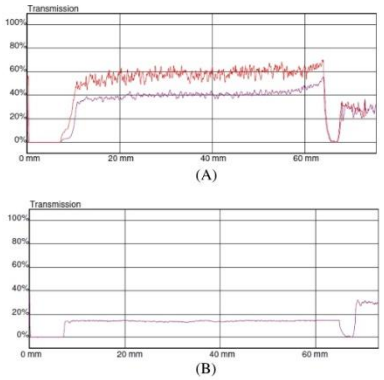

FIGURE 6 Transmission measured through samples of coacervate (a) 1:5 at 25°C (pH 4 [red] and pH 5 [purple]) and (b) 1:5 at 37°C and pH 5. This figure represents the light transmission percentage in the *y*-axis versus the height of the sample tube in the *x*-axis.

TABLE 2 Zeta potential results for coacervates with 1:5 alginate: Gelatin A volume ratio.

25°C		37°C	
pH 6	−25.66 ± 1.20 mV	pH 6	−24.00 ± 1.15 mV
pH 5	−13.76 ± 0.72 mV	pH 5	−17.90 ± 0.44 mV
pH 4	−13.76 ± 0.70 mV	pH 4	−16.73 ± 0.58 mV

Finally, zeta potential measurements were performed in order to characterize the systems surface net charge and further prove the temperature and pH effect on coacervate synthesis. The results are presented in Table 2.

These results in Table 2 confirm the protonation of the gelatin A when pH values decrease. This protonation of all the amino functional groups, whether they are in a full closed (25°C) or partially unraveled (37°C) coil. As proposed the isoelectric point of gelatin A is found between the values of 6 and 4, more concretely between 5 and 6. When protonation occurs, the net charge of the molecules will be more positive (thus, less negative).

Moreover, it has been stated that for several colloidal dispersions, a generalized value of less than −15 mV or more than 15 mV provides stability throughout time.[4] For this measurements, it is once again confirmed that a heating stage implementation to the synthesis process develops a more stable colloidal system. Table 2 results show that zeta potential is less than 15 mV for coacervates synthetized at pH 6 at both temperatures. These values suggest that there are enough electrostatic forces to provide stability to the colloidal system. For 25°C synthesized coacervates this could be the reason why occasionally precipitates were observed and certainly why the polydispersity index reported are higher, since aggregation amongst them could happen, as shown in the microscope images (Figures S7 and S8). However, it is important to note that not only this forces determine the stability

RIGHTSLINK

10991581, 2014, 8, Downloaded from https://onlinelibrary.wiley.com/doi/10.1002/pat.3154 by Universidad De Salamanca, Wiley Online Library on [05/11/2024]. See the Terms and Conditions (https://onlinelibrary.wiley.com/terms-and-conditions) on Wiley Online Library for rules of use; OA articles are governed by the applicable Creative Commons License

and aggregation in the colloidal dispersion of the samples. The interaction particle–particle or particle–medium is also important to analyze, and this is shown and commented in following results in this section.

3.2 | Turbidimetry results

Figure 6 shows the light transmitance throughout the cell used for tubidity measurement. *Y*-axis represents the values of transmittance along the tube that contains the coacervates sample where the height of tube is represented in *x*-axis in mm. Big steps are observed at the first measurements because it corresponds to bottom plug (0–10 mm) and another one is observed around 60 mm because it corresponds to the top of the sample (interphase gas–liquid).

This figure illustrates the results for the coacervate samples at 25°C (1:5 at pH 4 and 5) and 37°C (1:5 at pH 5). As it can be seen, the transmittance for coacervates at 25°C (60%) is far higher than the transmittance at 37°C (less than 20%), indicating how the temperature is a key parameter to obtain coacervates causing more turbidity. According to different studies, coacervates that showed more turbidity tend to be more stable.[1,4,38–40] This is due to the Tyndall effect provoked by the coacervates formed, which are in suspension in the sample bulk. The concentration of these coacervates promotes the turbidity of the sample, being able to absorb more light emitted by the turbidimeter. This is translated as a lower transmittance percentage, due to the lower percentage of light received in the turbidimeter detector. This light absorbance is caused by stable coacervates and their concentration in the bulk. Therefore, the more turbidity a sample shows, the more stable their coacervates will be.

Furthermore, the straight line in Figure 6B shows a high stability of the 37°C synthesized coacervates, meaning, a measurement with little to no noise, and a backscatter straight line. This phenomenon is not found in Figure 6A showing an unstable solution. Once again, this is translated into a homogeneous turbidity throughout the sample height in the sample tube, meaning the coacervates are more likely to be stable, monodisperse, and the concentration of these is balanced for the whole sample bulk.

Tyndall effect was more pronounced in the systems with no precipitates and where more coacervates were synthesized. The promotion of electrostatic interactions due to the gelatin A partially unraveled structure provokes a higher concentration of particles that presents a higher turbidity. This explains why the more stable systems present more turbidity. It is also important to indicate that a similar trend was observed for the different runs at different pHs and ratios (always a higher stability at 37°C than 25°C). Adding to these conclusions, the different turbidity of the samples agrees with the results that were obtained with dynamic and SLS.

3.3 | Salt effect on coacervates

As previously stated, the salt effect was also studied by turbidimetry. Small amounts of NaCl (50, 100, 150, and 200 mM) were added to the coacervates previously shown (Figure 6) for turbidimetry results (1:5 volume ratio, pH 5, and temperatures of 25 and 37°C). The salt effect was clearly visible at a macroscopic scale, since aggregates were progressively formed when the salt concentration increased in both temperatures. This is shown in Figure S9.

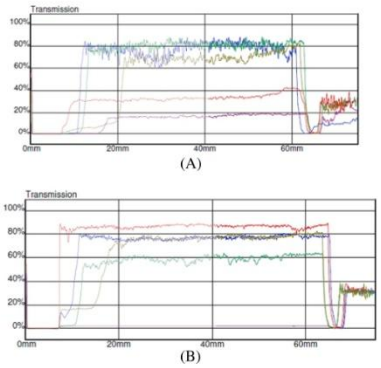

FIGURE 7 Transmission measurements of turbidity analysis of coacervates 1:5 and pH 5 and (a) 25°C synthesis with NaCl (mM): 0 (purple), 50 (red), 100 (gray), 150 (green), and 200 (blue); (b) 37°C synthesis with NaCl (mM): 0 (purple), 50 (green), 100 (gray), 150 (blue), and 200 (red). This figure represents the light transmission percentage in the *y*-axis versus the height of the sample tube in the *x*-axis.

According to the turbidimetry results, coacervates at 25°C showed precipitates at all salt concentrations, being the one without salt the only stable one. As salt concentration increased, so did the transmittance, indicating less stability of the coacervates. Also let it be noted that back scattering measurements went higher and more unstable as salt concentration increased. These backscatter measurements are shown in Figure S10a. This explains all the noise in the measurements signals reported in Figure 6A,B for the NaCl added samples. The precipitates formation causes a disparity in the transmittance of the sample throughout the tube height, since the concentration of the reagents will no longer be balanced. Thus, the more unstable is the sample, the more unstable will be the turbidity measurement. Moreover, the precipitates formation reduces the stable coacervates concentration, implying there will be less Tyndall effect, therefore less turbidity, more transmittance percentage, and less stability.

Coacervates (synthesized at 37°C) showed the same results when it came to salt effect, since the only visibly stable formulation was the one with no salt added. This is shown in transmittance measurements being more stable than the 25°C synthesized coacervates ones, and the backscatter measurements, shown in Figure S10b. The main results obtained by turbidimetry are shown in Figure 7 below.

RIGHTSLINK

10991581, 2014, 8, Downloaded from https://onlinelibrary.wiley.com/doi/10.1002/pat.3134 by Universidad De Salamanca, Wiley Online Library on [05/11/2024]. See the Terms and Conditions (https://onlinelibrary.wiley.com/terms-and-conditions) on Wiley Online Library for rules of use; OA articles are governed by the applicable Creative Commons License

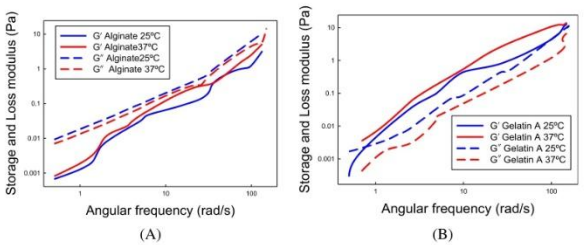

FIGURE 8 Oscillatory rheological analysis on (a) alginate and (b) gelatin A, both cold (25°C) and heated (37°C).

Salt effect on coacervates samples has been previously reported as a Debye length reducer, filtering repulsive interactions between the oppositely charged compounds in a system.[43] This can sometimes be a beneficial effect, like promoting fish gelatin and alginate coacervates formation as reported by Derkach et al., as long as salt concentration was lower than 50 ppm.[43] However, fish gelatin is a gelatin characterized to be significantly more monodisperse and smaller (13–15 nm) than the gelatin A that is used in this study. Gelatin A was characterized to have multiple peaks of bigger size distributions. Therefore, filtering interactions between gelatin A and alginate will promote the aggregates formations that will eventually precipitate, rather than coacervation process. Also, this effect has been reported as coacervation inhibitor when using inorganic acids to regulate pH. HCl would not induce correctly coacervation whereas acetic acid did because of the effect of diluted ions in water, preventing electrostatic interactions to happen.[42]

Nonetheless, it can be concluded that, once again, temperature must be controlled for an optimized synthesis. This is due to the presence of more stable solutions, even with precipitates, at 37 than 25°C. This was also proven by DLS measurements of these samples, being the PDI increased as the salt concentrations were. PDI values for 0, 50, 100, 150, and 200 mM NaCl added were: 0.63, 0.65, 0.76, 0.91, and 1.00 (at 25°C), and 0.14, 0.48, 0.58, 0.71, and 1.00 (at 37°C).

3.4 | Rheology characterization

Rheological oscillatory and statistical flow tests were performed on the samples to study the influence of the different experimental parameters on their elastic and viscous behavior.

3.4.1 | Oscillatory analysis

First, oscillatory analysis was performed on solutions of alginate and gelatin A (0.5% w/w both), at 25 and 37°C. Results are illustrated in Figure 8A,B. On the one hand, it can be seen how the storage modulus (G′) of the gelatin increases with the temperature whereas the viscous one decreases.

Furthermore, for both conditions the storage modulus is always higher, indicating the slightly elastic nature of the solutions. The change on the spectrum of the gelatin is caused by the change on the conformation of the gelatin (from organized fibers to a partially unraveled structure). In this unraveled conformation, there are more available charges that can interact between them, increasing therefore the storage modulus. This correlation of G′ values increasing when aqueous gelatin solutions are heated is supported by References 26,44.

On the other hand, alginate samples show a viscous-like behavior, since its loss modulus (G″) prevails over its storage modulus. This nature is not changed but restricted when heating due to an elastic modulus growth as well as viscous modulus decrease. Overall, it is demonstrated that heating these samples promotes their solid-nature, regardless of their natural behavior in aqueous solutions. This increase of the storage modulus is what probably induce a better coacervation process when mixing these solutions under heat.

Besides, the fact that the gelatin volume exceeds by 4–6 times the alginate volume, it is likely to predict the coacervates solid behavior.

Following these conclusions, the different moduli of the coacervates at different pH and temperature conditions were also determined. The results obtained for these experiences are illustrated in Figure 9A,B. It is possible to observe how the storage modulus increases with the temperature since the coacervate was formed due to the interactions alginate–gelatin A. As previously stated, the volume ratio of the solutions predicts their elastic nature.

Furthermore, storage modulus is always higher than the viscous modulus for all the experimental conditions, indicating the existence of interactions between both compounds being influenced mainly by the gelatin A presence. Figure 9B also highlights how the pH did not have an important influence on the storage modulus, since the values for these are similar for the different experimental. Nevertheless, there are slightly better results for pH 5.

However, in Figure 9A, the temperature is again proven to promote elasticity and stabilize the coacervate solutions, thus, pointing this parameter out as a fundamental one in the synthesis process. Finally, these results also indicated that the interactions are not strong enough to form a strong gel structure, since the storage modulus depends on the frequency.

RIGHTSLINK

10991581, 2014, 8, Downloaded from https://onlinelibrary.wiley.com/doi/10.1002/pat.3154 by Universidad De Salamanca, Wiley Online Library on [05/11/2024]. See the Terms and Conditions (https://onlinelibrary.wiley.com/terms-and-conditions) on Wiley Online Library for rules of use; OA articles are governed by the applicable Creative Commons License

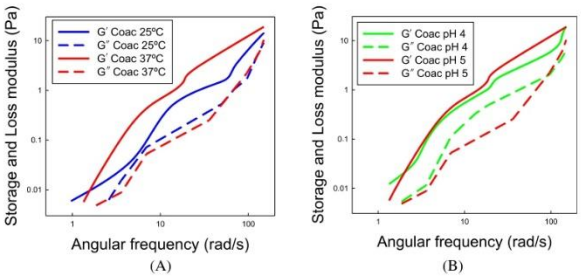

FIGURE 9 Oscillatory rheological analysis on coacervates with different (a) temperatures (cold at 25°C and heated at 37°C) and pH 5 and (b) pH values (at 4 and 5) and 37°C.

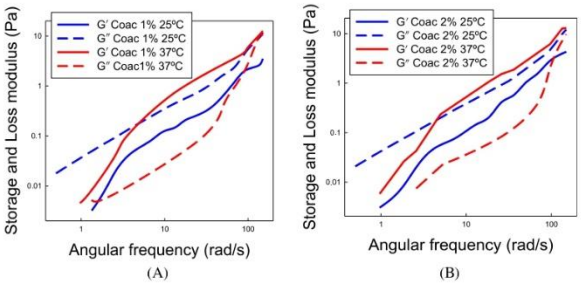

FIGURE 10 Oscillatory rheological analysis on concentrated coacervates of (a) 1% w/w and (b) 2% w/w, both cold (25°C) and heated (37°C) at pH 5.

Results with higher concentrations of gelatin and alginate (and coacervates) were also performed in order to study tendencies among the interactions further. This is motivated by the weak interactions detected in the results, due to the diluted character of the solutions. The results can be observed in Figure 10A,B, choosing a pH value of 5 due to present the best results. First, the solutions of gelatin change their tendency to a liquid-like behavior in the cold samples (25°C) as it is shown in Figure S11. However, this change in viscoelastic nature did not happen when studying alginate solutions. In this case, the viscous behavior was maintained, regardless the increasing concentration. Nevertheless, the temperature effect does not change, promoting the solid nature of the gelatin solutions until switching it back to a solid-like behavior (G′ values prevail, again, over G″ values). These results also predict the coacervates behavior, same as explained for lower concentrations.[49,50]

When the coacervation was induced on 1.0% and 2.0% w/w solutions at high temperature after reducing the pH to 5, due to previous results, the storage moduli also increased, highlighting that interactions occurred. In spite of this fact, precipitates and high values of PDI at 1.0% and 2.0% w/w concentrations were obtained. This phenomenon can be explained, taking into account that inducing interactions can increase the storage modulus, but also can promote precipitation and multimodal particle size.

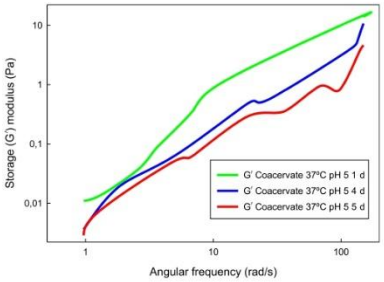

FIGURE 11 Oscillatory rheological analysis on storage G′ modulus from heated (37°C) coacervate at pH 5 throughout the days (stability).

In fact, storage moduli of the systems with concentrations of 0.5% w/w are similar to the storage moduli for 1.0% and 2.0% w/w, indicating that both systems have a similar number of interactions, in spite of the concentration. However, the remaining solids in 1.0% and

RIGHTSLINK

10991581, 2014, 8, Downloaded from https://onlinelibrary.wiley.com/doi/10.1002/pat.3154 by Universidad De Salamanca, Wiley Online Library on [05/11/2024]. See the Terms and Conditions (https://onlinelibrary.wiley.com/terms-and-conditions) on Wiley Online Library for rules of use; OA articles are governed by the applicable Creative Commons License

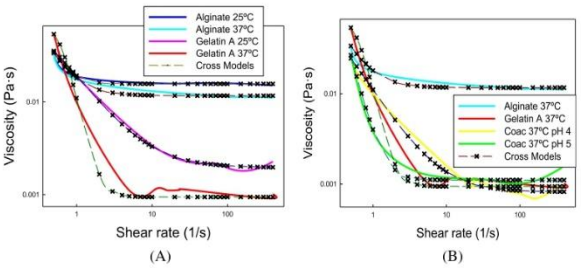

FIGURE 12 Static flow rheological analysis on (a) alginate and gelatin A cold (25°C) and heated (37°C), with their adjusted cross models (Equation 1) and (b) heated (37°C) alginate, gelatin A and coacervates solutions at 1:5 volume ratio and pH 4 and 5, with their adjusted cross models (Equation 1).

TABLE 3 Cross model parameters.

Solution	Temp (T, °C)	Zero-rate viscosity (η_0, Pa·s)	Consistency (K, s)	Critical strain ($\dot{\gamma}_c$, s^{-1})
Alg (0.5% w/w)	25	0.08	2.83	0.351
Alg (0.5% w/w)	37	0.34	7.16	0.139
Gelatin (0.5% w/w)	25	0.15	5.94	0.168
Gelatin (0.5% w/w)	37	0.07	1.58	0.632
Coacer (run 10)	37	0.28	3.25	0.306
Coacer (run 12)	37	0.41	1.28	0.781

2.0% w/w solutions cannot interact, resulting in the precipitation of small amounts of solids.

Oscillatory analyses were also performed on coacervates after the cooling–heating cycles. Figure 11 shows the change of the mechanical spectrum of the coacervates solutions after the respective cycles (1, 4, and 5 days). These results confirm the conclusions mentioned in the DLS section previously. This means, the properties for coacervates are lost during cold cycles (25°C), but recovered after heating (37°C). In this rheological study, the property is the elastic behavior (G′ values).

As it shows, the first day kept the initial rheological behavior of the solution (high storage modulus). However, this slightly predominant solid nature decreases after 4 days (4 cooling–heating cycles). This means the solution has a stronger tendency towards a liquid-like behavior at 25°C. Figure 10 shows how the elastic properties gradually decreases as more cycles are performed. This reflects the interactions between gelatin A and alginate decrease with time, due to possible re-assembly of the gelatin structure during the cooling stages.

The last mechanical spectrum is attributed to the hysteresis cycle of the cooling–heating of gelatin A that can induce different interactions (the transition between the different conformation of gelatin A structure).

It can be concluded that oscillatory results showed an increase of the elastic modulus when the synthesized coacervates were formed with a narrow PDI and proper values of turbidity. This phenomenon is due to the induced interactions, controlled by the temperature effect and the partial unraveling of gelatin A structure. Oscillatory analyses also indicate how the coacervates stability cannot be extended for more than 4–5 days.

Adding to previous DLS results, the G′ measurements for the sixth day presented significant unstability and value drops from the previous day. This characterized the end of the hysteresis cycle, since the coacervates properties are not recovered after the sixth heating cycle.

3.4.2 | Statistical flow analysis

Figure 12A,B and Table 3 show different viscosity-shear rate diagrams, as well as some of the obtained parameters after fitting the experimental results with Cross model, corresponding with Equation 2.

In Table 3, cold solutions (25°C) have a similar behavior in terms of pseudoplasticity, since their critical strain rates and zero-rate viscosities are almost identical. For all the solutions, a Newtonian plateau was obtained at large velocities of deformation (infinity shear viscosity close to 0). Moreover, a pronounced shear-thinning region was found at the beginning of the measurements for all the solutions due to the alginate and gelatin A structures. Table 3 also indicates how the temperature effect slightly modifies the values of the Cross model's parameters.

The formation of the coacervates, although increasing the zero-rate viscosity, did not modify significantly the pseudoplastic behavior of the polymers alone, showing a similar behavior in both of them. Zero-rate viscosities and critical strain rates are again similar, and are mainly independent of the temperature. Although the temperature is

RIGHTSLINK

10991581, 2014, 8, Downloaded from https://onlinelibrary.wiley.com/doi/10.1002/pat.3154 by Universidad De Salamanca, Wiley Online Library on [05/11/2024]. See the Terms and Conditions (https://onlinelibrary.wiley.com/terms-and-conditions) on Wiley Online Library for rules of use; OA articles are governed by the applicable Creative Commons License

determined as a factor that can affect the synthesized coacervates, statistical analyses did not provide a significant information concerning coacervates formation.

Furthermore, it is possible to observe the difference the pH makes in the coacervation process. Figure 12B highlights that the curve at pH 5, (best experimental conditions according to size and PDI), has an intermediate shape between the alginate and gelatin A behaviors. This phenomenon does not occur for pH 4 (shape of the curve similar to the gelatin one due to its excess).

4 | CONCLUSIONS

Alginate–gelatin A complex coacervation has been studied with dynamic and SLS, turbidimetry, and rheology. Different experimental parameters, such as alginate–gelatin A volume ratio, pH, and a previous gelatin A solutions heating (37°C) have been considered.

Experimental results indicated that a gelatin preheating with a pH reduction is required to form unimodal coacervate solutions. This preheating is mandatory to change gelatin A structure in order to facilitate the subsequent interactions between gelatin A and alginate at a lower pH, inducing coacervation.

Moreover, the alginate–gelatin A volume ratio and their respective concentrations must be controlled to reduce the PDI of the coacervates as well as the formation of precipitates. In fact, a particle size between 200 and 600 nm with a PDI of around 0.20 can be obtained depending on the experimental conditions (alginate–gelatin A volume ratio of 1:5 with a pH of 5 and a gelatin preheating at 37°C were the best experimental conditions).

Not only size distribution and PDI were proven to better with temperature, but also the electrostatic interactions between the compounds, even observing differences by optical microscopy. SLS measurements showed a negative second viral coefficient for the coacervate system when heated at 37°C, which highlighted stronger forces among particles than with the solvent.

It was also highlighted that the coacervates have to be heated again to recover their properties at 37°C (showing thermo-reversibility) because cooling stages increased their size and PDI. However, this cycle can be also performed for 4–5 days since the size increased every day due to the hysteresis cycle of the gelatin A structure, modifying the interactions. Results were confirmed also with rheology and its storage modulus.

Oscillatory analysis also highlighted the gelatin A pre-heating importance in coacervates synthesis, even changing the solutions from a liquid-nature to a solid-nature. Furthermore, these analyses confirmed the temperature to be an elasticity enhancer for the coacervates. However, statistical analysis, and also the Cross model, did not indicate significant changes amongst the different solutions, as presented in Table 3.

Besides, turbidimetry was also used to characterize the importance of the temperature effect and the disadvantages of the salt effect on this coacervates, resulting in precipitates when NaCl was added.

Therefore, a correct combination of pH, gelatin A preheating, as well as alginate–gelatin volume ratio, and their concentrations must be taken into account to synthesize in a reproducible way stable coacervates with a proper particle size and PDI, strong electrostatical forces, and elastic behavior.

ACKNOWLEDGMENTS

Marcos Blanco-López acknowledges the funds from the program "University of Salamanca - Banco Santander Ayudas para financiar contratos predoctorales."

CONFLICT OF INTEREST STATEMENT

The authors declare no conflicts of interest.

DATA AVAILABILITY STATEMENT

The data that supports the findings of this study are available in the supplementary material of this article.

ORCID

Antonio Tabernero https://orcid.org/0000-0003-1141-6629

REFERENCES

1. Sing CE, Perry SL. Recent progress in the science of complex coacervation. *Soft Matter*. 2020;16:2885-2914.
2. Astoricchio E, Alfano C, Rajendran L, Temussi PA, Pastore A. The wide world of coacervates: from the sea to neurodegeneration. *Trends Biochem Sci*. 2020;45:706-717.
3. Nakashima KK, Vibhute MA, Sprujit E. Biomolecular chemistry in liquid phase separated compartments. *Front Mol Biosci*. 2019;6:21-29.
4. Comert F, Malanowski F, Azarikia PL, Dubin PL. Coacervation and precipitation in polysaccharide–protein systems. *Soft Matter*. 2016;113:4154-4161.
5. Xue C-H, Shi M-M, Chen H-Z, Wu G, Wang M. Preparation and application of nanoscale microemulsion as binder for fabric inkjet printing. *Colloids Surf A Physicochem Eng Asp*. 2006;287:147-152.
6. Kim S, Huang J, Lee Y, et al. Complexation and coacervation of like-charged polyelectrolytes inspired by mussels. *Proc Natl Acad Sci U S A*. 2016;113:E847-E853.
7. Lazko J, Popineau Y, Legrand J. Soy glycinin microcapsules by simple coacervation method. *Colloids Surf B Biointerfaces*. 2004;37:1-8.
8. Bungenberg de Jong HG, Krujit HR. Potentialities of the poly(aminoethyl methacrylate) p(AMA) as gelatin-like polymer in complex coacervation. *Proc Acad Sci Amsterdam*. 1929;32:849-856.
9. Bhattacharya A, Niederholtmeyer H, Podolsky KA, et al. Lipid sponge droplets as programmable synthetic organelles. *Procl Natl Acad Sci USA*. 2020;117:18206-18215.
10. Poudyal RR, Pri Cakmak F, Keating CD, Bevilacqua PC. Physical principles and extant biology reveal roles for RNA-containing membraneless compartments in origins of life chemistry. *Biochemistry*. 2018;57:2509-2519.
11. Polk A, Amsden B, Yao D, Peng T, Goosen MFA. Controlled release of albumin from chitosan-alginate microcapsules. *J Pharm Sci*. 1994;83:178-185.
12. Wen S, Alexander H, Inchikel A, Stevenson WTK. Microcapsules through polymer complexation: part 3: encapsulation and culture of human Burkitt lymphoma cells in vitro. *Biomaterials*. 1995;16:325-335.

RIGHTSLINK

10991581, 2024, 8, Downloaded from https://onlinelibrary.wiley.com/doi/10.1002/pat.6514 by Universidad De Salamanca, Wiley Online Library on [05/11/2024]. See the Terms and Conditions (https://onlinelibrary.wiley.com/terms-and-conditions) on Wiley Online Library for rules of use; OA articles are governed by the applicable Creative Commons License

13. Johnson NR, Ambe T, Wang Y. Lysine-based polycation:heparin coacervate for controlled protein delivery. *Acta Biomater*. 2014;10:40-46.
14. Chu H, Gao J, Chen C-W, Huard J, Wang Y. Injectable fibroblast growth factor-2 coacervate for persistent angiogenesis. *Procl Natl Acad Sci USA*. 2011;108:13444-13449.
15. Lim ZW, Ping Y, Miserez A. Glucose-responsive peptide coacervates with high encapsulation efficiency for controlled release of insulin. *Bioconjug Chem*. 2018;29:2176-2180.
16. Tang JD, Caliari SR, Lampe KJ. Temperature-dependent complex coacervation of engineered elastin-like polypeptide and hyaluronic acid polyelectrolytes. *Biomacromolecules*. 2018;19:3925-3935.
17. Ulubayram K, Cakar AN, Korkusuz P, Ertan C, Hasirci N. EGF containing gelatin-based wound dressings. *Biomaterials*. 2001;22:1345-1356.
18. Chu H, Chen C-W, Huard J, Wang Y. Neural stem cells encapsulated in a functionalized self-assembling peptide hydrogel for brain tissue engineering. *Biomaterials*. 2013;34:1747-1756.
19. Chen WC, Lee BG, Park DW, et al. Controlled dual delivery of fibroblast growth factor-2 and interleukin-10 by heparin-based coacervate synergistically enhances ischemic heart repair. *Biomaterials*. 2015;72:138-151.
20. Xing F, Cheng G, Yi K, Ma L. Nanoencapsulation of capsaicin by complex coacervation of gelatin, acacia, and tannins. *Appl Polym Sci*. 2005; 96:2225-2229.
21. Dickinson E. Colloid science of mixed ingredients. *Soft Matter*. 2006; 2:642-652.
22. Noel TR, Krzeminski A, Moffat J, Parker R, Wellner N, Ring SG. Quartz crystal microbalance with dissipation monitoring: enabling real-time characterization of biological materials and their interactions. *Carbohydr Polym*. 2007;70:393-405.
23. Haug IJ, Draget KI, Smidsrod O. Physical behaviour of fish gelatin-κ-carrageenan mixtures. *Carbohydr Polym*. 2004;56:11-19.
24. Montilla A, Casal E, Moreno J, Belloque J, Olano A, Corzo N. Isolation of bovine β-lactoglobulin from complexes with chitosan. *Int Dairy J*. 2007;17:459-464.
25. Ward AG, Courts A. *The Science and Technology of Gelatin*. Academic Press; 1977:73-105.
26. Djabourov M, Leblond J, Papon P. Gelation of aqueous gelatin solutions. I structural investigation. *J Phys France*. 1988;49:319-332.
27. Veis A, Cohen J. Engineering the multiscale complexity of vascular networks. *Nature*. 1960;186:720-725.
28. Boedtker H, Doty P. A study of gelatin molecules, aggregates and gels. *J Phys Chem*. 1954;58:968-983.
29. Yang J-S, Xie Y-J, He W. Research progress on chemical modification of alginate: a review. *Carbohydr Polym*. 2011;84:33-39.
30. Lee KY, Mooney DJ. Alginate: properties and biomedical applications. *Prog Polym Sci*. 2012;37:106-126.
31. Gombotz WR, Wee SF. Protein release from alginate matrices. *Adv Drug Deliv Rev*. 1998;31:267-285.
32. Smidsrod O, Skjak-Brœk G. Alginate as immobilization matrix for cells. *Trend Biotechnol*. 1990;8:71-78.
33. Qin Y. Alginate fibres: an overview of the production processes and applications in wound management. *Polym Int*. 2008;57:171-180.
34. Tonnesen HH, Karlsen J. Alginate in drug delivery systems. *Drug Dev Ind Pharm*. 2002;28:621-630.
35. Kong HJ, Smith MK, Mooney DJ. Designing alginate hydrogels to maintain viability of immobilized cells. *Biomaterials*. 2003;24:4023-4029.
36. Joseph I, Venkataram S. Indomethacin sustained release from alginate-gelatin or pectin-gelatin coacervates. *Int J Pharm*. 1995;126: 161-168.
37. Devi N, Hazarika D, Deka C, Kakati DK. Gelatin and gelatin-polyelectrolyte complexes: drug delivery. *J Macromol Sci Phys*. 2012; 49:936-945.
38. Lau H-C, Jeong S, Kim A. Gelatin-alginate coacervates for circumventing proteolysis and probing intermolecular interactions by SPR. *Int J Biol Macromol*. 2018;117:427-434.
39. Serafin A, Culebras M, Collins MN. Synthesis and evaluation of alginate, gelatin, and hyaluronic acid hybrid hydrogels for tissue engineering applications. *Int J Biol Macromol*. 2023;233:123438.
40. Zamboni F, Ren G, Culebras M, et al. Curcumin encapsulated polylactic acid nanoparticles embedded in alginate/gelatin bioinks for in situ immunoregulation: characterization and biological assessment. *Int J Biol Macromol*. 2022;221:1218-1227.
41. Jeong S, Kim BW, Park M, Ban E, Lee S-H, Kim A. Improved diabetic wound healing by EGF encapsulation in gelatin-alginate coacervates. *Pharmaceutics*. 2020;12:334.
42. Saravanan M, Rao KP. Preparation and characterization of microcapsules based on biodegradable polymers: pectin/casein complex for controlled drug release systems. *Carbohydr Polym*. 2010;80:808-816.
43. Derkach SR, Voron'ko NG, Kuchina YA. Intermolecular interactions in the formation of polysaccharide-gelatin complexes: a spectroscopic study. *Polymers*. 2022;14:2777.
44. Brown FR 3rd, Hopfinger AJ, Blout ER. The collagen-like triple helix to random-chain transition: experiment and theory. *J Mol Biol*. 1972; 63:101-115.
45. Gandhi SS, Yan H, Kim C. Polymer gels: perspectives and applications. *ACS Macro Lett*. 2014;3:1210-1214.
46. Maki Y, Saito W, Dobashi T. Preparation and thermoresponsive behaviors of UV-crosslinked gelatine nanogels. *Biorheology*. 2018;32:15-19.
47. Ashan SM, Rao CM. Characterization of carboxymethyl cellulose-based antimicrobial films incorporated with plant essential oils. *Int J Biol Macromol*. 2017;95:1126-1134.
48. Picard J, Giraudier S, Larreta-Garde V. Controlled remodeling of a protein-polysaccharide mixed gel: examples of gelatin-hyaluronic acid mixtures. *Soft Matter*. 2009;5:4198-4205.
49. Priftis D, Megley K, Laugel N, Tirrell MV. The effect of salt on the complex coacervation of vinyl polyelectrolytes. *J Colloid Interface Sci*. 2013;398:39-50.
50. Tavares L, Zapata Noreña CP. Encapsulation of ginger essential oil using complex coacervation method: coacervate formation, rheological property, and physicochemical characterization. *Food Bioproc Tech*. 2020;13:1405-1420.
51. Xiong W, Ren C, Tian M, Yang X, Li J, Li B. Complex coacervation of ovalbumin-carboxymethylcellulose assessed by isothermal titration calorimeter and rheology: effect of ionic strength and charge density of polysaccharide. *Food Hydrocoll*. 2017;73:41-50.
52. Marciel AB, Srivastava S, Tirrell MV. Structure and rheology of polyelectrolyte complex coacervates. *Soft Matter*. 2018;14:2454-2464.
53. Yamamoto M, Ikada Y, Tabata Y. Controlled release of growth factors based on biodegradation of gelatin hydrogel. *J Biomater Sci Polym ed*. 2001;12:77-88.
54. Priftis D, Tirrell M. Phase behaviour and complex coacervation of aqueous polypeptide solutions. *Soft Matter*. 2012;8:9396-9405.

SUPPORTING INFORMATION

Additional supporting information can be found online in the Supporting Information section at the end of this article.

How to cite this article: Blanco-López M, Marcos-García A, González-Garcinuño Á, Tabernero A, Martín del Valle EM. Exploring the effect of experimental conditions on the synthesis and stability of alginate–gelatin coacervates. *Polym Adv Technol*. 2024;35(8):e6554. doi:10.1002/pat.6554

RIGHTSLINK

10991581, 2024, 8, Downloaded from https://onlinelibrary.wiley.com/doi/10.1002/pat.6554 by Universidad De Salamanca, Wiley Online Library on [05/11/2024]. See the Terms and Conditions (https://onlinelibrary.wiley.com/terms-and-conditions) on Wiley Online Library for rules of use; OA articles are governed by the applicable Creative Commons License

Supporting information

Exploring the effect of experimental conditions on the synthesis and stability of alginate-gelatin coacervates

Marcos Blanco-López[1], Alejandro Marcos-García[1], Álvaro González-Garcinuño[1,2], Antonio Tabernero[1,2,], Eva Martín del Valle[1,2].*

1) Department of Chemical Engineering. University of Salamanca. Plaza Los Caídos s/n, 37008 Salamanca (Spain).
2) Institute for Biomedical Research in Salamanca (IBSAL), Paseo de San Vicente 87, 37007, Salamanca (Spain).

**** Corresponding author at: Antonio Tabernero (antaber@usal.es)***

Figure S1: Precipitates formed from coacervates with 1:4 (left) and 1:5 (right) volume ratio and pH 7 after cold (25ºC) coacervation.

Figure S2: Coacervate sample of 1:5 volume ratio at 37ºC and pH 5 with clear Tyndall effect (run 8).

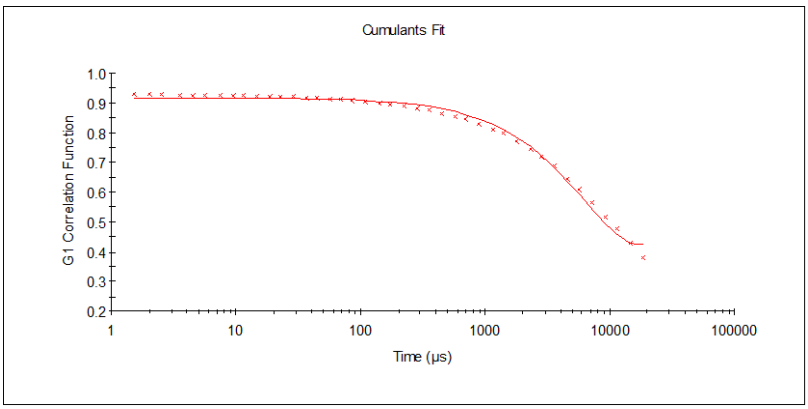

a)

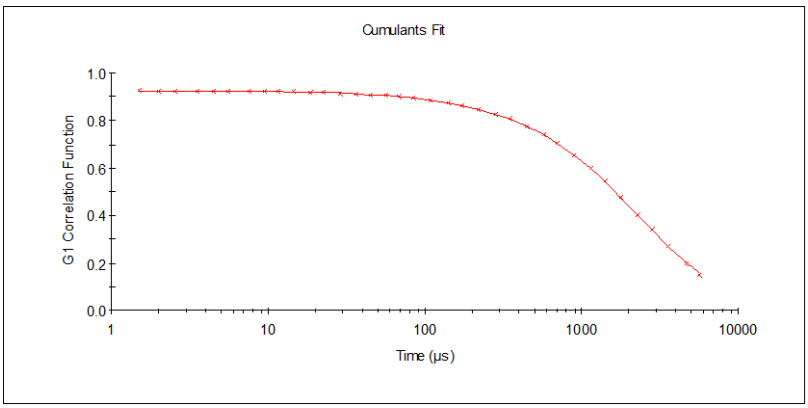

b)

Figure S3: Autocorrelation functions for coacervates at 1:5, pH 5 and a) 25ºC and b) 37ºC.

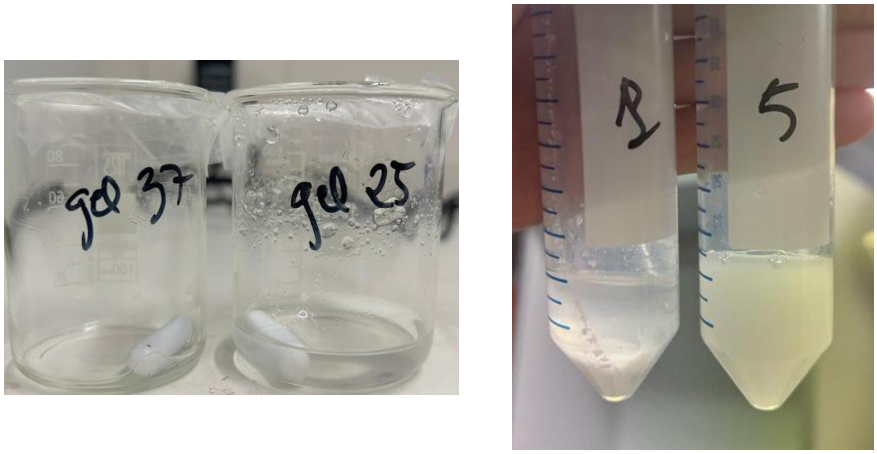

a) b)

Figure S4: a) Solutions of gelatin A at 37ºC (left) and 25ºC (right) and b) Coacervates samples at 1:4 pH4 and 25ºC (left, run 5) or 37ºC (right, run 6)

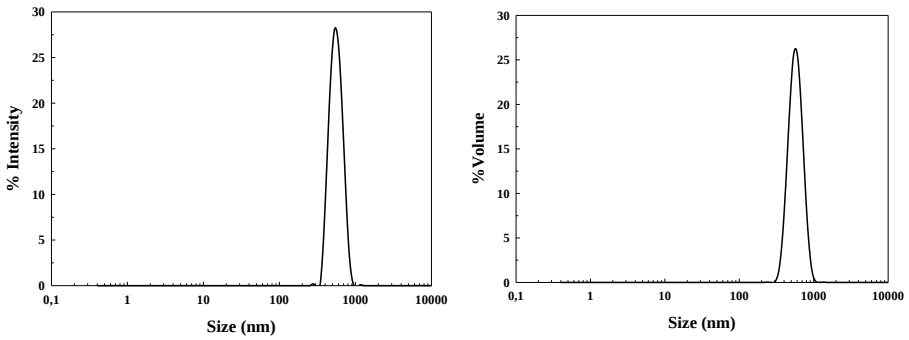

a) b)

Figure S5: Measurements in DLS for coacervates 1:5 at 37ºC and pH 5 (run 8 in Table 1 and Figure 3a) in manuscript) for a) intensity percentage and b) volume percentage

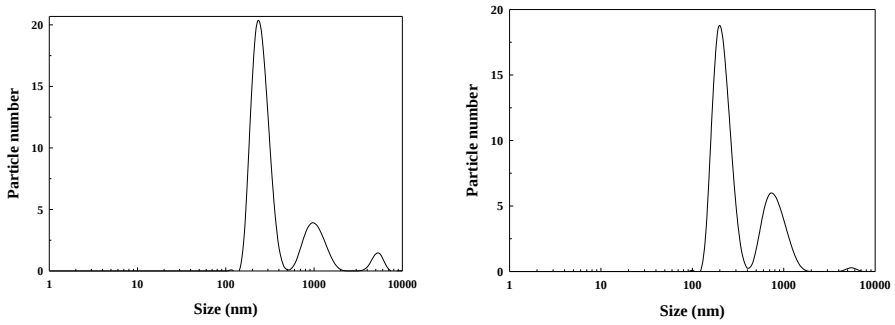

a) b)

Figure S6: DLS measurements for coacervates at 37ºC and pH 5 for volume ratios a) 1:3 and b) 1:7

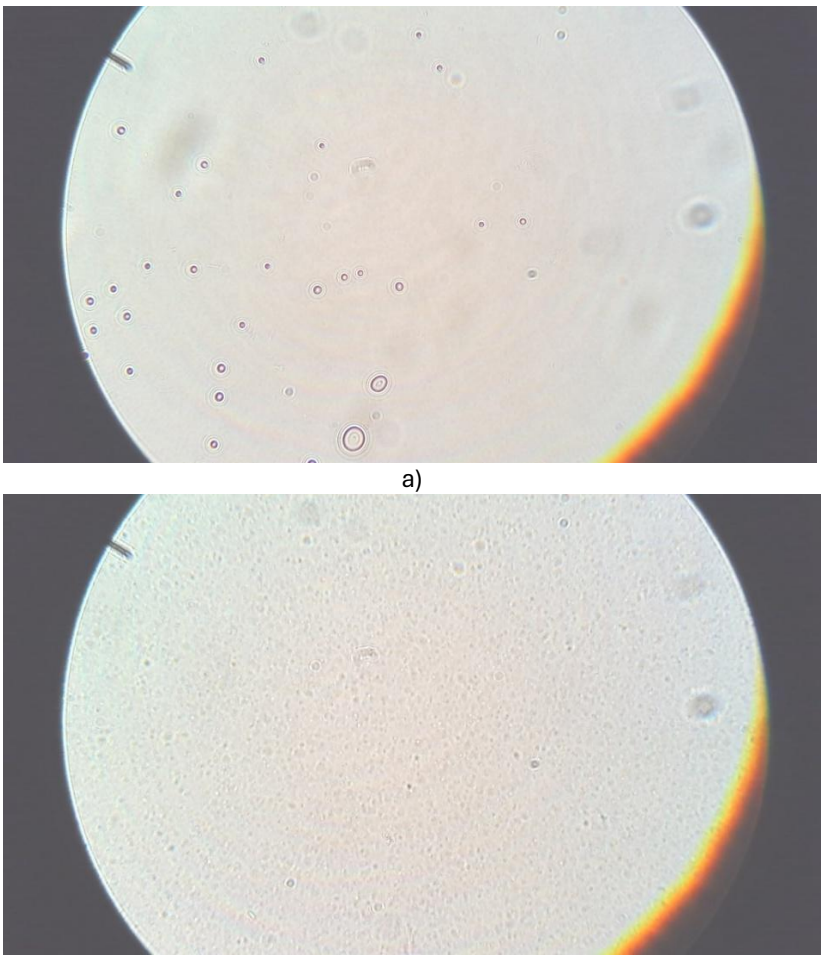

a)

b)

Figure S7: Optical microscopy images of samples of coacervates 1:5 and pH 5 synthesized at a) 25 ºC and b) 37ºC.

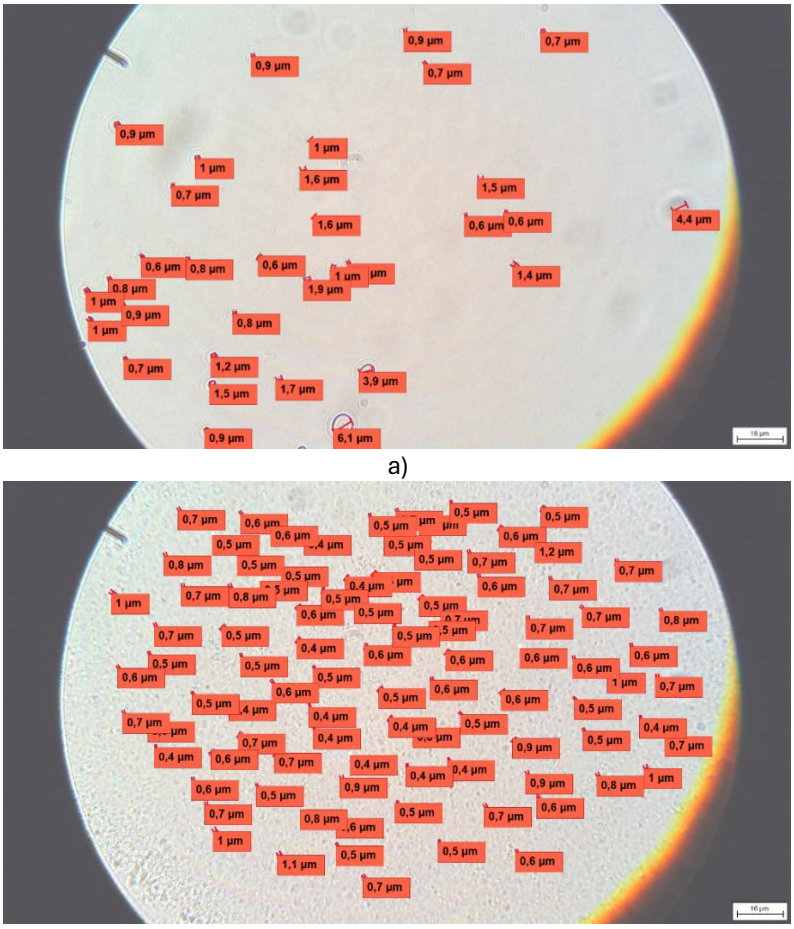

a)

b)

Figure S8: Particle measurements of optical microscopy images of samples of coacervates 1:5 and pH 5 synthesized at a) 25 ºC and b) 37ºC

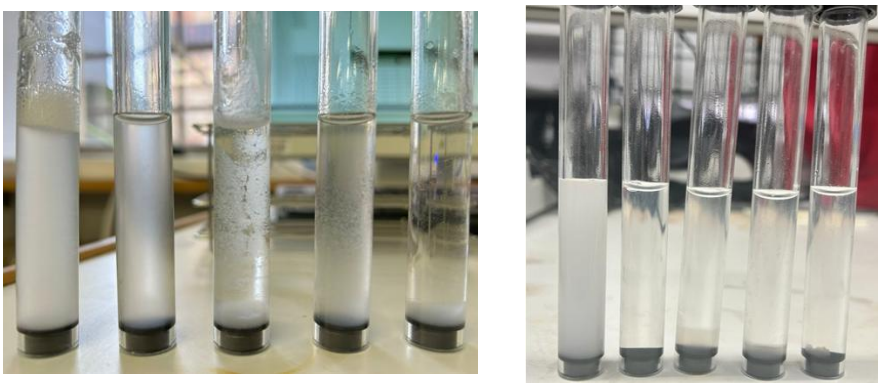

a) b)

Figure S9: Coacervates samples of 1:5 and pH 5 with increasing salt concentrations from left to right (0, 50, 100, 150, and 200 mM NaCl) at a) 25 ºC and b) 37 ºC

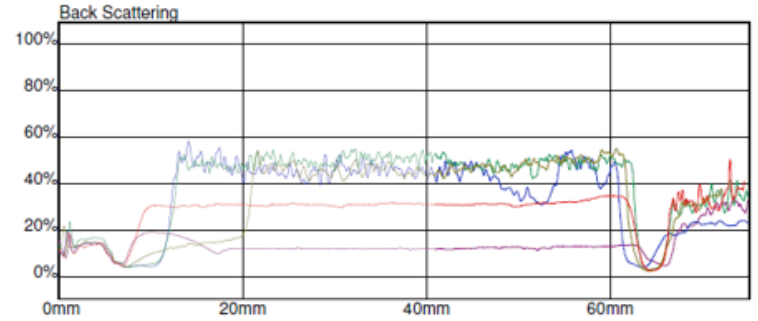

a)

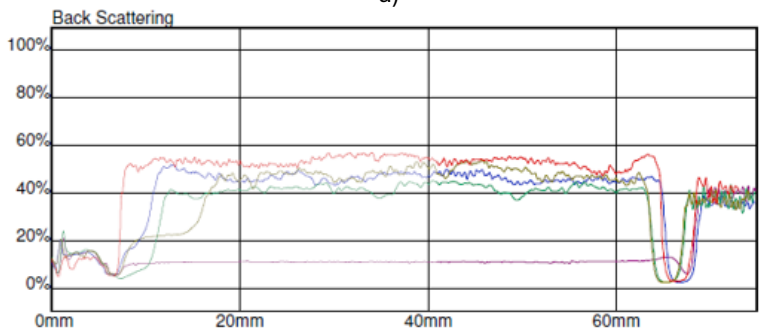

b)

Figure S10: Backscattering measurements of turbidity analysis of coacervates 1:5 and pH 5 and a) 25 ºC synthesis with NaCl (mM): 0 (purple), 50 (red), 100 (grey), 150 (green), and 200 (blue); b) 37 ºC synthesis with NaCl (mM): 0 (purple), 50 (green), 100 (grey), 150 (blue), and 200 (red).

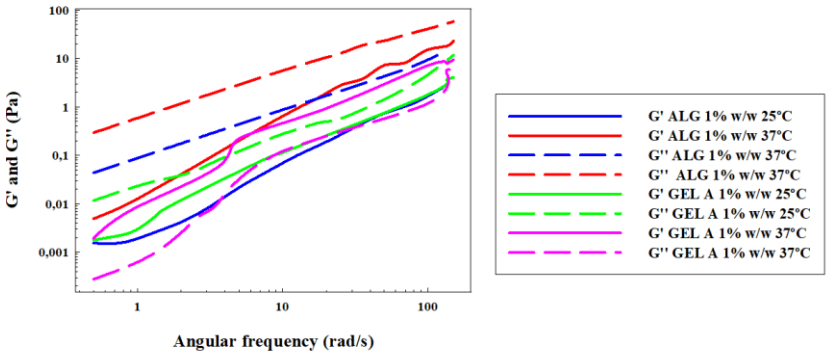

a)

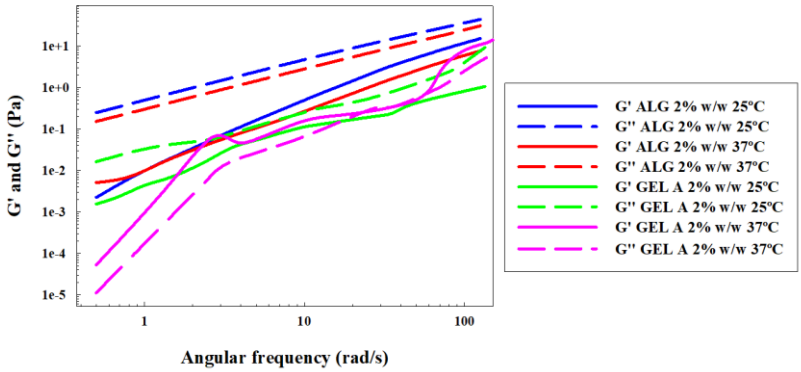

b)

Figure S11: Rheological oscillatory analyses on alginate and gelatin A at 25°C and 37°C with increased concentrations of a) 1% w/w and b) 2% w/w

4.5. Conclusions

As it was concluded in the article, a system based on alginate-gelatin A coacervates was successfully synthesized (400-750 nm with narrow size distribution, PDI<0.25), optimized, and fully characterized with different techniques.

However, this system did not present compatible physicochemical properties to be used for the intended dual-responsive breast cancer treatment. The thermo-responsive behaviour exhibited a hysteresis cycle that compromised coacervate stability at temperatures below 37ºC, while consecutive heating-cooling cycles progressively increased particle size and polydispersity (from 500 nm to 1µm in 5 days). Furthermore, the system did not show a gel structure or strong solid-like rheological behaviour at its stability peak. Consequently, the formulation was considered unsuitable for local administration.

Moreover, it was stated that, for viable polymer ratios, the optimal pH for coacervates stability was 5.0, showing instability at higher values. This implied the potential release of the drug in healthy tissues where the pH is higher, causing undesired cytotoxic effects on them. Conclusions are briefly summarized in Figure 4.3.

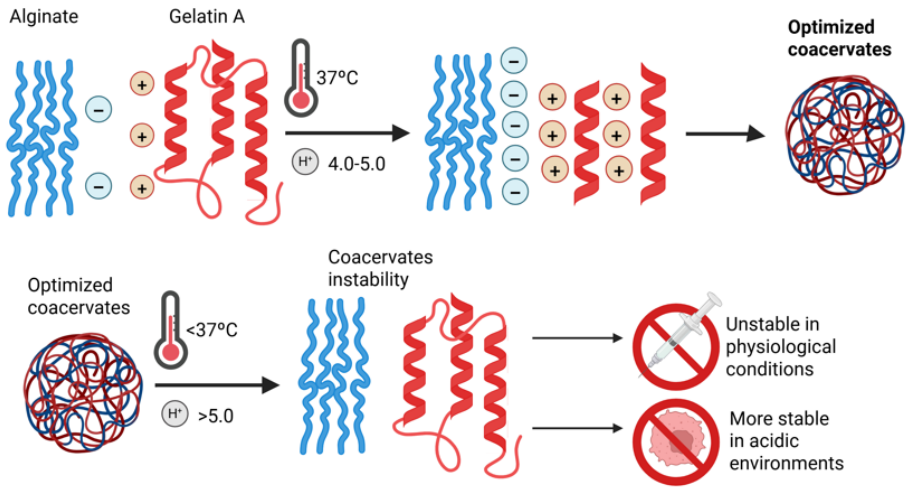

Figure 4.3. Conclusions of coacervates synthesis optimization and incompatibility with the intended application.

To conclude, although the work has contributed to develop an optimized coacervate system understanding many process variables effect, including the temperature novelty, the system is not compatible with the application it was designed for. Therefore, contingency plans are executed in following chapters for the synthesis of an efficient dual-response local administered platform for post-surgery breast cancer therapy preventing recurrences.

4.6. References also cited

[1] Cheng Y-H, He C, Riviere JE, Monteiro-Riviere NA, Lin Z. Meta-analysis of nanoparticle delivery to tumours using a physiologically based pharmacokinetic modelling and simulation approach. ACS Nano. 2020;14:3075-3095.

[2] Souri M, Yim W, Halder M, Jin Z, Jokerst JV. Coacervate-Based Delivery Systems: Bridging Fundamentals and Applications. ACS Appl Mater Interfaces. 2025;17:41513-53.

[3] Espinosa-Andrews H, Rodríguez-Rodríguez R. Complex coacervates for controlled drug delivery. In: Jana S, editor. Advances in pharmaceutical technology for drug delivery systems Volume 1: Recent progress in modern drug targeting strategies. Boca Raton (FL, USA): CRC Press; 2025. 297-325.

[4] Warnakulasuriya SN, Nickerson MT. Review on plant protein-polysaccharide complex coacervation and the functionality and applicability of formed complexes. J Sci Food Agric. 2018;98:5559-5571.

[5] Saravanan M, Rao KP. Pectin-gelatin and alginate-gelatin complex coacervation for controlled drug delivery: Influence of anionic polysaccharides and drugs being encapsulated on physicochemical properties of microcapsules. Carbohydr Polym. 2010;80:808-816.

[6] Lau H-C, Jeong S, Kim A. Gelatin-alginate coacervates for circumventing proteolysis and probing intermolecular interactions by SPR. Int J Biol Macromol. 2018;117:427-434.

[7] Kim BW, Ban E, Kim A. Gelatin-alginate coacervates optimized by DOE to improve delivery of bFGF for wound healing. Pharm. 2021;13:2112.

[8] Jeong S, Kim BW, Lau H-C, Kim A. Gelatin-alginate complexes for EGF encapsulation: Effects of H-bonding and electrostatic interactions. Pharm. 2019;11:530.

[9] Jeong S, Kim BW, Park M, Ban E, L S-H, Kim A. Improved diabetic wound healing by EGF encapsulation in gelatin-alginate coacervates. Pharm. 2020;12:334.

[10] Joseph I, Venkataram S. Indomethacin sustained release from alginate-gelatin or pectin-gelatin coacervates. Int J Pharm. 1995;126:161-168.

[11] Archut A, Klost M, Drusch S, Kastner H. Complex coacervation of pea protein and pectin: Contribution of different protein fractions to turbidity. Food Hydrocoll. 2023;134:108032.

[12] Ward AG, Courts A. The science and technology of gelatin. Academic Press. 1977:73-105.

[13] Shinde UA, Nagarsenker MS. Characterization of gelatin-sodium alginate complex coacervation system. Indian J Pharm Sci. 2009;71:313-317.

4.7. List of abbreviations

bFGF — Basic Fibroblast Growth Factor
BSA — Bovine Serum Albumin
DS — Diclofenac Sodium
EGF — Epidermal Growth Factor
HDF — Human Dermal Fibroblasts
IM — Indomethacin
MH — Metronidazole Hydrochloride

5. *Expanding the pH Window of Liposomal Drug Delivery Using Eudragit-Based Polymeric Coatings*

5.1. Introduction

As it was concluded in previous chapter, the initial approach to synthesize a dual-responsive drug delivery system based on alginate-gelatin A coacervates was not compatible with the intended therapeutic application. Particularly, stability under physiological conditions was not achieved due to undesired pH and temperature-responsive behaviour. Therefore, the sustained drug release at acidic environment could not be obtained from this system, limiting its applicability.

Thus, new alternative nanocarriers capable of providing stability at physiological conditions and the desired pH-responsiveness must be developed. In this context, liposomes represent one of the most exploited and efficient nanocarriers in commercialized drug delivery systems due to their structural similarity to biological membranes, which implies great biocompatibility, and ability to encapsulate therapeutic agents regardless of their hydrophilicity [1]. Besides, their surface can be easily tuneable for enhanced stimuli targeting and controlled release. In this sense, pH-sensitive liposomal systems are particularly attractive for tumour targeting strategies, since they can exploit the well-defined pH gradient from healthy conditions to acidified tumour microenvironment or intracellular cancer compartments [2].

Recently the most reported pH-sensitive liposomal systems are based on modifications of the lipid bilayer composition via incorporating pH-sensitive phospholipids which destabilize the membrane at physiological conditions. Therefore, even though they prove efficient acidic pH-response, their applicability and stability is significantly restricted [3]. Alternatively, a more versatile strategy consists of coating liposomes with a pH-responsive polymer, preserving their stability and expanding their applicability. Specifically, Eudragit® polymers offer different formulations to define different pH responses depending on the desired pH range for promoted release, or enhanced stability, regarding the intended application. Thus, Eudragit® polymers can be implemented in the liposomal systems in order to obtain different pH-responses that can operate a more expanded applications margin, besides acidic tumour targeting, like alkaline intestinal deliveries [4].

Hence, this chapter is focused on the development of pH-responsive coated liposomes with Eudragit® polymers as adaptable drug delivery systems operating at different pathological pH environments. More concretely, two different Eudragit® formulations with opposite functioning were tested on a common optimal and conventional liposomal base: Eudragit® S100, designed for alkaline triggered releases focused on intestinal or colorectal applications for oral formulations, and Eudragit® EPO, taking advantage of its acidic triggered release to target tumour microenvironment [4]. Furthermore, synthesis optimization, physicochemical characterization, release studies, and biological validation will be developed to ultimately establish a versatile liposomal platform for expanded smart drug deliveries in different applications.

5.2. Liposomes as drug delivery carriers

Liposomes can be defined as spherical vesicles formed by one or more lipidic bilayers mainly constituted by phosphatidylcholine (PC) and cholesterol (CHOL). They represent a strong bridge between biology and pharmaceutical technology since their composition imitates the cellular membranes. They can also encapsulate both hydrophilic and hydrophobic drugs either in their inner aqueous core or their lipidic bilayer, respectively [1]. Furthermore, liposomes show biocompatibility, biodegradability, and low immunogenicity, reducing the probabilities of adverse effects before reaching target site of delivery. However, some variables such as their size, number of bilayers, or surface charge can negatively influence in their efficacy in bloodstream or other administered pathways [5].

These limitations have been improved in order to reach fully approved therapies. Moreover, liposomes present versatility in many aspects: Their bilayer organization (Uni or multilamellar), size (Giant, large, medium or small vesicles), synthesis method (Thin film hydration, solvent injection, reverse phase evaporation), etc. This is illustrated in Figure 5.1. Regarding the synthesis method for lab scale, thin film hydration is usually chosen due to efficiency, reproducibility, and high passive encapsulation efficiency for hydrophilic and hydrophobic drugs [6]. Apart from being designed for certain size, bilayer organization, or

many other physicochemical properties regarding their application, they can also be conferred targeting capacity towards specific cells, tissues, intracellular compartments, etc. [7].

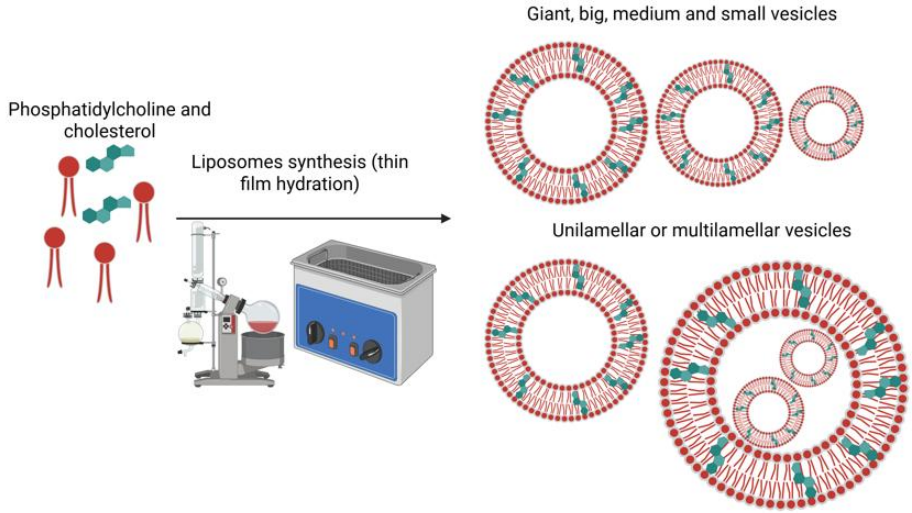

Figure 5.1. Different liposomal structural organization depending on the different synthesis variables.

5.3. Liposomes targeting capacity

Liposomes targeting capacity can be provided by different approaches: For instance, based on the EPR effect for passive targeting in tumour environments [6], or active by surface functionalization, like ligands attachment, such as folate, hyaluronic acid, peptides, antibodies, etc. In this case, the affinity between liposomes and the target molecule enhance their performance and efficiency [7].

Moreover, liposomes can also be designed to respond towards specific stimuli, such as pH, temperature, light, or redox conditions to release their payloads at target site. In this context, Table 5.1. summarizes the main advantages and limitations of the most commonly used stimuli-responsive liposomal systems [7]:

Table 5.1. Stimuli to respond for nanocarriers

Methodology	Benefits	Limitations
pH	Wide applicability Wide range of pH between healthy and affected tissues No external triggers needed	Difficult to maintain structure
Temperature	Enhances EPR effect	Off-target delivery Internal temperature difference is minimal and variable
Light	High precision Minimum invasiveness	Need for an external trigger Low penetration ability
Redox	High sensitivity	GSH-sensitive nanoparticles need endosome association

As it can be seen in Table 5.1, temperature does not present a promising stimulus due to off-target delivery and minimal gradient for liposomes to respond to, light requires an external trigger which can also cause systemic toxicity, and redox stimulus presents GSH-sensitivity which is not as reproducible as other stimuli. Therefore, pH is the preferred stimulus, since physio-pathological gradients usually present wide ranges for liposomes sensitivity design with better affordability and easiness. Thus, considering the wide and consistent pH differences among physiological and pathological environments within the human body, conventional liposomal off-target drug delivery can be redefined into a formulation capable of responding to specific pH environments [8].

5.4. pH-sensitive liposomes

As previously described, pH-sensitive liposomes react to pH differences provoking structural instability or reorganization that promotes drug release under certain conditions, whilst remaining stable in the opposite range. For tumour targeting, they remain stable at physiological pH (7.4) but become unstable under acidic conditions, such as those found in their microenvironments (6.8-4.0) [8]. In this context, developed pH-responsive liposomes with promising results in drug delivery are mentioned in Table 5.2.

Table 5.2. Reported pH-sensitive liposomal systems

Formulation	Drug/ Payload	Highlight	Ref
PEGylated DOPE/CHEMS	DOX SIM	High encapsulation (100 and 70% respectively) and 2:1 ratio caused synergistic cytotoxicity in *in vitro* assays	9
DOPE/CHEMS/ Cetuximab	DTX	SUV with high encapsulation (88%) showed better internalization and cytotoxicity of pH-response and active targeting	10
DOTAP/CHEMS CHOL/DOPE-mPEG /FU	GEM	Improvements in cellular internalization and endosomal escape (cationic charge). FU coating improves tumour targeting	11
DOPE/CHOL/ CHEMS/$MgCaFe_2O_4$	DOX	High encapsulation (98%) and synergy between pH-response and hyperthermia for cancer cellular growth inhibition	12
PEG-Hz-DOPE/TATp/mAb 2C5	DOX	Enhanced cytotoxicity and better internalization in cancer cells	13
DOPE-PEG-ES /CHEMS/ HSPC/CHOL	DOX	Higher cytotoxicity in breast cancer cells than non-pH-responsive treatments	14
DOPE/CHEMS/ F-PEO-DSPE	DOX	Higher drug accumulation at acidic pH (5.0) compared to 7.4.	15

As it can be seen, many pH-sensitive liposomal systems have been reported for successful drug delivery in tumour microenvironments. However, all of these systems reported the implementation of pH-responsive compounds, like DOPE, which reduce significantly liposomes stability at physiological conditions, as illustrated in Figure 5.2., limiting their application by inducing a non-lamellar phase transition (HII), requiring stabilizers in the vesicle bilayer, or complex surface functionalizations [3, 9-15]. In contrast, other strategies like coating with a pH-responsive polymer, can preserve the designed pH-response whilst adding improved performance, and enhanced structural stability. In this sense, Eudragit® polymers constitute a wide variety of pH-responsive polymers based on acrylic acid derivates [4].

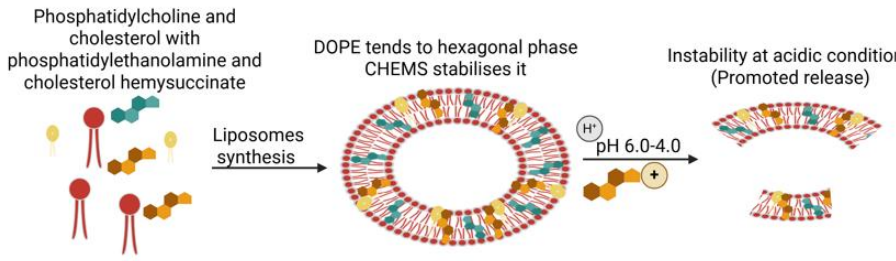

Figure 5.2. pH-responsive mechanism for liposomes with implemented DOPE and CHEMS, compromising their stability at physiological conditions.

5.4.1. Eudragit® coated pH-responsive liposomes

The Eudragit®polymer family represents a promising strategy for the development of pH-sensitive systems through electrostatically driven coatings. Their versatility and easy coating process position them as a preferred strategy, since a wide range of formulations can change the liposomal systems pH-responsive behaviour. Eudragit® polymers are mainly based on derivatives of methacrylate with different, but well defined, solubility profiles depending on the pH-response threshold. The different formulations have enabled their use in applications such as enteric coating, or sustained release, consolidating them as a key tool in drug delivery [16].

Despite few reported EU coated liposomal systems, this strategy has so far been restricted to very specific applications, mainly in the treatment of gastric and dermatological diseases. Therefore, systematic comparisons between different EU coatings, optimization of the size and monodispersity of EU-coated liposomes, and detailed kinetic analyses of drug release as a function of the coating employed remain scarce in the literature. Accordingly, two opposite functioning coatings selected for developing a broad pH-sensitive approach are EU S100 for alkaline releases and EU EPO for acidic ones.

5.4.1.1. Eudragit® S100 coated liposomes

Originally, Eudragit® S100 coatings are designed for protection of payloads in digestive tract (acidic pathway) in oral formulations until reaching the intestine for payload release (alkaline conditions). For this

purpose, Eudragit® S100 remains insoluble in acidic media but is dissolved in pH ranges higher than 7.0, presenting anionic behaviour [16]. Therefore, to enable liposomes to establish electrostatic interactions with this anionic polymer, their surface must be modified to exhibit a positive net charge through the incorporation of the positively charged stearylamine. Although this coating is not valid for acidic tumour targeting, it could serve as an additional stabilizing strategy for liposomal formulations in pH-responsive applications such as colorectal cancer, ulcerative colitis, Chron disease, etc [16]. Moreover, the EU S100 coated liposomes in literature lack biological validation of their pH-response.

5.4.1.2. Eudragit® EPO coated liposomes

In contrast, Eudragit® EPO presents a pH-response threshold around 5.0, being soluble under this value, exhibiting cationic behaviour. Thus, this coating is suitable for the pH-responsive tumour targeting capacity, which has not ever been reported in literature. Moreover, its cationic behaviour can enhance the interaction with biological membranes negatively charged, like cellular membranes, for a faster internalization in targeted tissues or cells. This represents a promising strategy to develop for the first time a coated liposomal system based on Eudragit® capable of targeting acidic tumour microenvironment. In this case, since the formulation is cationic, no liposome surface modification is required.

In this context, this chapter strategy aims to simultaneously optimize the liposome coating process with EU S100 and EU EPO, thereby obtaining a monodisperse and versatile liposomal platform that can be engineered to respond to opposite pH environments. This approach broadens the potential applicability of these systems for enhancing cancer therapy via different administration routes. The different coating procedures are illustrated in Figure 5.3.

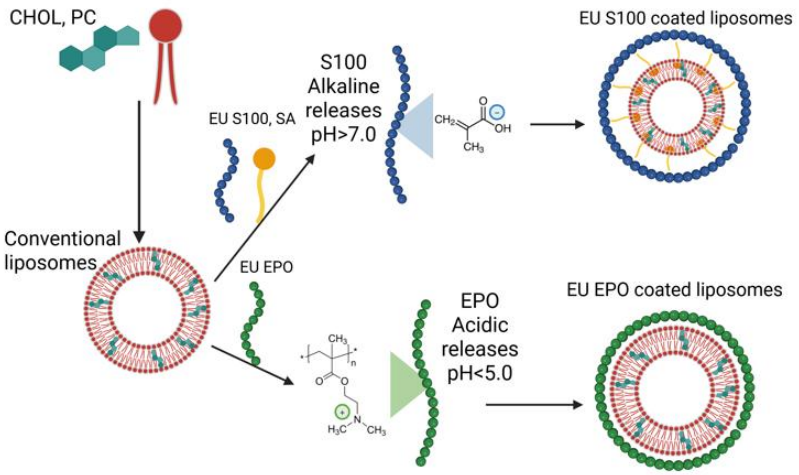

Figure 5.3. Eudragit® coating formulations for synthesis of pH-responsive liposomes.

5.5. Article related to this chapter

Following this section, the manuscript "Expanding the pH window of liposomal drug delivery using Eudragit®-based polymeric coatings" is presented as the results and discussions obtained within the framework of this experimental phase. This manuscript is currently under second revision for the journal Colloids and Surfaces A: Physicochemical and Engineering Aspects. The objective of this manuscript is not only developing and optimizing a coated pH-responsive liposomal system that can target acidic breast cancer cells, but also expanding onto it for different coatings and different applications. Therefore, an extended platform of pH-responsive liposomes design was developed in order to approach oppositely pH ranges.

For this purpose, two different pH-responsive coatings were implemented to a common optimized conventional liposomal system. Eudragit® S100 provided alkaline release, presenting a platform for oral formulations intended for colonic or intestinal diseases, even though the coating process showed micrometric aggregates. On the other hand, Eudragit® EPO provided a stable coated monodisperse liposomal system that stayed stable for at least 15 days, presenting the possibility of systemic administration due to their size.

Moreover, the liposomes showed high encapsulation efficiencies of the 5-FU model drug used for this work. Meanwhile conventional liposomes showed no pH-response, releasing the full concentration in hours, coated formulations provided a full release in one day for soluble ranges, whilst preventing it for insoluble pH values. Further mathematical models fittings supported the change of release mechanism due to polymer coating, establishing diffusion as the predominant one.

Furthermore, cell assays validated the pH-response, particularly in Eudragit® EPO coated liposomes, which targeted BT-474 breast cancer cells with a faster internalization, and induced more cell death compared to any other formulation, whilst slightly preserving healthy stromal HS-5 cells viability. This was potentially attributed to the successful implementation of a pH-responsive tumour-targeting strategy with enhanced cellular internalization.

Expanding the pH Window of Liposomal Drug Delivery Using Eudragit®-Based Polymeric Coatings

Marcos Blanco-López[1], Inmaculada de Dios-Pérez[1,3], Celia Nieto[1,2,], Antonio Tabernero[1,2,*], Patricia P. Esteban[3], Eva Martín del Valle[1,2].*

1) *Department of Chemical Engineering. University of Salamanca. Plaza Los Caídos s/n, 37008 Salamanca (Spain).*
2) *Institute for Biomedical Research in Salamanca (IBSAL), Paseo de San Vicente 87, 37007, Salamanca (Spain).*
3) *Healthcare Technologies Institute (HTI), University of Birmingham, B15 2TT, Birmingham (UK).*

**** Corresponding author at: Antonio Tabernero (antaber@usal.es)***

Abstract

Liposomes are among the most investigated nanocarriers for site-specific drug delivery in diseases such as cancer. Considerable efforts have therefore been devoted to improving their targeting capabilities, including the development of pH-responsive systems. One promising strategy consists of coating liposomes with pH-sensitive polymers, although this approach remains poorly explored in cancer nanomedicine.

In this work, cholesterol/phosphatidylcholine liposomes were optimized to obtain stable small unilamellar vesicles (SUVs) with diameters below 100 nm and unimodal size distributions (PDI<0.1). These liposomes were subsequently coated via electrostatic interactions with two pH-responsive Eudragit® (EU) polymers: EU S100 and EU EPO. EU EPO-coated liposomes showed average diameters of approximately 114 nm, compatible with potential systemic administration, whereas EU S100-coated formulations formed micrometric aggregates, making them more suitable for oral delivery.

Both coated formulations efficiently encapsulated 5-fluorouracil (5FU) and prevented its premature release, retaining up to 50% of the drug after 24 hours under conditions in which the coatings remained insoluble (pH<7.0 for EU S100 and pH>5.0 for EU EPO). Drug release kinetics were best described by first-order and Higuchi models, indicating diffusion through the lipid bilayer as the predominant release mechanism.

All formulations exhibited good biocompatibility. Among them, EU EPO-coated liposomes showed the greatest reduction in tumour cell viability, likely due to enhanced intracellular drug release and faster cellular internalization.

Overall, EU-coated liposomes may represent a versatile platform for pH-responsive drug delivery through different administrations routes.

1. Introduction

Nowadays, cancer remains one of the leading causes of mortality worldwide, accounting for approximately one in every six deaths in 2020 and ranking as the second cause of death after cardiovascular diseases. Over the years, the treatment of this complex disease has evolved considerably and currently includes several therapeutic approaches, such as surgery, radiotherapy, chemotherapy, and immunotherapy. In general, surgery and radiotherapy are primarily employed for early-stage cancers, whereas chemotherapy and immunotherapy are more commonly used in advanced tumours and metastatic diseases. Although the drugs used in these last two therapies are highly effective at inhibiting cancer cell proliferation, their clinical efficacy is often limited by their poor bioavailability and non-specific biodistribution, which can lead to severe side effects and even the development of drug resistances [1-4]. In this context, the development of drug nanocarriers has attracted substantial attention as a strategy to overcome some of the drawbacks associated with conventional therapies. These systems offer significant potential to increase drug accumulation at tumour tissues, enhance therapeutic efficacy, and reduce systemic toxicity [5, 6].

Among the various drug nanocarriers employed in cancer nanomedicine, lipid-based nanoparticles stand out because of their advantageous properties, especially liposomes. Liposomes are artificial spherical vesicles composed mainly of a lipid bilayer capable of encapsulating both hydrophilic and hydrophobic compounds [7]. In addition, their size and surface charge can be tailored according to the intended therapeutic application [8]. Owing to their structural similarity to cellular membranes, liposomes generally exhibit high cellular internalization rates and excellent biocompatibility [7]. However, conventional liposomes still lack sufficient targeting specificity and may therefore cause undesired toxicity [9, 10]. Consequently, considerable efforts have been devoted to engineering the liposomal surface to improve targeting capabilities and to develop systems able to respond to specific stimuli [11, 12], thereby enabling controlled drug release within the pathological microenvironment [13]. These stimuli may be endogenous (such as pH variations, the presence of specific enzymes,

changes in redox potential, temperature fluctuations, or alterations in metabolite concentration) [14-18], or exogenous (including light irradiation, magnetic fields, or ultrasound exposure) [19-21].

Given the physiological pH gradients that exist within the body, as well as the acidic microenvironment of tumour tissues and several cellular organelles involved in the endocytosis of drug delivery systems [14, 22-24], the design of pH-responsive liposomes represents a particularly promising strategy. Such systems may enable a more sustained and controlled release of chemotherapeutic agents, while simultaneously protecting them from premature degradation before reaching the target tissue. This feature is especially relevant for orally administered drugs, for which stability throughout the gastrointestinal tract is crucial [11, 25].

The most widely used strategy to confer pH sensitivity to liposomes consists of synthesizing them from charged lipids, such phosphatidylethanolamine (PE) and cholesterol hemysuccinate (CHEMS), which favour the release of the encapsulated drugs at acidic pH values, such as those existing in some cell organelles. Nevertheless, the release induced by these compounds occurs within narrow pH windows and is less effective for drugs with high molecular weight [26, 27], so liposome coating with pH-responsive polymers, such as Eudragit® S100 (EU S100) or Eudragit® EPO (EU EPO), may emerge as a powerful alternative [28, 29].

On one hand, EU S100 contains carboxylic groups, which confer an anionic character and make it soluble in aqueous media at alkaline values (pH>7.0), where it behaves as a branched macromolecule with hydrophilic termini due to its high molecular weight, enabling coating via electrostatic interactions [30]. Nonetheless, to achieve effective adsorption onto liposomes, and given their inherently anionic nature, it is necessary to include primary amine groups on their surface (e.g. through stearylamine (SA)), thereby shifting their zeta potential towards more positive values [31-33]. The resulting nanosystems, which can release their payload under alkaline conditions, have been mainly investigated in oral formulations for inflammatory bowel disease, with the aim of protecting drugs along the gastrointestinal tract [26]. For instance,

Alghurabi et al. developed liposomal formulations coated with EU S100 that promoted bile salt release at pH>7.0 [32], while Caddeo et al. demonstrated that encapsulation of quercetin in a similar system improved its stability in gastric fluids [33].

In contrast, EU EPO contains amine functional groups, which confer a cationic character; thus, it has been used, albeit to a limited extent, in the design of liposome-based nanocarriers intended for applications requiring enhanced drug release under acidic pH conditions [28, 34]. For example, Hasanovic et al. developed EU EPO-coated liposomes to enhance the skin penetration of acyclovir and minoxidil, taking advantage of the system's ability to interact with skin lipids [35].

As it can be seen from the examples cited above, despite the potential of coating liposomes with EU S100 and EU EPO, this strategy has so far been restricted to very specific applications, mainly in the treatment of gastric and dermatological diseases. Therefore, systematic comparisons between different EU coatings, optimization of the size and monodispersity of EU-coated liposomes, and detailed kinetic analyses of drug release as a function of the coating employed remain scarce in the literature.

In this context, the present work aimed to address this gap by optimizing the liposome coating process with EU S100 and EU EPO, thereby obtaining a monodisperse and versatile liposomal platform that can be engineered to respond to opposite pH environments. This approach broadens the potential applicability of these nanosystems for enhancing cancer therapy via different administration routes. To assess their pH-responsiveness, the model drug 5-fluorouracil (5FU), widely used in the treatment of several solid tumours [36, 37], was encapsulated within the EU-coated liposomes. Subsequently, the cellular internalization and antitumour activity of the resulting nanosystems were evaluated in breast cancer cells, while cytotoxicity was assessed in stromal cells.

Overall, the results obtained provide new insights into the design of polymer-coated liposomes and highlight their potential as adaptable and advantageous platforms for next-generation targeted drug delivery.

2. Materials and methods

2.1. Materials

Sigma Aldrich supplied Egg L-α-phosphatidylcholine (PC, MW 758 g/mol, 60% purity determined by TLC), cholesterol (CHOL, MW 386 g/mol), stearylamine (SA, pure, MW 270 g/mol), 5-fluorouracil (5FU, MW 130 g/mol) and thiazolyl blue tetrazolium bromide (MTT reagent). Chloroform (99.5% w/v) was obtained by PanReac AppliChem ITW Reagents. Pure phosphatidylcholine (99% purity) was purchased from Avanti Polar Lipids. The pH responsive polymers Eudragit® S100 (EU S100, MW 135,000 g/mol) and Eudragit® EPO (EU EPO, MW 47,000 g/mol) were kindly donated by Evonik OnCare. Dulbecco's Modified Eagle Medium (DMEM), fetal bovine serum (FBS), penicillin-streptomycin (P-S), phosphate-buffered saline (PBS), rhodamine B, and CellTracker® Green CMFDA were purchased from Fisher Scientific.

2.2. Liposome synthesis

Liposomes were synthesized following the thin-film hydration method [38]. Firstly, PC and CHOL were weighed at the desired molar ratio (50:50-100:0, respectively) and dissolved in 20 mL chloroform under magnetic stirring at 200 rpm and room temperature. After 30 minutes, a clear homogeneous solution was obtained. The organic phase was then transferred to a round-bottom flask and subjected to rotary evaporation.

Chloroform was completely removed by rotary evaporation at 55ºC for 30 minutes, resulting in the formation of a thin lipid film on the flask wall. Subsequently, 10 mL of PBS were added to hydrate and resuspend the lipid film by sonication for 1 hour at the selected temperature (25-65ºC). Once the lipid layer had been completely dispersed in the aqueous phase, the liposomal suspension was transferred to a preheated extrusion system.

The extrusion setup (Avanti Polar Lipids mixi-extruder, Alabama, U.S.A.) was previously assembled and equilibrated at the selected temperature (25-65ºC). PC hydrophilic membrane filters with a pore diameter of 0.1 μm (Cytiva Nuclepore, Fisher Scientific) were used during

the extrusion process. The liposomal suspension was passed repeatedly between two syringes through the membrane for a predetermined number of passes (1-17 passes), yielding a unimodal liposome dispersion with a final concentration of 1.30% (w/w).

2.2.1. Liposome coating with EU S100

To enable efficient coating of liposomes with EU S100, SA was firstly incorporated into the liposomal formulation in order to modify the zeta potential of the vesicles. Specifically, 9 mg of SA were weighed together with PC and CHOL, following the procedure described in Section 2.2. Afterwards, aqueous EU S100 solutions were prepared at different concentrations: 0.01, 0.025, 0.05, 0.1, and 0.25% (w/v). Each polymer solution was placed in a beaker under magnetic stirring at 1,000 rpm, after which the SA-contaning liposomal suspension were added at a 1:1 volume ratio. The resulting mixture was maintained under stirring was for 1 hour to allow the coating process to occur [33].

2.2.2. Liposome coating with EU EPO

For coating with EU EPO, the polymer was dissolved in sodium acetate buffer adjusted to pH 4.5 at different concentrations: 0.1, 0.25, and 0.5% (w/v). Then, conventional liposomes were poured over the polymer solution following the same procedure described in Section 2.7.

2.3. Characterization of conventional and EU-coated liposomes

2.3.1. Vesicle size, PDI and zeta potential

Both conventional and EU-coated liposomes were characterized by dynamic light scattering (DLS) using a Zetasizer instrument (Malvern Instruments, Worcestershire, UK) over a period of 21 consecutive days to determine their mean particle size, polydispersity index (PDI), and zeta potential. Automatic attenuation mode was selected, and the results were analysed based on particle number distribution. Measurements were performed using the standard peak integration method provided by the instrument software, with a detection angle of 173º.

2.3.2. Cryo-SEM

Cryogenic scanning electron microscopy (Cryo-SEM) was used to evaluate the morphology of both conventional and EU-coated liposomes (SEM-FEI FIB Quanta 3D, Brno, Czech Republic). Briefly, a 3 µL aliquot of each sample was deposited onto a grid, which was later immersed in liquid nitrogen to rapidly freeze the sample and preserve its native structure. The frozen grids were then transferred to a cryo-preparation chamber (Quorum PP3010 Prepdek, California, USA), coupled to the microscope chamber. Within this chamber, the samples underwent sublimation and gold sputter coating. Sublimation was carried out at -100°C for 5 minutes to remove the superficial ice layer, while sputter coating was performed using argon gas to provide a conductive metallic layer con the sample surface. Finally, the grids were transferred to the microscope chamber, where observations were conducted at -140°C using an accelerate voltage of 5kV and a working distance of 5 mm.

2.4. Loading of liposomes with 5FU

Liposomes were loaded with the hydrophilic anticancer model drug 5FU. 5FU was dissolved in PBS to obtain a final concentration of 50 ppm, according to the inhibitory concentration (IC_{50}) values previously reported in the literature for *in vitro* assays [39]. This drug-containing aqueous phase was later used to hydrate and resuspend the lipid film after rotary evaporation, thereby enabling passive drug loading. The resulting loaded liposomes were then subjected to the extrusion process under the same conditions described previously to obtain a unimodal dispersion.

2.5. Determination of 5FU encapsulation efficiency

To quantify the amount of drug encapsulated within the liposomes, non-encapsulated 5FU was separated from the liposomal suspension via ultracentrifugation. Loaded liposomes were centrifuged using a 70-TI rotor at 39,000 rpm (approximately 60,000 x g) at 4ºC for 1 hour. After centrifugation, a visible pellet corresponding to the liposomal fraction was obtained. The supernatant, containing the non-encapsulated drug,

was carefully collected, and the concentration of 5FU was determined by UV-vis spectrophotometry (Shimadzu UV-1800) at 260 nm.

For this procedure, liposomal formulations were synthesized in duplicated batches: one bacth containing 5FU and another without drug loading. Since certain lipid components also exhibit absorbance at 260 nm, the absorbance difference between loaded and unloaded liposomal supernatants at this wavelength was attributed to the non-encapsulated drug. The same procedure was applied to EU-coated liposomes.

Encapsulation efficiency (%EE) was calculated according to Eq.1:

$$\%EE = \frac{C_{50ppm\ pattern} - C_{supernanant}}{C_{50ppm\ pattern}} \times 100 \quad \text{(Eq. 1)}$$

Where $C_{supernanant}$ is the concentration of non-encapsulated 5FU determined from the absorbance difference between loaded and unloaded liposomal supernatants after centrifugation, and $C_{50ppm\ pattern}$ corresponds to the concentration of the standardized 5FU solution (50 ppm).

2.6. Drug release studies

Drug release experiments were performed using the dialysis membrane diffusion method. Briefly, 5 mL of each liposomal formulation were introduced into dialysis membranes (SpectraPor® 7, MWCO 1,000 Da, 18mm; Carl Roth, Karlsruhe, Germany) and immersed in buffered aqueous media at different pH values. The systems were incubated at 37ºC under orbital shaking at 50 rpm (Biosan ES-20, Riga, Latvia). The selected pH values conditions were 7.4 (physiological pH of healthy tissues), 6.5 (tumour extracellular microenvironment), 5.5 (endosomal pH), and 4.5 (lysosomal pH). Aliquots of the release medium were collected at predetermined time intervals (0, 0.5, 1, 2, 4, 8, 12, and 24 h), and the concentration of released 5FU was determined by UV-Vis spectrophotometry.

Also, for these experiments, formulations were synthesized in duplicate batches, with only half of the samples containing the drug. The absorbance difference between loaded and unloaded formulations was

attributed to the release of 5FU. Drug release profile at each time point was calculated according to Eq. 2:

$$\frac{C}{C_{max}} = \frac{C_{aliquot\ at\ time\ t}}{C_{aliquot\ at\ time\ t=24h}} \quad \text{(Eq. 2)}$$

Where $\frac{C}{C_{max}}$ represents the normalized cumulative drug release at each time point; $C_{aliquot\ at\ time\ t}$ corresponds to the concentration of 5FU released at time t (determined from the absorbance difference between loaded and unloaded liposomal formulations), and $C_{aliquot\ at\ time\ t=24h}$ represents the maximum concentration of 5FU released, corresponding to the final sampling time (24 hours), at which release plateau was observed.

In addition, the cumulative released of 5FU relative to the initial loading concentration in each experiment was calculated according to Eq. 3:

$$\%5FU\ released = \frac{C_{aliquot\ at\ time\ t=24h}}{C_{50ppm\ pattern}} \quad \text{(Eq. 3)}$$

Where again $C_{50\ ppm\ pattern}$ corresponds to the concentration of the standardized 5FU solution (50 ppm).

2.7. Theoretical model fitting

Experimental drug release obtained for both conventional and EU-coated liposomes were fitted to different theoretical kinetic models. All experimental release profiles were normalized to C_{max}, corresponding to the maximum drug concentration released in each system, as described in Eq. 2, rather than to the initial drug loading concentration.

The selected models included zero- and first-order kinetics, and the Higuchi and Korsmeyer-Peppas models. For the latter two, only experimental data corresponding to less than 60% cumulative drug release were considered [40]. These models were selected based on their widespread application in studies evaluating drug release from nanocarrier systems, which is due to their fitting enable assessment of whether the release process is concentration-dependent and, more

importantly, determination of the predominant transport mechanism, which is typically diffusion-controlled in liposomal systems.

The equations corresponding to each model are presented below:

Zero order kinetics: $\frac{C}{C_{max}} = k_0 \cdot t$ (Eq. 4)

Where $\frac{C}{C_{max}}$ is the cumulative fraction of drug released at a given time, k_0 is the zero-order release rate constant (h^{-1}), and t is time (h).

First order kinetics: $\frac{C}{C_{max}} = 1 - e^{-k_1 \cdot t}$ (Eq. 5)

Where k_1 is the first-order release rate constant (h^{-1}).

Higuchi model: $\frac{C}{C_{max}} = k_H \cdot \sqrt{t}$ (Eq. 6)

Where k_H is the Higuchi release constant ($h^{-0.5}$)

Korsmeyer-Peppas model: $\frac{C}{C_{max}} = k_{KP} \cdot t^n$ (Eq. 7)

Where k_{KP} is the kinetic constant of the Korsmeyer-Peppas model (h^{-n}), and n is the release exponent associated with the drug transport mechanism.

Model fitting was performed by maximizing the coefficient of determination (R^2), calculated according to Eq 8:

$$R^2 = 1 - \frac{SSE}{SST} = 1 - \frac{\sum_i^N (X_{i,exp} - X_{i,th})^2}{\sum_i^N (X_{i,exp} - \bar{X}_{exp})^2} \quad \text{(Eq. 8)}$$

Where SSE is the sum of squared errors, and SST is the total sum of squares. $X_{i,exp}$ corresponds to each experimental drug release value (C/C_{max}), $X_{i,th}$ represents the corresponding theoretical value predicted by the fitting model, and $\bar{X}_{exp}$ is the mean of the experimental release data.

2.8. *In vitro* evaluation of 5FU-loaded liposomes' antiproliferative activity

To evaluate the antiproliferative activity of conventional and EU-coated liposomes loaded with 5FU, cell viability assays were performed using two different types of cells: BT-474 breast carcinoma cells and HS5 stromal cells (ATCC, Manassas, VA, USA). BT-474 cell line was selected due to its high proliferative capacity, which facilitates the development of mildly acidic conditions in culture, whereas HS-5 stromal cells were chosen because they represent a key component of neoplastic tissues and are cultured under conditions that more closely resemble physiological pH. Both cell lines were cultured in DMEM supplemented with 10% (v/v) FBS and 1% (v/v) P-S (DMEM+) and maintained at 37ºC in a humidified atmosphere containing 5% CO_2.

The antiproliferative activity of the different liposomal formulations was assessed by MTT assays [41]. BT-474 and HS-5 cells were seeded in triplicate in flat-bottomed 24-well-plates at an initial density of 16,000 cells per well. Afterwards, cells were exposed to the different treatments for 24, 48, and 72 hours under standard cultured conditions, while untreated cells were used as control. After the corresponding incubation periods, MTT reagent was dissolved in PBS at a concentration of 5 mg/mL and added to each well at 10% of the total well volume. Following 1 hour of incubation, the DMEM+ containing MTT was removed, and the resulting formazan crystals were dissolved in 0.5 mL of DMSO per well. Absorbance was measured at 550 nm in a microplate reader (Tecan Spark, Vienna, Austria), and cell viability was calculated according to Eq. 9:

$$Cell\ viability\ (\%) = \frac{Avg\ OD\ sample\ wells - Avg\ OD\ medium\ control\ wells}{Avg\ OD\ cell\ control\ wells - Avg\ OD\ medium\ control\ wells} \quad \text{(Eq. 9)}$$

Initially, MTT assays were performed to determine the IC_{50} value of 5FU for both cell lines. Subsequently, a normalised dose based on previously determined IC_{50} values was selected to objectively evaluate the effect of the formulations. Accordingly, both loaded and unloaded liposomal systems (conventional and EU-coated) were synthesized and used to treat the cells. Drug-loaded formulations were diluted in DMEM+

to achieve the desired final IC_{50} concentration of 5FU, while unloaded formulations were diluted using the same procedure.

2.9. Assessment of liposomal cellular uptake

To complement the results obtained from the cell viability assays, the cellular uptake of the different liposomal formulations was evaluated in the BT-474 breast carcinoma cell line. For this purpose, cells were stained with CellTracker® Green CMFA (0.7 μM) according to the manufacturer's instructions and seeded in glass-bottom dishes at a density of 20,000 cells/mL. Then, cells were incubated at 37°C with the different liposomal formulations, in which rhodamine B had been previously encapsulated following the same procedure described for 5FU loading, reaching a final rhodamine concentration of 2 μg/ml. Cellular uptake was studied after incubation periods of 0,5, 1, 4, and 24 hours. Following each incubation period, cells were washed with PBS to remove non-internalized liposomes and imaged using confocal laser scanning microscopy (CLSM) (Leica SP8, Leica Camera, Wetzlar, Germany).

2.10. Statistical analysis

All data were presented as mean ± standard deviation (SD) for at least three independent experiments or measurements (n = 3). Comparisons between two groups were performed using unpaired Student's t-tests. Multiple-group comparisons were performed using one-way ANOVA for liposome synthesis and stability studies, and two-way ANOVA for drug release kinetics and cell viability assays. When statistically significant differences were identified, Tukey's post hoc test was applied for pairwise comparisons.

3. Results and discussion

3.1. Liposome synthesis optimization

3.1.1. Synthesis of conventional liposomes

The synthesis of conventional liposomes was initially optimized by evaluating the influence of several process variables, including the

number of extrusion passes, sonication and extrusion temperatures, the molar ratio (MR) between PC and CHOL, and the PC yield. Liposome stability was subsequently assessed through daily measurements of mean particle size and PDI. The particle size results are presented in Figure 1, while additional data are provided in Figure S1 (Supplementary Material) and Tables S1-S4 of the Supplementary Material.

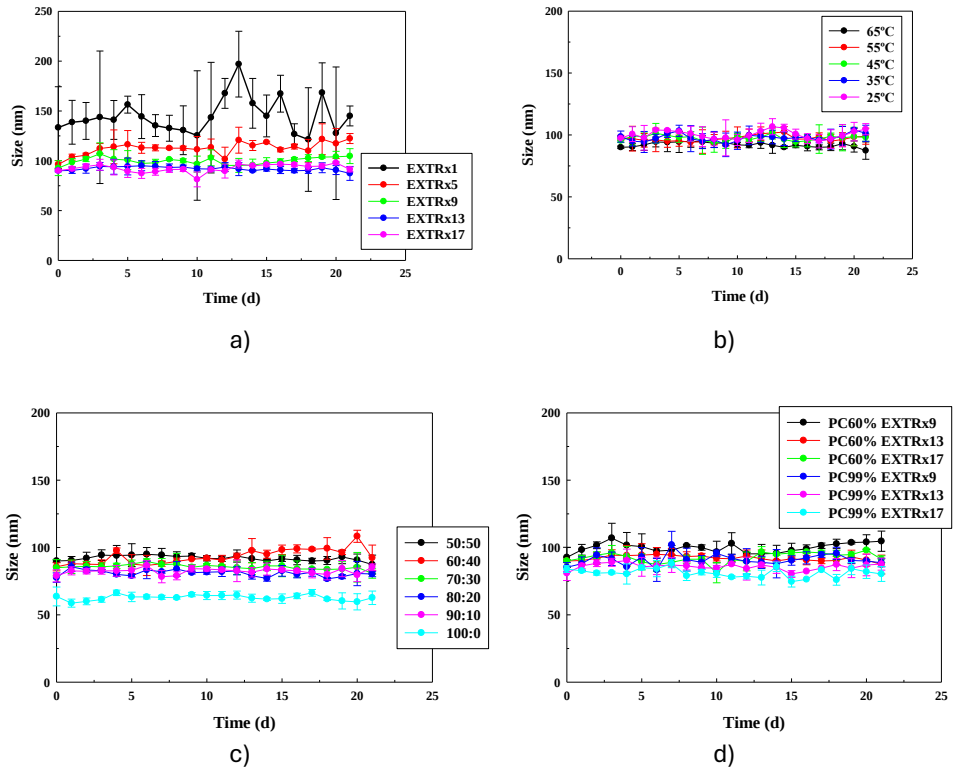

Figure 1: Liposomes size distribution over a period of 21 days as a function of: a) Extrusion number of passes, b) sonication and extrusion temperature, c) MR of PC:CHOL, and d) PC yield. Results are expressed as a mean values of 3 measurements ± SD.

Figure 1a shows the variation in liposome size as a function of the number of extrusion passes (1, 5, 9, 13, and 17 passes). As observed, the mean particle size decreased significantly as the number of passes through the membrane increased, a trend confirmed by statistical analysis ($p<0.0001$). This behaviour can be explained by the action of the membrane filter, which disrupts lipid structures larger than the pore size.

Therefore, repeated extrusion cycles promote the reassembly of lipid vesicles into smaller and more homogeneous populations, resulting in increasingly monodispersed systems (PDI<0.1) [42].

Based on these results, it was concluded that small unilamellar vesicle (SUV) systems could already be obtained after 9 extrusion passes. This number of passes ensured particles sizes within the recommended range for prolonged blood circulation (<200 nm), as such dimensions are compatible with passive accumulation in tumour tissues through the enhanced permeability and retention (EPR) effect, which facilitates nanoparticle extravasation through the leaky vasculature characteristic of tumours. In addition, nanoparticles within this size range are less susceptible to protein corona formation and subsequent clearance by the reticuloendothelial system, thereby improving their suitability for systemic administration [8]. Nonetheless, the optimal condition was achieved at 13 passes. This conclusion was further supported by Tukey's post hoc analysis, which revealed no statistically significant differences between 13 and 17 passes, while maintaining negligible mass loss, as shown in the yield data presented in Table S1 of the Supplementary Material.

Figure 1b illustrates the effect of temperature (25-65ºC) on liposome size and polydispersity. In this case, as observed, the mean liposome size decreased with increasing temperature. This fact can be attributed to the weakening of Van der Waal forces between PC molecules and other phospholipids at higher temperatures, which play a key role in the assembly and long-term stability of liposomal bilayers [31]. Furthermore, 65ºC was the only temperature condition that showed statistically significant differences compared with all other tested temperatures ($p<0.0001$).

Figure 1c shows the influence of the MR between PC and CHOL on liposome characteristics. Phospholipids are known to constitute the most abundant fraction of liposomal formulations due to their amphiphilic nature and structural similarity to cellular membranes [43]. The results indicate that increasing the PC proportion generally led to a reduction in particle size. However, formulations containing CHOL

proportions lower than 20% exhibited several bimodal populations throughout the 21-day studied period. This behaviour can be explained by the structural properties of the lipid components. PC possesses a cylindrical geometry that favours the formation of fluid bilayers with pronounced curvature, thereby promoting the formation of smaller liposomes. In contrast, CHOL increases membrane rigidity and bilayer thickness, reducing membrane curvature [2]. Hence, MR values of 70:30 and 80:20 (PC: CHOL) were identified as the optimal formulations, as they provide the best compromise between liposome size and PDI. Thus, statistical analysis revealed significant differences among all the tested groups, except between the 80:20 and 90:10 formulations. Ultimately, the 70:30 MR was selected for subsequent experiments because this composition provides a more rigid bilayer structure, which may contribute to delaying drug diffusion and release [31].

Finally, Figure 1d presents the effect of PC purity on liposome properties [1,31]. As shown, increasing PC purity resulted in smaller particle sizes, likely due to the reduced presence and the consequently higher proportion of PC in the formulation. Nevertheless, the impurities present in lower-purity PC include additional phospholipids and steroid compounds that may contribute to bilayer stabilization. As a result, although formulations prepared with lower-purity PC exhibited slightly larger particle sizes, they also showed lower PDI values and reduced size variability. Therefore, these results confirmed that lower-yield PC is also suitable for the synthesis of stable SUV systems, despite the statistically differences observed ($p<0.0001$).

Otherwise, conventional liposomes were also characterized via Cryo-SEM (Figure 2). This technique revealed that the samples generally exhibited homogeneous particle size distribution, supporting the low PDI values previously obtained by DLS analysis. Nevertheless, some aggregates and larger spherical structures were observed, most likely because of the sample preparation process. In particular, immersion in liquid nitrogen may induce expansion and aggregation of liposomes due to freezing their aqueous core [33]. In addition, the sublimation step carried out during Cryo-SEM preparation may further contribute to theses morphological alterations.

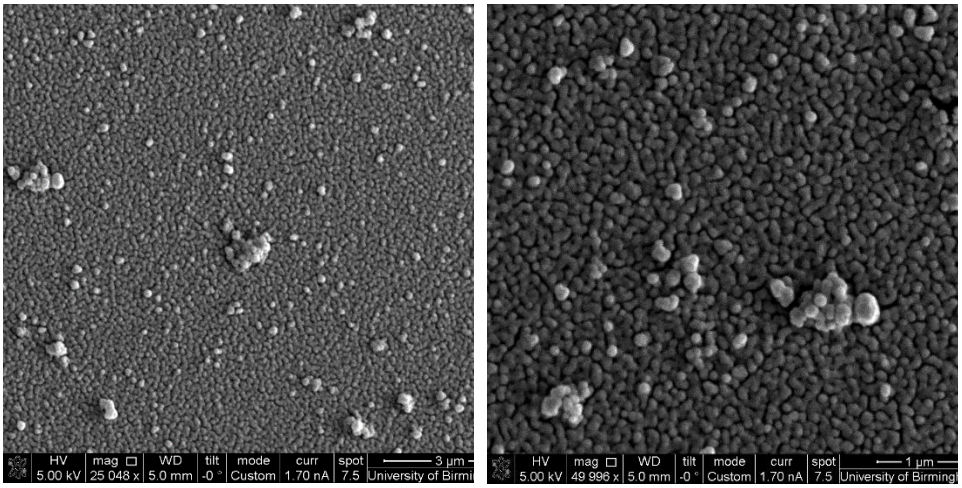

a) b)

Figure 2: Cryo-SEM micrographs of non-fractured conventional liposomes synthesized using a 70:30 PC:CHOL MR, an extrusion temperature of 65ºC, 13 extrusion passes, and low yield PC: a) 25,000x magnification and b) 50,000x magnification.

3.1.2. Synthesis of EU S100-coated liposomes

Due to the anionic nature of both EU S100 and conventional liposomes, SA was incorporated into the liposomal formulation to confer a positive surface charge and thereby enable electrostatic coating with EU S100. After SA incorporation and modification of the original 70:30 formulation, the results summarized in Table 1 were obtained.

Table 1: Size, PDI and zeta potential values of SA-containing liposomes.

Formulations	Size via DLS (nm)	PDI	Zeta Potential (mV)
Conventional lip 70:30	85.58	0.07	-8.30±1.08
70:30 + 9 mg SA	95 .33	0.14	+8.31±0.33
70:30 + 9 mg SA + 5FU	98.66	0.14	+7.90±0.33

Successful incorporation of SA was confirmed by the inversion of the surface charge from negative to positive values, indicating the formation of cationic liposomes. Moreover, as shown, incorporation of SA resulted in an increase in liposome size, which could be attributed to the structural effects associated with the inclusion of additional compounds during liposome assembly [7, 31]. This modification also led to a slight increase in the PDI value, reaching 0.14. Nevertheless, the resulting

dispersion remained stable over a period comparable to that observed for conventional liposomes.

Once a stable cationic liposomal system had been obtained, the coating process with EU S100 was performed. To this end, different concentrations of EU S100 were used to coat the SA-containing liposomal dispersions under magnetic stirring. The corresponding results obtained are shown in Table 2 and Figure 3.

Table 2: Size, PDI and zeta potential values of EU S100-coated liposomes.

[EU S100] (% w/v)	Size (DLS) (nm)	% of peaks in number of particles	PDI	Size ± SD (microscopy) (µm)	Zeta potential (mV)
0	95.0±12.6	100	0.16	-	+8.31±0.33
0.01	134.2±76.5 5,052±824.6	72 / 27	0.16	0.40±0.36	+7.26±0.25
0.025	131.4±12.1 4,320±1,190	40 / 60	0.43	3.97±1.07	+5.77±0.40
0.05	97.4±56.1 4,637±1,112	25 / 75	0.67	4.45±1.45	+3.54±0.43
0.1	90.8±19.6 2,088±590.2	9 / 91	1	2.15±1.11	-4.40±0.37
0.25	101.5±24.6 4,830±960.8	9 / 91	1	4.52±1.52	-4.95±0.36

The micrometric sizes of EU S100-coated liposomes that were observed by optical microscopy could be attributed to particle aggregation during the coating process. Indeed, coating occurs as a competitive phenomenon when the liposomal suspension is added to the EU S100 solution, favouring interactions not only between the polymer and individual liposomes, but also among coated liposomes themselves. This aggregation process was likely enhanced by the branched structure and high molecular weight of EU S100 [30]. Similar aggregation phenomena leading to micrometric particle sizes had also been reported in previous studies [44].

Although the aggregate sizes determined by optical microscopy vary among formulations, the lowest average particle size was observed for the formulation containing 0.1% (w/v) EU S100 (Figure 3a), suggesting that this concentration represents the optimal coating condition. This conclusion was further supported by the fact that this formulation

exhibited the highest proportion of coated liposomes within the sample (Figure 3b), together with a negative surface charge. In addition, zeta potential values reached a plateau at higher EU S100 concentrations, indicating successful coating saturation (Figure 3c).

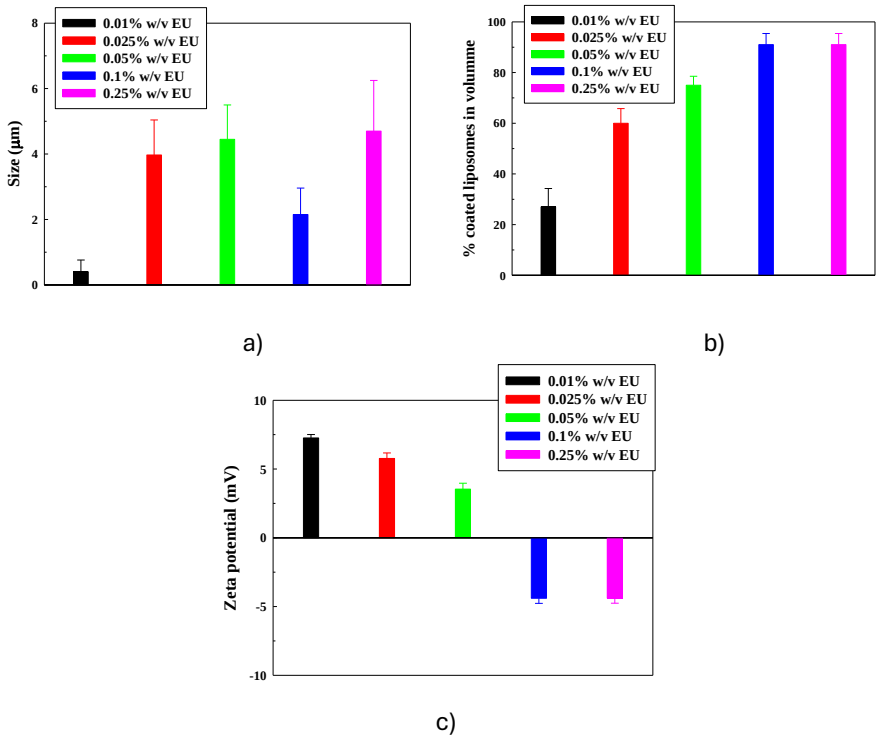

Figure 3: Results for EU S100 coated liposomes regarding: a) Aggregates sizes by optical microscopy analyses by FIJI, b) Percentage of coated liposomes in particle number by zetasizer, c) Zeta potential. Results are expressed as a mean values of 3 measurements ± SD.

Finally, Figure 4 illustrates the Cryo-SEM micrographs of EU S100-coated liposomes. As shown, aggregates with sizes consistent with those previously estimated by optical microscopy and DLS analyses were detected. In addition, at higher magnifications (Figure 4b), aggregation among individual liposomes could be clearly distinguished. Furthermore, numerous aggregates associated with the polymeric structure of EU S100 itself were identified, forming larger agglomerates, as illustrated in Figure 4c. The dimensions of these structures were consistent with the sizes previously measured experimentally [30]. This phenomenon has also been reported in previous works, in which both

coated liposomes and Eudragit® aggregates displaying similar morphologies were reported for comparable EU S100 concentrations [44].

Overall, the obtained results suggested that these large aggregates would not be suitable for intravenous administration, as they would be rapidly recognized and cleared by the immune system. Thus, these formulations appeared more appropriate for oral administration. In this regard, their use through this route could be particularly advantageous, since the anionic nature of the EU S100 coating may protect the encapsulated payload under acidic conditions, such as those encountered in the gastrointestinal tract.

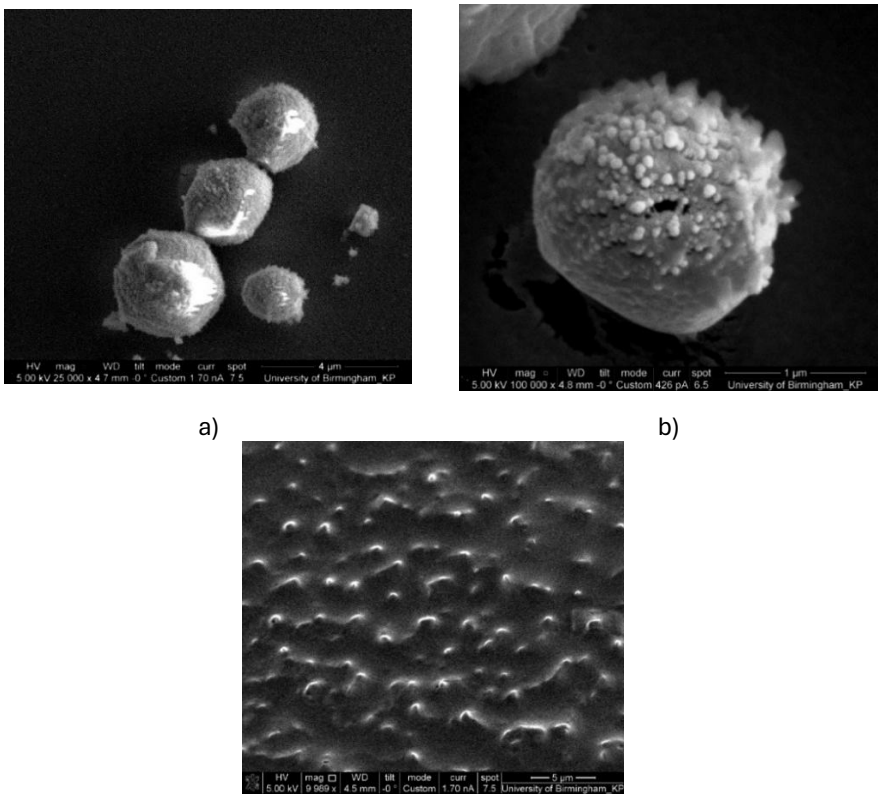

Figure 4: Cryo-SEM micrographs of non-fractured EU S100-coated liposomes at a) 25,000x magnification, b) 100,000x magnification, where individual conventional liposomes could be distinguished within the aggregates, and c) 10,000x magnification, illustrating the aggregation behaviour of the EU S100 polymer.

3.1.3. Synthesis of EU EPO-coated liposomes

To subsequently coat the liposomes with EU EPO, conventional liposomes were first synthesized at pH 7.4 and 4.5 using the three optimal extrusion conditions previously identified (5, 9, and 13 extrusion passes). The resulting formulations were then diluted in PBS acidified with HCl to evaluate their stability under acidic conditions, since EU EPO is only soluble at low pH values. Following this step, liposomes were coated with EU EPO at polymer concentrations ranging from 0.1% to 0.5 (w/v) [35]. The corresponding results are shown in Figure 5, Figure S3 (Supplementary Material), and Table 3:

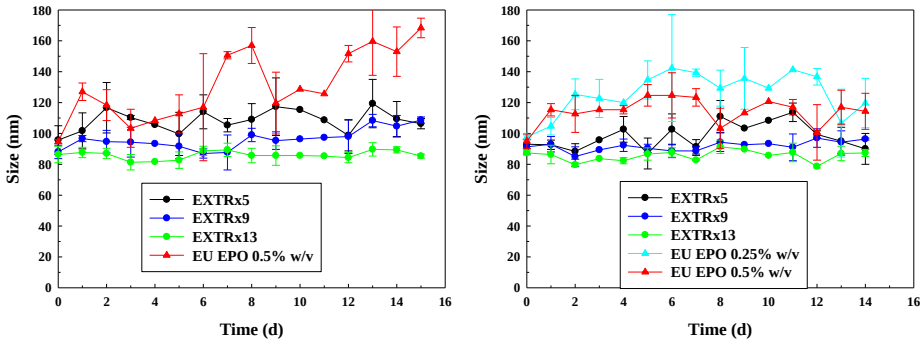

Figure 5: Evolution of particle size for conventional liposomes extruded at 5, 9, and 13 passes, as well as EU EPO-coated liposomes, under acidic conditions (pH 4.5). Liposomes were previously synthesized in: a) PBS at pH 7.4, and b) buffer at pH 4.5. Results are expressed as mean values ± SD from 3 independent measurements.

Firstly, conventional liposomes synthesized in PBS and diluted in medium at pH 4.5 did not exhibit significant changes in vesicles size, as shown in Figure 5a. This observation confirmed the stability achieved during the optimization of the liposome synthesis process. However, PDI values increased slightly, probably due to subtle changes in lipid-medium interactions, such as partial dehydration of polar head groups, which may affect bilayer flexibility in a non-uniform way [35]. Consequently, these results suggested that directly synthesizing liposomes under acidic conditions would not compromise their stability when high number of extrusion passes (9 or 13) are employed, as no statistically significant differences were observed.

Table 3: Particle size and zeta potential values of conventional and EU EPO-coated liposomes under acidic conditions. Liposomes were either initially synthesized in PBS (7.4) and later diluted in acidic medium or directly synthesized at pH 4.5. Results are expressed as mean values from 3 independent measurements.

pH	Passes in extrusion/ coating	Size (nm)	Size dev (nm)	PDI	Zeta potential (mV)
7.4	5	108.31	23.67	0.23	-6.06±0.66
	9	96.31	21.67	0.15	
	13	85.98	8.33	0.12	
	EPO 0.5%	130.98	73.67	0.18	+16.2±0.80
4.5	5	98.27	26.67	0.16	-5.83±0.85
	9	91.84	12.00	0.13	
	13	85.58	12.67	0.12	
	EPO 0.25%	125.69	44.67	0.17	+14.43±1.75
	EPO 0.5%	114.18	29.67	0.14	+19.07±1.00

Regarding EU EPO-coated liposomes, a minimum polymer concentration of 0.25% (w/v) was required to detect coated vesicles by DLS measurements. Below this concentration, DLS measurements mainly detected smaller particles, likely corresponding to dissolved polymer aggregated present in the samples [34]. In contrast, formulations containing 0.25% and 0.5% (w/v) EU EPO showed efficient coating, allowing proper characterization of the resulting liposomes, as illustrated in Figure 5b. Among the tested conditions, the formulation containing 0.5% (w/v) EU EPO provided the most favourable coating characteristics, yielding smaller coated liposomes, lower size deviations over time, and reduced PDI values, particularly when liposomes were directly synthesized at pH 4.5. Also, all statistically differences were observed among the different formulations ($p<0.0001$ and $p<0.05$ for EU EPO concentrations of 0.25% and EPO 0.5% (w/v), respectively).

However, liposomes coated with 0.25% (w/v) EU EPO may not possess a sufficiently stable polymer conformation at the liposomal surface. This polymer concentration might be insufficient to establish strong electrostatic interactions with the weakly anionic surface of conventional liposomes. Consistently, these formulations exhibited lower positive zeta potential values, suggesting less efficient coating and

lower colloidal stability over time due to weaker repulsive interactions among coated particles [35].

In the case of liposomes initially synthesized in PBS (pH 7.4), subsequent acidification of the medium decreased EU EPO solubility, favouring polymer self-aggregation and resulting in a less stable coating layer. This effect likely explained the instability observed for formulations containing lower polymer concentrations (0.25% w/v), as well as the larger size fluctuations detected over time. These findings confirmed that the optimized formulation correspond to liposomes directly synthesized at pH 4.5 and coated with 0.5% (w/v) EU EPO, which minimized particle size while maintaining improved stability.

Cryo-SEM characterization for this optimized system is presented in Figure 6. Small aggregates were observed in EU EPO-coated liposomes, probably due to both sample preparation effects and the presence of the polymer. However, these aggregates were significantly smaller than those observed for EU S100-coated liposomes ($p<0.0001$) [33]. In addition, several particles maintained a spherical morphology sizes close to the estimated 100 nm range, in agreement with DLS measurements. Within the small aggregates, individual conventional liposomes could still be distinguished.

Furthermore, the Cryo-SEM images shown in Figure 6 also revealed a markedly different behaviour of EU EPO under soluble conditions compared to EU S100. In particular, EU EPO appeared as dispersed particles rather than forming an extended polymer network. This distinct behaviour likely explained the more efficient coating process and the smaller particle sizes observed for EU EPO-coated liposomes compared with EU S100-coated liposomes in Figure 4, where the polymer network distribution can be clearly appreciated in Figure 4c.

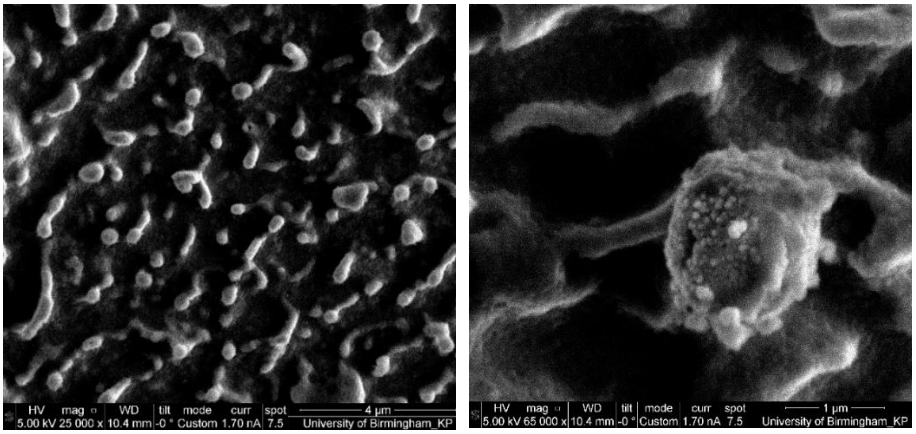

a) b)

Figure 6: SEM images obtained from non-cut samples of EU EPO coated liposomes at a) 25,000 magnification and b) 65,000 magnification, where the conventional liposomes could be observed.

Likewise, in contrast to EU S100-coated liposomes, the particle size of EU EPO-coated formulations remained compatible with systemic administration, as it may facilitate evasion from rapid immune clearance while still allowing passive accumulation at tumour sites through the enhanced permeability and retention (EPR) effect [8]. Although the measured zeta potential values were slightly positive, the presence of the polymeric coating may effectively shield the surface charge, thereby partially mitigating opsonisation.

3.2. Drug encapsulation efficiency and drug release

Encapsulation of 5FU was performed using the passive method [31], which has previously been reported to provide higher encapsulation efficiencies for liposomal systems compared with active loading approaches [43]. The encapsulation efficiency and loading capacity values obtained for all fabricated liposomal formulations are shown in Table 4:

Table 4: Encapsulation efficiency (%EE) and loading capacity values of 5FU in the different liposomal formulations. Results are expressed as a mean values ± SD from 3 independent experiments.

Liposomes system	%EE	Loading capacity (mg 5FU/mg lip)
Conventional 70:30	93.66±0.95	0.237±0.01
EU S100 coated	95.69±1.23	0.218±0.01
EU EPO coated	94.66±1.06	0.231±0.01

As it can be seen, the passive loading strategy resulted in nearly complete encapsulation of this hydrophilic drug, in agreement with previous studies [45]. This high encapsulation efficiency could be mainly attributed to the excellent solubility of 5FU in aqueous media, its small molecular size, and its neutral charge, all of which facilitate its incorporation into the aqueous core of liposomes during vesicle formation and extrusion.

Moreover, the loading capacities obtained in the present work are higher than those usually reported for hydrophilic drugs such as 5FU encapsulated in liposomes [46-48], and even higher than those described for certain lipophilic compounds [49, 50]. These findings further support the stability and monodispersity of the synthesized liposomal systems.

Interestingly, polymer-coated liposomes showed slightly higher encapsulation efficiencies than conventional liposomal formulations. This observation is consistent with previous reports indicating that polymeric coatings may contribute to improving drug retention and encapsulation efficiency in liposomal systems [33].

The drug release profiles obtained for the different formulations are shown in Figure 7:

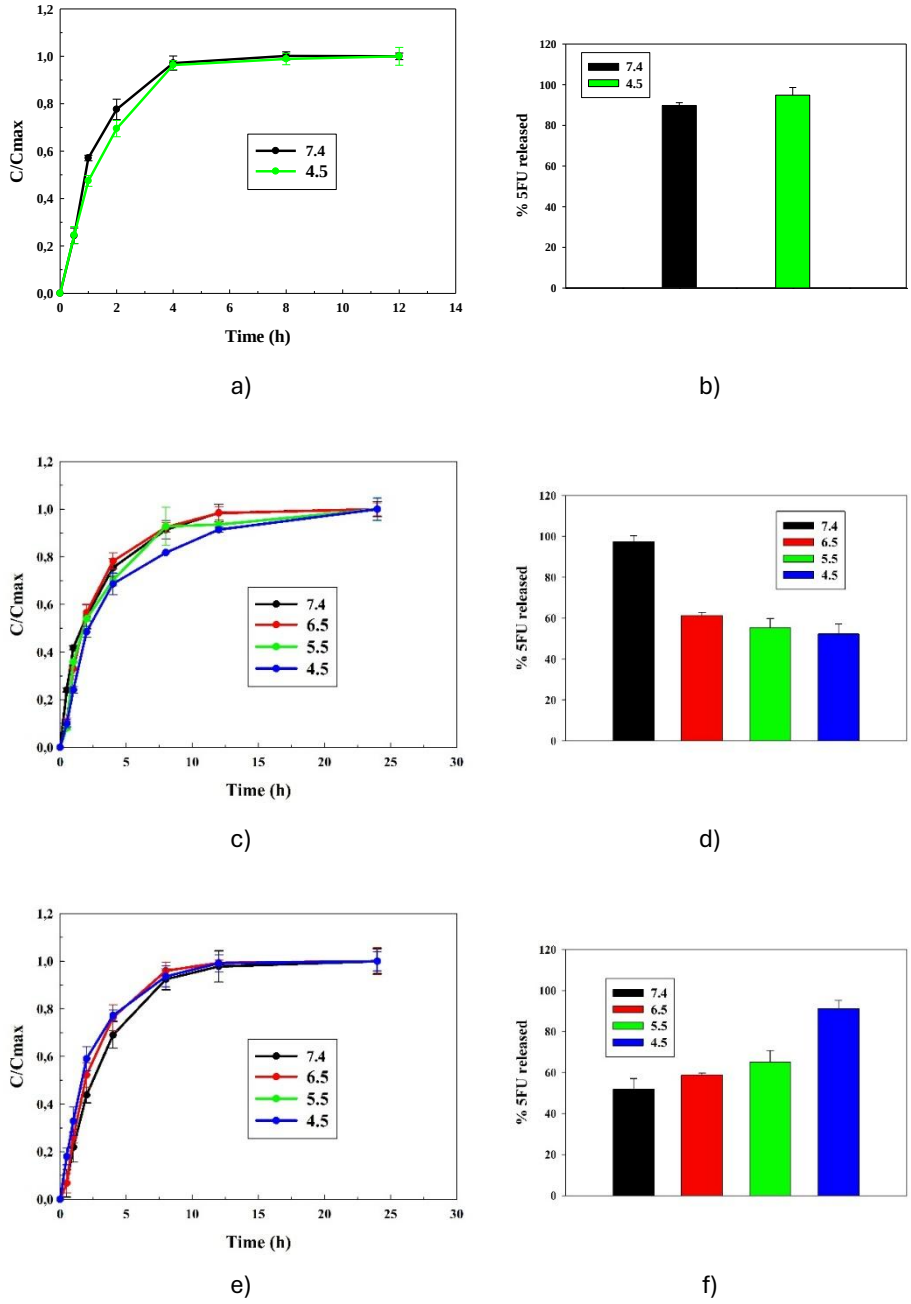

Figure 7: Cumulative drug release profiles and final percentage of released drug for: conventional liposomes (a, b), EU S100-coated liposomes (c,d), and EU EPO-coated liposomes (e, f). Results are expressed as mean values ± SD from three independent experiments.

As shown in Figures 7a and 7b, conventional liposomes did not exhibit pH-responsive behaviour, since nearly the entire drug payload was released into the medium within the first 4 hours. Furthermore, the stability of these liposomes under additional acidic pH conditions had previously been evaluated, revealing instability over a one-week period, as presented in Figure S2 (Supplementary Material).

The rapid release observed for conventional liposomes suggested that drug transport may be mainly governed by diffusion through the lipid bilayer. This behaviour was likely associated with the high membrane fluidity resulting from the elevated PC content and relatively low CHOL proportion, together with the hydrophilic nature and small molecular size of 5FU.

In contrast, pH-responsiveness was successfully achieved after coating the liposomes with Eudragit® polymers. EU S100-coated liposomes showed a clear pH-responsive behaviour, significantly reducing drug release under acidic conditions, where only approximately 50% of the encapsulated drug was released after 24 hours, as shown in Figure 7d. Nonetheless, the kinetic profiles presented in Figure 7c revealed similar release trends across the tested media. These findings agreed with previous studies involving EU S100-coated liposomal systems [32].

Similarly, EU EPO-coated liposomes also displayed pH-responsive behaviour, effectively limiting drug release under alkaline conditions. Under these conditions, approximately 50% of the drug payload remained retained after 24 hours, as shown in Figure 7f. In contrast, drug release progressively increased as the pH became more acidic, reaching complete release once the polymer reached its solubility threshold. As previously observed for permeation studies involving this coating, the kinetic profiles themselves did not exhibit major differences among conditions [35].

Statistically significant differences were found between conditions in which the polymer coatings remained soluble and those in which they were insoluble ($p<0.0001$ for all conditions except at $t=0$).

Overall, these findings demonstrate the successful development of a pH-responsive liposomal drug delivery system capable of responding to both acidic and alkaline environments. Particularly, the obtained results again reinforce the concept that EU-S100-coated liposomes may be especially suitable for oral drug administration, as they preferentially promote drug release under alkaline conditions within the gastrointestinal tract. Conversely, EU EPO-coated liposomes appear more appropriate for systemic administration, since they enhance drug release under the acidic conditions characteristic of the tumour microenvironment and intracellular endosomal/lysosomal compartments.

3.5. Theoretical model fitting

The experimental drug release data obtained for the developed liposomal systems were fitted to four different kinetic models: zero-order, first-order, Higuchi, and Korsmeyer-Peppas models. The corresponding fitting parameters are shown in Table 5 and Figure S4 (Supplementary Material):

Table 5: Fitting parameters obtained from the adjustment of the experimental drug release data to the zero-order, first-order, Higuchi, and Korsmeyer-Peppas kinetic models, together with their corresponding coefficients of determination (R^2).

Models		Zero order		First order		Higuchi		Korsmeyer-Peppas		
Liposomes		k_0 (h^{-1})	R^2	k_1 (h^{-1})	R^2	k_H ($h^{-0.5}$)	R^2	k_{KP} (h^{-n})	n	R^2
70:30	PBS	0.11	0.01	0.79	0.99	0.53	0.99	0.49	0.69	0.99
	4.5	0.11	0.08	0.63	1.00	0.48	0.99	0.43	0.68	0.95
EU S100	PBS	0.06	0.02	0.42	0.99	0.39	1.00	0.38	0.54	1.00
	6.5	0.06	0.08	0.34	0.99	0.33	0.98	0.30	0.96	0.99
	5.5	0.06	0.14	0.34	0.99	0.33	0.99	0.28	0.94	0.99
	4.5	0.06	0.31	0.27	0.98	0.28	0.98	0.25	0.95	1.00
EU EPO	PBS	0.06	0.32	0.28	0.99	0.25	0.98	0.21	0.85	1.00
	6.5	0.06	0.23	0.32	1.00	0.25	0.98	0.25	0.86	0.99
	5.5	0.06	0.20	0.35	0.99	0.30	0.98	0.26	0.81	0.99
	4.5	0.06	0.09	0.40	1.00	0.36	1.00	0.32	0.70	1.00

As presented, the zero-order kinetic model provided the poorest fitting performance, as evidenced by the lower R^2 values obtained. This

result was expected, since drug release from liposomal systems is intrinsically dependent on both drug concentration and time. Nevertheless, under conditions where the polymer coatings remained insoluble, the fitting to the zero-order model improved slightly, further supporting the delayed and sustained release behaviour induced by the coatings [40]. The concentration-dependent nature of drug release also explains why the first-order kinetic model provided the best overall fitting to the experimental data. Similarly, the Higuchi model showed excellent fitting performance during the early release stages (C/Cmax<60%), as reflected by R^2 values shown in Table 7. Both models have previously been reported as suitable for liposomal systems in which diffusion constitutes the predominant release mechanism [51, 52]. Furthermore, fitting results confirmed that polymer coating reduced the release rate, as demonstrated by the lower kinetic constant values obtained for coated formulations, particularly when the polymer remained insoluble.

Besides, analysis of the Korsmeyer-Peppas exponent (*n*) suggested that the polymeric coating significantly influenced the release mechanism, especially under insoluble conditions. In these cases, the *n* values approached those characteristics of Case II transport (n>0.8), rather than purely Fickian diffusion, while still maintaining satisfactory R^2 values. This fact probably indicated that the coating layer contributed to drug release through additional anomalous transport mechanisms, such as polymer relaxation or structural reorganization processes. Additionally, the relative magnitude of the kinetic constants further confirmed the slower release associated with insoluble polymer conditions.

Thus, in general, these findings demonstrated the enhanced stability and controlled-released properties achieved through optimization of the coating process. Similar conclusions have also been reported in previous studies, where the Korsmeyer-Peppas model successfully described drug release from liposomal systems [53], including formulations containing drugs such as letrozole and paclitaxel, for which quasi-Fickian diffusion mechanisms were observed [54]. Since the Higuchi and first-order models consistently provided the best fittings, it could be

concluded that diffusion remained the predominant release mechanism in the developed systems, as previously discussed [52].

3.6. *In vitro* evaluation of 5FU-loaded liposomes' antiproliferative activity

As previously described, the HS-5 and BT-474 cell lines were used to evaluate the effects of coated and uncoated liposomal formulations through MTT viability assays. Prior to these experiments, preliminary assays were conducted using different concentrations of free 5FU, ranging from 0 (control) to 30 μM, to determine the IC_{50} for each cell line. The obtained IC_{50} values at 48 hours were 2.5 μM for BT-474 cells (Figure 8a), which was lower than those reported in previous studies [39], and 30 μM for HS-5 cells (Figure 8b).

For subsequent experiments, the IC_{50} determined for BT-474 cells was selected as the normalised treatment concentration for both cell lines, since using the IC_{50} value obtained for HS-5 stromal cells would result in excessively low survival rates in BT-474 cells, thereby hindering an accurate evaluation of the effects associated with the different liposomal formulations [55, 56].

Once the IC_{50} of 5FU has been established at 2.5 μM, the following treatments were evaluated: loaded (L+5FU) and unloaded (L) conventional liposomes, loaded (S100+5FU) and unloaded (S100) EU S100-coated liposomes, and loaded (EPO+5FU) and unloaded (EPO) EU EPO-coated liposomes. All loaded formulations were diluted to achieve a final drug concentration equivalent to the selected IC_{50} value, while unloaded liposomal formulations were diluted using the same dilution factor. The results of MTT viability assays performed after 24, 48, and 72h of treatment in HS-5 and BT-474 cell lines are presented in Figure 8.

As expected, unloaded liposomal formulations did not significantly reduce cell viability, which is consistent with the known biocompatible of the reagents employed in their synthesis, as shown in Figures 8 c and 8d [28, 33, 57]. Nonetheless, the EU S100-coated liposomes exhibited slightly higher intrinsic toxicity, resulting in approximately 75% cell viability in BT-474 cells after 72 hours of treatment. Similar viability

values (80%) have been previously reported for other cell lines, such as HCT-116, after 48 hours of exposure to comparable formulations [58].

On the other hand, conventional loaded liposomes (L+5FU) did not show substantial differences compared with free 5FU until 72 hours, as confirmed by Tukey's post hoc analysis following two-way ANOVA in both cell lines. This fact was probably associated with the rapid release of 5FU from conventional liposomes, which occurs almost completely within the first 4 hours of treatment, resulting in a release profile that may proceed faster *in vitro* than the cellular internalization process itself [59].

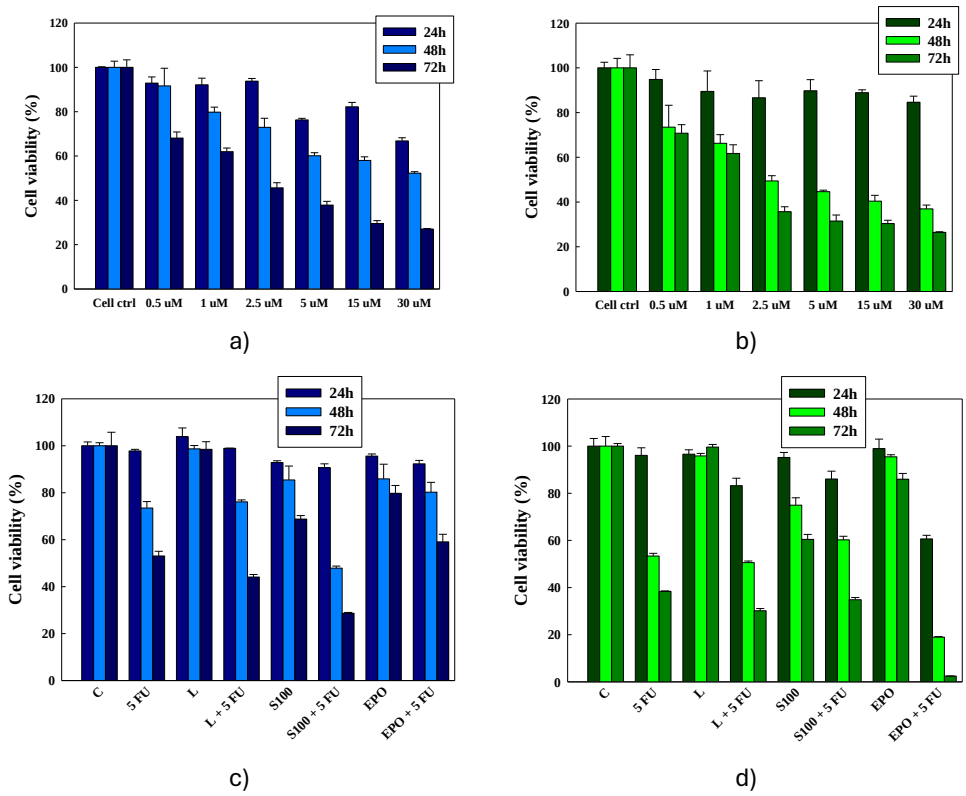

Figure 8: Cell viability (%) determined by MTT assays in HS-5 and BT-474 cell lines. Sub-panels (a and b) show the determination of the IC50 value of 5FU at 48 hours for HS-5 and BT-474 cells, respectively. Sub-panels c) and d) present the cytotoxicity and antiproliferative effects of the different liposomal formulations, including untreated control cells (C), free 5FU at the IC50 concentration determined for BT-474 cells, and the different designed treatments evaluated after 24, 48, and 72 hours in c) HS-5 and d) BT-474 cells. Results are expressed as mean values ± SD from 3 independent experiments.

By contrast, EU-coated liposomes exhibited significantly different effects compared with non-coated liposomes ($p<0.0001$). In this way, EU EPO-coated liposomes markedly reduced BT-474 cell viability, reaching values close to 5% after 72 hours of treatment. This enhanced antiproliferative activity may be associated with the pH-responsive behaviour of the formulation, which could favour intracellular release of 5FU under acidic conditions characteristic of tumour cells and endosomal compartments [22, 60]. For the same reason, EU EPO-coated liposomes produced a substantially lower reduction in HS-5 cell viability compared with the other 5FU-loaded formulations, maintaining approximately 60% viability after 72 hours of treatment.

Otherwise, the effect of EU S100-coated liposomes on BT-474 cells was relatively similar to that observed for conventional 5FU-loaded liposomes, reducing cell viability to approximately 35% after 72 hours. This behaviour may be related to the ability of the EU S100 coating to protect the encapsulated payload under acidic conditions, together with the larger particle size of these formulations, which could slow down their cellular internalization rate. However, EU S100-coated liposomes induced a greater reduction in HS-5 cell viability than conventional loaded liposomes, decreasing viability to approximately 40-45%, possibly due to the formation of large aggregates that may enhance nonspecific interactions with stromal cells.

3.7. Uptake

To further corroborate some of the results obtained in the viability assays described in the previous section, the cellular internalization of the different liposomal formulations in BT-474 cells was analysed by confocal microscopy. Images were acquired after 0.5, 1, 4, and 24 hours of treatment. As described in the Methodology section, rhodamine B was encapsulated within the liposomes, while cells were stained with Celltracker® Green. The resulting images are shown in Figure 9.

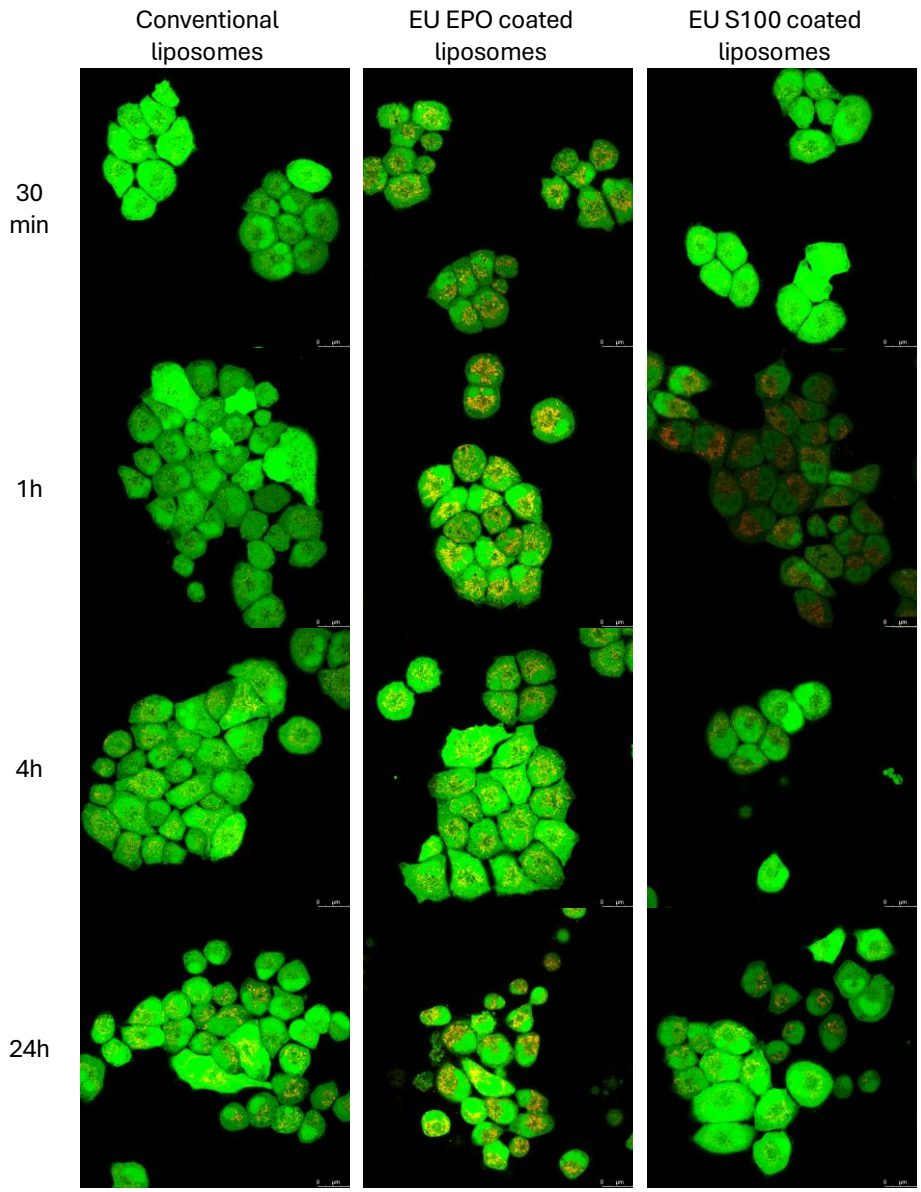

Figure 9: Representative confocal microscopy images showing the cellular uptake of the different liposomal formulations (red) in BT-474 cells (green) after 0.5, 1, 4, and 24 hours of treatment. Scale bar = 25 µm.

As shown in Figure 9, EU EPO-coated liposomes exhibited the fastest internalization rate, as fluorescent red signal could already be distinguished inside the cells only 30 minutes after treatment. This observation may be related to the slightly positive surface charge of these liposomes, which could favour their interaction with the negatively

charged cellular membrane. Such enhanced internalization may help explain why this formulation produced the greatest reduction in breast cancer cell viability. In contrast, internalization of EU S100-coated liposomes became evident after approximately 1 hour of treatment. However, the smaller fluorescent red signal area observed after 4 and 24 hours suggested that the liposomes were internalized to a lesser extent than EU EPO-coated formulations, most likely due to their larger particle size, as previously discussed. Finally, conventional liposomes exhibited the slowest cellular internalization profile, since red intracellular fluorescence was not clearly observed until 4 hours of treatment. Nevertheless, after 24 hours, conventional liposomes appeared to be internalized more efficiently by BT-474 cells than EU S100-coated liposomes, which may contribute to explaining the greater reduction in cell viability observed for this formulation in comparison with EU S100-coated systems.

4. Conclusions

In summary, this work presents a versatile liposomal formulation that could be used to selectively deliver chemotherapeutic agents, as well other drugs, to physiological and/or pathological microenvironments with opposite pH conditions.

Specifically, the developed formulation consists of a liposomal core composed of PC and CHOL, which proportion was optimized to obtain SUVs with particle sizes below 100 nm and PDI values lower than 0.1 over a 21-day period, thereby providing a robust and reproducible nanocarrier platform.

Afterwards, pH-responsiveness was conferred to this liposomal core through electrostatic coating with Eudragit® polymers. Coating with EU S100 exhibited a marked tendency to aggregate due to the high molecular weight of the polymer and its behaviour in buffered solutions, making this formulation more suitable for oral administration. In this case, optimal coating condition was achieved at a polymer concentration of 0.1% (w/v). In contrast, coating with EU EPO yielded stable nanosystems at a concentration of 0.5% (w/v), maintaining good monodispersity and

particle sizes below 200 nm, which highlights their potential suitability for systemic administration.

Despite their morphological differences, both coated liposomal formulations exhibited high encapsulation efficiencies for 5FU and prevented up to 50% of the encapsulated drug from being released within 24 hours under pH conditions in which the polymer coatings remained insoluble. Moreover, the pH-responsive modifications observed in the release kinetics were supported by the *n* values obtained from the Korsmeyer-Peppas model fitting, suggesting changes in the release mechanism when the coatings remained insoluble. Nevertheless, the best overall fittings were obtained for the first-order and Higuchi models, confirming diffusion as the predominant release mechanism.

Finally, *in vitro* assays demonstrated the biocompatibility of the developed liposomal formulations and further confirmed the pH-responsive behaviour of the coated systems. In particular, EU EPO-coated liposomes proved to be the most effective in reducing tumour cell viability while exhibiting the lowest toxicity towards healthy stromal cells. This fact was likely related to their enhanced ability to release the encapsulated drug under acidic conditions, such as those found in tumour cell cultures. Furthermore, the marked reduction observed in BT-474 cell viability may also be explained by the faster cellular internalization rate exhibited by EU EPO-coated liposomes compared with conventional liposomes and EU-S100-coated formulations.

Conflict of interest

Authors do not declare any conflict of interest.

Acknowledgements

M. Blanco-López wants to acknowledge the funds from “Programa propio III de la Universidad de Salamanca: Ayudas para financiar contratos predoctorales de la Universidad de Salamanca cofinanciados por el Banco Santander” for his PhD fellowship. The authors would like to express their gratitude to the Spanish Ministry of Science and

Innovation for the financial support, research project: PID2022-1405990B-I00.

References

[1] M. Xu, X. Han, H. Xiong, Y. Gao, B. Xu, G. Zhu, J. Li, 2023. Cancer nanomedicine: Emerging strategies and therapeutic potentials. Molecules. 28, 5145.

[2] R.L. Siegel, K.D. Miller, A. Jemal, Cancer statistics, CA Cancer J. Clin. 68 (2018) 7-30.

[3] M. Germain, F. Caputo, S. Metcalfe, G. Tosi, K. Spring, A.K.O. Aslund, A. Pottier, R. Schiffelers, A. Ceccaldi, R. Schmid, Delivering the power of nanomedicine to patients today, J.C.R. 326 (2020) 164-171.

[4] World Health Organization, Cancer, WHO Fact Sheets, 2024. https://www.who.int/news-room/fact-sheets/detail/cancer (Accessed 12 May 2026).

[5] P.R. Karn, Z. Vanic, I. Pepic, N. Skalko-Basnet, Mucoadhesive liposomal delivery systems: The choice of coating material, Drug. Dev. Ind. Pharm. 37 (2011) 482-488.

[6] S. De Leo, D. Berti, F. Di Francesco, 2018. Encapsulation of curcumin-loaded liposomes for colonic drug delivery in a pH-responsive polymer cluster using a pH-driven and organic solvent-free process. Mol. 23, 739.

[7] B. Barea, A. Franco, M.T. Tomas-Ugarte, 2020. Ternary nanocomposite carriers based on organic clay-lipid vesicles as an effective colon-targeted drug delivery system: Preparation and in vitro/in vivo characterization. J. Nanobiotechnology. 18, 17.

[8] Y. Barenholz, G. Cevc, Physical chemistry of biological surfaces. Structure and properties of membranes, Marcel Dekker, 2000.

[9] G.M. Soliman, Nanoparticles as safe and effective delivery systems of antifungal agents: Achievements and challenges, Int. J. Pharm. 523 (2017) 15–32.

[10] R.M. Straubinger, R.D. Arnold, R. Zhou, R. Mazurchuk, J.E. Slack, Antivascular and antitumor activities of liposome-associated drugs, Anticancer Res. 24 (2004) 397–404.

[11] M.D. Fulton, W. Najahi-Missaoui, 2023. Liposomes in cancer therapy: How did we start and where we are now. Int. J. Mol. Sci. 24, 6615.

[12] L.W. Allahou, S.Y. Madani, A. Seifalian, 2021. Investigating the application of liposomes as drug delivery systems for diagnosis and treatment of cancer. Int. J. Biomater. 1, 3041969.

[13] S.B. Mascarenhas, M. Koland, S.M. Ghetia, Development and investigation of Eudragit S-100 encapsulated chitosan-coated liposomes of prednisolone for colon targeting, J Young Pharm. 11 (2019) 7–11.

[14] C. J. Chu, F.C. Szoka, pH-Sensitive Liposomes, J. Liposome Res. 4 (1994) 361–395.

[15] J. Lou, M.D. Best, A general approach to enzyme-responsive liposomes, Chem. Eur. J. 26 (2020) 8597-8607.

[16] W. Ong, Y. Yang, A.C. Cruciano, R.L. McCarley, Redox-triggered contents releasefrom liposomes, J. AM.Chem. Soc. 130 (2008) 14739-14744.

[17] K. Kono, H. Hayashi, T. Takagishi, Temperaure-sensitive liposomes: Liposomes bearing poly(N-isopropylacrylamide), J. Control. Release. 30 (1994) 69-75.

[18] J. Lou, R. Sagar, M.D. Best, Metabolite-responsive liposomes employing synthetic lipid switches driven by molecular recognition principles, Acc. Chem. Res. 55 (2022) 2882–2891

[19] S.J. Leung, M. Romanowski, Light-activated content release from liposomes, Theranostics. 2 (2012) 1020-1036.

[20] H. Marie, L. Lemaire, F.Franconi, S. Lajnef, Y-M. Frapart, V. Nicolas, G. Frebourg, M. Trichet, C. Menager, S. Lesieur, Superparamagnetic liposomes for MRI monitoring and external magnetic field-induced selective targeting of malignant brain tumors, Adv. Funct. Mater. 25 (2015) 1258-1269.

[21] S-L. Huang, R.C. MacDonald, Acoustically active liposomes for drug encapsulation and ultrasound-triggered release, BBA Membr. 1665 (2004) 134-141.

[22] Y. Lee, D.H. Thompson, 2017. Stimuli-responsive liposomes for drug delivery. WIREs Nanomed Nanobiotechnol. 9, 1407.

[23] S. Marchun, C.R. Dass, P. Sriamornsak, Targeted therapy for cancer using pH-responsive nanocarrier systems, Life Sciences. 90 (2012) 381-387.

[24] R. Tenchov, R. Bird, A.E. Curtze, Q. Zhou, Lipid nanoparticles: From liposomes to mRNA vaccine delivery: a landscape of research diversity and advancement, ACS Nano. 15 (2021) 16982–17015.

[25] K.M. Hosny, O.A. Ahmed, R.T. Al-Abdali, Enteric-coated alendronate sodium nanoliposomes: A novel formula to overcome barriers for the treatment of osteoporosis, Exp. Opin. Drug Deliv. 10 (2013) 741-746.

[26] S. Aib, K. Iqbal, N. Khan, S. Khalid, M. Adnan, S.M. Umair, M.J. Dar, 2022. pH-sensitive liposomes for colonic co-delivery of mesalazine and curcumin for the treatment of ulcerative colitis. J. Drug Deliv. Sci. Technol. 72, 103335.

[27] H. Karanth, R.S.R.Murphy, pH sensitive liposomes-principle and application in cancer therapy, J. Pharm. Pharmacol. 59 (2007) 469-483.

[28] C.N. Patra, R. Priya, S. Swain, G.K. Jena, K.C. Panigrahi, D. Ghose, Pharmaceutical significance of Eudragit: A review, Futur. J. Pharm. Sci. 3 (2017) 33-45.

[29] T.M.Allen, P.R. Cullis, Liposomal drug delivery systems: From concept to clinical applications, Adv Drug Deliv Rev. 65 (2013) 36–48.

[30] T.V. Sakhno, N.N. Barashkov, I.S. Irgibaeva, S.V. Pustovit, Y.E. Sakhno, Polymer coatings for protection of wood and wood-based materials, ACES. 6 (2016) 93-110.

[31] G. Bozzuto, A. Molinari, Liposomes as nanomedical devices, Int. J. Nanomed. 10 (2015) 975–999.

[32] H. Alghurabi, T. Tagami, K.Ogawa, T. Ozeki, 2022. Preparation, characterization and in vitro evaluation of Eudragit S100-coated bile salt-containing liposomes for oral colonic delivery of budesonide. Polym. 14, 2693.

[33] C. Caddeo, M. Gabriele, X. Fernández-Busquets, D. Valenti, A.M. Fadda, L. Pucci, M. Manconi, Antioxidant activity of quercetin in Eudragit-coated liposomes for intestinal delivery, Int. J. Pharm. 565 (2019) 64-69.

[34] J. Li, I.W. Lee, G.H. Shin, X. Chen, H.J. Park, Curcumin-Eudragit E PO solid dispersion: A simple and potent method to solve the problems of curcumin, Eur. J. Pharm. Biopharm. 94 (2015) 322-332.

[35] A. Hasanovi, C. Hollick, K. Fischinger, C. Valenta, Improvement in physicochemical parameters of DPPC liposomes and increase in skin permeation of acyclovir and minoxidil by the addition of cationic polymers, Eur. J. Pharm. Biopharm. 75 (2010) 148-153.

[36] Q. Ke, K. Jiang, H. Li, L. Zhang, B, Chen. Hierarchically micro-, meso-, and macro-porous MOF nanosystems for localized cross-scale dual-biomolecule loading and guest-carrier cooperative anticancer therapy, ACS Nano. 18 (2024) 21911-21924.

[37] Z. Zhou, Q. Ke, M. Wu, L. Zhang, K. Jiang, Pore space partition approach of ZIF-8 for pH responsive codelivery of ursolic acid and 5-fluorouracil, ACS Materials Lett. 5 (2023) 466-472.

[38] H. Zhang, Thin-Film Hydration Followed by Extrusion Method for Liposome Preparation, Methods Mol. Biol. 1522 (2017) 17–22.

[39] C. Karthika R. Sureshkumar, D.V. Sajini, G.Md. Ashraf, Md.H. Rahman, 5-fluorouacil and curcumin with pectin coating as a treatment regimen for titanium dioxide with dimethylhydrazine-induced colon cancer model, Environ. Sci. & Pollut. Res. 29 (2022) 63202-63215.

[40] A. Jain, S.K. Jain, In vitro release kinetics model fitting of liposomes: An insight, Chem. Phys. Lipids. 201 (2016) 58-40.

[41] R.E. Duncan, M.C. Archer, Farnesol induces thyroid hormone receptor (THR) beta1 but inhibits THR-mediated signaling in MCF-7 human breast cancer cells. Biochem. Biophys. Res. Commun. 343 (2006) 239–243.

[42] Avanti® Research, How to use the Avanti® Mini-Extruder. https://www.sigmaaldrich.com/ES/es/technical-documents/protocol/materials-science-and-engineering/drug-delivery/avanti-mini-extruder?utm, 2025 (accessed 15 December 2025)

[43] G. Gregoriadis, 2016. Liposomes in Drug Delivery: How It All Happened. Pharmaceutics. 8, 19.

[44] MJ. Barea, MJ. Henkins, MH. Gaber, RH. Bridson, Evaluation of liposomes coated with a pH responsive polymer, Int. J. Pharm. 402 (2010) 89-94.

[45] P. Crosasso, P. Brusa, F. Dosio, S. Arpicco, D. Pacchioni, F. Schuber, L. Cattel, 1997. Antitumoral activity of liposomes and immunoliposomes containing 5-fluorouridine prodrugs. J. Pharm. Sci. 86, 7.

[46] M. Fresta, A. Villari, G. Puglisi, G. Cavallaro, 5-Fluoracil: Various kinds of loaded liposomes: Encapsulation efficiency, storage stability and fusogenic properties, Int. J. Pharm. 99 (1993) 145-156.

[47] C.A.M. da Costa, A.M. Moraes, Encapsulation of 5-fluoroacil in liposomes for topical administration, Acta Sci. Technol. 25 (2003) 53-61.

[48] S. Handali, E. Moghimipour, M. Kouchak, Z. Ramezani, M. Amini, K.A. Angali, S. Saremy, F.A. Dorkoosh, M. Rezaei, New folate receptor targeted nano liposomes for delivery of 5-fluorouacil to cancer cells: Strong implication for enhanced potency and safety, Life Sci. 227 (2019) 39-50.

[49] S.M.G. Ong, L.C. Ming, K.S. Lee, K.H. Yuen, 2016. Influence of the encapsulation efficiency and size of liposome on the oral bioavailability of griseofulvin-loaded liposomes. Pharmaceutics. 8, 25.

[50] T. Nii, F. Ishii, Encapsulation efficiency of water-soluble and insoluble drugs in liposomes prepared by the microencapsulation vesicle method, Int. J. Pharm. 298 (2005) 198-205.

[51] P. Jayachandran, S. Ilango, V. Suseela, R. Nirmaladevi, M.R. Shaik, M. Khan, B. Shaik, 2023. Green synthesized silver nanoparticle-loaded liposome-based nanoarchitectonics for cancer management: In vitro drug release analysis. Biomedicines. 11, 217.

[52] N. Karimi, B. Ghanbarzadeh, F. Hajibonabi, Z. Hojabri, K. Ganbarov, H.S. Kafil, H. Hamishehkar, M. Yousefi, R.R. Mokarram, F.S. Kamounah, Turmeric extract loaded nanoliposome as a potential antioxidant and antimicrobial nanocarrier for food applications, Food Biosci. 29 (2019) 110–117.

[53] F. Haghiralsadat, G. Amoabediny, M.N. Helder, S. Naderinezhad, M.H. Sheikhha, T. Forouzanfar, B. Zandieh-Doulabi, A comprehensive mathematical model of drug release kinetics from nano-liposomes, derived from optimization studies of cationic PEGylated liposomal doxorubicin formulations for drug-gene delivery, Artif. Cells Nanomed. Biotechnol. 46 (2018) 169–177.

[54] M.T. Vu, N.T.T. Le, T.L-B. Pham, N.H. Nguyen, D.H. Nguyen, 2020. Development and characterization of soy lecithin liposome as potential drug carrier systems for codelivery of letrozole and paclitaxel. J. Nanomater. 8896455.

[55] S. Jung, S. Lee, H. Lee, J. Yoon, E.K. Lee, Oleic acid-embedded nanoliposome as a selective tumoricidal agent, Colloids Surf. B Biointerfaces. 146 (2016) 585-589.

[56] V.V. Serra, A. Zamarron, M.A.F. Faustino, M.C. Iglesias-de la Cruz, A. Blázquez, J.M.M. Rodrigues, M.G.P.M.S. Neves, J.A.S. Cavaleiro, A. Juarranz, F. Sanz-Rodriguez, New porphyrin amino acid conjugates: Synthesis and photodynamic effect in human epithelial cells, Bioorg. Med. Chem. 18 (2010) 6170-6178.

[57] S. Inam, M. Irfan, N. Lali, H.K. Syed, S. Asghar, I.U. Khan, S-U-D. Khan, M.S. Iqbal, I. Zaheer, A. Khames, H.A. Abou-Taleb, M.A.S. Abourehab, 2022. Development and characterization of Eudragit EPO-based solid dispersion of rosuvastatin calcium to foresee the impact on solubility, dissolution, and antihyperlipidemic activity. Pharm. 18, 492.

[58] S. Guo, G. Wang, T. Wu, F. Bai, J. Xu, X. Zhang, Solid dispersion of berberine hydrochloride and Eudragit S100: Formulation, physicochemical characterization and cytotoxicity evaluation, J. Drug Deliv. Sci. Technol. 40 (2017) 21-27.

[59] K. Sen, S. Banerjee, M. Mandal, Dual drug loaded liposome bearing apigenin and 5-fluorouracil for synergistic therapeutic efficacy in colorectal cancer, Colloids Surf. B. 180 (2019) 9-22.

[60] O. Udofot, K. Affram, B. Israel, E. Agyare, Cytotoxicity of 5-fluorouracil-loaded pH-sensitive liposomal nanoparticles in colorectal cancer cell lines, Integr. Cancer Sci. Ther. 2 (2015) 245-252.

Supporting information

Expanding the pH Window of Liposomal Drug Delivery Using Eudragit®-Based Polymeric Coatings

Marcos Blanco-López[1], Inmaculada de Dios-Pérez[1,3], Celia Nieto[1,2,], Antonio Tabernero[1,2,*], Patricia P. Esteban[3], Eva Martín del Valle[1,2].*

1) *Department of Chemical Engineering. University of Salamanca. Plaza Los Caídos s/n, 37008 Salamanca (Spain).*
2) *Institute for Biomedical Research in Salamanca (IBSAL), Paseo de San Vicente 87, 37007, Salamanca (Spain).*
3) *Healthcare Technologies Institute (HTI), University of Birmingham, B15 2TT, Birmingham (UK).*

**** Corresponding author at: Antonio Tabernero (antaber@usal.es)***

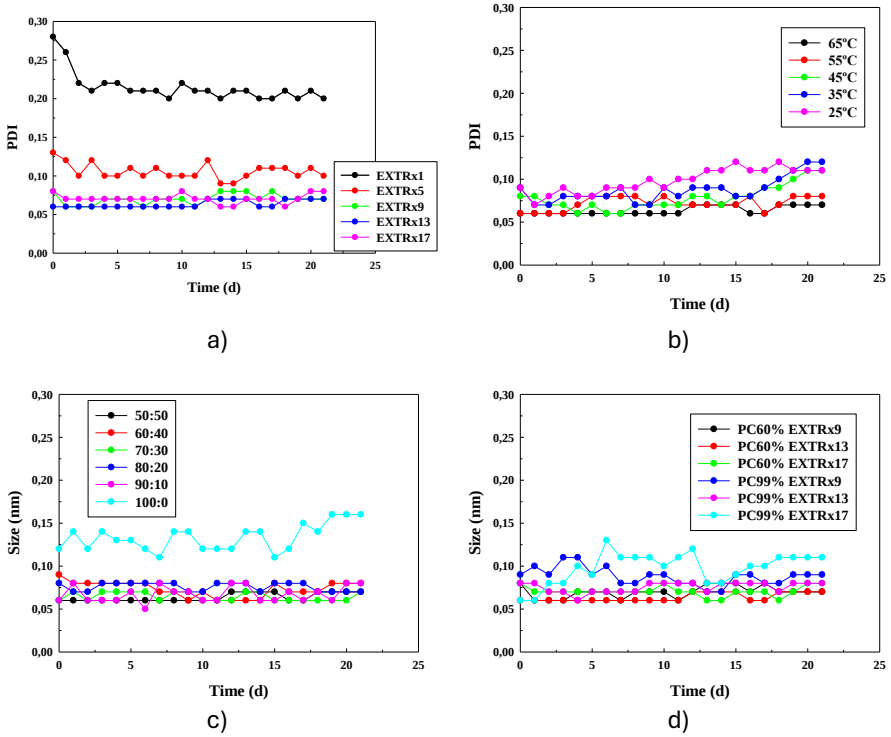

Figure S1: Evolution of the PDI of liposomes over 21 days as a function of: a) number of extrusion passes, b) sonication and extrusion temperature, c) PC:CHOL molar ratio, and d) PC yield.

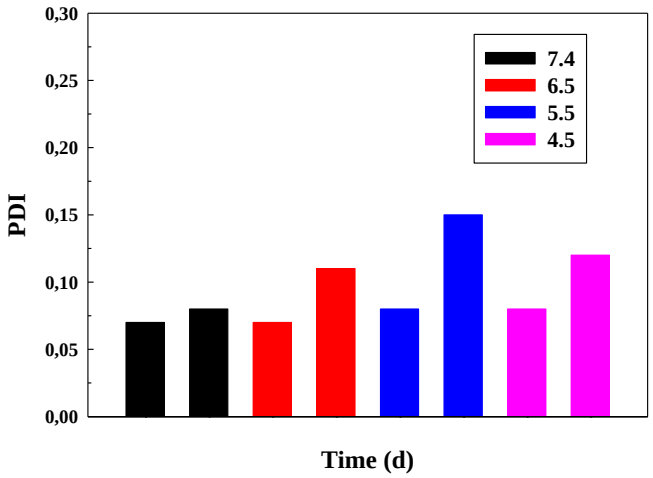

Figure S2: PDI of conventional liposomes immediately after dilution (day 0, left) and after 7 days of incubation (right) in different acidic media indicated in the legend.

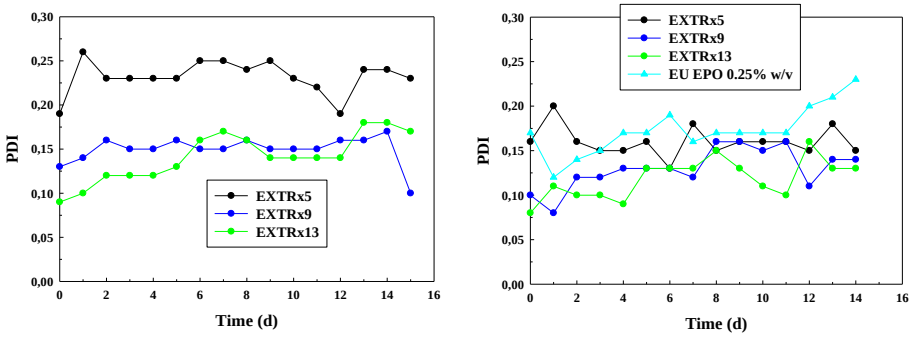

a) b)

Figure S3: Evolution of particle size over time for conventional liposomes extruded at 5, 9, and 13 passes and for EU EPO-coated liposomes in acidic medium (pH 4.5). Liposomes were previously synthesized either in: a) PBS at pH 7.4, or b) acidic medium at pH 4.5.

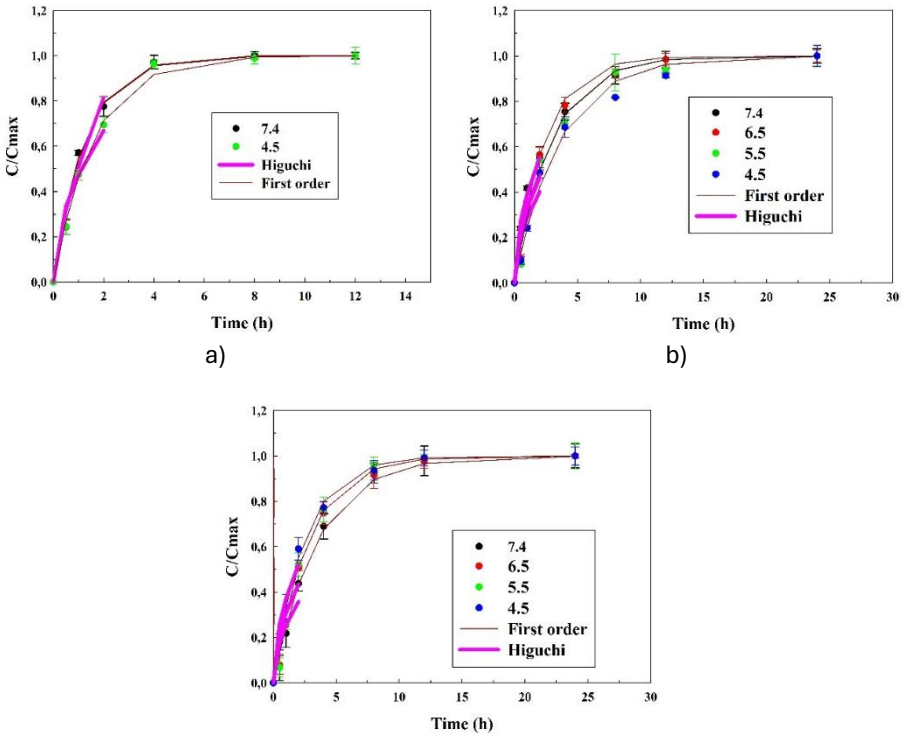

a) b)

c)

Figure S4: Fitting of experimental drug release data to first-order and Higuchi kinetic models for: a) conventional liposomes, b) EU S100-coated liposomes, and c) EU EPO-coated liposomes, all synthesized at 70:30 PC:CHOL molar ratio.

Table S1: Vesicle mean size, size deviation, PDI and mass yield of liposomes as a function of the extrusion process conditions.

Number of passes	Size (nm)	Size dev. (nm)	PDI	Yield (%mass)
1	146.08	96.00	0.22	100
5	111.88	25.33	0.11	99.95
9	99.45	14.33	0.07	99.93
13	92.30	5.00	0.06	99.88
17	92.27	15.33	0.07	99.85

Table S2: Vesicle mean size, size deviation, and PDI of liposomes as a function of sonication and extrusion temperatures.

Temperature (ºC)	Size (nm)	Size dev (nm)	PDI
65	92.30	5.00	0.06
55	97.33	8.33	0.07
45	97.37	7.99	0.07
35	97.29	11.33	0.08
25	100.71	10.66	0.09

Table S3: Vesicle mean size, size deviation, and PDI of liposomes as a function of PC:CHOL molar ratio.

RM PC:CHOL	Size (nm)	Size dev (nm)	PDI
50:50	92.30	5.00	0.06
60:40	92.50	13.66	0.07
70:30	85.58	9.00	0.07
80:20	80.98	9.00	0.07
90:10	82.39	18.33*	0.13
100:0	62.79	43.66*	0.15

**More than one population of liposomes was detected in the samples during the evaluation period.*

Table S4: Vesicle mean size, size deviation, and PDI of liposomes as a function of PC yield.

PC (%w)	Number of passes	Size (nm)	Size dev (nm)	PDI
60	9	99.45	14.33	0.07
	13	92.30	5.00	0.06
	17	92.27	15.33	0.07
99	9	90.69	18.67	0.09
	13	86.36	9.33	0.07
	17	81.57	10.33	0.09

5.6. Conclusions

As previously stated, the failed attempt to obtain a dual-responsive drug delivery system based on coacervates justified the exploration of an alternative pH-responsive strategy, based on a nanocarrier. Regarding this, liposomes have proven a robust and versatile platform for developing stimuli-responsive drug delivery formulations. In fact, a stable conventional liposomal system was successfully synthesized and optimized, providing SUV (85 nm) with good reproducibility, polidispersity (PDI <0.1) and high 5FU encapsulation efficiency (94%). This system demonstrated a robust baseline for further pH-responsive functionalization.

Furthermore, Eudragit® coatings provided different pH-responsive liposomal platforms via surface modification with electrostatic interactions among oppositely charged functional groups of liposomes surface and coating polymers. The main advantage for this methodology compared with other pH-sensitive liposomal system was that the liposome integrity was preserved at physiological conditions. However, the two different Eudragit® formulations showed distinct behaviours due to the physicochemical properties of each coating polymer. Eudragit® S100 showed micrometric aggregates, but the alkaline pH-responsive behaviour proved to be effective, conserving its potential for oral formulations. On the other hand, Eudragit® EPO yielded a more stable nanoscale coated liposomes (114 nm) maintaining narrow size distribution (PDI <0.15) and stability for at least 2 weeks, implying promising properties for tumour targeting.

Drug release studies confirmed that polymer coating induced an additional resistance, significantly reducing drug initial burst and showing different drug release cumulative percentage depending on the media pH. When fitting experimental data to mathematical models, the diffusion was confirmed as the predominant release mechanism with the coating layer acting as controllable kinetic barrier. Moreover, cell studies validated the biocompatibility and functional relevance of the pH-responsive coatings. Importantly, Eudragit® EPO coated liposomes showed the most promising behaviour, enhancing cytotoxic activity

against BT-474 breast cancer cells by up to 30% compared to other formulations, whilst preserving cell viability in healthy stromal cells.

In conclusion regarding the thesis objectives, the polymer-coated liposomes emerged as a suitable platform for the proposed development of a pH-responsive drug delivery platform to incorporate into the dual-responsive strategy, after the coacervates failed attempt. The conclusions of this chapter are summarized in Figure 5.4.

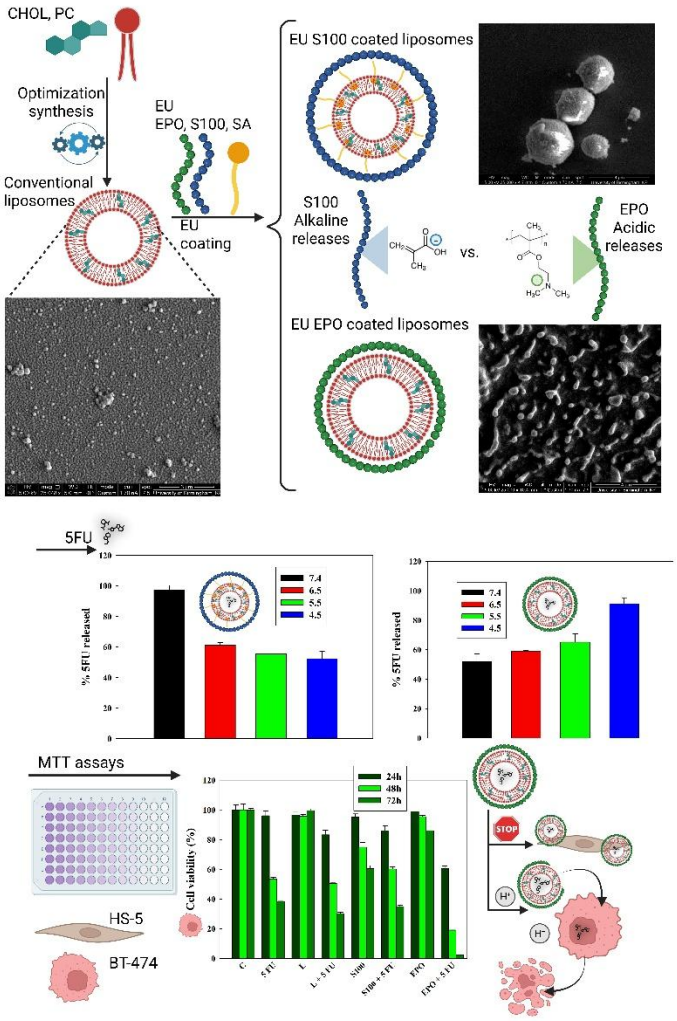

Figure 5.4. Summarized conclusions of the synthesis of conventional and EU coated liposomes, and the EU EPO coated liposomes tumour targeting evidence.

5.7. References also cited

[1] Antimisiaris SG, Marazioti A, Kannavou M, Natsaridis E, Gkartziou F, Kogkos G et al. Overcoming Barriers by Local Drug Delivery with Liposomes. Adv Drug Deliv Rev. 2021;174:53–86.

[2] Yu J, Chu X, Hou, Y. Stimuli-Responsive Cancer Therapy based on Nanoparticles. Chem Commun. 2014;50:11614–11630.

[3] Hafez IM, Ansell S, Cullis PR. Tunable pH-Sensitive Liposomes Composed of Mixtures of Cationic and Anionic Lipids. Biophys J. 2000;79:1438-46.

[4] Patra CN, Priya R, Swain S, Jena GK, Panigrahi KC, Ghose D. Pharmaceutical significance of Eudragit: A review. Futur J Pharm Sci. 2017;3:33-45.

[5] Skotland T, Ekroos K, Kauhanen D, Simolin H, Seierstad T, Berge V et al. Molecular Lipid Species in Urinary Exosomes as Potential Prostate Cancer Biomarkers. Eur J Cancer. 2017;70:122–132.

[6] Raikwar S, Panda PK, Saraf S, Bidla PD, Rathee S, Jain SK. Liposomes as a Drug Carrier. In: Jana S, editor. Advances in pharmaceutical technology for drug delivery systems Volume 1: Recent progress in modern drug targeting strategies. Boca Raton (FL, USA): CRC Press; 2025. 199-233.

[7] AlSawaftah NM, Awad NS, Pitt WG, Husseini GA. pH-Responsive Nanocarriers in Cancer Therapy. Polymers. 2022;14:936.

[8] Yu J, Chu X, Hou, Y. Stimuli-Responsive Cancer Therapy based on Nanoparticles. Chem Commun. 2014;50:11614–11630.

[9] Duarte JA, Gomes ER, De Barros ALB, Leite EA. Co-Encapsulation of Simvastatin and Doxorubicin into pH-Sensitive Liposomes Enhances Antitumoral Activity in Breast Cancer Cell Lines. Pharmaceutics. 2023;15:369.

[10] Moreira TDS, Silva ADO, Vasconcelos BRF, Santos EDS, De Sousa ACC, De Freitas JVB, et al. DOPE/CHEMS-Based EGFR-Targeted Immunoliposomes for Docetaxel Delivery: Formulation Development, Physicochemical Characterization and Biological Evaluation on Prostate Cancer Cells. Pharmaceutics. 2023;15:915.

[11] Li M, Chen H, Peng D, Lu X, Kong J, Luo S, et al. FU-coating pH-sensitive liposomes for improving the release of gemcitabine by endosome escape in pancreatic cancer cells. J Drug Deliv Sci Technol. 2023;80:104135.

[12] Pacheco ARF, Cardoso BD, Pires A, Pereira AM, Araújo JP, Carvalho VM, et al. Development of pH-Sensitive Magnetoliposomes Containing Shape Anisotropic Nanoparticles for Potential Application in Combined Cancer Therapy. Nanomaterials. 2023;13:1051.

[13] Koren E, Apte A, Jani A, Torchilin VP. Multifunctional PEGylated 2C5-immunoliposomes containing pH-sensitive bonds and TAT peptide for enhanced tumor cell internalization and cytotoxicity. J Control Rel. 2012;160:264–73.

[14] Paliwal SR, Paliwal R, Pal HC. Estrogen-anchored pH-sensitive liposomes as nanomodule designed for site-specific delivery of doxorubicin in breast cancer therapy. Mol Pharm. 2012;9:176–86.

[15] Xia G, An Z, Wang Y. Synthesis of a novel polymeric material folate-poly(2-ethyl-2-oxazoline)-distearoyl phosphatidyl ethanolamine tri-block polymer for dual receptor and pH-sensitive targeting liposome. Chem Pharm Bull (Tokyo). 2013;61:390–8.

[16] Patra ChN, Priya R, Swain S, Kumar Jena G, Panigrahi KC, Ghose D. Pharmaceutical significance of Eudragit: A review. Future J Pharm Sci. 2017;3:33-45.

5.8. List of abbreviations

5-FU — 5-Fluorouracyl
BT-474 — Breast Tumour Cell Line
CHEMS — Cholesterol Hemysuccinate
CHOL — Cholesterol
DDS — Drug Delivery System
DLS — Dynamic Light Scattering
DMEM — Dulbecco's Modified Eagle Medium
DMSO — Dimethyl Sulfoxide
DOPE—1,2-Dioleoyl-sn-Glycero-3-Phosphoethanolamine
DOTAP — 1,2-Dioleoyl-3-Trimethylammonium-Propane
DOX — Doxorubicin
DSPE — 1,2-Distearoyl-sn-Glycero-3-Phosphoethanolamine
DTX — Docetaxel
EDTA — Ethylenediaminetetraacetic Acid
EE — Encapsulation Efficiency
EPR — Enhanced Permeability and Retention
EU — Eudragit®
FBS — Foetal Bovine Serum
GEM — Gemicitabine
GSH — Glutathione
HCl — Hydrochloric Acid
HCT-116 — Human Colon Tumour Cell Line
HS-5 — Human Bone Marrow Stromal Cell Line
HSPC — 1,2-Distearoyl-sn-Glycero-3-Phosphocoline
Hz — Hydrazone
IC_{50} — Inhibitory Concentration 50
mAb — Monoclonal Antibody
MCF-7 — Michigan Cancer Foundation Breast Cancer Cell Line
MDA-MB-231 — MD Anderson Mammary Breass Cancer Cell Line
mPEG — Methoxy-Poly(Ethylene Glycol)
MR — Molar Ratio
MTT — 3-(4,5-dimethylthiazol-2-yl)-2,5-diphenyltetrazolium Bromide
MW — Molecular Weight
MWCO — Molecular Weight Cut Off

PBS — Phosphate Buffer Saline
PC — 1,2-Diacyl-sn-Glycero-3-Phosphocholine (Phosphatidylcholine)
PDI — Polidispersity Index
PEG — Poly(Ethylene Glycol)
PEO — Poly(Ethylene Oxide)
PS — Penicillin-Streptomycin
SA — Stearylamine
SD — Standard Deviation
SEM — Scanning Electron Microscopy
SIM — Simvastatin
SUVs — Small Unilamellar Vesicles
TATp — Trans-Activator of Transcription Peptide
UV — Ultraviolet

6. Innovative Thermo-sensitive Composite Materials: Merging Poloxamer PF-127 and Polysaccharides for Enhanced Functional Properties

6.1. Introduction

As it was described in the introduction, one of the main advantages of the system developed in this thesis for post-surgical breast cancer treatment is its local administration, which solves the systemic administration limitations of current approaches, such as low therapeutic efficiency and systemic toxicity. Proposing a local administration implies the direct accumulation of high drug concentrations directly at surgical bed, where up to 95% of residual cancer cells can be found after tumour resection. Therefore, this approach represents a promising approach for preventing tumour recurrence [1].

Previous chapters 4 and 5 focused on the development of platforms for pH-responsive tumour targeting strategies. Although the developed coacervates did not exhibit sufficient stability for compatibility with the intended application, liposomes were successfully synthesized, optimized, and coated to achieve the desired pH-responsive behaviour, targeting the acidic tumour microenvironment. However, for efficient local administration, liposomes require a matrix capable of adapting to the irregular cavity left during the surgery, providing sustained drug release as a local drug depot. In this sense, macroscopic hydrogels represent particularly suitable platforms for this application [2].

According to the thesis objectives, the matrix designed must present adaptability to the cavity, mechanical stability and biodegradability. Consequently, for a better implantation and integration, an injectable hydrogel is proposed, undergoing gelation after it is administered in the surgical bed, providing mechanical resistance and sustained drug release. Moreover, the *in situ* gel transition must be driven by the increase of temperature, constituting a thermo-sensitive injectable matrix. Regarding this, hydrogel physicochemical properties can be designed to enable injectability of the liquid precursor at room temperature, and to obtain a strong gel in surgical bed after *in situ* gelation at physiological temperature [2].

Therefore, this chapter focuses on the design, synthesis, and optimization of the thermo-responsive hydrogel platform proposed for local administration after breast tumour resection. Concretely, the selection of appropriate hydrogel components for an optimized thermo-responsive behaviour must be characterised overall by rheological analyses.

6.2. Polymers in thermo-sensitive hydrogel networks

Polymer chains ultimately confer the hydrogel matrix properties and gelling mechanisms by either physical or chemical interactions, and they can come from two different sources

6.2.1. Natural polymers

Natural polymers can be used in thermo-sensitive hydrogels overall due to their high biocompatibility, biodegradability, and structural similarity with the extracellular matrix (ECM) components. Most natural polymers do not present thermo-response by themselves, but can still be implemented in hydrogels for their biocompatibility advantages, like collagen[3], hyaluronate [4], alginate [5], or chitosan [6].

In order for them to present the desired thermal transition, additional compounds must be added to the network. For instance, collagen can be conjugated with glutaraldehyde whilst chitosan is mostly incorporated with β-glycerophosphate as crosslinking agent, which present a transition temperature around 37ºC, making this formulation suitable for injection [6]. Although chemically crosslinked hydrogels present improved resistant properties, usually these methodologies implement agents or chemical reactions that compromise the biocompatibility of the system, as well as their shear-thinning or self-healing behaviour, complicating its injection. Hence, synthetic polymers which usually present physical crosslinking, which is better for injectability, are frequently preferred [7].

6.2.2. Synthetic polymers

Synthetic polymers rather offer more structural and thermo-responsive control over natural polymers, which promotes them as injectable drug reservoirs for delivery systems.

6.2.2.1. Poly(N-Isopropylacrylamide) (PNIPAAM)

Thermo-sensitive polymer PNIPAAM presents a LCST around 32ºC, providing their hydrogels with injectability but also a potential burst release in application. Below LCST values, PNIPAAM is hydrophilic, which presents an abrupt transition to a hydrophobic state once passed LCST. Polymer chains collapse due to the reduced interactions with media as temperature rises [8]. Moreover, properties can be defined based on PNIPAAm molecular weight or chain distribution [8].

Although PNIPAAM presents well defined and tuneable thermal transition, it does not exhibit a good biodegradability in *in vivo* conditions, potentially causing cytotoxic effects by residual monomers or their synthesis by-products [8].

6.2.2.2. Poly(Ethylene Oxide) (PEO) and Poloxamers

PEO is a highly hydrophilic polymer which is not thermo-sensitive on its own but can present this characteristic by its combination with other copolymeric blocks, presenting better biocompatibility than other synthetic polymers. In these systems, PEO acts as the modulator of more complex structures [9].

For di-block copolymers, the other segment usually presents hydrophobic nature in order to obtain amphiphilic compounds able to self-assembly in aqueous solutions and transition to physical crosslinked hydrogels. The main design characteristic is the ratio between the polymers, showing more hydration and less structural stability when the hydrophilic content increases [9]. A common example is hydrogels PEO-PLA where the polylactic acid introduces stiffness and hydrophobicity [10].

However, an improved alternative to this diblock structure is the triblock poloxamer architecture, which exhibits enhanced structural stability and gelation capacity due to the micellar aggregation capacity (MAC) with increasing temperature. Specifically, Pluronics (tri-block copolymers PEO-PPO-PEO poloxamers) highly outstand the other combinations. Poly(Propylene Oxide) PPO provides the hydrophobicity and thermo-responsiveness. These systems self-assembly in micelles under aqueous solutions and over critical micellar concentration (CMC), and undergo gel transition when temperature increases, providing injectability using body temperature for their sol-gel transition [11].

A widely studied FDA approved Pluronic for injectable hydrogels is Pluronic F-127 or Poloxamer P407 (PF-127). PF-127 is a non-ionic surfactant presented in flakes at room temperature (F) with a molecular weight of 12,600 g/mol (12), presenting the following structure: $(PEO)_{99}$-$(PPO)_{69}$-$(PEO)_{99}$. This structure determines a PPO/PEO ratio of approximately 0.70 (7).[12] PF-127 polymeric chains form micelles in aqueous media, which further rearrange in gel form by their micellar aggregation capacity.

This gelation mechanism is conferred by temperature increase which causes the hydrophobic interactions of PPO blocks and induce micellar auto organisation, followed by their packaging, as illustrated in Figure 6.1. Main advantages of this process are the encapsulation of therapeutic agents in liquid state before the injection, avoidance of drug burst right after the administration, and sustained drug delivery in local reservoirs [11]. It also exhibits excellent biocompatibility and biodegradability, making it a promising platform for the protection and delivery of various anticancer drugs [11].

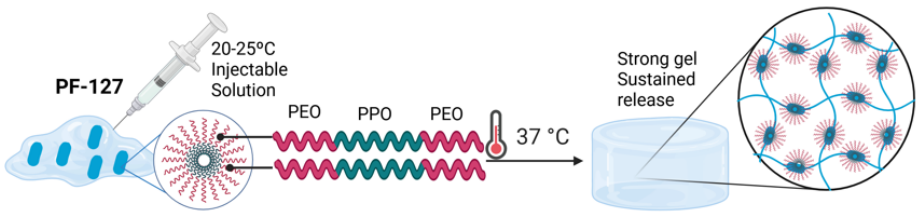

Figure 6.1. Thermo-sensitivity in PF-127 for injectable hydrogel design

6.3. PF-127 hydrogels for breast cancer treatment

As previously mentioned, different PF-127 based hydrogel systems have been reported for breast cancer treatment. However, regarding its durability, PF-127 biggest limitation is the low mechanical resistance due to relatively weak physical interaction among micelles in MAC. This is mainly addressed by the incorporation of different compounds that can strengthen the network mechanical properties. This can already be seen in Table 6.1. references.

Table 6.1. Reported PF-127 hydrogels for breast cancer therapy

Hydrogel formulation (+PF-127)	Drug/ Payload	Highlights	Ref
HA/GSNO/ SiO_2 NPs	Cis NO	Synergic effect reduced MDA-MB-231 cell viability to 29%	13
CS/DOPA	Photo thermal rGO	Photothermic effect reduced MCF-7 cells viability to 32%, and provided antibacterial activity	14
ALG/Ca/α-CD	DOX rGO	Reduced MCF-7 viability to 23% with NIR irradiation	15
PHB-b-PDMAEMA	Oligo nucleotide Sur-ASON	Gene therapy reduced tumour volume by 55.4% in mice (MCF-7)	16
Liposomes	PTX	Reduced KB cell line viability to 11.6% with greater cellular uptake	17
Fud (Nanogel)	PTX Cur	Combined system reported less toxicity than PTX alone (68% vs 30%) in MCF-7	18

As Table 6.1. illustrates, different compounds have been added to PF-127 formulations, providing better therapeutic efficacy since the mechanical resistance is improved and a targeting strategy is added to the system. Moreover, the most promising characteristic of these systems is the versatility which can modify the sol-gel transition in a biocompatible way, and many other viscoelastic properties, by establishing different compounds into the network. The thermo-response of PF-127 and its modifications due to compound addition can be characterised by rheology, indicating transition temperature, confirming gel state, or MAC stability.

6.4. Rheological characterization of hydrogel thermo-response

Generally, any injectable hydrogel intended for drug reservoir or drug delivery must present good injectability at room temperature and a strong gel behaviour at physiological temperature. Consequently, it must be adapted to its desired kinetic profile [7]. In order to characterize the gelling transition, rheology is presented as an essential tool enabling the evaluation of viscoelastic changes of the biomaterial associated with structural changes. Parameter determination such as the first temperature to present gel state, gel completion temperature (gct), elastic modulus, viscous modulus, or viscosity of the system is key to determine the mechanical resistance and stability of the hydrogel [7].

6.4.1. Oscillatory flow analysis

Oscillatory flow analyses apply an oscillatory stress or strain to the hydrogel to determine its elastic (G') or solid-like behaviour and viscous (G'') or liquid-like behaviour. When gelation occurs, in a sweep temperature test, it can be observed when the system becomes highly elastic (after cgt), exhibiting solid-like behaviour [7].

Moreover, frequency sweep tests evaluate how the viscoelastic behaviour changes with oscillatory deformation over a range of frequencies at a constant strain and temperature. When the elasticity of the system is completely independent from the frequency applied, a strong gel state is defined. Therefore, it is possible to determine whether the gel state has been achieved at a certain temperature [7].

6.4.2. Static flow analysis

On the other hand, static flow analyses study the flow behaviour under increasing shear rates, which enables the determination of the viscosity of the system, determination of shear-thinning behaviour, or other needed properties to evaluate injectability and resistance of the hydrogel. PF-127 micellar aggregation capacity has been reported to present three different stages under this test. First, the pre-gel stage is characterized by Newtonian behaviour, in which viscosity is only

dependent of the hydrogel concentration. Subsequently, the gel transition stage shows a progressive increase in viscosity proportional to temperature as structural arrangement occurs. Finally, the stable gel is reached, where a strong gel network is established and viscosity becomes independent of temperature [7]. Illustrated examples of suitable hydrogel properties regarding rheological analyses can be seen in Figure 6.2.

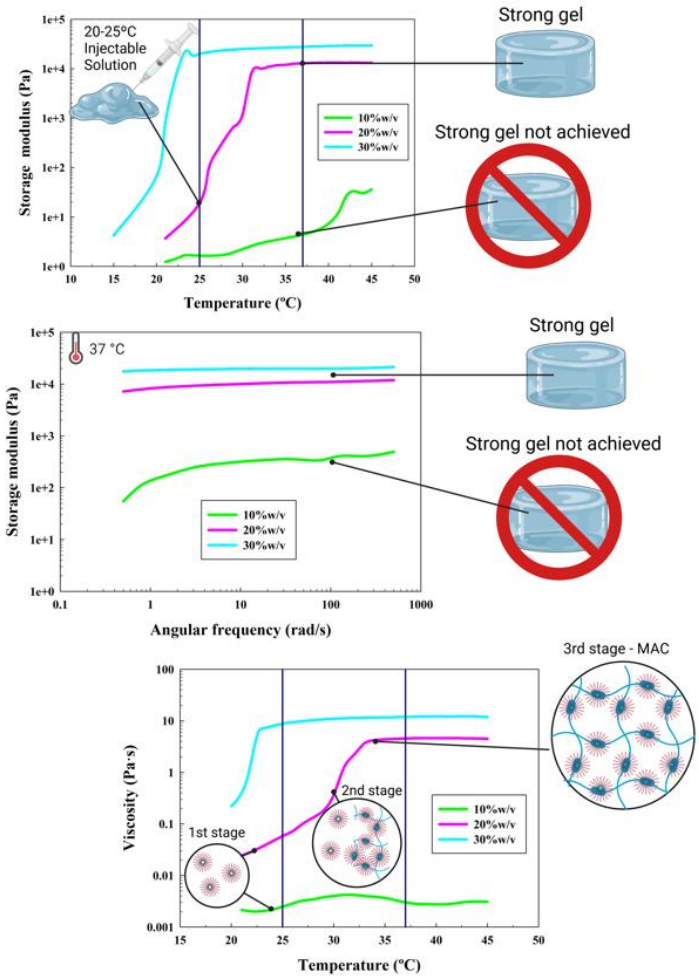

Figure 6.2. Rheological analyses on thermo-sensitive PF-127 hydrogels showing suitable properties for the intended application.

Throughout the studies mentioned in Table 1.6, rheological tests have been performed in order to establish the improvements of the PF-127

viscoelastic properties when adding different compounds, as well as other studies non-related to breast cancer. However, little research contemplates how the behaviour of the micellar aggregation and the final gel properties may vary depending on the structural nature of the compounds added. As of today, more investigation is required exploring how different polysaccharides with different behaviours under aqueous solutions affect the gelation process, as well as drug release. [19]

6.5. Article related to this chapter

Following this section, the published article "Innovative Thermosensitive Composite Materials: Merging PF-127 with Polysaccharides for Enhanced Funtional Properties" is presented as the results and discussions obtained during this experimental phase. The objective of this article was studying how different structural configurations of polysaccharides affected the properties of the PF-127 based hydrogel. Selecting different structural organizations in polymers, poloxamer concentration, or polysaccharides concentrations, the developed formulations were thoroughly studied in rheological tests to evaluate how the different parameters influenced the thermal transition of the PF-127 and which formulations were improved towards the desired application, regarding injectability and sustainability.

Finally, several formulations of different implemented polysaccharides which gelled within the suitable temperature range for injectability, achieved strong gel state at physiological temperature, and improved hydrogels viscosity without collapsing the MAC were subjected to drug release tests. Their kinetic profile was further studied, determining how the improved properties influenced the delay of the 5-FU release in terms of degradation rate, or erosion mechanism.

- Blanco-López M, de Dios-Pérez I, González-Garcinuño Á, Tabernero A, Martín del Valle EM. Innovative thermosensitive composite materials: Merging Poloxamer PF-127 and polysaccharides for enhanced functional properties. Macromol Mater Eng. 2025;2400457.

RESEARCH ARTICLE

Macromolecular Materials and Engineering
www.mame-journal.de

Innovative Thermosensitive Composite Materials: Merging Poloxamer PF-127 and Polysaccharides for Enhanced Functional Properties

Marcos Blanco-López, Inmaculada de Dios-Pérez, Álvaro González-Garcinuño, Antonio Tabernero, and Eva Martín del Valle*

Currently, new cancer treatment options are being developed following tumor resection surgery, with a focus on minimizing invasiveness and reducing systemic toxicity to lower the risk of recurrence. In this context, the thermosensitive poloxamer Pluronic Acid F-127 (PF-127) is modified by incorporating polysaccharides with varying structures—xanthan gum (XG), alginate (ALG), gellan gum (GG), and levan (LEV). Hydrogels are synthesized using different ratios of polysaccharides and PF-127. Rheological results reveal that adding polysaccharides to the hydrogel matrix increases storage moduli from 8 to 11–18 kPa and viscosity from 4.5 to 6.1–7.1 Pa s. Additionally, the micellar aggregation capacity (MAC) and gelation temperature shift from 34 °C to between 22 and 31 °C. Studies on 5-fluorouracil (5-FU) release from these composites indicate that enhanced MAC prolongs drug release 4 times longer compared to the hydrogel made with PF-127 alone. A mathematical model is applied to analyze these experimental results, taking into account polymer chain release. Hydrogel's degradation rate and viscosity are primary determinants of drug release duration. Thus, by modifying the hydrogel composition, MAC, thermosensitivity, and drug release profile can be finely controlled based on the polysaccharide used.

1. Introduction

Cancer remains a significant medical and societal burden, posing an ongoing challenge for healthcare and scientific research. In particular, breast cancer's high heterogeneity complicates treatment strategies, since conventional therapies, like radiotherapy and chemotherapy, are often associated with severe side effects and systemic toxicity that also impact healthy breast tissue cells.[1] To improve efficacy, selectivity, and patient quality of life, research is increasingly directed toward developing personalized and more effective therapies.

In cases requiring tumor resection, current surgical techniques aim for minimal invasiveness to preserve surrounding healthy tissue. Adjuvant therapies, including immunotherapy and targeted therapy, focus on selectively eliminating residual cancer cells while safeguarding healthy cells in the peritumoral region.[2]

One promising approach in personalized treatment strategies involves alternative methods of drug delivery post-tumor removal, using advanced localized drug delivery systems. Such localized delivery is particularly advantageous in breast cancer treatment, as it provides sustained release of therapeutic agents directly at the tumor site, reducing unwanted systemic distribution and thus minimizing the risk of recurrence.[2]

Biocompatible compounds are at the forefront of these alternative treatment systems, acting as drug delivery systems (DDSs). The primary DDS options being explored include liposomes, nanoparticles, and hydrogels. Among these, hydrogels offer unique advantages: they have the potential for stimulus-responsive synthesis, and can fill tissue cavities, serving as matrices for embedding additional therapeutic particles.[3–5]

Hydrogels have long demonstrated versatile applications, especially in tissue engineering,[6] cell growth matrices,[7] and drug encapsulation and delivery.[8] For drug delivery, hydrogels offer significant potential for localized breast cancer treatment, particularly after tumor resection, as they allow for drug protection, targeting, and efficient encapsulation.[9] Postresection, the hydrogel can be directly injected into the cavity, aiming to prevent recurrence through a more precise delivery method that minimizes harm to healthy cells and systemic toxicity.[10] Moreover, injectable hydrogels for localized drug delivery provide several advantages over conventional methods like oral or intravenous

M. Blanco-López, I. de Dios-Pérez, Á. González-Garcinuño, A. Tabernero, E. Martín del Valle
Department of Chemical Engineering
University of Salamanca
Plaza Los Caídos s/n, Salamanca 37008, Spain
E-mail: antaber@usal.es
Á. González-Garcinuño, A. Tabernero, E. Martín del Valle
Institute for Biomedical Research in Salamanca (IBSAL)
Paseo de San Vicente 87, Salamanca 37007, Spain

The ORCID identification number(s) for the author(s) of this article can be found under https://doi.org/10.1002/mame.202400457

© 2025 The Author(s). Macromolecular Materials and Engineering published by Wiley-VCH GmbH. This is an open access article under the terms of the Creative Commons Attribution License, which permits use, distribution and reproduction in any medium, provided the original work is properly cited.

DOI: 10.1002/mame.202400457

ADVANCED SCIENCE NEWS
www.advancedsciencenews.com

Macromolecular Materials and Engineering
www.mame-journal.de

delivery, which often suffer from low bioavailability and lack target specificity.[11]

This localized approach positions the drug close to the lesion, preventing local relapse of breast tumors after breast-conserving therapy.[12] Consequently, it offers a promising alternative focused on minimizing side effects and enhancing targeted drug delivery to cancerous cells.[2]

However, hydrogels often face limitations for injectability and initially rapid drug release, typically addressed by incorporating thermosensitivity to respond to temperature changes.[13] Thermosensitive injectable hydrogels have been explored in applications like DNA vaccine delivery,[14] bone regeneration,[15] wound healing, and cancer therapy.[16,17] For localized drug release, thermosensitive hydrogels are particularly valuable as they adapt to temperature variations, enabling controlled drug delivery and reducing the initial burst release.[10] Their aqueous, injectable form transitions to a gel state within the body, where they control release and fill cavities in a stable matrix, a key advantage for alternative treatments aimed at maximizing therapeutic efficiency.[18]

Thermosensitive hydrogels are also highly versatile, biocompatible, and biodegradable.[19] They undergo gelation at a specific transition temperature. This gelation process involves a shift from a liquid solution at room temperature (25 °C) to a gel at physiological temperature (37 °C) within the body.[20] This transition allows the gel to serve as a drug reservoir, gradually releasing the encapsulated agent at the injection site.[21]

A widely studied compound for thermosensitive hydrogel synthesis is Pluronic Acid F-127, or Poloxamer P407 (PF-127), a biocompatible, FDA-approved poloxamer capable of forming said hydrogels.[21] PF-127 is a nonionic surfactant composed of triblock polymers with two hydrophilic polyethylene oxide (PEO) ends and a hydrophobic polypropylene oxide (PPO) center. Concretely, it is a Pluronic (P) presented in flakes at room temperature (F) with a molecular weight of ≈12 600 g mol^{-1} (12), presenting the following structure: $(PEO)_{99}$–$(PPO)_{69}$–$(PEO)_{99}$. This structure determines a PPO/PEO ratio of ≈0.70 (7).[22]

The gelation transition of PF-127 falls within the target range for this application (25–37 °C), allowing the polymer micelles to gel through its micellar aggregation capacity (MAC) when heated, which leads to a stable hydrogel network as water evaporates.[23] Pluronic triblock copolymer structures present lipotropic and thermotropic behaviors. This means that PF-127 undergoes two different aggregation phenomena when in aqueous solution: micellization over the critical micellization temperature (cmt) when their concentration is higher than the minimum micellar concentration, and gellification, starting at critical gelation temperature (cgt) and stabilizing at the gelation completion temperature (gct).[24]

The transition from unimers to micelles comes from the dehydration of the PPO blocks, caused by an endothermic heat of micellization. After micellization, PF-127 has been reported to self-assembly in spherical micelles, since PEO/PPO ratio is higher than 0.5. The spherical micelles constitute a liotropic liquid phase (L_1) with isotropic behavior in aqueous solutions. Additionally, thermotropic behavior is expected. This implies that there is no need to increase the PF-127 concentration in order to appreciate a phase transition or structure reorganization, as presented in the phase diagram in **Figure 1**. When the temperature is increased, at a constant concentration, the spherical micelles undergo a first order transition by hard sphere interaction into a cubic phase (BCC) (Q_2) which is transparent, optically isotropic, highly viscous, and more elastic.[25] This cubic phase can present crystals when the concentration is closer to 100 wt%. Moreover, only a tight two-phase region is presented between the L_1 and the Q_2 phase, coinciding the MAC gelling transition. It must be noted that for other Pluronic compounds, such as P123, L122, or L121, this cubic phase is decreased in their diagram in order to promote the hexagonal or lamellar phase, due to the decrease of the PEO/PPO ratio.[25] Phase diagram for PF-127 is presented in Figure 1 below.

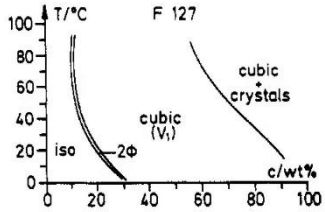

Figure 1. Phase diagram of PF-127. Reproduced with permission.[25] Copyright 1994, American Chemical Society.

PF-127 hydrogels have been proved to many different applications, not only as a vehicle for DDS but also as an active agent for being able to modify multidrug resistant cancer cells. The PF-127 binds with the plasma membrane of said cells affecting its fluidization, induces inner mitochondrial membrane polarization, and depletes ATP, decreasing antiapoptotic defense.[26] Rheological properties put this compound as an eligible support material for 3D printing tissue for biomimetic scaffolds,[27] due to the thermoplastic nature and yield stress it exhibits in gel form. This last application is also derived from tissue engineering, where noninvasive methods, such an injectable scaffold, are also a main objective.[28] More concretely, it can be included in regenerations of cartilage,[29] bone,[30] and even accelerates wound healing.[31]

Some of the most novelly applications for this material may also include neuroregeneration of the peripheral nervous system, where PF-127 with PLGA semipermeable nanosized porous structure would serve as a nerve guide and would allow blood vessels to grow and supply nutrients to growing axons,[32] or gene therapy, where PF combined with polyethileneimine (PEI) and conjugated with cell-penetrating peptide to the DR5-receptor in cancerous cells was used as a biodegradable and nontoxic system which showed higher gene transfection to cancerous cells than PEI alone.[33]

Moreover, PF-127-based hydrogels can effectively deliver drugs while adhering to biological tissues and minimizing surface tension, which aids in tissue targeting and protects the drug from degradation.[34] However, PF-127 hydrogels often dissolve quickly in physiological fluids, limiting their residence time, stability, and mechanical strength.[35,36] These limitations can be addressed by structural modifications, such as incorporating conjugated nanoparticles or copolymers to enhance strength and

 © 2025 The Author(s). Macromolecular Materials and Engineering published by Wiley-VCH GmbH

15292691, 0, Downloaded from https://onlinelibrary.wiley.com/doi/10.1002/mame.202400457 by Universidad De Salamanca, Wiley Online Library on [09/12/2025]. See the Terms and Conditions (https://onlinelibrary.wiley.com/terms-and-conditions) on Wiley Online Library for rules of use; OA articles are governed by the applicable Creative Commons License

promote tumor-specific drug delivery.[37] For instance, Ju et al. achieved localized delivery of paclitaxel using PF-127 hydrogels modified with carboxymethyl chitosan, resulting in a 40% increase in drug retention at the tumor site through cross-linking with glutaraldehyde.[38] Interaction with some drugs (overall when they are hydrophobic) may cause changes in the micellization and gelation process, presenting a more resistant structure depending on the drug concentration. This was described by Wei et al. with Ibuprofen interpenetrating micelles and restricting their motion.[24] In this context, hydrophobic materials have been used to modify the PF-127 network and enhance its effectiveness.[39]

Thus, modifying PF-127 with additional copolymers can mitigate rapid drug release without compromising thermosensitivity or injectability.[40,41] Other approaches embed intelligent nanoparticles into the hydrogel matrix, enhancing drug targeting and providing resistance against rapid degradation. Examples include alginate (ALG) microparticles, which have shown 10 times slower drug release rates than PF-127 alone,[42] dendrimers like polyamidoamine, which increase drug loading efficiency and exhibit cytocompatibility and anticancer activity,[43,44] and liposomes, which improve bioavailability and prolong drug residence time in treatments like retinal drug delivery.[45]

Another strategy is to create micelle systems with other Pluronics or surfactants, such as Tween 80,[46] P105,[47] P123,[48,49] or PF-68, optimizing drug release profiles for biomedical applications.[21,50,51] Additionally, incorporating polysaccharides can stabilize micelles and improve gel network properties without increasing toxicity, as polysaccharides are inherently biocompatible and biodegradable.

In this context, Bhowmick et al. studied the integration of xanthan and guar gum with PF-127 for ophthalmologic use,[52] and Dewan et al. found that adding tamarind seed polysaccharide improved elasticity, reduced porosity, and increased diffusion rates.[53] Brambilla et al. explored PF-127 with various polymeric excipients, including xanthan gum (XG), carrageenan, and HPMC, correlating sol–gel transition temperature, viscosity, and drug release.[54] Lupu et al. demonstrated that adding xanthan gum,[55] κ-carrageenan, alginate, and gellan gum enhanced the hydrogel's elastic modulus and viscosity.[56] De Dios-Pérez et al. (2023) observed that adding gellan gum and cyclodextrin complexes increased the elastic modulus up to 15 kPa in optimized formulations.[57]

While many approaches have improved localized delivery, cytotoxicity, and stability, few focus on the structural modifications that optimize the hydrogel properties for controlled drug release. Therefore, this work investigates the implementation of polysaccharides with distinct structures to PF-127 to precisely tune its thermosensitive properties. Rheological studies examine how polysaccharide–PF-127 networks alter gelation temperature and control drug release, specifically for 5-fluorouracil (5-FU).

Four polysaccharides are tested: XG with a helical structure; ALG and gellan gum (GG) with linear structures (GG also exhibits branches); and levan (LEV), a fructose polysaccharide that forms nanoparticles via self-assembly in water. Finally, a mathematical model correlates hydrogel stability and drug release behavior, accounting for transport resistance in the matrix.[58]

This study establishes a methodology for enhancing PF-127 hydrogels through polysaccharide incorporation, creating thermosensitive systems with customed properties for precise drug release and gelation control.

2. Experimental Section

2.1. Materials

Poloxamer PF-127 (#G2443), 5-FU (#G2443) and the following polysaccharides: XG (#G1253) with an average molecular weight around 1000 kDa, alginic sodium salt from brown algae (#G2033) with an average molecular weight around 150 kDa and a mannuronic to guluronic acid ratio of ≈1.56, and GG as Gelzan CM Gelrite (#1910) low acyl, with an average molecular weight around 1000 kDa were all purchased from Sigma-Aldrich. For levan synthesis D(+)-sucrose pure, pharma grade of molecular weight 342.30 Da was purchased from PanReacc AppliChem, the levansucrase enzyme (fructosyltransferase 68A) from Creative Enzymes, and ethanol (98% w/v) from Honeywell.

2.2. PF-127 Hydrogel Synthesis

10 mL of distilled water was poured in a beaker and left stirring at 4 °C. Once the water reached this temperature, the PF-127 was slowly added to the water while stirring to prevent aggregates. This mixture was left stirring overnight at 4 °C for PF-127 to be completely dissolved and obtain a homogeneous liquid hydrogel solution. The concentrations of PF-127 in these solutions were 10, 20, or 30% w/v.

2.3. Levan Synthesis

For levan synthesis, a cell-free methodology was used (molecular weight of the obtaining levan around 2000 kDa) described in references.[59] The levansucrase enzyme was added (0.2 mg L^{-1}) to a water solution of sucrose (90 g L^{-1}) in an AFORA reactor of 250 mL at 37 °C. After 72 h, the reaction was stopped, and the polymer was isolated by adding three volumes of ethanol to the reaction mixture. This new mixture was left at −20 °C for 24 h so the polymer precipitation could be induced. Afterward, the mixture was taken to centrifugation, using a tube Falcon centrifuge 5804 from Eppendorf (Madrid, Spain) at 10 000 rpm during 10 min, so levan could be separated from the supernatant. Finally, the polymer was taken to lyophilization, in a freeze dryer Telstar LyoQuest (Barcelona, Spain), prior freezing (−85 °C for 5 min), at −55 °C and 0.005 bar for 24 h.

2.4. PF-127 and Polysaccharide Hydrogel Synthesis

For hydrogel solutions with added polysaccharides (XG, ALG, GG, LEV), the process was similar to the one previously described in Section 2.2, with the only difference that the PF-127 was now dissolved in a polysaccharide aqueous solution instead of distilled water. For these polysaccharide aqueous solutions of 10 mL, concentrations of 0.5% and 1.0% w/v of the polysaccharides were added to distilled water at room temperature, except from gellan

 © 2025 The Author(s). Macromolecular Materials and Engineering published by Wiley-VCH GmbH

15029514, 0, Downloaded from https://onlinelibrary.wiley.com/doi/10.1002/mame.202400457 by Universidad De Salamanca, Wiley Online Library on [09/12/2025]. See the Terms and Conditions (https://onlinelibrary.wiley.com/terms-and-conditions) on Wiley Online Library for rules of use; OA articles are governed by the applicable Creative Commons License

ADVANCED SCIENCE NEWS
www.advancedsciencenews.com

Macromolecular Materials and Engineering
www.mame-journal.de

15926754, 0, Downloaded from https://onlinelibrary.wiley.com/doi/10.1002/mame.202500457 by Universidad De Salamanca, Wiley Online Library on [09/12/2025]. See the Terms and Conditions (https://onlinelibrary.wiley.com/terms-and-conditions) on Wiley Online Library for rules of use; OA articles are governed by the applicable Creative Commons License

Table 1. Formulations of polysaccharides and PF-127 hydrogels.

Formulation	Hydrogel [% w/v]	Formulation	Hydrogel [% w/v]	Formulation	Hydrogel [% w/v]
1	10% PF	10	0.5% ALG + 10% PF	19	1.0% GG + 10% PF
2	20% PF	11	0.5% ALG + 20% PF	20	1.0% GG + 20% PF
3	30% PF	12	0.5% ALG + 30% PF	21	1.0% GG + 10% PF
4	0.5% XG + 10% PF	13	1.0% ALG + 10% PF	22	0.5% LEV + 10% PF
5	0.5% XG + 20% PF	14	1.0% ALG + 20% PF	23	0.5% LEV + 20% PF
6	0.5% XG + 30% PF	15	1.0% ALG + 10% PF	24	0.5% LEV + 30% PF
7	1.0% XG + 10% PF	16	0.5% GG + 10% PF	25	1.0% LEV + 10% PF
8	1.0% XG + 20% PF	17	0.5% GG + 20% PF	26	1.0% LEV + 20% PF
9	1.0% XG + 30% PF	18	0.5% GG + 30% PF	27	1.0% LEV + 30% PF

gum, which dilution was obtained at 85 °C, and stirred for 1 h on a heating and magnetic stirring plate Isotemp from Fisherbrand (Madrid, Spain). After this time, homogeneous polysaccharide solutions were achieved. In this context, **Table 1** indicates the compositions of the different formulations PF-127 with the polysaccharides.

Once the polysaccharide solutions were at room temperature (GG solution needed an extra step cooling down from 80 °C to room temperature), these were taken to the cold chamber and were left with stirring at 4 °C until this temperature was reached. After that, the PF-127 was added with the same concentrations and following the procedure in Section 2.2. Finally, all of the hydrogels presented transparency in both solution and gel state, except from the LEV ones, which presented turbidity due to their characteristic Tyndall effect.[59] This turbidity slightly increased with the LEV concentration. The hydrogel samples can be seen in Figures S1 and S2 in the Supporting Information.

2.5. Rheology

The rheometer used was an AR 1500ex model from TA instruments (Madrid, Spain), equipped with a 4 cm diameter aluminum plate and a 1 mm gap. The rheological analysis was performed once the solutions were fully prepared and taken back to room temperature. Samples of 1.5 mL of the hydrogel (in liquid state) were loaded on the peltier and geometry gap was set to 1 mm.[20,57,60,61] Also, a solvent trap was used in the rheological measurements in order to control water evaporation. This solvent trap used vacuum grease and lightweight, low-viscosity, nonvolatile machine oil placed in the surroundings of the flat geometry head.

Both temperature and frequency sweep tests (oscillatory analysis) were performed on the hydrogels. The main variables measured were the elastic or storage (G') modulus and the viscous or loss (G'') modulus, obtaining the gct and elasticity of the gel systems. For temperature sweep tests, the temperature range studied was from 15 to 45 °C with a 1 °C min^{-1} rate, as described.[62,63] Also a temperature 5 °C min^{-1} rate was used in order to study the poloxamer's hysteresis. Fixed variables were frequency (10 Hz) and strain percentage (0.2%) so that the hydrogel provided results within its linear viscoelastic region. For frequency sweep tests, the frequency range studied was 0.5–500.0 rad s^{-1}. Fixed variables were temperature (37 °C), so that measured gel properties were the ones at physiological conditions, and strain percentage (0.2%).

Temperature ramp static flow analyses (static analysis) were also performed. For this type of analysis, the measured variable was the viscosity of the hydrogel, which provided information about the sol–gel transition. Tests kept the same temperature range studied in the oscillatory analysis (15–45 °C). Temperature ranges took into account storage temperature, operating room temperature,[64] and physiological temperature. The fixed variable for this analysis was the shear rate at 50 s^{-1} in order to observe the MAC effect on viscosity.[20]

2.6. Synthesis of the Loaded Hydrogels

Hydrogels were loaded with the antimetabolite drug 5-FU following previous Sections 2.2 and 2.4. For these hydrogels, a 5-FU standard solution was added to the distilled water or polysaccharide aqueous solution once it was stirring at 4 °C and prior to adding PF-127. The final concentration of 5-FU was 50 ppm, since it was reported as the IC_{50} in MTT assays.[65]

Let it be noted that, although PF-127 was proven to improve drugs solubility in aqueous phases,[66] the 5-FU IC_{50} was lower than its saturated concentration in water and a higher amount of 5-FU might promote side effects if the formulation was administered.

2.7. Drug Release Experiments

For drug release experiments, 5 mL of the loaded synthesized hydrogels (liquid state at 25 °C) was weighed in a 35 mm diameter Petri dishes and taken to incubation at 37 °C for 30 min. This time enabled the samples to fully undergo the gelification process in the incubator EN025, Nuve Incubator (Ankara, Turkey). Afterward, the Petri dish was placed in a support inside a 100 mL beaker full of distilled water, on a heating and stirring plate at 37 °C and 100 rpm. This system was connected to the spectrophotometer Cary 60 UV–vis from Agilent Technologies (Santa Clara, CA, USA) via a probe that enabled continuous measurements of the bulk. The temperature was controlled as well via probe connected to the plate. The bulk was measured periodically by the spectrophotometer probe at 260 nm (peak of 5-FU detection) at a temperature of 37 °C.[65] An experimental diagram explaining all

 © 2025 The Author(s). Macromolecular Materials and Engineering published by Wiley-VCH GmbH

ADVANCED SCIENCE NEWS
www.advancedsciencenews.com

Macro-olecular Materials and Engineering
Open Access
www.mame-journal.de

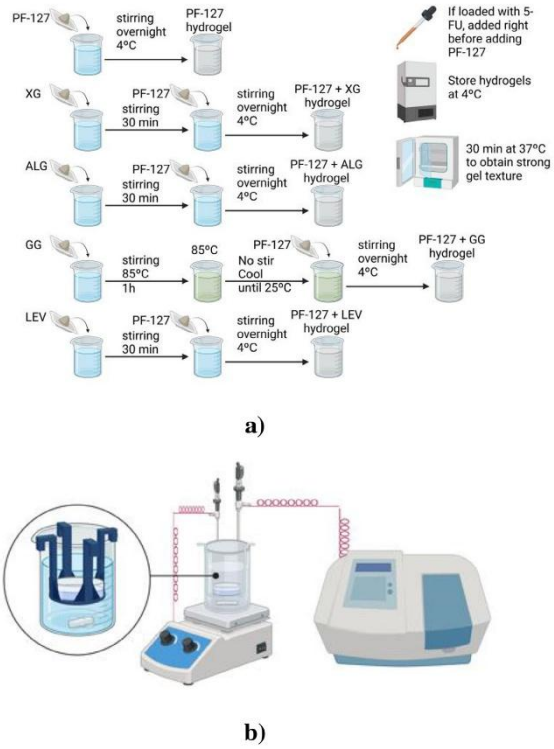

Figure 2. a) Experimental diagram of hydrogels synthesis processes, and b) scheme of the system setup for drug release experiments. This figure was created with BioRender.

of the hydrogels' synthesis and these experiments' setup is further illustrated in **Figure 2**.

2.8. Mathematical Modeling of the Drug Release Experiments

Drug release experimental results were fitted to a mathematical model in order to determine the constants values which explained the contribution of the polysaccharide and the PF-127 to the drug release. It was stated that the mass released of 5-FU was directly proportional to the degradation rate of the hydrogel,[57] and degradation rate was a function of the relative loss of mass of both polymers involved (W) and the fraction of chains released from the internal structure of the hydrogel (F).[58] This was expressed in the kinetic equation for these experiences Equation (1) below

$$M^{rel}{}_{5FU} = K_r \cdot \left(W_{PF} \cdot F_{PF} + W_X \cdot F_X\right) \quad (1)$$

being $M^{rel}{}_{5FU}$ the percentage of mass for 5-FU released, K_r the release constant, including all the resistances taking place in the transport phenomena (dimensionless), W and F the paremeters

 © 2025 The Author(s). Macromolecular Materials and Engineering published by Wiley-VCH GmbH

11/09/2025, Downloaded from https://onlinelibrary.wiley.com/doi/10.1002/mame.202400457 by Universidad De Salamanca, Wiley Online Library on [09/12/2025]. See the Terms and Conditions (https://onlinelibrary.wiley.com/terms-and-conditions) on Wiley Online Library for rules of use; OA articles are governed by the applicable Creative Commons License

ADVANCED SCIENCE NEWS
www.advancedsciencenews.com

Macromolecular Materials and Engineering
www.mame-journal.de

explained before, and subtitles PF and X the reference to the compound being either the poloxamer (PF) or the polysaccharide, if any, respectively.

In order to estimate the F value, the model described another parameter P, a variable function of time according to Equation (1) and that depended on the degradation rate parameter, k_d. This parameter was further defined in Equation (2) shown below

$$P = 1 - \exp\left(k_d \cdot t\right) \tag{2}$$

being P the unitary fraction of degradation (dimensionless), k_d the degradation rate of the hydrogel chains (s^{-1}), and t the time (s). Once defined P, the released chains of both polymers of the system could now be calculated following Equations (3) and (4) shown below

$$F_X = \left(1 - (1 - P)^2\right)^N \tag{3}$$

$$F_{PF} = P^2 + P \cdot (1 - P) \cdot F_X \tag{4}$$

being N the erosion parameter (dimensionless, and ranges from 0 to 1 values). As a conclusion, three parameters would be estimated for this model: the release constant, the degradation rate, and the erosion parameter.

Parameter estimation was carried out by Solver add-in complement in Excel, where the relative error was the function that should be minimized by varying the three parameters mentioned above. This relative error definition followed the Equation (5) shown below

$$E_r = \frac{E_{abs}}{n} = \left|\frac{V_{th} - V_{exp}}{V_{th}}\right| \cdot \frac{100}{n} \tag{5}$$

being E_r and E_{abs} the relative and absolute errors, V_{th} and V_{exp} the theoretical and experimental values, respectively, and n the total number of experimental values collected during the experiences. All parameters of Equation (5) were dimensionless.

Furthermore, the Stokes–Einstein equation was also discussed in order to relate the diffusion coefficient/bulk diffusion and the viscosity of the hydrogels. This equation was shown below as Equation (6)

$$D = \frac{k_B \cdot T}{6\pi\mu R_0} \tag{6}$$

being D the diffusion coefficient ($m^2\ s^{-1}$), k_B the Boltzmann's constant (5.67×10^{-8} W m^{-2} K^{-4}), T the temperature (K), μ the solvent viscosity (Pa s), and R_0 the solute's radius (m).

3. Results and Discussion

3.1. Rheological Results

First, the rheological characterization of the hydrogels is presented evaluating parameters such as gct (which is determined as the first temperature presenting gel behavior)[24] in the temperature sweep test, and values of the storage moduli in the frequency sweep tests. Gct is the studied parameter concerning hydrogel injectability and thermal response to room and tissue temperatures. Let it be noted that thermosensitivity needs to happen between 25 and 37 °C (gct between these values) in order for formulations to be eligible for injectability and filling properties.[35,58] This is why these two temperatures are marked in the rheological analyses graphs below.

Also, the MAC is studied through temperature ramp tests. MAC is defined as the aggregation which causes the phase transition from isotropical aqueous solution to the BCC solid-like structure with increasing temperature. This phase transition has been studied by many authors in references for Pluronics.[22,24,25,57] More concretely, this characterization of the MAC is described by Shriky et al.[20] Results are taken into account for deciding the best hydrogel systems, based on their elastic and viscous properties that depend on their formulation.

3.1.1. PF-127 Hydrogel System

The hydrogel based off of PF-127 alone was first studied and characterized by all the rheological tests explained in Section 2.5. The main results of the poloxamer concentrations at 10, 20, and 30% w/v (formulations 1 to 3) are illustrated in **Figure 3**.

Figure 3a shows the temperature sweep test (oscillatory flow analysis) results for 10, 20, and 30% w/v concentrations of PF-127 hydrogels. As it can be seen in this figure, hydrogels with concentrations higher than 10% w/v underwent gelation when the temperature increased. This was represented when the G' increased exponentially from unstable measurements at low values, below 10 Pa, until a stable gel region, reaching values higher than 10 and 30 kPa for formulations 2 and 3, respectively.

This analysis not only proved that PF-127 hydrogels needed a concentration higher than 10% w/v in order to be thermosensitive and reach a gel state (since formulation 1 never reached it), but also that this gelation process showed a lower gct (34 and 23 °C) and a higher elastic nature (G' of around 11 and 25 kPa) when the concentration of PF-127 increased (formulations 2 and 3). This confirms previous studies about the thermosensitivity of PF-127.[20,56] In addition, let it be noted that for formulations 2 and 3, the elastic nature was confirmed since the storage moduli prevailed over the loss moduli. This is shown in Figure S3a (Supporting Information). Moreover, another interesting data that could be considered are the temperature where the hydrogel starts transitioning from liquid to solid (T_{LTS}), found in the onset of the steep increase of the complex modulus (G^*). T_{LTS} values are shown in **Table 2**, and representation of this complex moduli can be found in Figure S9a (Supporting Information).

Moreover, additional measurements were performed in order to confirm their reproducibility, as shown in Figure S4a (Supporting Information). Also, the hysteresis cycle of the poloxamer was studied. A cooling stage was added and it showed that the system returned to a solution state in a solid-to-liquid transition temperature[66,67] around 17 °C as reported.[68] Besides, the hysteresis cycle breadth was proven to shrink when the heating and cooling rates were lowered, as well as proven with other Pluronics like F68.[66,67] These results can be seen in Figure S4b (Supporting Information). Moreover, expanding the temperature sweep to lower temperatures determines the cmt for F2 at ≈7.5 °C,

 © 2025 The Author(s). Macromolecular Materials and Engineering published by Wiley-VCH GmbH

15292654, 0, Downloaded from https://onlinelibrary.wiley.com/doi/10.1002/mame.202400457 by Universidad De Salamanca, Wiley Online Library on [09/12/2025]. See the Terms and Conditions (https://onlinelibrary.wiley.com/terms-and-conditions) on Wiley Online Library for rules of use; OA articles are governed by the applicable Creative Commons License

ADVANCED SCIENCE NEWS
www.advancedsciencenews.com

Macromolecular Materials and Engineering
www.mame-journal.de

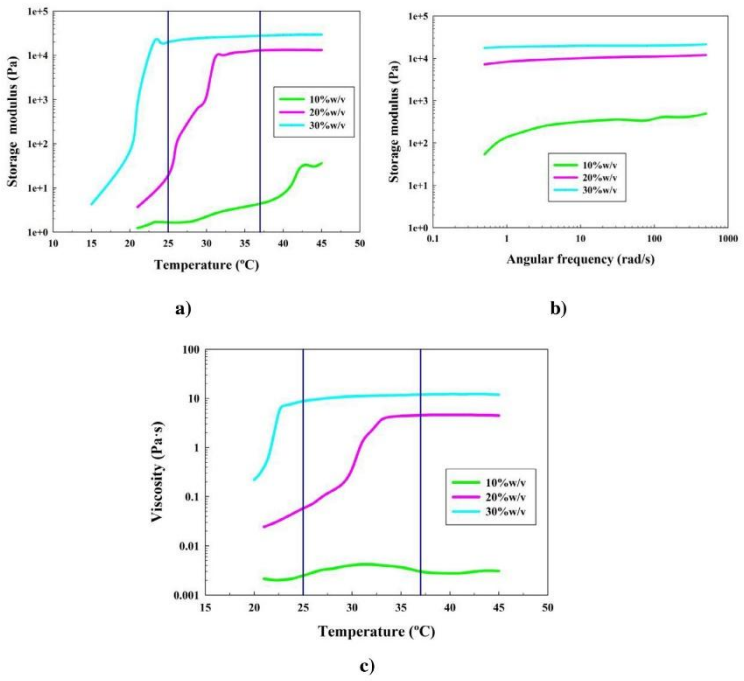

Figure 3. Rheological analyses of PF-127 hydrogels: a) temperature sweep oscillatory flow test, b) frequency sweep oscillatory flow test, and c) temperature ramp steady flow test.

corresponding to a minimum loss modulus value[66] when fitting experimental data to a polynomic trend, as shown in Figure S4c (Supporting Information). The cmt is found to be lower than other Pluronics like F68 at higher concentrations.[24] This might be due to the PEO/PPO ratio in the compounds.[25]

Figure 3b shows the angular frequency sweep of the PF-127 hydrogels at 37 °C. This test was performed in order to find a strong gel behavior of the systems specifically at physiological temperature. This fact was demonstrated since the elastic moduli of the systems were independent of the frequency. Also, these were always higher than the viscous moduli, exhibiting the elastic nature of the gel, as shown in Figure S3b (Supporting Information).

It was shown that this strong gel state was present at 37 °C for concentrations higher than 10% w/v, agreeing with previous results.[20,53,56] As stated before, when the PF-127 concentration increased (formulations 2 and 3), so did the elastic nature of the systems at any temperature, since elastic moduli values increased from 8 to 19 kPa. Moreover, the difference between elastic and loss moduli increased from 7 to 18 kPa, shown in Figure S3b (Supporting Information).

Figure 3c shows the 1 °C min^{-1} ramp temperature in static flow analysis. The heating rate was chosen as described.[62,63] It has been reported that this rate can affect the hysteresis cycle of Pluronic F68, but does not cause a significant difference (±1 °C) in the temperatures where the Pluronic F68 starts gelling or the gct.[66,67] This test is essential in order to understand the MAC that PF-127 exhibits. According to Figure 3c, three different stages were found. The first one (solution with liquid-like behavior) corresponds with a Newtonian formulation, since the viscosity values are low and only depend on the PF-127 concentration.

 © 2025 The Author(s). Macromolecular Materials and Engineering published by Wiley-VCH GmbH

15292654, 0, Downloaded from https://onlinelibrary.wiley.com/doi/10.1002/mame.202400457 by Universidad De Salamanca, Wiley Online Library on [09/12/2025]. See the Terms and Conditions (https://onlinelibrary.wiley.com/terms-and-conditions) on Wiley Online Library for rules of use; OA articles are governed by the applicable Creative Commons License

ADVANCED SCIENCE NEWS
www.advancedsciencenews.com

Macromolecular Materials and Engineering
www.mame-journal.de

Table 2. Rheological analyses results, being T_{MAC} the temperature where MAC stabilizes at the start of the third stage.[20]

Form	Hydrogel [% w/v]	Rheology					
		Oscillatory flow				Steady flow	
		T_{sweep}		$Freq_{sweep}$		T_{ramp}	
		T_{LTS} [°C]	gct[°C]	G' [kPa]	$G' - G''$ [kPa]	T_{MAC} [°C]	μ [Pa s]
1	10% PF	No gelation process[a]					
2	20% PF	26	34	8.63 ± 2.36	7.16 ± 0.77	34	4.53 ± 0.21
3	30% PF	19	24	19.40 ± 1.94	18.68 ± 0.90	24	11.21 ± 2.19
4	0.5% XG + 10% PF	No gelation process					
5	0.5% XG + 20% PF	No gelation process					
6	0.5% XG + 30% PF	24	28	8.89 ± 1.20	8.33 ± 0.26	No MAC[b]	
7	1.0% XG + 10% PF	No gelation process					
8	1.0% XG + 20% PF	27	28	6.74 ± 2.45	6.12 ± 0.25	No MAC	
9	1.0% XG + 30% PF	20	24	11.49 ± 1.61	10.66 ± 0.87	No MAC	
10	0.5% ALG + 10% PF	No gelation process					
11	0.5% ALG + 20% PF	26	31	11.00 ± 3.07	9.74 ± 0.92	29	7.04 ± 1.67
12	0.5% ALG + 30% PF	18	23	10.31 ± 1.92	9.06 ± 0.75	22	13.15 ± 3.30
13	1.0% ALG + 10% PF	No gelation process					
14	1.0% ALG + 20% PF	26	31	10.76 ± 0.69	10.76 ± 0.69	29	7.18 ± 0.15
15	1.0% ALG + 30% PF	17	22	29.33 ± 1.64	28.36 ± 1.56	No MAC	
16	0.5% GG + 10% PF	No gelation process					
17	0.5% GG + 20% PF	26	32	15.88 ± 3.54	14.65 ± 0.58	32	6.98 ± 0.60
18	0.5% GG + 30% PF	18	25	10.31 ± 1.92	9.06 ± 0.75	No MAC	
19	1.0% GG + 10% PF	No gelation process					
20	1.0% GG + 20% PF	No gelation process					
21	1.0% GG + 30% PF	17	22	25.59 ± 5.60	23.21 ± 1.49	No MAC	
22	0.5% LEV + 10% PF	No gelation process					
23	0.5% LEV +20% PF	25	30	18.69 ± 2.46	17.31 ± 2.02	30	6.11 ± 0.86
24	0.5% LEV + 30% PF	19	23	8.38 ± 2.16	7.32 ± 2.47	No MAC	
25	1.0% LEV + 10% PF	No gelation process					
26	1.0% LEV+ 20% PF	25	28	18.09 ± 2.54	17.12 ± 1.55	30	6.39 ± 0.62
27	1.0% LEV + 30% PF	18	22	34.52 ± 2.60	32.98 ± 2.53	21	11.42 ± 3.04

[a] No gelation process was observed in the temperature sweep oscillatory flow analysis; [b] No MAC was observed due to unstable viscosity in temperature ramp steady flow analysis.

The gelation process starts in a second phase, where the viscosity starts being dependent and directly proportional to the temperature. Micelles start associating in the Q_2 phase since the water molecules evaporate. Finally, a more ordered structure and stable gel behavior is reflected in the third and final stage, where the viscosity becomes an independent variable from the temperature again.

Figure 3c also shows that an increase on the PF-127 concentration from formulation 2 to 3 affects the MAC, making the gel transition (when the third stage begins) decrease from 34 to 23 °C and the viscosity increase from 4 to 11 Pa s, respectively.

3.1.2. PF-127 and XG Hydrogels

In order to study the effect of the implementation of XG to the PF-127 hydrogels, the concentrations of 0.5 and 1.0% w/v of said polysaccharide were implemented to the system (formulations 4–9). The results obtained are shown in **Figure 4**.

Figure 4a,b represents the temperature sweep test for said formulations. The first observation was that the implementation of this polysaccharide never reached a gel state if the PF-127 concentration is 10% w/v (formulations 4 and 7). The other PF-127 concentrations underwent this gelation process. However, formulation 5 gel state did not show a clear stabilization, since the elastic modulus starts decreasing toward the end of the test. This is due to steric hindrance problems of few micelles linking with high ordered XG helix structure. These mentioned formulations were consequently discarded from future analyses.

Analyzing the XG implementation on the elastic moduli, it was observed that for formulations 6, 8, and 9, the storage moduli values were around 11, 7, and 16 kPa, respectively. This shows that increasing the XG concentration also increases the G' values.

 © 2025 The Author(s). Macromolecular Materials and Engineering published by Wiley-VCH GmbH

11029154, 0, Downloaded from https://onlinelibrary.wiley.com/doi/10.1002/mame.202400457 by Universidad De Salamanca, Wiley Online Library on [09/12/2025]. See the Terms and Conditions (https://onlinelibrary.wiley.com/terms-and-conditions) on Wiley Online Library for rules of use; OA articles are governed by the applicable Creative Commons License

ADVANCED SCIENCE NEWS
www.advancedsciencenews.com

Macromolecular Materials and Engineering
www.mame-journal.de

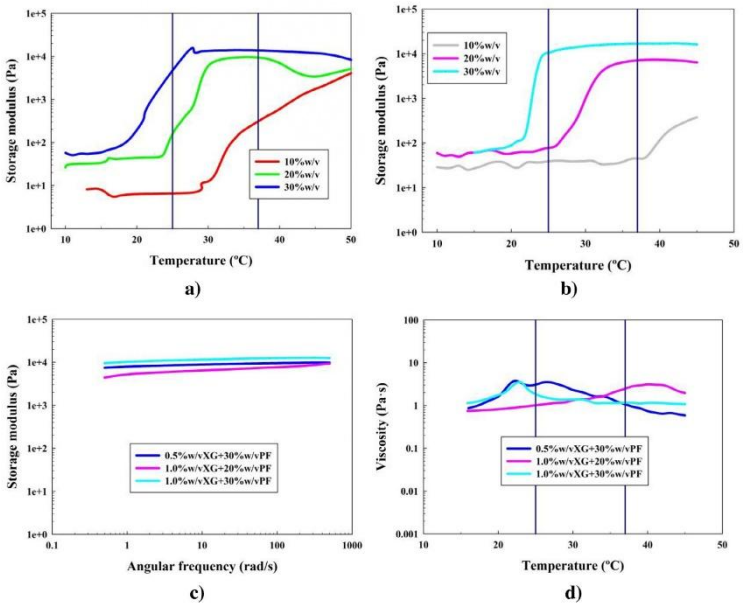

Figure 4. Rheological analyses of PF-127 and XG hydrogels: a) temperature sweep oscillatory flow test for 0.5% w/v XG, b) temperature sweep oscillatory flow test for 1.0% w/v XG, c) frequency sweep oscillatory flow test on gel formulations, and d) temperature ramp steady flow test on gel formulations.

However, these results obtained did not present any higher G' values than the hydrogels based off of PF-127 only. This means that XG implementation also caused difficulties to reach gel states as strong as PF-127 hydrogels. This was also shown with the gct values of these formulations, being 28, 28, and 24 °C for formulation 6, 8, and 9, respectively.

The stable gel state formulations shown in the temperature sweep test (formulations 6, 8, and 9) were taken to the frequency sweep test at 37 °C. In Figure 4c, this analysis showed a strong gel behavior for all formulations at this temperature. Storage moduli values reported were around 9, 7, and 12 kPa for formulations 6, 8, and 9, respectively. These results confirmed that the PF-127 concentration had a higher effect on gellation, since formulations with high XG concentration did not present higher G' values than those with low XG, or PF-127 alone hydrogels. Once again, XG implementation does not improve elastic nature of the hydrogels. Moreover, this elastic nature of XG and PF-127 hydrogels was confirmed in Figure S5a (Supporting Information), and G^* is shown in Figure S9b (Supporting Information).

Figure 4d shows the temperature ramp for the steady flow analysis. These results clearly showed that none of the formulations 6, 8, or 9 showed the MAC zones compared to PF-127 alone, since there is never a gel state stabilization. In this context, XG is a helicoidal polysaccharide,[69] which has a complex helix 3D structure that, according to the results, is difficult to coexist with the micelles present as colloids in the liquid bulk of the aqueous solution. This means that, as the temperature increased, the micelles started associating among them, increasing the viscosity but ended collapsing at the fixed shear rate of the static flow experiments, as shown in Figure 4d.[70] Therefore, a gel was formed with an internal structural disorder that provided the system with low viscosity values.

3.1.3. PF-127 and ALG Hydrogels

For the polysaccharide ALG, the rheological analyses are the ones shown in **Figure 5** (formulations 10–15).

 © 2025 The Author(s). Macromolecular Materials and Engineering published by Wiley-VCH GmbH

15029514, 0, Downloaded from https://onlinelibrary.wiley.com/doi/10.1002/mame.202400457 by Universidad De Salamanca, Wiley Online Library on [09/12/2025]. See the Terms and Conditions (https://onlinelibrary.wiley.com/terms-and-conditions) on Wiley Online Library for rules of use; OA articles are governed by the applicable Creative Commons License

ADVANCED SCIENCE NEWS
www.advancedsciencenews.com

Macromolecular Materials and Engineering
www.mame-journal.de

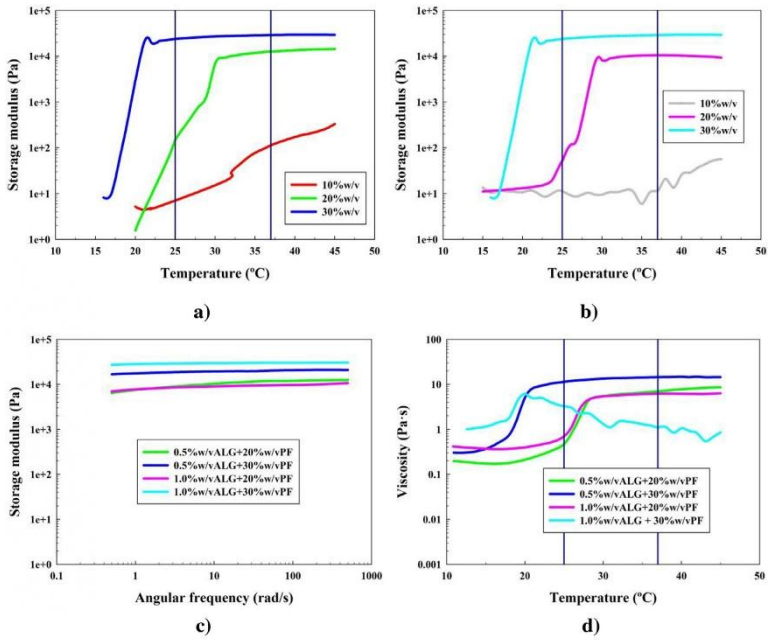

Figure 5. Rheological analyses of PF-127 and ALG hydrogels: a) temperature sweep oscillatory flow test for 0.5% w/v ALG, b) temperature sweep oscillatory flow test for 1.0% w/v ALG, c) frequency sweep oscillatory flow test on gel formulations, and d) temperature ramp steady flow test on gel formulations.

Figure 5a,b shows the results for all formulations 10–15 of the hydrogels in the temperature sweep tests. As it can be seen, once again, it was confirmed that for low concentrations of PF-127 (10% w/v, formulations 10 and 13), the gelation process was nonviable, no matter the ALG concentration added. However, the rest of the other formulations showed an efficient gelation process.

For this case, the gcts were 31 and 23 °C for formulations 11 and 12, and 31 and 22 °C for formulations 14 and 15, respectively. For this polysaccharide, only the increasing PF-127 concentration established an acceleration in the gelation process.

Moreover, the G' values were found to be equal or higher than the ones for PF-127 hydrogels. It was shown, for a 20% w/v PF-127 concentration, that ALG effect was more visible in its lower concentration (formulation 11), since its G' value does not promote with increasing ALG concentration.

These four formulations were taken to frequency sweep tests in order to confirm the strong gel behavior at the physiological temperature of 37 °C. Test results in Figure 5c first confirmed the strong gel behavior. The G' values were 11, 19, 11, and 29 kPa for formulations 11, 12, 14, and 15, respectively. First, these G' values were shown to be higher than the ones for PF-127 hydrogels, confirming the positive effect of ALG implementation.

As it can be seen, for a 20% w/v of PF-127 concentration, the alginate addition promoted the storage modulus value independently of its concentration, suggesting that lower ALG concentration was optimal for this PF-127 concentration.

Besides, when it came to considering the difference between the storage and loss moduli, the reported values were around 9, 18, 11, and 28 kPa, respectively. These are represented with their G'' in Figure S6 (Supporting Information) and $G^{\pm}$ is shown in Figure S9c (Supporting Information). For $(G' - G'')$ values, the ALG effect was more visible. When increasing ALG concentration, so did the elastic nature of the gels. This was also due to the elastic nature that ALG solutions have as well.[71]

 © 2025 The Author(s). Macromolecular Materials and Engineering published by Wiley-VCH GmbH

15292654, 0, Downloaded from https://onlinelibrary.wiley.com/doi/10.1002/mame.202400457 by Universidad De Salamanca, Wiley Online Library on [06/11/2025]. See the Terms and Conditions (https://onlinelibrary.wiley.com/terms-and-conditions) on Wiley Online Library for rules of use; OA articles are governed by the applicable Creative Commons License

ADVANCED SCIENCE NEWS
www.advancedsciencenews.com

Macromolecular Materials and Engineering
Open Access
www.mame-journal.de

Figure 5d shows the ramp temperature with steady flow analysis. First, formulation 15 clearly showed that the micelles are not stable and collapse at the fixed shear rate. The rest of the formulations did show a successful MAC. On the other hand, it was also observed a big difference in the gel stabilization temperatures when increasing PF-127 concentration, being these 29 °C for both formulations 11 and 14, and 22 °C for formulation 12. ALG hydrogels also reached higher viscosity values of 7, 13, and 7 Pa s, greater than the ones of PF-127 hydrogels. Moreover, it was shown that increasing ALG concentration did increase the viscous properties and confers the structure more strength toward external deformation forces. Finally, regarding formulation 12 gct, it is shown that the gelation occurs at lower temperatures than room temperature (25 °C).

In these systems, the PF-127 hydrophilic blocks (PEO) tend to mainly form hydrogen bonds with other functional groups with hydrogen in them (mainly alcohols and carboxylic acids). In the alginate case, the carboxylic acid groups can easily tend toward these interactions, as well as other electrostatic interactions.[71,72] The PF-127 and alginate system has been reported to form mesh macrostructures that increase their size when the PF-127 concentration does. Basically, the pluronic micelles are organized in cubic domains and induce the distortion of alginate chains.[73] Following this, different size meshes coexist in a nonhomogeneous spatial distribution of the micelles in the polymeric network, as long as the PF-127 concentration exceeds the value of 10% w/v, as shown in the results. The micelles organize into dense aggregates in which packing increases with the PF-127 concentration.[74] This also explains why the PF-127 concentration was more determinant in the experimental results in Figure 5d. For PF-127 formulations 11 and 14, the ones with 20% w/v PF, are the ones in which structure is potentially compatible for the application.

3.1.4. PF-127 and GG Hydrogels

The same procedure was followed to study GG implementation to the PF-127 hydrogels (formulations 16–21). The rheological analyses are shown in **Figure 6**.

First, looking at the temperature sweep tests in Figure 6a,b, it was once again proven that GG was not an exception for low concentrations (10% w/v) of PF-127 to undergo the gelation process. Moreover, for formulation 20, this process never occurred as well. Thus, we could first state that high concentrations of GG were not able to show the gelation process, since probably the branched and more spatially complex structure of the GG caused a collapse in the hydrogel structure.[75]

For the rest of the formulations, this gelation process was observed. The gcts were 32, 25, and 22 °C, for formulations 17, 18, and 21, respectively. All of these results did not present a significant increase when comparing with the PF-127 hydrogels. Therefore, GG did not interrupt the PF-127 gelation process, but surely did not promote it.

Results for the frequency sweep test in Figure 6c at 37 °C showed strong gel behavior for all the potential formulations. Storage moduli values were around 16, 10, and 25 kPa, which did not imply a significant difference for formulation 21 compared to formulation 3 (without polysaccharides). However, for formulation 17, it was found that the gel had significantly improved elastic properties compared to formulation 2, showing higher storage modulus value, and a higher difference between this one and the viscous one, around 15 kPa. This can be seen in Figure S7 (Supporting Information) and G^* is shown in Figure S9d (Supporting Information).

Figure 6d shows the temperature ramp steady flow test. As it can be seen, only the formulation 17 was able to reach the stabilization of its viscosity at a value close to 7 Pa s, greater than PF-127 hydrogel viscosity, and similar to the ones reported in the ALG systems.

In these formulations, the PF-127 also interacts via hydrogen bonds, with its strength increasing when the polysaccharide concentration does too. However, if the concentration increased from 0.5% w/v, the GG and its structure interfered with the PF-127 network making it unstable and collapsing the MAC at the fixed shear rate in Figure 6d.[75]

3.1.5. PF-127 and LEV Hydrogels

The last polysaccharide to be added to the system was LEV that was synthesized enzymatically from a sucrase solution, as described in previous sections (formulations 22–26). The results are the ones shown in **Figure 7**.

For LEV systems in Figure 7a,b, it was also confirmed that without enough PF-127 concentration, the gelation mechanism did not happen (formulations 22 and 25). There was also an exception concerning formulations 23 and 24, where the increasing PF-127 concentration caused a negative effect on the elastic modulus of the system. This can be seen in Figure 7a.

Nonetheless, the gel state was efficiently achieved for formulations 23, 24, 26, and 27. The gcts for these were 30, 23, 28, and 22 °C, respectively. These results implied that, apart from the exception, LEV effect was shown positive, since the gcts were lowered when it was added. Moreover, it is shown that LEV implementation improved the desired elastic properties of the PF-127 hydrogels, comparing their G' values with G' from PF-127 hydrogels.

These formulations were taken to the fixed temperature 37 °C, and were analyzed by a frequency sweep test in Figure 7c, showing that all of the hydrogels had a strong gel behavior. Let it also be noted that formulations 23 and 24 overlap each other, regardless of the polysaccharide concentration (green and purple lines in Figure 7c). As previously said, the results for this PF-127 concentration were improved by LEV addition, but not its concentration increase. The elastic moduli values reported were around 19, 8, 18, and 34 kPa, respectively. For formulations 23 and 26, LEV concentration had the same effect, while for formulations 24 and 27, the LEV effect was clear and visible, reaching G' higher than 30 kPa for both high concentrations.

For all the cases, besides formulation 24, the LEV addition caused a clear improvement over the elasticity of the PF-127 hydrogels. Not only when it came to elastic moduli values but also the difference between this and the viscous ones, being around 17, 7, 17, and 33 kPa, respectively. G'' of the formulations can be seen in Figure S8 (Supporting Information) and G^* is shown in Figure S9e (Supporting Information).

Studying the MAC through the temperature ramp test in Figure 7d, it was seen that the formulation 24 failed to show

 © 2025 The Author(s). Macromolecular Materials and Engineering published by Wiley-VCH GmbH

15029514, 0, Downloaded from https://onlinelibrary.wiley.com/doi/10.1002/mame.202400457 by Universidad De Salamanca, Wiley Online Library on [09/12/2025]. See the Terms and Conditions (https://onlinelibrary.wiley.com/terms-and-conditions) on Wiley Online Library for rules of use; OA articles are governed by the applicable Creative Commons License

ADVANCED SCIENCE NEWS
www.advancedsciencenews.com

Macromolecular Materials and Engineering
www.mame-journal.de

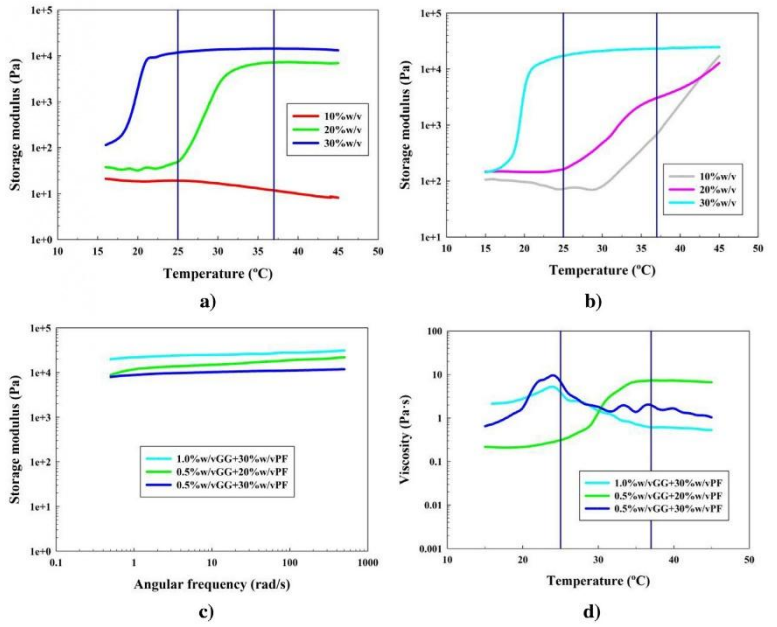

Figure 6. Rheological analyses of PF-127 and GG hydrogels: a) temperature sweep oscillatory flow test for 0.5% w/v GG, b) temperature sweep oscillatory flow test for 1.0% w/v GG, c) frequency sweep oscillatory flow test on gel formulations, and d) temperature ramp steady flow test on gel formulations.

a stable MAC at the studied shear rate. However, the rest of the formulations achieved this structure stabilization at temperatures of 30, 30, and 21 °C for formulations 23, 26, and 27. Reported viscosity values were around 6, 7, and 11 Pa s, respectively. These values were once again higher than the ones reported in PF-127 hydrogels, but the lowest of all polysaccharide systems. In order to explain the structure collapse of the formulation 24, it is important to take into account that levan is a self-assembly polysaccharide constituted of fructose units (—OH groups for hydrogen bonds), that forms nanoparticles inside the PF-127 micellar network. The addition of the nanoparticles explains why, if there was not enough PF-127 concentration, this ordered structure can collapse with high concentrations of LEV at a fixed shear rate, as shown in Figure 7d.[37] However, for formulations 23 and 26, both concentrations of LEV present the desired characteristics. Finally, observing the gct, it was possible to affirm that the formulation 27 had a gel state at room temperature.

It is therefore shown that the LEV effect highly improved the elastic nature of the hydrogels, since LEV is a self-assembly polysaccharide that does not present any complex structure to collapse the MAC. Besides, it also improved viscous properties, overall with higher concentrations, since more concentration means more viscosity taken by the hydrogel matrix to be more resistant against flow.

3.1.6. Selection of Optimal Formulations for Drug Release Experiments

Taking into account all the results obtained by the rheological analyses, Table 2 summarizes the final results for all formulations.

It is important to emphasize that for its use after a tumor resection, a strong gel has to be obtained at the physiological temperature (37 °C). This formulations need to present the MAC (ob-

 © 2025 The Author(s). Macromolecular Materials and Engineering published by Wiley-VCH GmbH

15292691, 0, Downloaded from https://onlinelibrary.wiley.com/doi/10.1002/mame.202400457 by Universidad De Salamanca, Wiley Online Library on [09/12/2025]. See the Terms and Conditions (https://onlinelibrary.wiley.com/terms-and-conditions) on Wiley Online Library for rules of use; OA articles are governed by the applicable Creative Commons License

ADVANCED SCIENCE NEWS
www.advancedsciencenews.com

Macromolecular Materials and Engineering
www.mame-journal.de

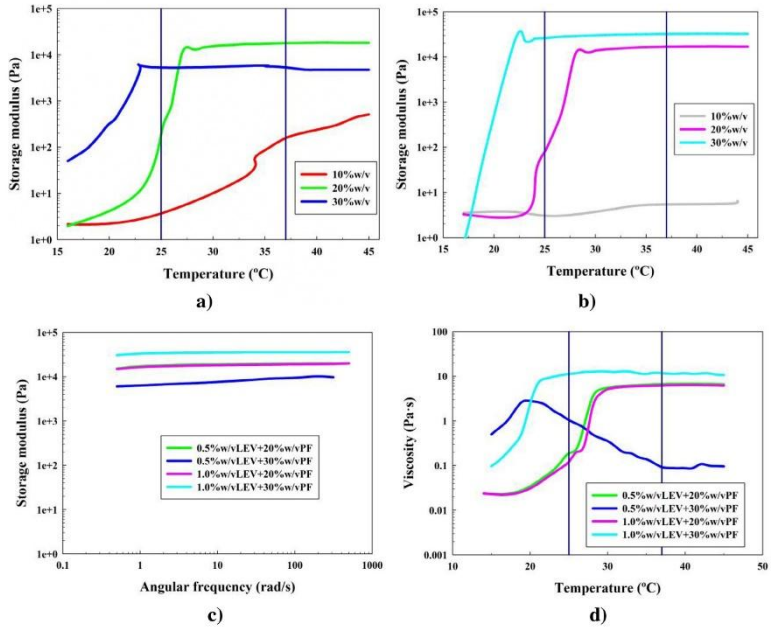

Figure 7. Rheological analyses of PF-127 and LEV hydrogels: a) temperature sweep oscillatory flow test for 0.5% w/v LEV, b) temperature sweep oscillatory flow test for 1.0% w/v LEV, c) frequency sweep oscillatory flow test on gel formulations, and d) temperature ramp steady flow test on gel formulations.

served in the temperature ramp steady flow analyses), reaching a stable higher viscosity once the gel state is achieved. It is also essential to present liquid state and aqueous solution behavior at room temperature (25 °C) in order to be injectable.[43] These characteristics must be studied through the understanding of interaction between the polysaccharides and the PF-127 hydrogel network.

Consequently, the potential formulations that were considered as potential DDS for the application mentioned were: 20% w/v PF-127, 0.5% and 1.0% w/v ALG with 20% w/v PF-127, 0.5% w/v GG with 20% w/v PF-127, and 0.5% and 1.0% w/v LEV with 20% w/v PF-127 (2, 11, 14, 17, 23, and 26, respectively).

3.2. Drug Release Experiments

All of these selected hydrogel systems were then loaded as described in Section 2.6 with a 5-FU concentration of 50 ppm, and then, the drug release experiments were performed as described in Section 2.7. Results for these experiments are shown in both **Figure 8** and **Table 3** below.

As it can be seen in Figure 8 and Table 3, for every system with any implemented polysaccharide at any concentration, the drug release was highly delayed, proving the point that polysaccharide structural implementation improved rheological properties and suits the hydrogels better for the desired application.[35] The PF-127 alone hydrogel presented a t_{10} lower than 1 min, t_{50} of 16 min, and t_{100} of 87 min. However, with polysaccharide structural effects, these times were delayed to 5–30 min for t_{10}, 70–145 min for t_{50}, and 260–440 min for t_{100}. This implied a minimum delay of 173 min (198% delay from PF-127 hydrogel) and a maximum delay of 353 min (405% delay from PF-127 hydrogel). Therefore, it can be stated that polysaccharides implemented systems contributed from double to quadruple the drug release time of the PF-127 hydrogels.

 © 2025 The Author(s). Macromolecular Materials and Engineering published by Wiley-VCH GmbH

15292654, 0, Downloaded from https://onlinelibrary.wiley.com/doi/10.1002/mame.202400457 by Universidad De Salamanca, Wiley Online Library on [09/12/2025]. See the Terms and Conditions (https://onlinelibrary.wiley.com/terms-and-conditions) on Wiley Online Library for rules of use; OA articles are governed by the applicable Creative Commons License

ADVANCED SCIENCE NEWS
www.advancedsciencenews.com

Macromolecular Materials and Engineering
www.mame-journal.de

Table 3. Drug release studied parameters, being t_{10}, t_{50}, and t_{100} the times where 10%, 50%, and 100% of the drug concentration was released, respectively.

Form	Hydrogel [% w/v]	t_{10} [min]	t_{50} [min]	t_{100} [min]	G′ [kPa]	Viscosity [Pa s]
2	20% PF-127	<1	16	87	8.63 ± 2.36	4.53 ± 0.21
11	0.5% ALG + 20% PF-127	9	81	315	11.00 ± 3.07	7.04 ± 1.67
14	1.0% ALG + 20% PF-127	31	145	440	11.49 ± 1.83	7.18 ± 0.15
17	0.5% GG + 20% PF-127	12	96	430	15.88 ± 3.54	6.98 ± 0.60
23	0.5% LEV + 20% PF-127	5	70	260	18.69 ± 2.46	6.11 ± 0.86
26	1.0% LEV + 20% PF-127	10	86	335	18.09 ± 2.54	6.39 ± 0.62

Systems exhibiting prolonged drug release correlated with higher viscosities rather than elevated G′ values. This phenomenon is attributed to the structural characteristics of the polysaccharides and their interactions with PF-127 via hydrogen bonds.

Among the polysaccharides studied, LEV demonstrated the shortest drug release times, primarily due to its self-assembly organization. This configuration forms a lower pore interconnected and higher elastic, but more permeable gel matrix. In drug release experiments, water permeated the structure, leading to an easier dissolution of the micelles. The distilled water established hydrogen bonds with the network compounds, promoting disaggregation into colloids, accelerating its drug release.

Rheological analysis further supports this explanation, as LEV exhibited the lowest viscosity among the polysaccharide-based gels (observed in temperature ramp tests). Although LEV hydrogels were the most elastic systems, their viscous properties were the weakest. This indicated that its ability to resist against external stresses was lower than the other formulations, resulting in faster disaggregation. However, higher levan concentrations increased the system viscosity, enhancing resistance and extending drug release times.

By contrast, alginate showed relatively slower drug release due to its linear structure. This linear structure limits water permeability and resists disaggregation due to spatial constraints. This is due to the alginate matrix, which is organized as chains entrapped within micelle domains, that forms more hydrogen bonds per polysaccharide unit. Consequently, while ALG did not exhibit an elastic modulus as high as LEV, it provided greater resistance to drug release.

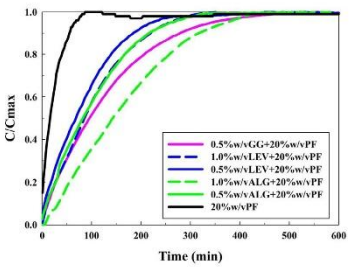

Figure 8. Drug release experiments with 5-FU-loaded PF-127 hydrogels.

This effect was also observed in the increased viscosity values in the temperature ramp test, showing higher values than PF-127 and LEV systems. Additionally, as the concentration of polysaccharide increased, so did the viscous properties and drug release time.

The addition of branches in GG introduces further structural complexity. However, this structural conformation can interfere with the PF-127 gel stabilization, which limited the GG concentrations to 0.5% w/v, as discussed earlier (see Sections 3.1.4 and 3.1.6).

In terms of drug release, GG performed better than ALG at the same concentration, due to its viscous properties. The structural complexity of GG created a denser, more tortuous matrix, reducing pore size and hindering water permeability more effectively than simpler polysaccharides at the same low concentration range.

Ultimately, the system with ALG yielded the best drug release results, as its higher concentration compensated for the structural GG structure. A similar trend was observed with LEV, which outperformed the GG system due to its higher concentration. Notably, higher drug release times order nearly correspond with higher viscosity (see Section 3.3 for model fittings).

Additionally, it has been demonstrated that the structural characteristics of these polysaccharides enhance the hydrogel matrix, resulting in increased elasticity, a more consistent gel state, and overall, greater viscosity and resistance against external stresses. Consequently, drug release times in these composite hydrogels are slowed to between half and a quarter of those in PF-127 hydrogels alone.

3.3. Modeling and Parameter Estimation of Drug Release Experiments

As previously explained in Section 2.8, experimental results shown in Figure 8 were fitted to a model previously described. The results of this modeling are shown in **Table 4**.

Taking into account the previous results, after a first estimation it was decided to fix the K_r value of the formulation 2 to 1.000, since the release constant includes all of the resistances against the phenomena transport. This model stablishes that almost all of the release phenomenon is due to the hydrogel degradation, with added resistance when adding polysaccharides. These

 © 2025 The Author(s). Macromolecular Materials and Engineering published by Wiley-VCH GmbH

15292691, 0, Downloaded from https://onlinelibrary.wiley.com/doi/10.1002/mame.202400457 by Universidad De Salamanca, Wiley Online Library on [09/12/2025]. See the Terms and Conditions (https://onlinelibrary.wiley.com/terms-and-conditions) on Wiley Online Library for rules of use; OA articles are governed by the applicable Creative Commons License

ADVANCED SCIENCE NEWS
www.advancedsciencenews.com

Macromolecular Materials and Engineering
Open Access
www.mame-journal.de

Table 4. Drug release modeling.

Form	Formulation concentrations [% w/v]	k_d [s^{-1}]	N	K_r	E_{abs}	E_r [%]
2	20% PF-127	2.521	0.010	1.000	3.172	2.665
11	0.5% ALG and 20% PF-127	0.469	0.010	1.063	3.209	2.697
14	1.0% ALG and 20% PF-127	0.256	0.435	1.181	5.942	4.993
17	0.5% GG and 20% PF-127	0.416	0.027	1.063	1.345	1.130
23	0.5% LEV and 20% PF-127	0.667	0.010	1.003	3.556	2.988
26	1.0% LEV and 20% PF-127	0.512	0.101	1.038	4.099	3.445

PF-127 hydrogels were observed to not swell while studying their degradation process, with a good fitting to a model adapted to study this mechanism,[57] indicating the main contribution for degradation was the PF-127 and polysaccharide chain disaggregation. Also, let it be noted that the parameter N must be a positive value between 0 and 1, since erosion has an influence in the drug release mechanism.

As shown in Table 4, the degradation rate constant k_d decreased with increasing polysaccharide concentration, indicating a slower drug release. The highest k_d value was observed in the PF-127 alone hydrogel, presenting its weak resistance against degradation.[36] In fact, k_d was reduced until 10 times in the polysaccharide systems, confirming the necessity of their implementation to achieve controlled drug release. The most delayed release (lowest k_d) was observed in the formulation 14 (1.0% w/v ALG), attributed to the high concentration of the second-most structurally complex polysaccharide, showing the highest viscosity value, as discussed in Section 3.2.

Analyzing the k_d values from the highest (fastest degrading) to the lowest (slowest degrading), it is shown that the degradation rate strongly influenced the drug release order, and was closely correlated with the viscosity of each formulation. This suggests that increased viscosity correlates with a lower degradation rate, indicating that more viscous systems resist against external stresses more effectively, and thus delays drug release time.

The N factor, related to erosion, increased with polysaccharide concentration, and all values remained below 0.5, suggesting that the erosion process is predominantly controlled by water diffusion through the gel matrix (permeability). This permeability decreased with increasing polysaccharide concentrations, since the entangled structures hindered water permeation.

The highest N value was observed for the formulation 14, affirming that the most controlled release occurred in the structure that limited water permeability the most. Polysaccharide systems at 1.0% w/v showed the highest N values, confirming their increased resistance to permeation. The high N for formulation 26 (1.0% w/v LEV) may explain its slightly higher drug release time compared to formulation 23 (0.5% w/v ALG), despite showing a lower k_d value. On the other hand, the 0.5% w/v formulations 11 and 23 had the lowest N values, similar to PF-127. Additionally, the branched structure of the formulation 17 (0.5% w/v GG) hindered permeation more than simpler polysaccharide systems at the same concentration, explaining its lower k_d.

When observing the release constant K_r, it was noted that this parameter reflected both degradation and additional transport phenomena. All systems exhibited K_r values greater than 1.000, indicating diffusion as the gel degraded. Comparing the PF-127 to polysaccharide implemented systems, it was noted that polysaccharides reduced the gel porosity and increased the system tortuosity, consequently lowering effective diffusion compared to bulk diffusion.

This contribution to tortuosity was the highest in ALG, followed by GG, and finally LEV implemented systems, correlating with each polysaccharide structural organization. Moreover, it was observed that higher viscosity correlated with lower bulk diffusion, supporting more consistent and sustained release. For K_r, formulation 14 showed the highest resistance to drug release, also corresponding to the highest viscosity among all of the systems. This correlation between K_r and viscosity further supports the conclusion that hydrogel matrix

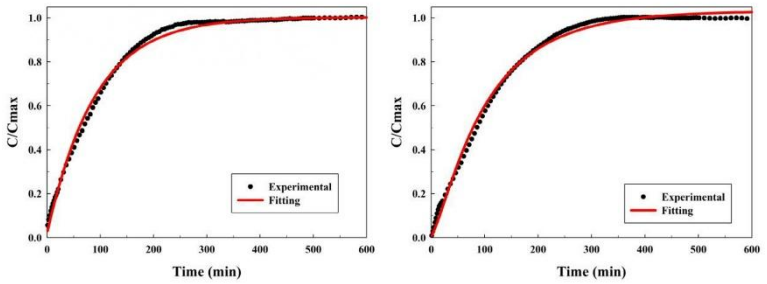

Figure 9. Graphical fittings to experimental drug release data for: a) formulation 17 and, b) formulation 14.

 © 2025 The Author(s). Macromolecular Materials and Engineering published by Wiley-VCH GmbH

15029514, 0, Downloaded from https://onlinelibrary.wiley.com/doi/10.1002/mame.202400457 by Universidad De Salamanca, Wiley Online Library on [09/12/2025]. See the Terms and Conditions (https://onlinelibrary.wiley.com/terms-and-conditions) on Wiley Online Library for rules of use; OA articles are governed by the applicable Creative Commons License

viscosity plays an essential role in controlling drug release kinetics.

Finally, commenting on the error values (E_r), as it can be seen in Table 4, all errors obtained are lower than 5.000%, which imply these models can be considered valid. A graphic proof of the models can be observed below in **Figure 9** showing the lowest (formulation 17) and the highest (formulation 14) errors (1.33% and 4.99%, respectively) obtained in the systems in Figure 9a,b, respectively. For the rest of the fittings, these can be seen in Figure S10 (Supporting Information).

4. Conclusions

This work examined the impact of the implementation of various polysaccharides to PF-127 hydrogels on their gelation behavior and control of 5-FU release. Analysis of gelation revealed that PF-127 concentrations above 10% w/v significantly increased the rheological properties of the system, enhancing elasticity, viscosity, and resistance to flow. Generally, the addition of polysaccharides increased the storage modulus and strengthened the gel structure at 37 °C, with higher viscosity values due to the supported MAC.

Six formulations were confirmed to undergo gelation between 25 and 37 °C, synthesizing consistent gels. These formulations included 20% w/v PF-127 alone, and in combination with 0.5% and 1.0% w/v ALG, 0.5% w/v GG, and 0.5% and 1.0% w/v LEV.

Drug release experiments with 5-FU-loaded hydrogels demonstrated that polysaccharide implementation significantly delayed release times by 2–4 times compared to the PF-127 hydrogel alone. Results indicated that higher polysaccharide concentrations and increased structural complexity promoted the systems viscosity and further delayed their drug release time.

Kinetic modeling of the drug release data confirmed polysaccharide and PF-127 chain disaggregation as the primary mechanism. Degradation rates, erosion factors, and release constants were calculated, showing that systems with higher viscosity, greater structural complexity, and prolonged drug release times exhibited lower degradation rates.

Finally, the release constant revealed that polysaccharide-implemented systems showed greater resistance to transport phenomena, resulting in reduced effective diffusion and enhanced viscosity. This release constant order correlated with viscosity trends from temperature ramp rheological analysis, confirming the relationship between viscosity and controlled release in the hydrogel systems.

Supporting Information

Supporting Information is available from the Wiley Online Library or from the author.

Acknowledgements

M.B.-L. wants to acknowledge the funds from the "Programa propio III de la Universidad de Salamanca: Ayudas para financiar contratos predoctorales de la Universidad de Salamanca cofinanciados por el Banco Santander" for his Ph.D. fellowship. The authors would like to express their gratitude to the Spanish Ministry of Science and Innovation for the financial support, research project: No. PID2022-1405990B-I00.

Conflict of Interest

The authors declare no conflict of interest.

Data Availability Statement

The data that support the findings of this study are available from the corresponding author upon reasonable request.

Keywords

drug release, mathematical model, PF-127, polysaccharides

Received: December 13, 2024
Revised: March 20, 2025
Published online:

[1] N. Harbeck, F. Penault-Llorca, J. Cortes, M. Gnant, N. Houssami, P. Poortmans, K. Ruddy, J. Tsang, F. Cardoso, *Nat. Rev. Dis. Primers* **2019**, *5*, 66.
[2] R. N. Woodring, E. G. Gurysh, E. M. Bachelder, K. M. Ainslie, *ACS Appl. Bio Mater.* **2023**, *6*, 934.
[3] H. Daraee, A. Etemadi, M. Kouhi, S. Alimirzalu, A. Akbarzadeh, *Artif. Cells, Nanomed., Biotechnol.* **2016**, *44*, 381.
[4] W. H. De Jong, *Int. J. Nanomed.* **2008**, *3*, 133.
[5] Y. Li, J. Rodrigues, H. Tomás, *Chem. Soc. Rev.* **2012**, *41*, 2193.
[6] K. Y. Lee, D. J. Mooney, *Chem. Rev.* **2001**, *101*, 1869.
[7] D. Puppi, F. Chiellini, A. M. Piras, E. Chiellini, *Prog. Polym. Sci.* **2010**, *35*, 403.
[8] T. R. Hoare, D. S. Kohane, *Polym. J.* **2008**, *49*, 1993.
[9] C. Sandoval-Yañez, L. Escobar, C. A. Amador, *Processes* **2020**, *8*, 1331.
[10] M. Wang, M. Chen, W. Niu, D. D. Winston, W. Cheng, B. Lei, *Biomater. Res.* **2020**, *261*, 120301.
[11] S. Chatterjee, P. C. L. Hui, C. W. Kan, W. Wang, *Sci. Rep.* **2019**, *9*, 11658.
[12] X. Chen, M. Wang, X. Yang, Y. Wang, L. Yu, J. Sun, J. Ding, *Theranostics* **2019**, *9*, 6080.
[13] P. J. Rose Jaquilin, O. S. Oluwafemi, S. Thomas, A. O. Oyedeji, *J. Drug Delivery Sci. Technol.* **2022**, *72*, 103390.
[14] V. H. G. Phan, H. T. T. Duong, T. Thambi, T. L. Nguyen, M. H. Turabee, Y. Yin, S. H. Kim, J. Kim, J. H. Jeong, D. S. Lee, *Biomater. Res.* **2019**, *195*, 100.
[15] S. H. Kim, T. Thambi, V. H. G. Phan, D. S. Lee, *Carbohydr. Polym.* **2020**, *233*, 115832.
[16] T. M. D. Le, B.-K. Jung, Y. Li, H. T. T. Duong, T. L. Nguyen, J. W. Hong, C.-O. Yun, D. S. Lee, *Biomater. Sci.* **2019**, *7*, 4195.
[17] T. M. D. Le, H. T. T. Duong, T. Thambi, V. H. G. Phan, J. H. Jeong, D. S. Lee, *J. Biol. Macromol.* **2018**, *19*, 3536.
[18] A. C. Marques, P. C. Costa, S. Velho, M. H. Amaral, *Gels* **2023**, *9*, 593.
[19] J. Shi, L. Yu, J. Ding, *Acta Biomater.* **2021**, *128*, 42.
[20] B. Shriky, A. Kelly, M. Isreb, M. Babenko, N. Mahmoudi, S. Rogers, O. Shebanova, T. Snow, T. Gough, *J. Colloid Interface Sci.* **2020**, *565*, 119.
[21] N. U. Khaliq, J. Lee, S. Kim, D. Sung, H. Kim, *Pharm. J.* **2023**, *15*, 2102.
[22] P. Zarrintaj, J. D. Ramsey, A. Samadi, Z. Atoufi, M. K. Yazdi, M. R. Ganjali, L. M. Amirabad, E. Zangene, M. Farokhi, K. Formela, M. R. Saeb, M. Mozafari, S. Thomas, *Acta Biomater.* **2020**, *110*, 37.
[23] J. J. Escobar-Chavez, M. Lopez-Cervantes, A. Naik, Y. N. Kalia, D. Quintanar-Guerrero, A. Ganem-Quintanar, *J. Pharm. Pharmaceut. Sci.* **2006**, *9*, 339.
[24] D. Wei, L. Ge, R. Guo, *Colloids Surf., A* **2018**, *553*, 1.
[25] G. Wanka, H. Hoffmann, W. Ulbricht, *Macromolecules* **1994**, *27*, 4145.

 © 2025 The Author(s). Macromolecular Materials and Engineering published by Wiley-VCH GmbH

15292654, 0, Downloaded from https://onlinelibrary.wiley.com/doi/10.1002/mame.202400457 by Universidad De Salamanca, Wiley Online Library on [09/12/2025]. See the Terms and Conditions (https://onlinelibrary.wiley.com/terms-and-conditions) on Wiley Online Library for rules of use; OA articles are governed by the applicable Creative Commons License

ADVANCED SCIENCE NEWS
www.advancedsciencenews.com

Macromolecular Materials and Engineering
Open Access
www.mame-journal.de

[26] D. Y. Alakhova, *Mol. Pharmaceutics* **2014**, *11*, 2566.
[27] J. P. K. Armstrong, M. Burke, B. M. Carter, S. A. Davis, A. W. Perriman, *Adv. Healthcare Mater.* **2016**, *5*, 1724.
[28] P. Zarrintaj, M. Jouyandeh, M. R. Ganjali, B. S. Hadavand, M. Mozafari, S. S. Sheiko, M. Vatankhah-Varnoosfaderani, T. J. Gutiérrez, M. R. Saeb, *Eur. Polym. J.* **2019**, *117*, 402.
[29] D. Seol, M. J. Magnetta, P. S. Ramakrishnan, G. L. Kurriger, H. Choe, K. Jang, J. A. Martin, T.-H. Lim, *J. Biomed. Mater. Res., Part B* **2013**, *101*, 1508.
[30] A. Gigout, M. D. Buschmann, M. J. B. Jolicoeur, *Biotechnol. Bioeng.* **2008**, *100*, 975.
[31] J. Wu, J. Zhu, C. He, Z. Xiao, J. Ye, Y. Li, A. Chen, H. Zhang, X. Li, L. Lin, Y. Zhao, J. Zheng, J. Xiao, *ACS Appl. Mater. Interfaces* **2016**, *8*, 18710.
[32] S. H. Oh, J. H. Kim, K. S. Song, B. H. Jeon, J. H. Yoon, T. B. Seo, U. Namgung, I. W. Lee, J. H. Lee, *Biomaterials* **2008**, *29*, 1601.
[33] Z. Wu, S. Zhan, W. Fan, X. Ding, X. Wu, W. Zhang, Y. Fu, Y. Huang, X. Huang, R. Chen, M. Li, N. Xu, Y. Zheng, B. Ding, *Nano Res.* **2016**, *11*, 122.
[34] K. K. Jain, *Methods Mol. Biol.* **2020**, *2059*, 1.
[35] M. S. H. Akash, K. Rehman, *J. Controlled Release* **2015**, *209*, 120.
[36] C. He, S. W. Kim, D. S. Lee, *J. Controlled Release* **2008**, *127*, 189.
[37] W. I. Choi, Y. Hwang, A. Sahu, K. Min, D. Sung, G. Tae, J. H. Chang, *Biomater. Sci.* **2018**, *6*, 2627.
[38] C. Ju, J. Sun, P. Zi, X. Jin, C. Zhang, *J. Pharm. Sci.* **2013**, *102*, 2707.
[39] N. A. Di Spirito, N. Grizzuti, R. Pasquino, *Phys. Fluids* **2024**, *36*, 111302.
[40] D. S. Pellosi, I. R. Calori, L. B. de Paula, N. Hioka, F. Quaglia, *Mater. Sci. Eng.* **2017**, *71*, 1.
[41] A. González-Garcinuño, A. Tabernero, M. Blanco-López, E. Martín del Valle, S. Kenjeres, *Eur. J. Pharm. Sci.* **2024**, *203*, 106917.
[42] M. Cidade, D. Ramos, J. Santos, H. Carrelo, N. Calero, J. Borges, *Materials* **2019**, *12*, 1083.
[43] Z. Gu, M. Wang, Q. Fang, H. Zheng, F. Wu, D. Lin, Y. Xu, Y. Jin, *Drug Dev. Ind. Pharm.* **2015**, *41*, 812.
[44] T. T. C. Nguyen, C. K. Nguyen, T. H. Nguyen, N. Q. Tran, *Mater. Sci. Eng., C* **2017**, *70*, 992.
[45] S. Blazaki, C. Tsika, M. Tzatzarakis, E. Naoumidi, A. Tsatsakis, C. Tsatsanis, M. K. Tsilimbaris, *Graefe's Arch. Clin. Exp. Ophthalmol.* **2017**, *255*, 2375.
[46] Y. Yang, J. Wang, X. Zhang, W. Lu, Q. Zhang, *J. Controlled Release* **2009**, *135*, 175.
[47] Y. Chen, W. Zhang, J. Gu, Q. Ren, Z. Fan, W. Zhong, X. Fang, X. Sha, *Int. J. Pharm.* **2013**, *452*, 421.
[48] W. Zhang, Y. Shi, Y. Chen, S. Yu, J. Hao, J. Luo, X. Sha, X. Fang, *Eur. J. Pharm. Biopharm.* **2010**, *75*, 341.
[49] W. Zhang, Y. Shi, Y. Chen, J. Ye, X. Sha, X. Fang, *Biomaterials* **2011**, *32*, 2894.
[50] P. D. Kelishady, E. Saadat, F. Ravar, H. Akbari, F. Dorkoosh, *Pharm. Dev. Technol.* **2015**, *20*, 1009.
[51] Y. Chen, W. Zhang, Y. Huang, F. Gao, X. Sha, X. Fang, *Int. J. Pharm.* **2015**, *488*, 44.
[52] M. Bhowmik, P. Kumari, G. Sarkar, M. K. Bain, B. Bhowmick, Md. M. R. Mollick, D. Mondal, D. Maity, D. Rana, D. Bhattacharjee, D. Chattopadhyay, *Int. J. Biol. Macromol.* **2013**, *62*, 117.
[53] M. Dewan, K. Dutta, D. Rana, A. Basu, A. Bhattacharya, A. Adhikary, D. Chattopadhyay, *New J. Chem.* **2020**, *44*, 15708.
[54] E. Brambilla, S. Locarno, S. Gallo, F. Orsini, C. Pini, M. Farronato, D. V. Thomaz, C. Lenardi, M. Piazzoni, G. Tartaglia, *Polymers* **2022**, *14*, 3624.
[55] A. Lupu, M. Bercea, M. Avadanei, L. M. Gradinaru, L. E. Nita, V. R. Gradinaru, *Macromol. Mater. Eng.* **2024**, 2400341, https://doi.org/10.1002/mame.202400341.
[56] A. Lupu, I. Rosca, V. R. Gradinaru, M. Bercea, *Polymers* **2023**, *15*, 355.
[57] I. de Dios-Pérez, A. González-Garcinuño, A. Tabernero, M. Blanco-López, J. A. García-Esteban, V. Moreno-Rodilla, B. Curto, P. Pérez-Esteban, E. M. Martín del Valle, *Eur. J. Pharm. Sci.* **2023**, *191*, 106618.
[58] J. Xu, E. Feng, J. Song, *J. Am. Chem. Soc.* **2014**, *136*, 4105.
[59] A. González-Garcinuño, A. Tabernero, G. Marcelo, V. Sebastián, M. Arruebo, J. Santamaría, E. M. Martín del Valle, *Int. J. Biol. Macromol.* **2019**, *137*, 62.
[60] Y.-I. Chung, S.-Y. Lee, G. Tae, *Colloids Surf., A* **2006**, *284*, 480.
[61] G. E. Newby, I. W. Hamley, S. M. King, C. M. Martin, N. J. Terrill, *J. Colloid Interface Sci.* **2009**, *329*, 54.
[62] A. P. Constantinou, V. Nele, J. J. Doutch, J. S. Correia, R. V. Moiseev, M. Cihova, D. C. A. Gaboriau, J. Krell, V. V. Khutoryanskiy, M. M. Stevens, T. K. Georgiou, *Macromolecules* **2022**, *55*, 1783.
[63] O. Kontogiannis, D. Selianitis, D. R. Perinelli, G. Bonacucina, N. Pippa, M. Gazouli, S. Pispas, *Int. J. Mol. Sci.* **2022**, *23*, 13814.
[64] F. P. Ellis, *Br. J. Ind. Med.* **1963**, *20*, 284.
[65] C. Karthika, R. Sureshkumar, D. V. Sajini, G. Md. Ashraf, Md. H. Rahman, *Environ. Sci. Pollut. Res.* **2022**, *29*, 63202.
[66] N. A. Di Spirito, N. Grizzuti, M. Casalegno, F. Castiglione, R. Pasquino, *Int. J. Pharm.* **2023**, *644*, 123353.
[67] S. Costanzo, A. Di Sarno, M. D'Apuzzo, P. Renato Avallone, E. Raccone, A. Bellissimo, F. Auriemma, N. Grizzuti, R. Pasquino, *Phys. Fluids* **2021**, *33*, 043113.
[68] S.-Y. Lee, G. Tae, Y.-H. Kim, *J. Biomater. Sci., Polym. Ed.* **2007**, *18*, 1335.
[69] G. Sworn, in *Handbook of Hydrocolloids*, 3rd ed., (Eds: G. O. Phillips, P. A. Williams), Woodhead Publishing Series in Food Science, Technology and Nutrition, Woodhead Publishing, Sawston, England **2021**, p. 833.
[70] M. Suhail, I. Chiu, Y. Lai, A. Khan, N. S. Al-Sowayan, H. Ullah, P. C. Wu, *Gels* **2023**, *9*, 640.
[71] M. Blanco-López, A. González-Garcinuño, A. Tabernero, E. M. Martín del Valle, *Polymers* **2021**, *13*, 966.
[72] M. Blanco-López, A. Marcos-García, A. González-Garcinuño, A. Tabernero, E. M. Martín del Valle, *Polym. Adv. Technol.* **2024**, *35*, 6554.
[73] M. Abrami, I. D'Agostino, G. Milcovich, S. Fiorentino, R. Farra, F. Asaro, R. Lapasin, G. Grassic, M. Grassi, *Soft Matter* **2014**, *10*, 729.
[74] I. Frisman, D. Seliktar, H. Bianco-Peled, *Acta Biomater.* **2012**, *8*, 51.
[75] M. Dewan, G. Sarkar, M. Bhowmik, B. Das, A. K. Chattoapadhyay, D. Rana, D. Chattopadhyay, *Int. J. Biol. Macromol.* **2017**, *102*, 258.

 © 2025 The Author(s). Macromolecular Materials and Engineering published by Wiley-VCH GmbH

15292654, 0, Downloaded from https://onlinelibrary.wiley.com/doi/10.1002/mame.202400341 by Universidad De Salamanca, Wiley Online Library on [09/12/2025]. See the Terms and Conditions (https://onlinelibrary.wiley.com/terms-and-conditions) on Wiley Online Library for rules of use; OA articles are governed by the applicable Creative Commons License

Supporting information

Innovative Thermosensitive Composite Materials: Merging Poloxamer PF-127 and Polysaccharides for Enhanced Functional Properties

Marcos Blanco-López[1], Inmaculada de Dios Pérez[1], Álvaro González-Garcinuño[1,2], Antonio Tabernero[1,2,], Eva Martín del Valle[1,2].*

1) *Department of Chemical Engineering. University of Salamanca. Plaza Los Caídos s/n, 37008 Salamanca (Spain).*
2) *Institute for Biomedical Research in Salamanca (IBSAL), Paseo de San Vicente 87, 37007, Salamanca (Spain).*

**** Corresponding author at: Antonio Tabernero (antaber@usal.es)***

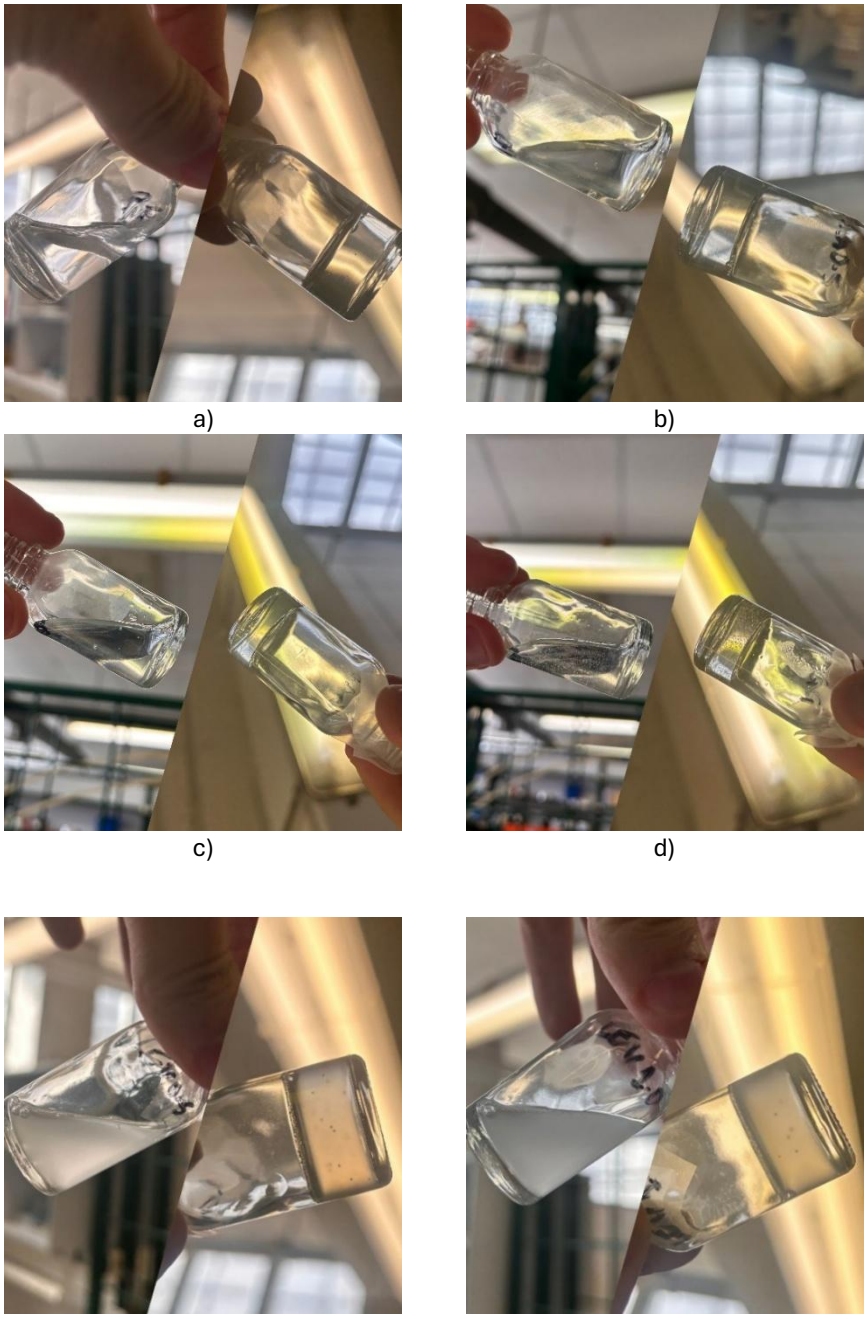

Figure S1. PF-127 20% w/v hydrogel samples in sol (left) and gel (right) state of: a) Formulation 2 (no polysaccharides), b) Formulation 11 (0.5% w/v ALG), c) Formulation 14 (1.0% w/v ALG), d) Formulation 17 (0.5% w/v GG), e) Formulation 23 (0.5% w/v LEV), and f) Formulation 26 (1.0% w/v LEV).

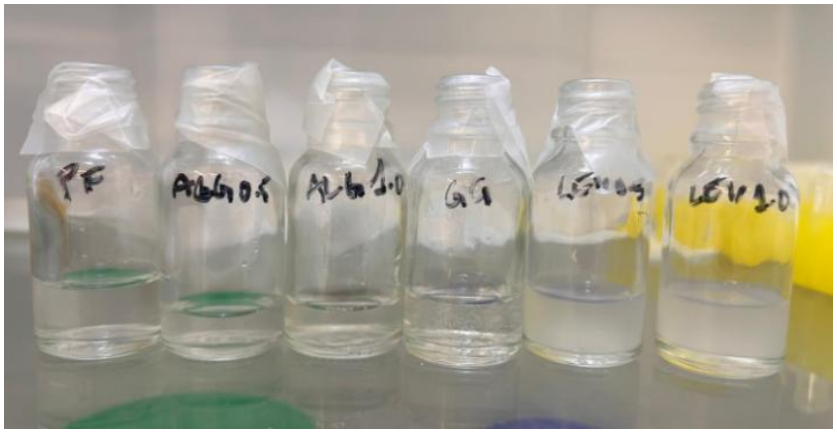

Figure S2. PF-127 20% w/v hydrogel samples in sol state (left). From left to right: Formulation 2 (no polysaccharides), Formulation 11 (0.5% w/v ALG), Formulation 14 (1.0% w/v ALG), Formulation 17 (0.5% w/v GG), Formulation 23 (0.5% w/v LEV), and Formulation 26 (1.0% w/v LEV).

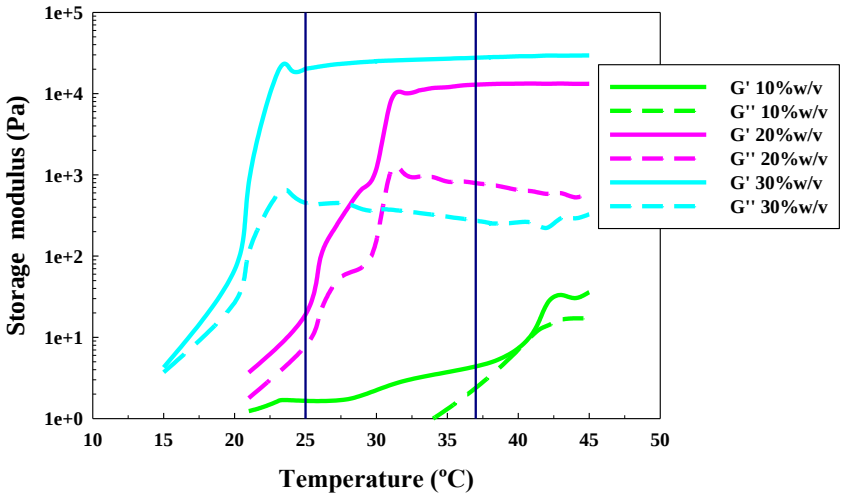

a)

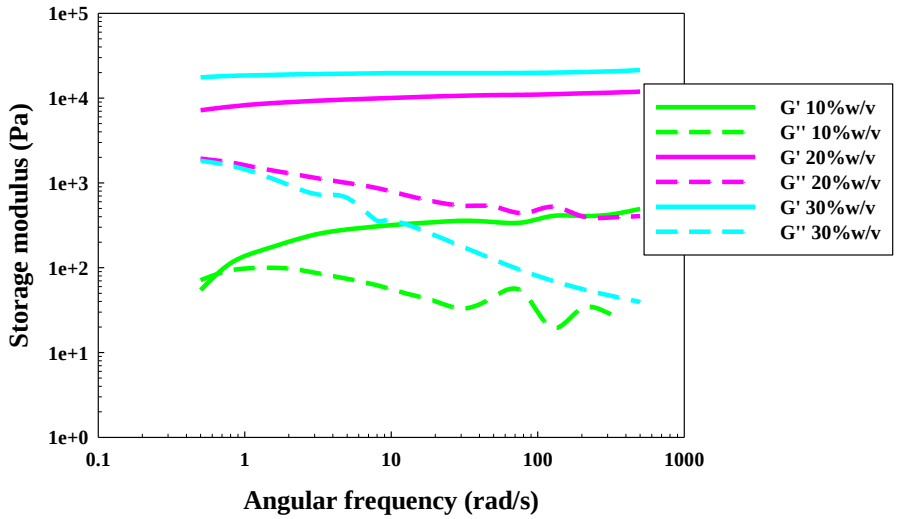

b)

Figure S3. PF-127 hydrogel system oscillatory flow analyses: a) Temperature sweep, and b) Frequency sweep.

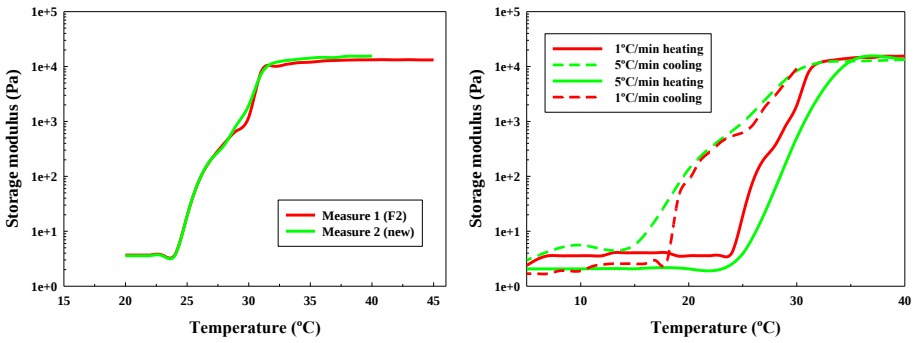

a) b)

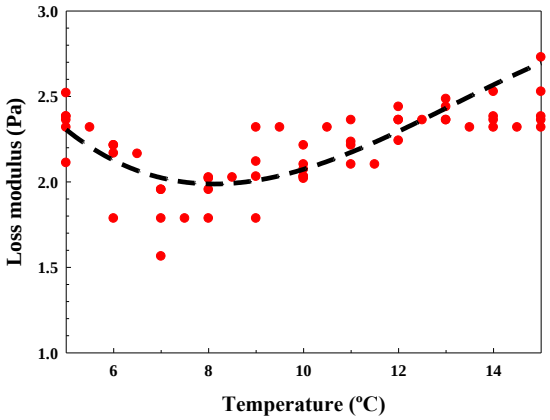

c)

Figure S4. Measurements on Formulation 2 (PF-127 20% w/v): a) Reproducibility of rheological analyses, b) Hysteresis cycles at 1.0ºC/min (red) and 5.0ºC/min (green) temperature sweep rates, and c) Loss moduli at low temperatures range with fitted polynomic trend.

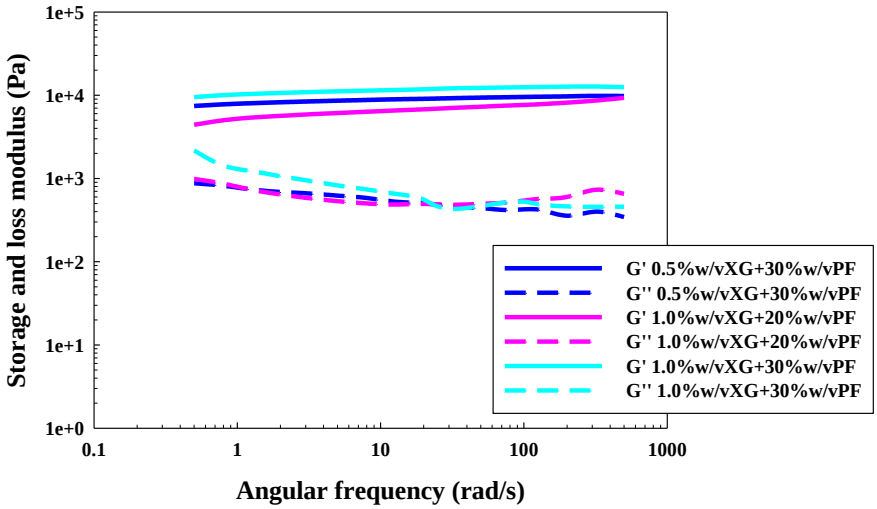

Figure S5. PF-127 and XG hydrogel frequency sweep oscillatory flow analysis.

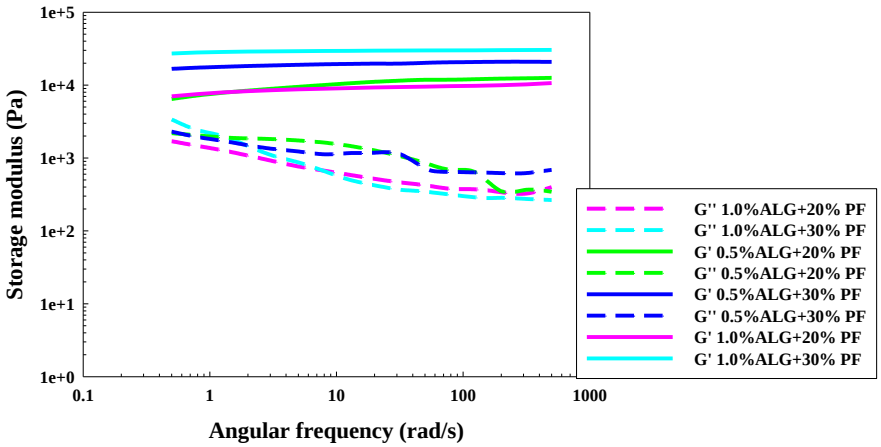

Figure S6. PF-127 and ALG hydrogel frequency sweep oscillatory flow analysis.

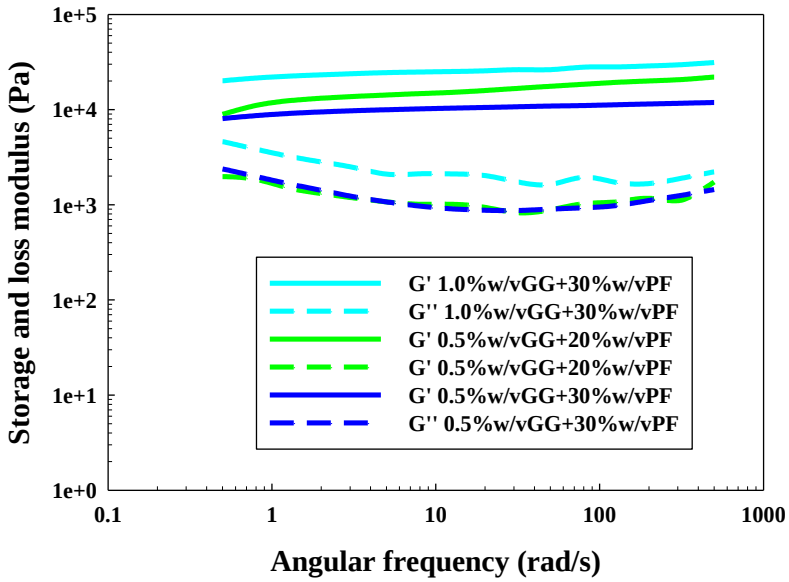

Figure S7. Frequency sweep oscillatory flow test for GG and PF-127 potential gel formulations.

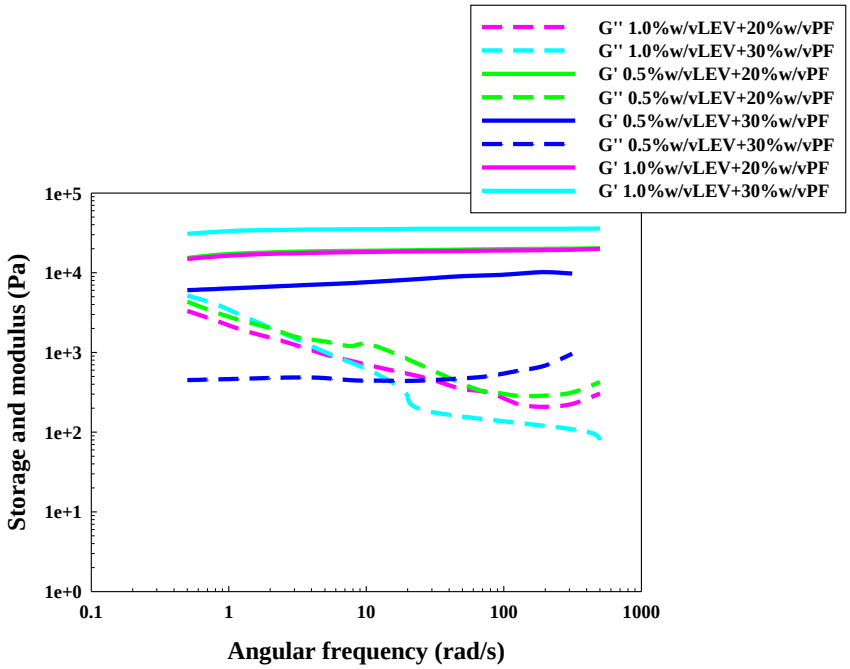

Figure S8. Frequency sweep oscillatory flow test for LEV and PF-127 potential gel formulations.

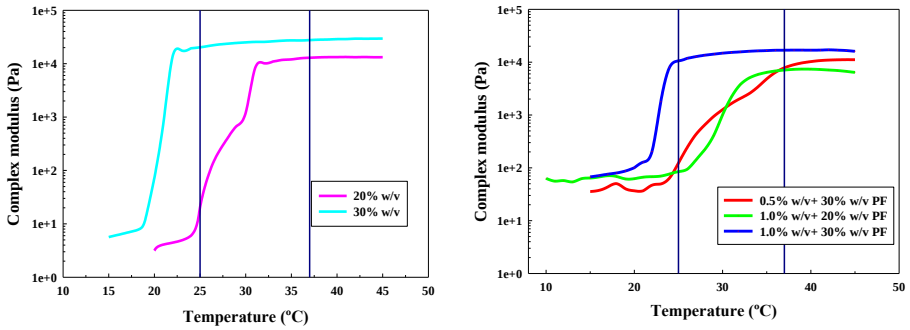

a) b)

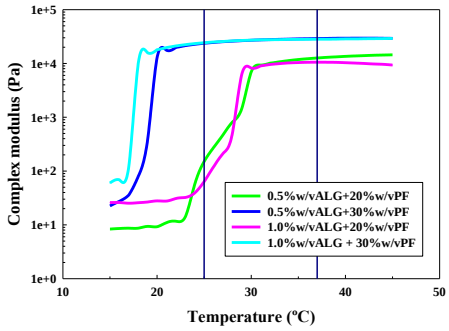

c)

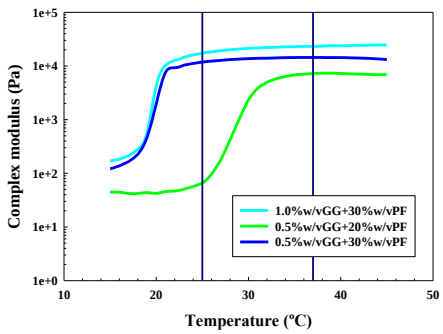

d)

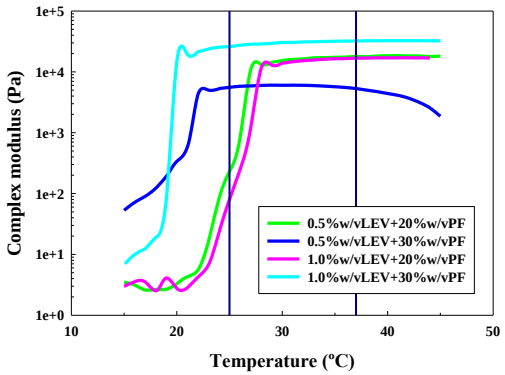

e)

Figure S9. Complex modulus of PF-127 20% w/v hydrogel: a) Without polysaccharides b) with XG, c) with ALG, d) with GG, and e) with LEV.

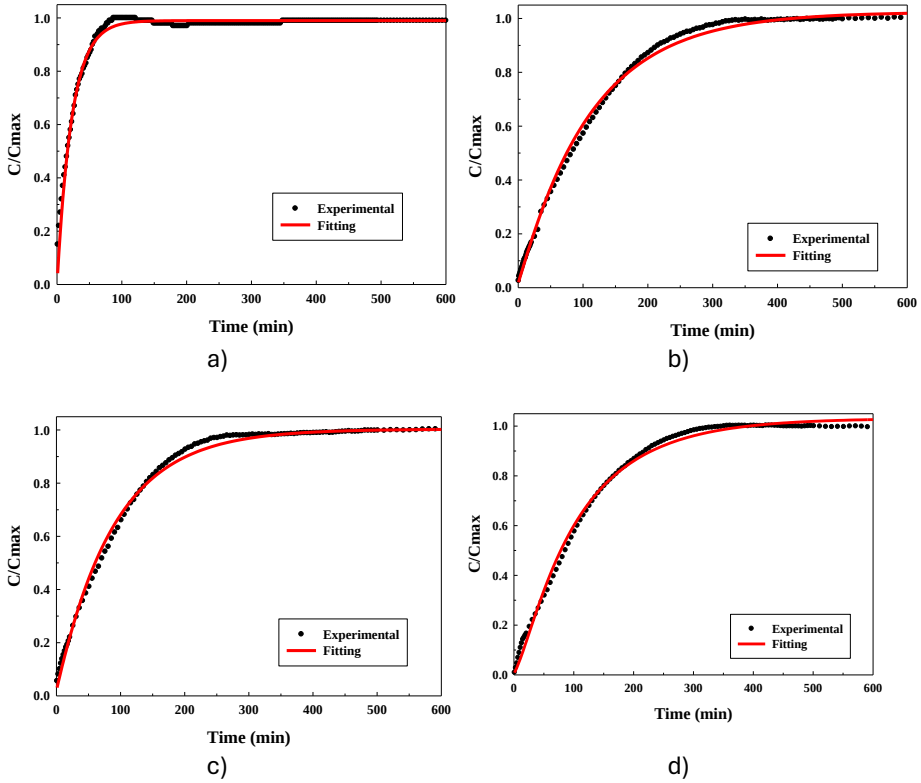

Figure S10. Graphical fittings to experimental drug release data for: a) Formulation 2, b) Formulation 11, c) Formulation 23, and d) Formulation 26.

6.6. Conclusions

Concluding, the successful design and optimization of thermo-responsive hydrogel formulations based on PF-127 and implemented polysaccharides was achieved and rheologically studied. Moreover, it was demonstrated that polysaccharides implementation was required for improving the poloxamer intrinsic mechanical limitations to achieve a better performance for the desired post-surgical application. Specifically, polysaccharides addition proved effectiveness modulating the network properties depending on the polysaccharides structural organization and compounds concentrations, and their subsequent effect on the micellar aggregation capacity. These modifications would ultimately affect the sol-gel transition in the gelation completion temperature (from 34ºC to 28ºC), elastic moduli values (from 8 to 11-18

kPa) or viscosity (from 4.1 to 6.1-7.1 Pa·s) determined by rheological analyses.

After obtaining the optimal formulations which exhibited the required viscoelastic properties for injection and strong gel at physiological temperature with a stable MAC, 5-FU drug release tests were performed. These confirmed that optimized hydrogels formulations delayed drug release over unmodified PF-127 formulation up to 4 times, in 8 hours. Moreover, the release kinetics obtained in mathematical model fitting were significantly influenced by polysaccharides implementation regarding degradation rate, established as a key parameter, or resistance against water permeation through the polymeric network.

Overall, the results obtained validated the development of a thermo-sensitive injectable hydrogel matrix based on PF-127 compatible with the post-resection breast tumour application. Therefore, this formulation establishes a robust base for subsequent integration of the pH-responsive nanocarrier developed in previous chapter, finally forming the proposed dual-responsive system. These conclusions can be seen summarized in Figure 6.3.

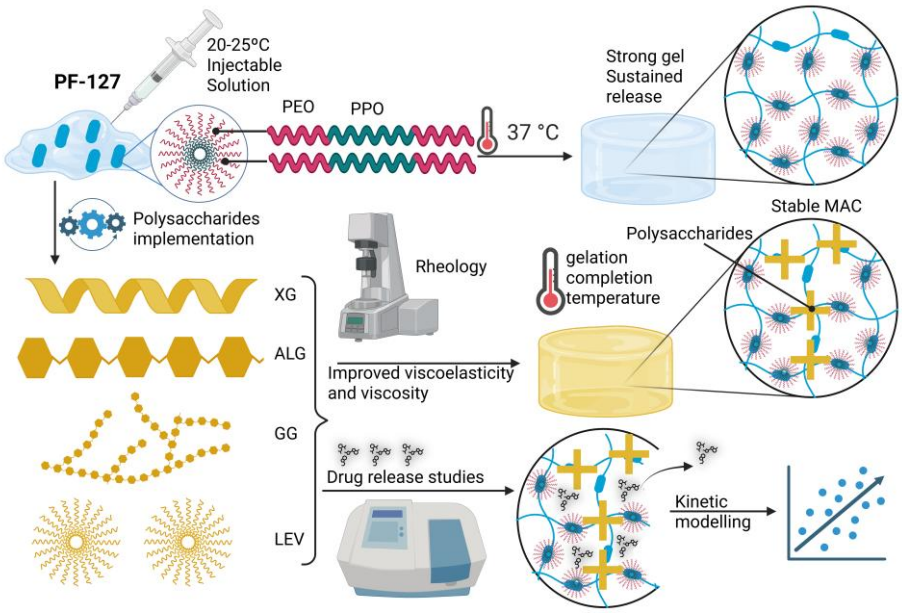

Figure 6.3. General conclusions on development of PF-127 thermo-sensitive hydrogels formulations for sustained 5-FU release.

6.7. References also cited

[1] Wahl AO, Rademaker A, Kiel KD, Jones EL, Marks LB, Croog V, et al. Multi-Institutional Review of Repeat Irradiation of Chest Wall and Breast for Recurrent Breast Cancer. Int J Radiat Oncol. 2008;70:477-84.

[2] Norouzi M, Nazari B, Miller DW. Injectable hydrogel-based drug delivery systems for local cancer therapy. Drug Discov Today. 2016;21:1835-49.

[3] Goel H, Gupta N, Santhiya D, Dey N, Bohidar HB, Bhattacharya A. Bioactivity Reinforced Surface Patch Bound Collagen-Pectin Hydrogel. Int J Biol Macromol. 2021;174:240–253.

[4] Gao Y, Vogus D, Zhao Z, He W, Krishnan V, Kim J et al. Injectable Hyaluronic Acid Hydrogels Encapsulating Drug Nanocrystals for Long-term Treatment of Inflammatory Arthritis. Bioeng Transl Med. 2021;7:e10245.

[5] Freeman I, Kedem A, Cohen S. The Effect of Sulfation of Alginate Hydrogels on the Specific Binding and Controlled Release of Heparin-Binding Proteins. Biomaterials. 2008;29:3260–3268

[6] Abdel-Bar HM, Abdel-Reheem AY, Osman R, Awad GAS, Mortada N. Defining cisplatin incorporation properties in thermosensitive injectable biodegradable hydrogel for sustained delivery and enhanced cytotoxicity. Int J Pharm. 2014;477:623-30.

[7] Stojkov G, Niyazov Z, Picchioni F, Bose RK. Relationship between structure and rheology of hydrogels for various applications. Gels. 2021;7:255.

[8] Zhang Y, Yu J, Ren K, Zuo J, Ding J, Chen, X. Thermosensitive Hydrogels as Scaffolds for Cartilage Tissue Engineering. Biomacromolecules. 2019;20:1478–1492.

[9] Madry H, Gao L, Rey-Rico A, Venkatesan JK, Müller-Brandt K, Cai X et al. Thermosensitive Hydrogel Based on PEO–PPO–PEO Poloxamers for a Controlled in Situ Release of Recombinant Adeno-associated Viral Vectors for Effective Gene. Adv Mater. 2019;32:1906508.

[10] Munim SA, Raza ZA. Poly(Lactic Acid) Based Hydrogels: Formation, Characteristics and Biomedical Applications. J Porous Mater. 2019;26:881–901.

[11] Quah SP, Smith AJ, Preston AN, Laughlin ST, Bhatia SR. Large-Area Alginate/PEO-PPO-PEO Hydrogels with Thermoreversible Rheology at Physiological Temperatures. Polymer. 2018;135:171–177.

[12] Zarrintaj P, Ramsey JD, Samadi A, Atoufi Z, Yazdi MK, Ganjali MR et al. Poloxamer: A tri-block copolymer for biomedical applications. Acta Biomater. 2020;110:37-67.

[13] Santana BM, Pieretti JC, Gomes RN, Cerchiaro G, Seabra AB. Cytotoxicity towards Breast Cancer Cells of Pluronic F-127/Hyaluronic Acid Hydrogel Containing Nitric Oxide Donor and Silica Nanoparticles Loaded with Cisplatin. Pharmaceutics. 2022;14:2837.

[14] Pouso MR, Melo BI, Goncalves JJ, Mendoca AG, Correia IJ, Melo-Diogo D. Development of dual-crosslinked Pluronic F127/Chitosan injectable hydrogels incorporating graphene nanosystems for breast cancer photothermal therapy and antibacterial applications. Eur J Pharm Biopharm. 2024;203:114476.

[15] Goncalves JJ, Melo BI, Pouso MR, Correia IJ, Melo-Diogo D. Dual-crosslinked injectable in situ forming Alginate/$CaCl_2$/Pluronic F127/α-Cyclodextrin hydrogels incorporating Doxorubicin and graphene-based nanomaterials for cancer chemo-photothermal therapy. J Drug Deliv Sci Techol. 2025;114:107520.

[16] Zhao D, Song H, Zhou X, Chen Y, Liu Q, Gao X et al.Novel facile thermosensitive hydrogel as sustained and controllable gene release vehicle for breast cancer treatment. Eur JPharm Sci. 2019;134:145-152.

[17] Nie S, Hsiao W, Pan W, Yang Z. Thermoreversible Pluronic F127-based hydrogel containing liposomes for the controlled delivery of Paclitaxel: In vitro drug release, cell cytotoxicity and uptake studies. Int J Nanomed. 2011;6:151-166.

[18] Nguyen NT, Nguyen VT, Vu TT, Nguyen TV, Nguyen TTT, Huynh PD. Efficient and controllable co-delivery of paclitaxel and curcumin from fucoidan-pluronic F127 nanogels for synergistic breast cancer treatment. Macromol Res. 2024;32:427-442.

[19] Gao X, Caruso BR, Li W. Advanced Hydrogels in Breast Cancer Therapy. Gels. 2024;10:479.

6.8. List of abbreviations

5-FU — 5-Fluorouracyl
b — Block
CMC — Critical Micellar Concentration
CS — Chitosan
Cur — Curcumin
DDS — Drug Delivery System
DOPA — 3,4-Dihydroxy-L-Phenylalanine
DOX — Doxorubicin
ECM — Extracelullar Matrix
Fud — Fucoidan
gct — Gellation completion temperature
GSNO — S-Nitrosoglutathione
HA — Hyaluronic Acid
LCST — Low Critical Solution Temperature
MAC — Micellar Aggregation Capacity
MCF-7 — Michigan Cancer Foundation Breast Cancer Cell Line
MDA-MB-231— MD Anderson Mammary Breass Cancer Cell Line
NIR — Near Infrared
PDMAEMA — Poly(2-(Dimethylamino)Ethyl Methacrylate)
PEG — Poly(Ethylene Glycol)
PEO — Poly(Ethylene Oxide)
PF-127 — Pluronic in Flakes 12,000 g/mol and PPO/PEO ratio 0.7.

PHB —Poly(3-Hydroxybutyrate)
PLA — Poly(Lactic Acid)
PLGA — Poly(Lactic-co-Glycolic Acid)
PNIPAAM — Poly(N-Isopropylacrylamide)
PPO — Poly(Propylene Oxide)
PTX — Paclitaxel
rGO — Reduced Graphene Oxide
Sur-ASON — Survivin-Antisene Oligo Nucleotide

7. Developing a dual-responsive drug delivery system based on injectable thermo-sensitive PF-127 hydrogel incorporating pH-responsive liposomes

7.1. Introduction

As it has been discussed throughout this thesis, the main limitations of current approaches in post-surgical breast cancer therapies are the difficulty of accumulating high drug doses in tumour site and the presence of systemic toxicity [1]. Previous chapter 6 described the development of an alternative platform for improved thermo-sensitive injectable local therapy aimed at overcoming these limitations by adapting to the cavity after tumour resection, and providing sustained release [2]. However, the drug reservoir synthesized for injectability and drug sustained release lacks a tumour targeting strategy. Regarding this, previous chapter 5 describes the development of the complementary drug delivery system based on coated liposomes which present pH-responsiveness enabling targeting of the acidic tumour environment [3].

Based on the conclusions presented in both chapters, the current chapter explores the integration of both systems, conforming a dual-responsive drug delivery platform [4]. This hybrid formulation combines the local retention and controlled release of the thermo-responsive hydrogel network with the pH-sensitive drug delivery of coated liposomes towards cancer cells, assembling a more effective and safer strategy for breast cancer recurrence prevention.

Therefore, this chapter describes the synthesis, physicochemical and viscoelastic characterization, and validation of the final optimal dual-response platform. Concretely, interactions established between the liposomes and the hydrogel matrix will be evaluated, determining their effect on the thermo-response, injectability, and rheological properties. Also, possible changes in the pH-responsiveness will be assessed due to liposomes incorporation into the hydrogel matrix. Finally, the biological performance of the optimized dual-response formulation will be evaluated using *in vitro* breast cancer models, including 2D cell cultures compared with healthy stromal fibroblasts, and 3D tumour spheroids, for an approximate prediction of its therapeutic potential in in vivo conditions.

7.2. Synthesis of liposomal hydrogels

As stated previously, liposomes may be synthesized following different methodologies, and hydrogels can be formed via physical or chemical interaction. However, their combination can be described in three different arrangements: Incorporation of liposomes into the hydrogel network, hydrogels generated by liposomes gelation, or hydrogel embedding in liposomes inner core, as illustrated in Figure 7.1 [5].

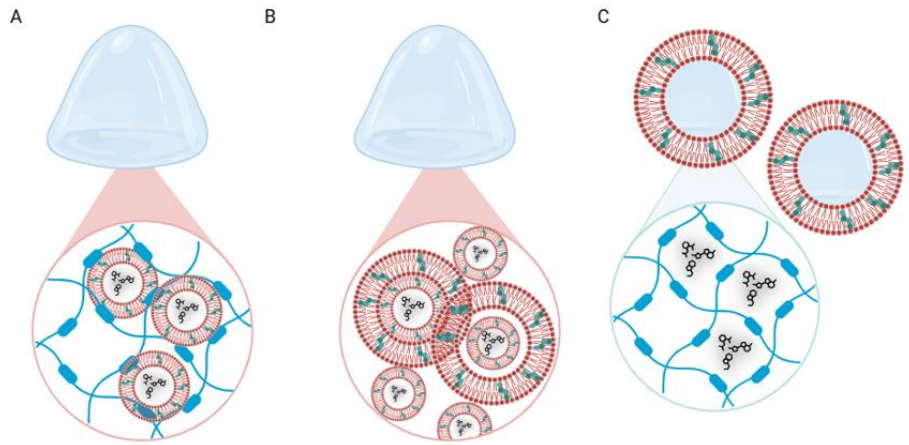

Figure 7.1. Arrangements of liposomal hydrogels: a) Liposomes incorporated into hydrogel matrix, b) Hydrogel formation due to liposomes gelation, and c) Lipid coated micro/nano hydrogels.

Although there are numerous studies for each liposomal hydrogel arrangement in literature, the majority of the reported systems follow the first procedure, such as the one presented in this work, due to better mechanical properties of fibrous network organization, better local retention, and easier synthesis procedures which do not require unilamellar vesicles mandatorily. Liposomes and hydrogels may function as two independent components but interactions among them exist, whether they are hydrogen bonding, electrostatic interactions, Van der Waals forces, covalent bonding, or pore entrapment [5]. These interactions constitute the base of hybrid systems which combine the benefits of both components and compensate the limitations they present separately. This is briefly summarized in Table 7.1.

Table 7.1. Benefits and limitations of hybrid and separate liposomes and hydrogels systems

System	Benefits	Limitations	Ref
Liposomes	Compatibility with hydrophilic and hydrophobic drugs Penetration in mucoses, etc. Easily stimuli-responsive	Lack of stability against physiological conditions Uncontrolled release Poor localized retention	6
Hydrogels	High stability Adhesion Sustained drug release	Lack of compatibility with hydrophobic drugs Weak penetration abilities	7
Liposomal Hydrogels	Enhanced liposomes stability Better compatibility with drugs Prolonged drug releases with multiple resistances Simultaneous adhesion and penetration Improved mechanical properties		8

As mentioned in Table 7.1, the liposomes lack stability against physiological conditions causing burst releases, and more importantly, cannot be retained after local administration at tumour site. On the other hand, hydrogels present high stability and sustained drug release, but they cannot provide strong internalization or targeting at micro or nano-sized scale.

Therefore, the main interest of these hybrid systems is the combination of both platforms for the delivery of different therapeutic agents since their combined release can be locally retained and sustained at desired sites, as illustrated in Figure 7.2. [8]. Moreover, as stated in the introduction, the design of these liposomal hydrogels for stimuli-response strategies enhances their performance and tumour targeting.

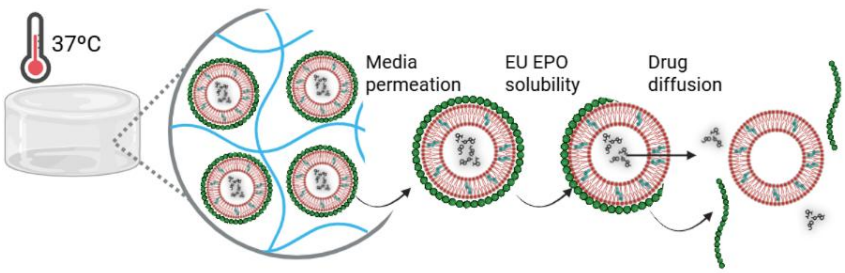

Figure 7.2. Proposed joint drug release mechanism scheme based on sustained release from strong gel (drug reservoir at 37ºC) with incorporated pH-response in acidic media

7.3. Stimuli-responsive liposomal hydrogels for breast cancer therapy

Stimuli-responsive hydrogels provide a more successful drug delivery and therapeutic efficiency. In this context, thermo-responsive injectability enables the local administration and *in situ* gelation for an easier accumulation at desired site, usually involving less side effects and systemic toxicity. This thermo-response and injectability can be evaluated through rheological assays, determining how the hydrogel changes as it gels with temperature increase. The rheological tests used for evaluating hydrogels gelation are explained in previous chapter 6. Thus, strong solid-like gels are formed within the body at physiological temperature, and then are degraded, releasing the loaded liposomes [9]. This can happen with any liposomal hydrogel arrangement, for instance, Mao et al. used thiolated chitosan-coated liposomes which gelled at 37ºC to deliver curcumin to breast cancer cells [10].

However, injectable hydrogels only present one stimulus response which does not target directly cancer cells, compromising therapeutic efficiency and exposing healthy tissues to cytotoxicity. In order to solve this, dual-response hydrogels have also been explored for breast anticancer therapies [4]. These systems are based on a thermo-responsive injectable hydrogel network and another stimulus response, like acidic pH. As stated in the introduction, many dual-response hydrogels present thermo- and pH-sensitive behaviour. Nevertheless, both responses rely on the hydrogel matrix only, thereby limiting the selectivity of drug delivery towards tumour environment. Despite its targeting capacity, hydrogels exhibit weak penetration abilities, which restricts selective intracellular delivery. When liposomes are incorporated in these dual-response hydrogels, the drug delivery and penetration improves [5], but the targeting strategy associated to the hydrogel matrix remains inefficient. This can be seen in reported studies like Fathi et al [11], Mohan et al [12], Ahmadi et al [13], for dual-responsive hydrogel matrices, or Li et al [14] for liposomal incorporated dual thermo- and pH-responsive hydrogels.

Therefore, the proposed strategy is to design the liposomes to respond to pH so that the local drug release is sustained, but also its delivery is inherently tumour-targeting using a pH-responsive carrier, enhancing its performance. For this mechanism, only Chen et al [15] developed a cleavable liposomal system incorporated into an injectable hydrogel intended for vaginal delivery. However, thermal gelation for this system was not studied through rheology, determining the interactions between the liposomes and hydrogel and how they may affect injectability and gelation. Moreover, this system was underdeveloped by only proving pH-response in drug release tests and cellular viability with a human embryonic kidney derived cell line for unloaded formulations of the hydrogel. Therefore, a more thorough study of this dual-responsive strategy with: Rheological analyses to optimise formulation in terms of injectability based on the liposomes interactions with the network, together with pH-response validation through kinetic modelling and cellular assays, and evaluation of the dual-response in tumour spheroids, are required for the development of a potential hybrid system for breast cancer recurrence prevention.

7.4. Article related to this chapter

Considering the current state of art, the manuscript “Developing an injectable thermo-responsive PF-127 hydrogel incorporating pH-responsive Eudragit®-coated liposomes for dual-stimuli controlled drug delivery in post-surgical breast cancer therapy” is presented as the results and discussions obtained within the framework of the final experimental phase. The aim of this study was to develop the final dual-responsive liposomal hydrogel in which thermo-sensitivity was provided by an injectable hydrogel matrix enabling local administration and sustained release, while pH-responsiveness was conferred by a coated liposomal platform with tumour-targeting capacity for selective drug delivery. This system was ultimately successfully synthesized and rheologically evaluated to confirm suitable injectability for administration within the surgical bed.

Moreover, the pH-response of the coated liposomal system was confirmed to remain after hydrogel incorporation, preventing drug

release at physiological pH values whilst promoting it at acidic intracellular compartment pH range. However, the hydrogel effect could be clearly seen, providing sustained release, analysed by one and two-stages model that confirmed the delay of loaded liposomes release.

Furthermore, cell assays validated the pH-response by increased breast cancer cell mortality due to acidic pH-targeting of the coated liposomes, whilst preserving minimal release in stromal healthy cells. Although the dual-responsive hydrogel was not tested on animal models, in vivo conditions of cancer cells were achieved by obtaining breast tumour spheroids and exposing them to the treatment, confirming its enhanced performance.

Developing an injectable thermo-responsive PF-127 hydrogel incorporating pH-responsive Eudragit® -coated liposomes for dual-stimuli controlled drug delivery in post-surgical breast cancer therapy

Marcos Blanco-López[1], Inma de Dios-Pérez[1,3], Antonio Tabernero[1,2,], Patricia Pérez-Esteban[3], Eva Martín del Valle[1,2].*

1) *Department of Chemical Engineering. University of Salamanca. Plaza Los Caídos s/n, 37008 Salamanca (Spain).*
2) *Institute for Biomedical Research in Salamanca (IBSAL), Paseo de San Vicente 87, 37007, Salamanca (Spain).*
3) *Healthcare Technologies Institute (HTI), University of Birmingham, B15 2TT, Birmingham (UK).*

**** Corresponding author at: Antonio Tabernero (antaber@usal.es)***

Abstract

Currently, breast cancer treatments look for better targeting of tumour cells and less systemic toxicity. Therefore, liposomes were designed to respond to acidic tumour microenvironment, providing stable SUV system with a pH-responsive polymer, Eudragit® EPO (110 nm, PDI<0.15). However, the development of a dual-responsive hydrogel exhibiting thermo-sensitive injectability for local administration together with a sustained release of 5-FU loaded pH-responsive liposomes represents the innovative approach proposed in this work.

This system combined the benefits of injectability for local administration as a drug reservoir with pH-responsive drug release triggered in the acidic tumour microenvironment. Rheology assays confirmed the suitable injectability for operation room temperature, decreasing the completion gelation temperature to 28ºC and providing a higher elastic gel network (G' value of 15 kPa) at physiological temperature when liposomes were incorporated.

Both the hydrogel effect and the pH-response behaviour of the coated liposomes were evaluated through drug release studies followed by fitting to one and two-stage kinetic models. Drug release was prevented up to 50% at physiological pH values over 2 days, enhancing the sustained 5FU delivery. Moreover, the determined parameters in Korsmeyer Peppas, Peppas Sahlin and Weibull models confirmed the delayed release associated with the hydrogel matrix and the coating layer solubility. Importantly, pH-responsive behaviour of hydrogels targeted BT-474 cells over HS-5 in the dual response formulation, providing sustained drug release, resulting in delayed cell death. Furthermore, breast tumour spheroids confirmed the efficiency of the dual-response hydrogel in 3D cell models that were disaggregated by it in a 3-day period, presenting promising results in in vivo conditions.

Keywords: Drug delivery, liposomes, hydrogels, pH-response, thermosensitivity, rheology, model fitting, in vitro assays.

1. Introduction

Cancer remains a leading cause of mortality worldwide and represents a major biomedical challenge due to its multifactorial nature, molecular heterogeneity and adaptive resistance to therapy [1-4]. Breast cancer is the most frequently diagnosed malignancy in women and continues to be a primary cause of cancer-related death despite advances in early detection, conservative surgery and adjuvant treatments [5, 6]. Conventional management relies on tumour resection combined with systemic chemotherapy or radiotherapy to eradicate tumour recurrences [7, 8]. However, these approaches suffer insufficient prevention of recurrence, and off-target toxicity [9, 10]. Consequently, targeting strategies are being actively explored [11].

One of the most used strategies to actively target cancer cells and increase therapeutic efficiency focuses on the physio-pathological pH gradient between healthy tissues at 7.4 and cancer cells which alter their metabolism overproducing lactate which acidifies their extracellular environment (down to 6.5) as well as intracellular compartments (from 6.0 to 4.5 in endosomes and lysosomes) [12]. This strategy is carried out by nanocarriers designed to respond to this stimulus. Out of all reported nanocarriers lipid vesicles outstand due to their structural resemblance with cellular membranes, particularly liposomes composed of a lipid bilayer [13]. They are capable of encapsulating hydrophobic drugs in their bilayer whilst hydrophilic drugs can be retained in their aqueous core, such as 5-fluorouracyl (5FU), an antineoplastic antimetabolite widely used for many types of cancer, including breast [1, 4].

In order to induce pH-response, liposomes can be coated with polymers that present this characteristic. Eudragit® is a commercial brand of methacrylate pH-responsive polymers used for sustained drug releases, approved by FDA [14]. More concretely, Eudragit® EPO (EU EPO) formulation presents cationic functional groups [15], which can establish electrostatic interactions with liposomes with negative surface charge [16]. This compound is soluble in pH < 5.0 and its molecular weight (47,000 g/mol) shows individual chains when dissolved in acidic aqueous media [17]. Only Hasanovic et al. have previously used this for

coated liposomes, encapsulating acyclovir and minoxidil for better skin permeation, showing pH-responsive drug release [18]. Therefore, this coating was further developed in previous studies for pH-responsive release of 5FU with kinetic modelling and cell viability [19]. However, the use of free liposomes usually involves an initial burst release. Consequently, different authors promoted the implementation of these vesicles into macroscopic hydrogels matrices, sustaining drug release [20, 21]. On the other hand, hydrogels can also be used for local administration, which enhances the targeting of tumour site by directly accumulating higher drug concentrations at the site, while reducing systemic toxicity [22-28].

Hydrogels can be locally administered via intratumoural or post-resection injection into the tumour bed, enabling enhanced payload retention, localized drug delivery, better pharmacokinetic parameters, and avoidance of first-pass metabolism [28-30]. Therefore, injectable hydrogels are presented as a promising platform for minimally invasive administration directly in the surgical bed after tumour resection, where they can act as local drug reservoir and adapt to the irregular geometry of breast tissue [31]. Furthermore, injectable hydrogels present thermo-responsive sol-gel behaviour [32, 33], enabling the development of dual-responsive drug delivery systems upon incorporation of pH-sensitive liposomes. Thereby enhancing therapeutic efficiency.

Thermo-responsive systems remain liquid at room temperature, facilitating injection, and gel rapidly at physiological temperature, allowing retention at the administration site [34, 35]. One of the most common structures found in injectable hydrogels are triblock copolymers, consisting of an ABA structure where A represents hydrophilic ends and B a hydrophobic chain in between [36]. More specifically, poloxamers made of polyethylene oxide (PEO) as A and polypropylene oxide (PPO) as B are widely used due to biocompatibility, FDA approval and range of thermo-response[37].

PF-127, or poloxamer 407, is a Pluronic (P) in flakes form (F), with a molecular weight of 12,600 g/mol (12) and a PPO/PEO ratio of 0.7 (7) [38]. The gelation transition of this poloxamer falls between the 25-37ºC

range, being suitable for *in situ* forming at physiological conditions [39]. Firstly, unimer chains form micelles at low critical micellar concentration (cmc) and temperature (cmt) by PPO dehydration [40]. Micelle phase is reported as an injectable liquid phase (sol state) [41]. Reorganization of micelles into a strong gel state by reaching the completion gelation temperature (cgt) [42] is defined by the micellar aggregation capacity [38, 39]. Although PF-127 based hydrogels are perfectly suitable for injectable applications, they often dissolve quickly in physiological fluids, decreasing their stability and mechanical strength [43, 44]. Previous works have increased its resistance against degradation by interaction with encapsulated drugs [42] or different types of polysaccharides as referenced in Bhowmick et al. with xanthan and guar gum [45], Brambilla et al. with xanthan gum and carrageenan [46], de Dios-Pérez et al. with gellan gum [47], and Blanco-López et al. [48] with polysaccharides presenting different structural organizations.

In this context, the incorporation of nanoparticles like liposomes can also enhance hydrogel properties like polysaccharides do [49]. In contrast, thermo and pH dual-responsive systems have also been reported. Li et al. reported thermo and pH-responsive injectable chitosan hydrogels loaded with DOX and CUR for sustained release in solid tumours treatment. Co-encapsulation of these two drugs in a rapid-*in situ*-gelling at 37ºC network demonstrated long sustained release and good cytotoxicity in MCF-7 cell line [50]. Although this formulation presented a successful dual response, these were only dependant on the hydrogel, lacking an additional platform to specifically deliver the drugs into the cancer cells. Accordingly, only Chen et al. developed a dual thermo and pH-sensitive liposomal injectable hydrogel based on novel cleavable mPEG-Hz-CHEMS and a mixture of poloxamers for vaginal delivery. Drug release proved a broad pH-response due to cleavable presence, and dual-response gel showed low cytotoxicity towards HEK293 cell line, presenting a potential platform for vaginal delivery of hydrophobic drugs, even though thermo-response was not deeply analysed or optimized regarding injection [51].

Despite these reported advances, an efficient dual-responsive hybrid injectable hydrogel system for breast cancer treatment remains

unavailable. Reported dual-responsive hydrogels generally rely on both stimuli responses governed solely by their network, limiting the optimization of each response separately. In contrast, separating thermo- and pH-responsive functionalities into different components could enable a more efficient and sustained drug delivery mechanism based on independently tuneable release barriers. Moreover, studies rarely report how the addition of these nanoparticles improve injectability and the rheological properties of the hydrogel. In this context, this work proposes the development of an alternative local drug delivery system based on pH sensitive coated liposomes loaded with 5FU incorporated into a thermo-sensitive PF-127 hydrogel designed for injection after tumour resection. This system presents a simple and non-toxic synthesis of highly biocompatible compounds which enables the optimization of two stimuli-responses separately for a better joint response of 5-FU delivery targeting cancer cells, tested not only in monolayer but also spheroid cellular systems.

2. Materials and methods

2.1. Materials

Poloxamer PF-127, Egg L-α-phosphatidylcholine (PC, MW 758 g/mol) with a 60% of yield determined by TLC, cholesterol (CHOL, MW 386 g/mol), drug 5-fluoroacyl (5FU, MW 130 g/mol) and Thiazolyl Tetrazolium Bromide (MTT) were purchased on Sigma Aldrich. Chloroform (99,5% w/v) was provided by PanReacc AppliChem ITW Reagents. pH responsive Eudragit® EPO (EU EPO, MW: 47,000 g/mol) was kindly donated by Evonik OnCare. Dulbecco's Modified Eage Medium (DMEM), Foetal Bovine Serum (FBS), penicillin-streptomycin (P-S), trypsin 0.05% EDTA, and Phosphate Buffer Saline (PBS) were purchased from Fisher Scientific.

2.2. Dual response system synthesis

2.2.1. Conventional liposomes

Conventional liposomes were synthesized following thin film hydration methodology [52]. Briefly, reagents (PC, CHOL) were weighed

at 70:30 molar ratio (MR) and dissolved in chloroform. Afterwards, chloroform was completely removed with rotary evaporator at 55ºC, and the thin lipid film was re-suspended in PBS, sonicated and extruded (Avanti Polar Lipids mini-extruder, Alabama, U.S.A.) through a 0.1 μm filter (Cytivia Nuclepore, Fisher Scientific) 13 times at 65ºC. This system was stable for more than 15 days with average size of 85 nm and PDI<0.1 according to our previous work [19]. Liposomes synthesis process is illustrated in Figure 1a.

2.2.2. Coating with EU EPO

The coating methodology can be found elsewhere [18]. Firstly, liposomes were re-suspended in acidic aqueous buffered solution (PBS at 4.5) after chloroform evaporation due to EU EPO solubility. Their size or stability did not present a significant difference compared to conventional liposomes, as statistical analysis pointed [19].

EU EPO was dissolved in an acidic sodium acetate buffer (pH 4.5) at 0.5% w/v. The conventional liposomes (pH 4.5) were poured over in a 1:1 volume ratio, and stirred at 1,000 rpm for 1h at room temperature. This process provided coated liposomes of 115 nm and PDI<0.2 stable for 15 days as well [19]. Coating of liposomes method is illustrated in Figure 1 b below.

2.2.3. Implementing liposomes in PF-127 hydrogel

Conventional and coated liposomes solutions were mixed and stirred with PF-127 flakes overnight at 4ºC to synthesize the hydrogel, applying the cold method [53, 54]. The final concentration of PF-127 was set at 20% w/v in order to enable injectability, since the cgt determined a liquid-like solution at room temperature and a strong gel solid-like behaviour at physiological conditions, after previous results [48]. Hydrogels synthesis process is illustrated in Figure 1 c below.

2.2.4. Loading liposomes with 5FU

The liposomes embedded in the hydrogel matrix were loaded with 5FU. 5FU was dissolved in aqueous solution up to a final concentration

of 50 ppm, according to its inhibitory concentration 50 (IC_{50}) [55]. This loaded aqueous phase is the one used to resuspend the lipid film after rotary evaporation, therefore making it a passive loading method. Loaded liposomes go through the extrusion process as well, in order to obtain the same unimodal dispersion, and then coated and embedded in the hydrogel as previously explained [19]. Loading process is illustrated in Figure 1 a and b.

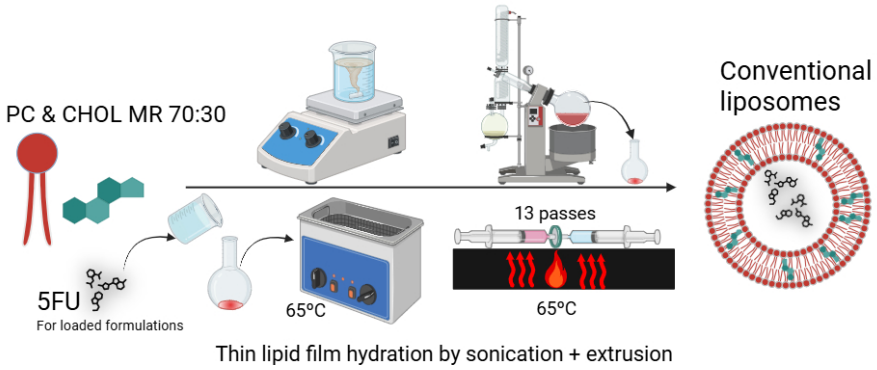

a)

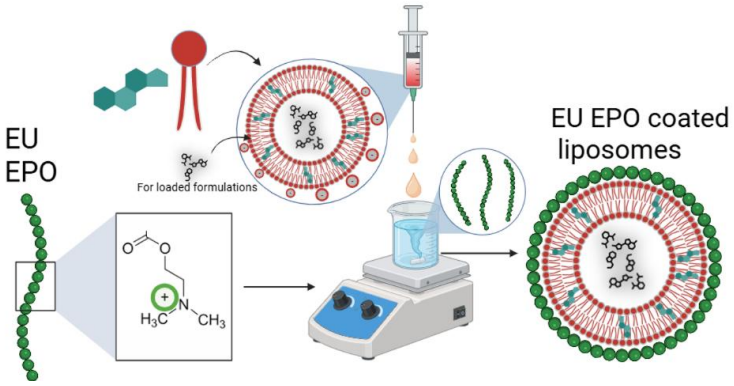

b)

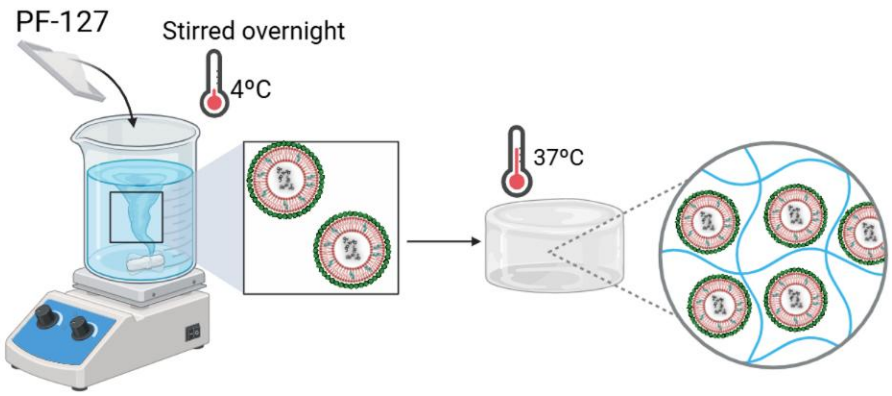

c)

Figure 1: Methods of dual-response system synthesis: a) Synthesis of (loaded) conventional liposomes via thin film hydration and extrusion, b) Coating process of (loaded) EU EPO coated liposomes, and c) Hydrogel formation via cold method with (loaded) conventional or EU EPO coated liposomes embedded.

2.3. Characterization of dual response hydrogel

2.3.1. Rheology

Rheology was performed to evaluate the viscoelastic properties of the thermo-sensitive hydrogels (TA rheometer AR 15000ex, Madrid, Spain). A flat geometry was used with a 4 cm diameter aluminium plate and a 1mm gap, as referenced [56, 57]. Samples of 1.5 mL of the hydrogel at room temperature (sol state) were loaded on the peltier and geometry was brought to the set gap. Moreover, a solvent trap was used in order to control water evaporation.

Both temperature and frequency sweep tests (oscillatory analysis) were performed on hydrogels. Storage or elastic (G') and loss or viscous (G'') moduli were measured, determining the cgt and elasticity of gel systems. It should be noted that gct is defined as the first temperature point where the system presents a gel state by ending exponential growth of G' after transition [42].

Temperature sweep tests used a 5-45ºC range at 1ºC/min rate as described [58, 59], which defined well enough poloxamer nature taking into account its hysteresis cycle. Frequency (10 Hz) and strain

percentage (0.2%) were fixed to assure an experimental viscoelastic region of the material. Frequency sweep tests were at fixed temperature (37ºC) to observe the gel behaviour at physiological conditions, from 0.5 to 500 rad/s of frequency range.

In contrast, temperature ramp static flow maintained the same temperature range with static flow conditions. This time the viscosity was measured in function of the temperature. The fixed variable was a shear rate of 50 s^{-1} to observe the micellar aggregation capacity [56].

2.3.2. Cryo-SEM

Cryogenic Scanning Electron Microscopy (SEM-FEI FIB Quanta 3D, Brno, Czech Republic) was used in order to characterize the hydrogels with conventional liposomes and EU EPO coated liposomes. 3µL of the samples were placed in the grid at room temperature (sol state). This grid was carefully placed in liquid nitrogen to freeze the sample and conserve its native structure. Afterwards it was taken to the cryo-chamber (Quorum PP3010 Prepdek, California, USA) preparation system. In this chamber the samples were cut (face fracture) with a blade and afterwards were sublimated and gold sputtered. Sublimation in order to remove the surface ice layer was performed at -100°C during 5 minutes and sputter used Argon gas to coat the samples metallically. Afterwards the grid was transferred to the microscope chamber where temperature was kept at -140°C and the distance to the lens was 5 mm with a voltage of 5kV.

2.4. Drug release

For drug release experiments 5mL of the loaded hydrogels were measured in Petri dishes at room temperature and were taken to incubation at 37ºC (Nuve Incubator EN025, Ankara, Turkey) for 30 min.

Once in gel state, the 5mL hydrogel was introduced in a supported 3D printed structure shown in Figure 2 in a 100 mL media beaker with buffered solutions at different pH at 37ºC [48].

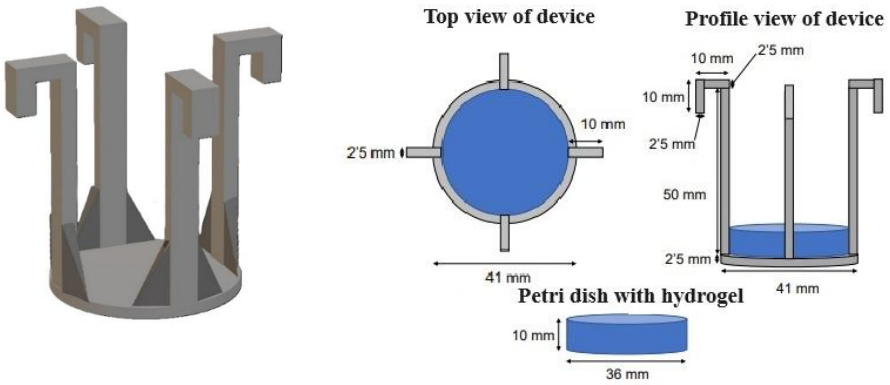

a) b)

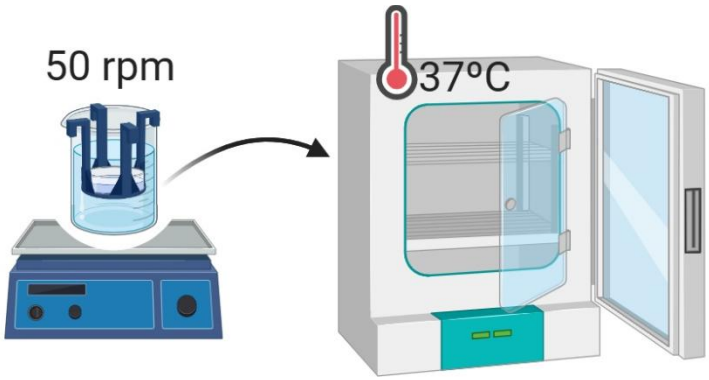

c)

Figure 2: Gel support for drug release as: a) Brief scheme, b) Measurements of the device for a 100 mL beaker, and c) Drug release experiment setup.

As shown in Figure 2 c, beakers were always set at 37ºC and orbital shaking (50 rpm) conditions to assure laminar flow with homogenized media (Biosan ES-20, Riga, Latvia). Aliquots of 0.5mL were taken from the media at set times: 0, 0.5, 1, 2, 4, 8, 12, 24, 36, and 48h and replaced with fresh buffered solution. 5FU concentration in aliquots was measured via spectrophotometry (Shimadzu UV-1800, Buenos Aires, Argentina) at λ of 260 nm (peak detection of 5FU). The concentration of 5FU released at each time (C) was divided by the maximum concentration of 5FU released in each system (Cmax).

It is important to note that drug release tests were always replicated with samples with and without 5FU in order to determine exactly the absorbance caused by the drug release exclusively [19].

2.5. Theoretical models fitting

Experimental data on liposomes and EU EPO coated liposomes hydrogels drug release was fitted to theoretical models. The models used were zero and first order kinetics, Higuchi and Korsmeyer-Peppas. For the latter two, only experimental points with less than 60% of drug released were fitted, following references [60].

Equations for the selected models are as follow:

Zero order kinetics: $\frac{C}{C_{max}} = k_0 \cdot t$ (Eq. 1)

Being $\frac{C}{C_{max}}$ the fraction of drug released at a certain time, k_0 the rate constant of this model (h^{-1}), and t the time (h).

First order kinetics: $\frac{C}{C_{max}} = 1 - e^{-k_1 \cdot t}$ (Eq. 2)

Being k_1 the rate constant of this model (h^{-1}).

Higuchi model: $\frac{C}{C_{max}} = k_H \cdot \sqrt{t}$ (Eq. 3)

Being k_H the rate constant of this model ($h^{-0.5}$)

Korsmeyer-Peppas model: $\frac{C}{C_{max}} = k_{KP} \cdot t^n$ (Eq. 4)

Being k_{KP} the constant rate for this model (h^{-n}), and n the exponent that associates the release with the type of transport of drug. Briefly, for $n \approx 0.43$ the transport is pure Fickian diffusion, between 0.43 and 0.85 it is abnormal transport, and for over 0.85 it is considered a transport II case [60].

For wider range fitting in these systems, two-stage models can also be used. In this work Peppas-Sahlin [61] and complementary Weibull [62] models were used, which equations are the ones below:

Pepas-Sahlin model: $\frac{C}{C_{max}} = k_1 \cdot t^m + k_2 \cdot t^{2m}$ (Eq. 5)

Being k_1 the kinetic constant due to diffusion (h^{-m}), k_2 the kinetic constant due to relaxation (h^{-m}), and m the exponent that describes system geometry and the temporal form of the transport. Briefly, for $m \approx 0.4 - 0.5$ spherical systems (such as liposomes) present a Fickian diffusion dominance [61].

Weibull model: $\frac{C}{C_{max}} = 1 - e^{\left[-\left(\frac{t}{\alpha}\right)^{\beta}\right]}$ (Eq. 6)

Being α the parameter of temporal scale (h), and β the shape parameter of the release curve.

2.6. Validation of liposomes and coated liposomes by *In Vitro* Tests.

In order to validate the effects of dual response system, cell viability assays were performed on two different cell lines: Fibroblast normal HS5 (ATCC® CRL11882™), and breast carcinoma BT-474 (ATCC® HTB20™). The cell lines were obtained from the American Tissue Collection (Manassas, VA, USA).

Culture media DMEM was supplemented with 10% FBS and 1% P-S (DMEM+) in order to culture the cells. They were maintained at 37ºC in a 5% CO_2 atmosphere. At 80-90% confluence, the cells were subcultured using trypsin.

In order to measure cell viability, MTT assays were performed in cells in exponential growth. Cells were plated by triplicate in flat-bottomed 24-well-plates (Costar) at an initial concentration of 16,000 cells per well. Plates were incubated for 24, 48, and 72 hours at 37ºC and 5% CO_2 in a humidified incubator. Cells were subjected to the different treatments involving hydrogels in their gel form immersed in DMEM+ in

order to replicate phenomenologically the physiological conditions of the application, apart from medium and cell control.

2.6.1. Viability assays on cell lines

MTT assays work as a colorimetric test to determine cytotoxicity of treatments on cell lines [63]. Briefly, thiazolyl blue tetrazolium bromide (MTT reagent) is dissolved in PBS up to a concentration of 5 mg/mL, and later added to the wells in a 10% volume measurement. MTT reacts with living cells producing violet formazan crystals via mitochondrial metabolism during incubation for the first hour after addition. Afterwards, DMEM+ with MTT solution must be removed from the well so that formazan crystals stay attached in the bottom. These crystals are dissolved with 0.5 mL of DMSO per well. Wells absorbance is measured using UV light (550 nm) in a Microplate reader (Techan Spark, Viena, Austria), and cell viability can be calculated as Eq. 7 below follows:

$$Cell\ viability\ (\%) = \frac{Avg\ OD\ sample\ wells - Avg\ OD\ medium\ control\ wells}{Avg\ OD\ cell\ control\ wells - Avg\ OD\ medium\ control\ wells} \quad \text{(Eq. 7)}$$

In order for cell viability to be as accurate as possible in physiological conditions with the original hydrogel formulations, a new gel support device was developed, resembling transfer wells [64]. Gel supports for cell wells were 3D printed (Creality, Shenzen Creality 3D Technology Co., China, using Panchroma Translucent Natural Filament). This way, 0.5 mL of hydrogel were poured on each well, which enabled its thermal transition to strong gels, suspended and completely covered in 1 mL of DMEM+ without touching the cells attached in the bottom. Lateral slits favoured the system transfer to the well bulk. Figure 3 presents a brief scheme of these supported structures below:

a) b)

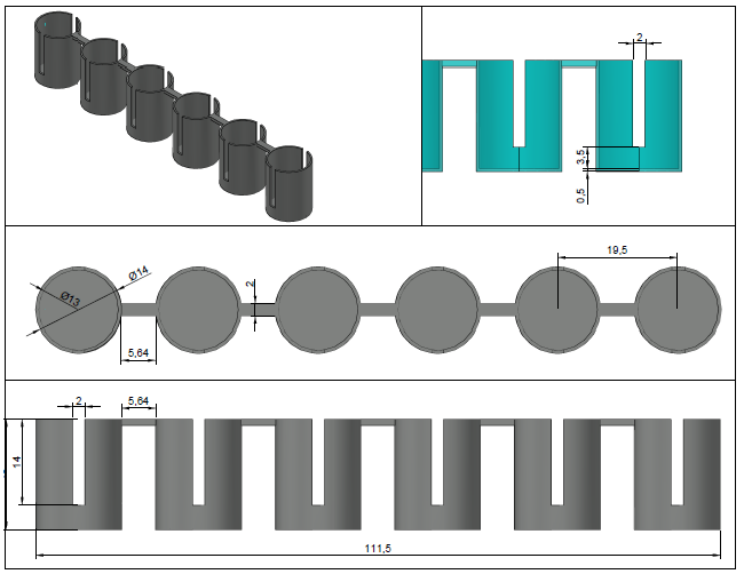

c)

Figure 3: Gel support device for 24-well plates for *in vitro* assays. The device allows the support of gel formulations in wells fully covered by DMEM+: a) Support device in well plates, b) Side view to assure the bottom is not reached, and c) Design of support device made in AutoCAD.

It must be noted that every gel support and PF flakes were sterilised before MTT assays by UV light radiation for 1h in sterile cell hood. Gel supports were also fully immersed in IMS solution before UV radiation.

Treatments used in MTT assays were the following: 5FU (directly diluted in DMEM+), PF-127 (G), loaded PF (G+5FU), hydrogel with unloaded and loaded conventional liposomes (G+L and G+L+5FU

respectively), and hydrogel with unloaded and loaded EU EPO coated liposomes (G+L+EPO and G+L+EPO+5FU respectively). Loaded formulations were synthesized to reach a final concentration of 2.5 μM in each well, due to 5FU IC_{50} preliminary assays [19]. They were used on both cell lines in MTT assays to observe their influence at 24, 48, and 72h.

2.6.2. Viability assays on spheroids

Multicellular Tumour Spheroids (MCTS) were obtained culturing BT-474 cells in Nuclon™ Sphera™ 96-well U-shaped bottom microplates (Thermo Fisher Scientific, Eugene, OR, USA) with a concentration of 2,000 cells /mL for 4 days to allow growth, as referenced [65]. Once the spheroids were grown, there were subjected to 5-FU solution (5-FU), EU EPO coated liposomal gel (G+L+EPO) and its loaded version (G+L+EPO+5-FU) in cell-counting and Live/Death assays at 24h, 48h, and 72h.

Cell-counting assay was performed in the same wells where the MCTS were developed. In order to keep resemblance with previous *in vitro* assays, 1/3 of media volume was replaced with the formulations in each well and loaded formulations kept a final concentration of 5-FU of 2.5 μM per well. Control wells remained untouched and each treatment was applied to 4 wells per day. Every day after treatment exposure, the 4 spheroids per treatment were collected, separated by centrifugation 1,400rpm for 4 minutes (Centronic-BL II from JP Selecta, Barcelona, Spain), disaggregated, and resuspended in 75 μL of DMEM+. Afterwards, the cells were quantified (InvitrogenCountess II FL Automated Cell Counter, ThermoFisher Scientific) with Trypan Blue.

Furthermore, cell viability was double assayed with Live/Death fluorescence staining. For this assay, 5 spheroids per treatment and day were placed in flat glass-bottom dishes after growth, and treated with DMEM+ and 1/3 of the volume of each treatment keeping the same drug concentration. At 48h and 72h, the spheroids were incubated with calcein AM (0.1 μM) and propidium iodide (0.94 μM) fluorescent dyes for 15 min. The stained samples were then imaged by Confocal Laser Scanning Microscopy (CLSM) (Leica TCS SP5, Leica Microsystems,

L'Hospitalet de Llobregat, Barcelona, Spain) with an excitation / detection of 494/517 and and 535/617 respectively.

2.7. Statistical analysis

Data for measurements, drug release tests, and cell viability is reported as mean value ± standard deviation (SD) for n=3 experiments. Specific comparison between groups was studied through unpaired Student's t-tests.

For multiple group comparisons, two-way ANOVA for drug release tests and cell viability assays were used. When statistically significant differences were confirmed, Tukey test was used as a post-hoc analysis.

3. Results and discussion

3.1. pH-T dual response system synthesis

3.1.1. Rheology

The hydrogels systems were characterized by rheological measurements to evaluate their viscoelastic properties. The results are illustrated in Figure 4 and Table 1 below:

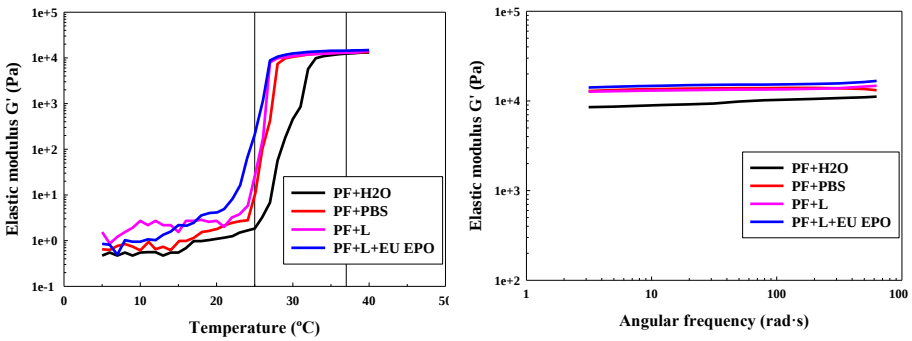

a) b)

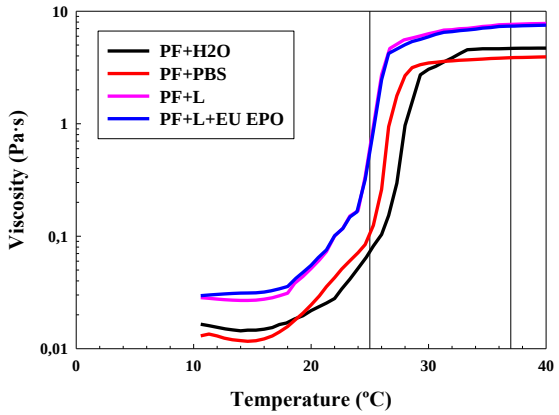

c)

Figure 4: Rheological analyses of PF-127 hydrogels in water (H2O) and PBS, with liposomes in acidic pH (L) and EU EPO coated liposomes (L+ EU EPO): a) Temperature sweep oscillatory flow test, b) Frequency sweep oscillatory flow test, and c) Temperature ramp steady flow test.

Table 1: Results of rheological measurements of PF-127 hydrogels in different solvents and with liposomes embedded

Formulation	Oscillatory flow			Steady flow	
	Tsweep	Freqsweep		Tramp	
	cgt (ºC)	G' (kPa)	G'-G'' (kPa)	T_{MAC} (ºC)	μ (Pa·s)
PF+H2O	34	9.78±1.33	7.16±0.77	34	4.53±0.21
PF+PBS	30	13.82±0.46	12.64±1.32	30	3.91±0.34
PF+L	29	13.45±1.04	12.42±1.08	28	6.51±1.64
PF+L+EU EPO	28	15.21±1.31	13.72±1.57	28	6.82±1.51

As it can be seen all the systems presented thermo-sensitivity. When the temperature sweep oscillatory test was analysed in Figure 4 a, it can be observed that all formulations presented sol state at room temperature (25ºC) which enabled their injectability, also seen in Figure S1a in Supplementary Material where viscous moduli are higher than the elastic ones. However, when the temperature increased, the storage moduli also increased exponentially until stable values from 10 kPa up to 15 kPa were reached for temperatures higher than the physiological one (37ºC), and predominant elastic behaviour, as shown in Figure S1 a in Supplementary Material.

Furthermore, when water solvent was changed with PBS, the cgt decreased, showing an earlier gel transition. This was mostly due to the

salting-out effect that the salts in the buffered solution caused. Ions in solution tended to compete with the hydrophilic PEO chains for the available water molecules. This implied that PPO chains tended to aggregate among themselves at lower temperatures, promoting their formation and aggregation before.

Not only this, but when liposomes were implemented, this effect slightly increased more, due to an intersection between the small size of the liposomes and poloxamer micelles, promoting the MAC. This is also observed when self-assembly polysaccharides were implemented into the PF-127 matrix, as shown in previous results [48, 66], and was also supported by previous results with liposomes in hydrogel [67].

Figure 4 b showed how at 37ºC a strong gel behaviour was confirmed by constant high values of G' independent from the frequency used. As observed, saline buffered solutions promoted the elasticity of the gel formed. This is due to the salting-out effect of saline buffered solvent, which promoted the elasticity of the gel [67]. Once again, the liposomes implementation promoted more this behaviour, as self-assembly polysaccharides had shown previously [48]. Not only the elastic moduli increased, but also its difference with the viscous one, as shown in Figure S1 b in Supplementary Material.

Finally, Figure 4 c proved a successfully predominant mechanism of gelation through the MAC of the poloxamer in static flow analysis. This was due to the three-phase gelation process characterized [56]: Firstly, at lowest temperature ranges, the systems showed a Newtonian formulation behaviour, the sol-gel transition was reflected in the viscosity increase, which finished with a stable structure and independent viscosity at higher temperature range. MAC was identified as the main mechanism in thermo-response since this temperature was also confirmed as the cgt in oscillatory flow analyses [42].

As expected, the salting-out effect promoted a lower temperature of MAC, but the viscosity did not increase, being less resistant against flow. This might be due to less hydrophilicity of PEO chains because of ions presence which causes less friction among micelles under flow [56].

However, when liposomes were implemented, viscosity increased. This was due to the presence of small vesicles strengthening the PF-127 matrix by interactions with the poloxamer micelles. These interactions promoted resistance against flow, as many other structures implemented had shown in previous results [45-48]. In this case, the size and structure of liposomes were so similar that no big difference was found between the systems with conventional or coated liposomes, supported by statistical analysis.

3.1.2. Cryo-SEM

When conventional liposomes and EU EPO coated liposomes were embedded in PF-127 hydrogel, face fracture cryo-SEM was used to characterize the systems via microscopy. The pictures can be seen in Figure 5.

As it can be seen in Figure 5 a, the pictures taken from microscopy showed a porous characteristic hydrogel matrix, previously reported [53, 54]. The structure did not change their size when the liposomes were embedded, in Figures 5 c and e. However, it can be seen that liposomes and EU EPO coated liposomes (even if the size is bigger due to aggregation because of the cryogenic process) were present within the hydrogel matrix fracture-induced cavities in Figure 5 c. This proved that liposomes morphology and characteristics remain after the implementation process and they did not interfere with the hydrogel matrix or were degraded.

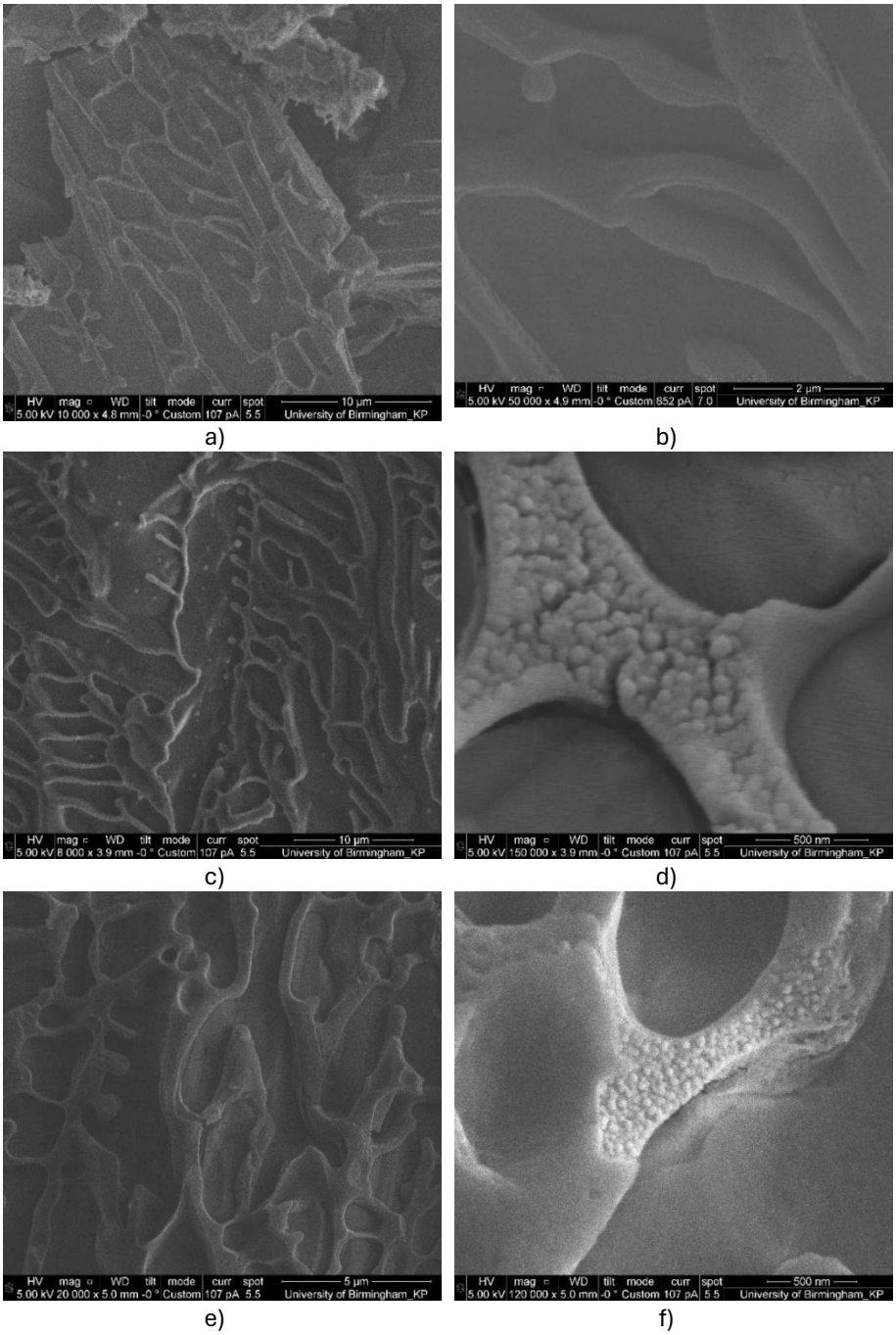

Figure 5: Face fracture Cryo-SEM pictures from PF-127 hydrogel matrix: a-b) alone, c-d) with conventional liposomes, and e-f) with EU EPO coated liposomes, and their close-ups (b, d, and f, respectively).

Moreover, these liposomes tended to accumulate on the hydrogel polymeric matrix overall. This was clearly shown in the close-ups. When the PF-127 alone was analysed in Figure 5 b no trace of liposomes or spheres was detected when the magnification increased. However, when the liposomes were implemented, Figures 5 d and f clearly showed that liposomes were successfully embedded within the hydrogel matrix. Not only that, but it was confirmed that the size of this liposomes remained around 100-200 nm, which coincided with the sizes provided by zetasizer in previous studies [19].

3.2. Drug release tests and modelling

3.2.1. Drug release tests

Loaded liposomes presented high 5FU encapsulation efficiencies as already reported [19] were embedded in the hydrogel matrix, constituting loaded hydrogels. Specifically, this was an encapsulation of >90% due to high solubility of the drug, small size of liposomes, extrusion procedure and coating effect (when it is applied) [68]. This encapsulation efficiency had been previously shown in hydrophilic and hydrophobic drugs for similar liposomal formulations [69, 70].

The drug release at 37ºC of the PF-127 hydrogel with conventional and EU EPO coated liposomes implemented are presented in Figure 6 below:

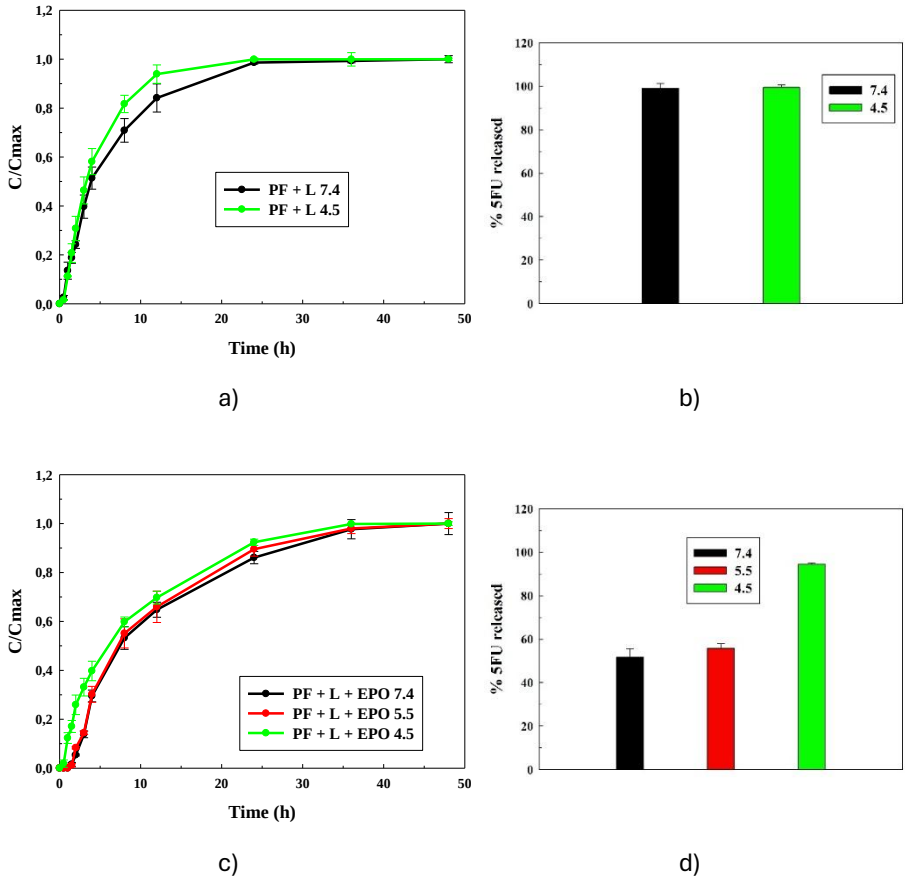

Figure 6: Results of 5FU release experiments for percentage of drug released in: Conventional liposomes (a and b), and EU EPO coated liposomes (c and d) embedded in PF-127 hydrogel: a and c) Kinetic profiles, and b and d) Amount of 5FU released compared to 5FU loaded. Results are expressed as a mean value of 3 experiments ± SD. Cmax was defined as the maximum 5FU concentration released in each experiment, as should be done prior to model fitting.

As it was observed in Figures 6 a and b, the conventional liposomes lacked pH-sensitivity, since the whole loaded drug was released almost identically regardless of pH of the media, showing a similar kinetic profile. This was due to the liposomal structure, since PC and CHOL did not present any pH response [66].

This was the same reason why this formulation of liposomes was found to be stable around different acidic pHs for a week time, as shown in Figure S2 in Supplementary Material, without significant statistical

difference either. Therefore, it could be stated that release is mainly produced via diffusion through the bi-lipidic membrane, due to the high PC content in the MR [21, 71]. In fact, diffusion was confirmed as predominant release mechanism in previous model fitting of liposomal formulations drug release studies [19].

Moreover, the time for this drug release to reach a plateau was found around 24 hours, which implied a clear delay of release time when it was compared liposomes alone release (4h) [19], supported by statistical significance ($p<0.0001$). This illustrated the significant effect of the hydrogel when it released the liposomes due to main erosion effect and water permeability, as previously discussed [72]. Furthermore, 5FU was also observed to have a faster release with the PF-127 alone or with polysaccharides [48], outlining the beneficial synergy between both systems, again, statistically different ($p<0.001$) (liposomes and poloxamer).

On the other hand, when the liposomes were EU EPO coated, it could be seen that pH sensitivity was induced due to the pH response of the polymer. As observed in Figure 6 d, when this polymer was insoluble (pH > 5.0), only half of the loaded drug was released in 2 days, in contrast with the whole concentration for pH where this polymer was soluble, such as 4.5. It was also observed that the kinetic release profiles showed a difference overall in the first release times until reaching plateau. Moreover, pH sensitive drug release profiles had been previously observed for this polymer coating in similar deliveries [18].

This was due to the synergistic effect that presented both the hydrogel network against water permeation, and the additional coating layer which introduced an extra diffusion barrier affecting drug release, even trapping it when insoluble. Therefore, it was confirmed that when EU EPO coated liposomes were embedded in a PF-127 hydrogel formulation, an efficient dual response T/pH system was achieved. This system not only responded to the transition pH point of the coating polymer (microtumoural environment), but also successfully delayed the drug release up to a day more due to the hydrogel network properties and its interaction with the embedded liposomes.

3.2.2. Theoretical model fitting

As previously stated, the drug release data from the hydrogels with liposomes embedded were fitted to different theoretical models aimed at explaining the mechanisms involved during drug release.

Zero order, first order, Higuchi and Korsmeyer-Peppas models were used as a first approach for a drug release from liposomal system, overall for early stages in the last two models mentioned (C/Cmax<60%). However, this study was completed through two-stage models, such as Peppas-Sahlin and another complementary model, Weibull. Fittings of one-stage and two-stage models are illustrated in Figures S3 and S4 in Supplementary Material, respectively.

Results for one-stage data fitting are shown in Table 2 below:

Table 2: Results of fitting experimental data to zero, first order kinetics, Higuchi, and Korsmeyer-Peppas model

Models		Zero order	First order	Higuchi	Korsmeyer-Peppas	
Hydrogels w		k_0 (h^{-1})	k_1 (h^{-1})	k_H ($h^{-0.5}$)	k_{KP} (h^{-n})	n
L	PBS	0.03	0.16	0.20	0.13	0.98
	4.5	0.03	0.19	0.21	0.14	0.99
L + EU EPO	PBS	0.02	0.08	0.12	0.03	1.34
	5.5	0.02	0.08	0.12	0.03	1.31
	4.5	0.02	0.11	0.17	0.12	0.89

Firstly, as it can be seen in Figure S3, zero order kinetic was never the best model to fit the release profiles. However, the graphical fitting increased significantly each time the kinetics showed slower release due to coating of liposomes and further insolubility of the coating, proving pH-sensitivity. In fact, zero order kinetics was previously characterized as best fit when the release in hydrogel was slower than in liposomes alone with hydrophobic drugs, like Paclitaxel [72].

However, in this case, best fittings were found in a first order kinetics and Korsmeyer-Peppas model. Higuchi also showed a robust fitting denoting diffusion as principal release mechanism, as referenced previously [67]. In addition, kinetic constants values and order in all of

these models further proved the significant release delay due to hydrogel matrix, and furthermore the (insoluble) polymer coating [19].

Once again, kinetic constants for Korsmeyer-Peppas model can be found in other studies where diffusion through conventional liposomes embedded in hydrogels were proven as the principal release mechanism (0.05-0.2) [73]. Nonetheless, exponents n on this model pointed to case II transport or higher values for systems with higher resistance against drug release. For this parameter, we can also numerically see the difference when the drug diffusion encountered polymer coating resistance, whether insoluble or soluble.

For conventional liposomal hydrogel the n is approximate to 1 due to the best fitting of the curve being a first order kinetic, which is not representative of the significance of a predominant mechanism. In complex systems, n>1 reflects temporary changes in resistance against transport. This can explain how, when the coating became insoluble, the resistance activated the n exponent trend to values higher than 1. However, for this case n should be referenced as a comparative parameter which shapes the release curve, rather than a release mechanism classifier.

Moreover, since there was a hydrogel matrix affecting the diffusional release of the drug from the liposomes, complementary studies were performed. The effect of the hydrogel in release constants was clear since the values of these same constants for liposomes systems alone decreased significantly (delayed drug release), also previously reported [21, 72].

Models selected for a whole fitting of the release curve (up to 36h) included the Peppas-Sahlin equation, which contains a diffusional and a relaxation term, and also a complementary Weibull model. The results for the fittings of these models are shown in Table 3.

Table 3: Results of fitting experimental data to Peppas-Sahlin and Weibull model

Models		Peppas-Sahlin			Weibull	
Hydrogels w		k_1 (h^{-m})	K_2 (h^{-2m})	m	α (h)	β
L	PBS	0.22	0	0.5	6.23	1.04
	4.5	0.23	0	0.5	4.73	1.06
L + EU EPO	PBS	0.14	0.03	0.5	11.39	1.26
	5.5	0.14	0.02	0.5	10.74	1.29
	4.5	0.20	0	0.44	8.83	0.90

As it can be observed, in Peppas-Sahlin model the m exponent lied between 0.4 and 0.5 which implied diffusional drug release mechanism associated for spherical systems, such as liposomes [61]. In addition, it could be seen the diffusional term of the equation was always predominant over a negligible relaxation term.

This could be interpreted as no effect from the gel matrix, but nonetheless this effect had been confirmed for low values of kinetic constants and in previous results [19], even for negative terms of this equation, as proposed by Mourtas et al. fittings to liposomal carbopol 974 NF and HEC gels [73]. To sum up, the gel delay effect on drug release was illustrated in the diffusional term rather than in the relaxation one.

It could be concluded that mechanism suggested firstly a release of liposomes from the hydrogel network, followed by the drug diffusion through the liposome bilayer, as referenced in liposomal hydrogels [74]. Consequently, negligible relaxation term was justified by no drug being released directly from the hydrogel network. This potential release mechanism is illustrated in Figure 7 below.

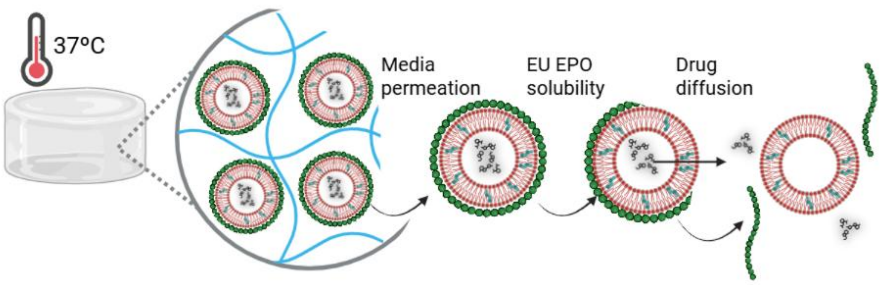

Figure 7: Potential drug release mechanism scheme. Media permeation enables hydrogel network relaxation liberating coated liposomes in media. Afterwards, for pH soluble range, EU EPO coating layer is dissolved in media, and 5FU is released via diffusion through bilipidic membrane.

Moreover, the relaxation term only became slightly positive when the polymer coating was insoluble at pH > 5.0. This indicated a minor, but additional secondary contribution associated to slow structural changes such as hydration, or re-ensemble of diffusional paths [61], which the insoluble layer constituted. This result contrasted with the n exponent trend surpassing 1 in previous Korsmeyer Peppas fit.

Furthermore, for contrast, Weibull model was applied for better graphical fittings shown in Figure S4. As it can be seen, the parameter regarding temporal scale (α) increased whenever the diffusional path encountered a new resistance, such as the coating layer, and overall its insolubility. All of these variables presented differences in this parameter due to the delay they caused to the diffusion drug release.

β parameter, which models the curve shape, is found around 1.00 when the release was homogeneous without changes in time, such as non-coated and soluble coated systems. However, for the dual-response system, the pH-response of insoluble coating increased this parameter up to 1.26, which stated an efficiency in the pH-response [62].

The contribution of this model to this study further proved that, when the coating resistance is added, the drug release delay was presented with lower diffusion kinetic constants in Peppas Sahlin, which corresponded with higher temporal scale parameters in Weibull. Moreover, the increase in β parameter, caused for insoluble coating layer, corresponds with the low increase in relaxation term of the

Peppas-Sahlin model, and even n increase over 1 in Korsmeyer Peppas model, proving the efficiency of pH-response.

3.3. Cell viability assays

3.3.1. MTT assays on 2D cell culture

Cell lines HS5 and BT474 were used in MTT assays to quantify the treatment with dual-response system and the other hydrogel formulations. Concentrations of loaded 5FU were set at 2.5μM, since it was determined as the IC_{50} for BT474 cell line at 48h in preliminary assays [75].

For this assay 3D printed gel supports device was used to place the treatments preserving their original concentration. This meant that PF aqueous solutions were placed on the gel supports, and afterwards introduced in the wells with cells attached in the bottom, and immersed in 1mL of DMEM+ per well. When the well plates were incubated, the gel was rapidly formed at 37ºC in under 2 minutes, as reported with other poloxamer gels formulations before [49]. Consequently, this approach was a more accurate study of the original hydrogel formulations in physiological conditions.

Preliminary tests were performed *in vitro* without cells in order to evaluate which volume of hydrogel formulations should be used for MTT assays for endured gel effect. This qualitative test indicated that 0.5 mL of treatment per gel support (or well) immersed in 1mL of DMEM+ could endure up to 8 hours without being fully dissolved or degraded. Consequently, 0.5 mL of treatments were placed in gel supports (maximum allowed due to lateral slits). Results of this preliminary test can be found in Figure S5 in Supplementary Material. Results of MTT assays are shown in Figure 8 below:

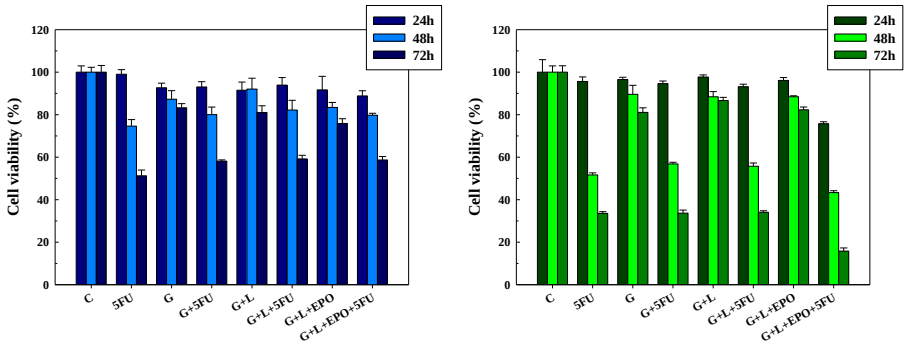

a) b)

Figure 8: Cell viability (%) of MTT assays for cell control (C), IC_{50} of 5FU (5FU), and PF-127 treatments (G) containing conventional (L) and EU EPO coated (EPO) liposomes as strong gel form on gel support device at 24, 48, and 72h on: a) HS5 and b) BT474.

Results shown in Figures 8 a and b showed a clear difference in the cell viability compared with liposomes treatments without PF-127 [19], which confirmed a significant gel effect on the treatments under *in vitro* conditions (Statistical analysis showed a majority $p<0.001$ between liposomes alone and G formulations at 48 and 72h). Firstly, it could be seen that when PF-127 concentration increased and gelled, this created more toxicity to both cell lines when unloaded. The use of a PF-127 based strong gel on cell viability assay has already shown a slight decrease in periods of 3 and 7 days [76, 77]. It has to be noted that cell viability was never found lower than 85% which was still considered a viable value.

For loaded formulations, the slower release rate of 5FU caused a slower arrival of the drug to the cells, and therefore, higher cell viability than previously. This effect even counteracted the higher toxicity of G formulations in contrast to liposomal ones [19]. These results further proved that gel effect was consistent and necessary if a controlled release is desired, confirmed via statistical analysis ($p<0.0001$ for 48 and 72h).

Moreover, the dual response T/pH treatment could also be observed in Figures 8 a and b, since the EU EPO coated liposomes with 5FU still caused more toxicity to BT474 cells than HS5 ones. Also, this difference in toxicity between cell lines was the most significant out of all the

formulations tested, being statistically significant when compared with non-coated liposomes or hydrogel-only treatments ($p<0.0001$). However, this pH-response was not as high (yet significant), as in previous assays due to the delayed drug release in G formulations.

This defined a synergy between both responses to stimuli for a sustained release without losing pH-responsiveness, since the delayed drug release due to thermo-sensitivity does not interfere negatively in the pH targeting of the EU EPO coated liposomes.

3.3.2. Viability assays on 3D MCTS

In vitro 3D culture systems have shown to replicate the *in vivo* growth conditions of solid tumours better than 2D systems or monolayer cultures, promoting them for drug toxicity models [78]. In fact, previous studies have already determined that spheroids bigger than 500 μm developed inner necrosis with time due to the lack of nutrients that arrive to their core, presenting dead cells surrounded by a rim of proliferating cells [79]. Therefore, the same procedures of 2D cell models were tested in MCTS to study more accurately their effect under *in vivo* conditions. The treatments selected were 5FU (in solution), and the loaded (G+5FU) and unloaded (G) dual-response system (G+ L+ EPO +5FU and G+ L+ EPO, respectively).

Firstly, cell-counting assay presented similar results to the ones provided in monolayer BT-474 cell line culture viability assay. Unloaded formulations viability decreased with time due to necrosis of its core, preserving similar results from the control to the dual-response hydrogel, proving its biocompatibility (65-67% at 48h and 48% at 72 h). In contrast, 5-FU solution caused more cell deaths due to its therapeutic efficiency (54% at 48h), whilst the loaded hydrogel showed the deadliest rates, proving its efficacy by better targeting cancer cells with implemented coated liposomes (40% at 48h and 29% at 72h). This fact demonstrates improvements compared to other strategies which showed same cytotoxicity as the drug solution or worse spreading [80]. These results are illustrated in Figure 9 a and b, whilst results for 24h can be found in Figure S6. Moreover, Live/Dead assay images confirmed the previous

results showing inner necrosis in control spheroids [79] and presenting smaller sizes and more disaggregated stages under 5FU and overall G+5FU treatment. These images are illustrated in Figure 9 c and d, where spheroids can be seen getting smaller, disaggregated and thus, transitioned into more mono-layered organizations with 5FU treatments and time, especially with G+5FU, where the aureole fully lost its integrity.

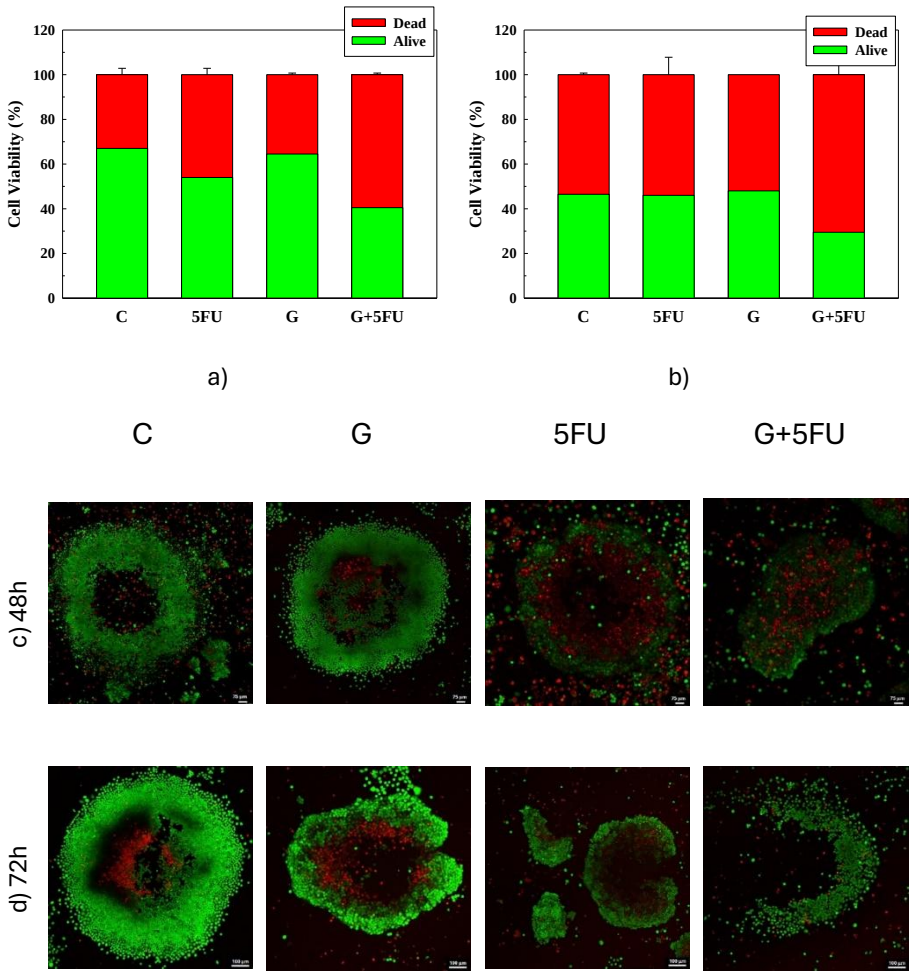

Figure 9: Cell viability (%)assays for cell control (C), IC_{50} of 5FU (5FU), and EU EPO liposomal PF-127 treatments unloaded (G) and loaded (G+5FU) at 48 (a and c) and 72h (b and d) on: a and b) Cell-counting assays and c and d) CLSM images of Live/Death assays.

4. Conclusions

In this work, different formulations of liposomes were embedded in a thermo-sensitive hydrogel matrix in order to synthesize a novel thermo and pH dual-response DDS useful for injection after tumour resection in breast cancer treatment. The synthesis and optimization of the system was achieved by implementing EU EPO coated liposomes into PF-127 hydrogel matrix, presenting an injectable system characterized by rheology. Moreover, liposomes incorporation improved viscoelastic properties of the system (G' from 9.7 to 15.6 kPa and viscosity from 4.5 to 6.0 Pa·s) without changing their structure or gelation mechanism.

Dual-responsive hydrogels also proved pH-sensitivity in 5-FU release preventing up to 50% of loaded drug to be released in a to 2-day period for pH values over 5.0, delaying its release compared to liposomal systems. The coating layer and its insolubility also added a resistance, slightly changing the release mechanism studied by one-stage (n exponent in Korsmeyer-Peppas) and two-stages (degradation term in Peppas-Sahlin and β parameter in Weibull) mathematical models fitting.

Finally, formulations demonstrated biocompatibility in cell lines of HS5 and BT474. MTT assays showed the dual-response efficiency, delaying cell death at 48h and 72h due to the gel effect, but maintaining its significant pH-responsiveness towards cancer cells. Moreover, 3D BT-474 MCTS supported previous results by showing enhanced cytotoxic effects against tumour cells with the dual-responsive formulation.

Consequently, this work provides the full synthesis, characterization, and functionalization of an injectable hydrogel that acts as a thermo and pH dual response DDS for sustained release of 5FU selectively towards breast cancer cells without the need of toxic solvents or complex chemical reactions or long synthesis. This provides a novel strategy for localized therapies in breast cancer treatment.

Conflict of interest

Authors do not declare any conflict of interest.

Acknowledgements

M. Blanco-López wants to acknowledge the funds from “Programa propio III de la Universidad de Salamanca: Ayudas para financiar contratos predoctorales de la Universidad de Salamanca cofiananciados por el Banco Santander” for his PhD fellowship. The authors would like to express their gratitude to the Spanish Ministry of Science and Innovation for the financial support, research project: PID2022-1405990B-I00.

References

[1] G.R. Bhat, I. Sethi, H.Q. Sadida, B. Rah, R. Mir, N. Algehainy, I.A. Albalawi, T. Masoodi, G.K. Subbaraj, F. Jamal, M. Singh, R. Kumar, M.A. Macha, S. Uddin, A.S.A-S. Akil, M. Haris, A.A. Bhat. Cancer cell plasticity: from cellular, molecular, and genetic mechanisms to tumor heterogeneity and drug resistance. Cancer Metastasis Rev. 2024, 43, 197-228. https://doi.org/10.1007/s10555-024-10172-z

[2] P. Piña-Sánchez, A.Chávez-González, M. Ruíz-Tachiquín, E. Vadillo, A. Monroy-García, J.J. Montesinos, R. Grajales. M.G. de la Barrera, H. Mayani. Cancer biology, epidemiology, and treatment in the 21st century: Current status and future challenges from a biomedical perspective. Cancer Control. 2021, 28. https://doi.org/10.1177/10732748211038735

[3] R.M. Espinosa. Breast cancer. Rev. Méd. Sinerg. 2017, 2, 8-12. ISSN 2215-4523

[4] K.P. Trayes, S.E.H. Cokenakes. Breast cancer treatment. Am. Fam. Physician. 2021, 104, 171-178.

[5] R.L. Siegel, K.D. Miller, A. Jemal. Cancer statistics. ACS. 2019, 69, 1. https://doi.org/10.3322/caac.21551

[6] Las cifras del cáncer en España. SEOM y REDECAN. 2025. https://seom.org/prensa/el-cancer-en-cifras#:~:text=El%20n%C3%BAmero%20de%20c%C3%A1nceres%20diagnosticados,y%20la%20Red%20Espa%C3%B1ola%20de ISBN: 978-84-09-69154-8. Last access: 01.28.2026.

[7] A. Zafar, S. Khatoon, M.J. Khan, J. Abu, A. Naeem. Advancements and limitations in traditional anti-cancer therapies: A comprehensive review of surgery, chemotherapy, radiation therapy, and hormonal therapy. Discov. Onc. 2025, 16, 607. https://doi.org/10.1007/s12672-025-02198-8

[8] P-P. Zheng, J.Li, J.M. Kros. Breakthroughs in modern cancer therapy and elusive cardiotoxicity: Critical research-practice gaps, challenges, and insights. Med. Res. Rev. 2017, 38, 325-376. https://doi.org/10.1002/med.21463

[9] K.L. Maughan, M.A. Lutterbie, P.S. Ham. Treatment of breast cancer. Am. Fam. Ohysician. 2010, 81, 1339-1346. PMID: 20521754.

[10] A.G. Waks, E.P. Winer. Breast cancer treatment. JAMA. 2019, 321, 288-300. 10.1001/jama.2018.19323

[11] K.H. Lau, A.M. Tan, Y. Shi. New and emerging targeted therapies for advanced breast cancer. Int. J. Mol. Sci. 2022, 23, 2288. https://doi.org/10.3390/ijms23042288

[12] Y. Lee, D.H. Thompson. Stimuli-responsive liposomes for drug delivery. WIREs Nanomed Nanobiotechnol. 2017, 9, 1407. 10.1002/wnan.1450

[13] B. Barea, A. Franco, M.T. Tomas-Ugarte. Ternary nanocomposite carriers based on organic clay-lipid vesicles as an effective colon-targeted drug delivery system: Preparation and in vitro/in vivo characterization. J. Nanobiotechnology. 2020, 18, 17. 10.1186/s12951-020-0579-7

[14] C.N. Patra, R. Priya, S. Swain, G.K. Jena, K.C. Panigrahi, D. Ghose. Pharmaceutical significance of Eudragit: A review. Futur. J. Pharm. Sci. 2017, 3, 33-45. https://doi.org/10.1016/j.fjps.2017.02.001

[15] N. Fine-Shamir, A. Dahan. Methacrylate-copolymer Eudragit EPO as a solubility-enabling excipient for anionic drugs: Investigation of drug solubility, intestinal permeability, and their interplay. Mol. Pharmaceutics. 2019, 16, 2884-2891. https://doi.org/10.1021/acs.molpharmaceut.9b00057

[16] G. Bozzuto, A. Molinari. Liposomes as nanomedical devices. Int. J. Nanomed. 2015, 10, 975–999. 10.2147/IJN.S68861

[17] J. Li, I.W. Lee, G.H. Shin, X. Chen, H.J. Park. Curcumin-Eudragit E PO solid dispersion: A simple and potent method to solve the problems of curcumin. Eur. J. Pharm. Biopharm. 2015, 94, 322-332. 10.1016/j.ejpb.2015.06.002

[18] A. Hasanovi, C. Hollick, K. Fischinger, C. Valenta. Improvement in physicochemical parameters of DPPC liposomes and increase in skin permeation of acyclovir and minoxidil by the addition of cationic polymers. Eur. J. Pharm. Biopharm. 2010, 75, 148-153. 10.1016/j.ejpb.2010.03.014

[19] M. Blanco-López, I. de Dios-Pérez, C. Nieto, A. Tabernero, E. Martín del Valle. Expanding the pH window of liposomal drug delivery using Eudragit-based polymeric coatings. Manuscript in Chapter 5.

[20] S. Yang, Z. Li, S. Li, J. Zhang, J. Huang, J. Ren, X. Wu. Advances in drug delivery systems based on liposome-composite hydrogel microspheres. J. Mater. Chem. B. 2025, 13, 11885-11908. 10.1039/D5TB01369K

[21] S. Mourtas, M. Haikou, M. Theodoropoulou, C. Tsakiroglou, S.G. Antimisiaris. The effect of added liposomes on the rheological properties of a hydrogel: A systematic study. J. Colloid Interface Sci. 2008, 317, 611-619. https://doi.org/10.1016/j.jcis.2007.09.070

[22] S. Pernas, S.M. Tolaney. HER2-positive breast cancer: New therapeutic frontiers and overcoming resistance. Ther. Adv. Med. Oncol. 2019. 10.1177/1758835919833519.

[23] M. Sambi, S. Haq, V. Samuel, B. Qorri, F. Haxho, K. Hill, W. Harless, M.R. Szewczuk. Alternative therapies for metastatic breast cancer: Multimodal approach targeting tumor cell heterogeneity. Breast Cancer. 2017, 9, 85-93. https://doi.org/10.2147/BCTT.S130838

[24] A. Szulc, M. Wozniak. Targeting pivotal hallmarks of cancer for enhanced therapeutic strategies in triple-negative breast cancer treatment- In vitro, in vivo and clinical trials literature review. Cancers. 2024, 16, 1483. https://doi.org/10.3390/cancers16081483

[25] O. Obidiro, G. Battogtokh, E.O. Akala. Triple negative breast cáncer treatment options and limitations: Future outlook. Pharm. 2023, 15, 1796. https://doi.org/10.3390/pharmaceutics15071796

[26] P. Tagde, A. Najda, K. Nagpal, G.T. Kulkarni, M. Shah, O. Ullah, S. Balant, Md.H. Rahman. Nanomedicine-based delivery strategies for breast cáncer treatment and management. Int. J. Mol. Sci. 2022, 23, 2856. https://doi.org/10.3390/ijms23052856

[27] S. Nagini. Breast cancer: Current molecular therapeutic targets and new players. Anticancer Agents Med. Chem. 2017, 17, 152-163. https://doi.org/10.2174/1871520616666160502122724

[28] R. Chaudhari, V. Patel, A. Kumar. Cutting-edge approaches for targeted drug delivery in breast cancer: Beyond conventional therapies. Nanoscale Adv. 2024,6, 2270-2286. 10.1039/D4NA00086B

[29] U. Kafle, S. Agrawal, A.K. Dash. Injectable nano drug delivery systems for the treatment of breast cancer. Pharm. 2022, 14, 2783. https://doi.org/10.3390/pharmaceutics14122783

[30] A.R. Hegde, R. Raychaudhuri, A. Pandey, G. Kalthur, S. Mutalik. Exploring potential formulation strategies for chemoprevention of breast cancer: A localized delivery perspective. Nanomed. 2021, 16, 1111-1132. https://doi.org/10.2217/nnm-2021-0018

[31] M.Wang,M. Chen,W. Niu, D. D. Winston,W. Cheng, B. Lei. Injectable muscle-adhesive antioxidant conductive photothermal bioactive nanomatrix for efficiently promoting full-thickness skeletal musclae regeneration. Biomater. Res. 2020, 261, 120301. https://doi.org/10.1016/j.bioactmat.2020.11.005

[32] S. Chatterjee, P. C. L. Hui, C.W. Kan,W.Wang. Dual-responsive (pH/temperature) Pluronic F-127 hydrogel drug delivery system for textile-based transdermal therapy. Sci. Rep. 2019, 9, 11658. https://doi.org/10.1038/s41598-019-48254-6

[33] P. J. Rose Jaquilin, O. S. Oluwafemi, S. Thomas, A. O. Oyedeji. Recent advances in drug delivery nanocarriers incorporated in temperature-sensitive Pluronic F-127- A critical review. J. Drug Delivery Sci. Technol. 2022, 72, 103390. 10.1016/j.jddst.2022.103390

[34] R. N. Woodring, E. G. Gurysh, E. M. Bachelder, K. M. Ainslie. Drug delivery systems for localized cancer combination therapy. ACS. Appl. Bio Mater. 2023, 6, 934. 10.1021/acsabm.2c00973

[35] K. K. Jain. An overview of drug delivery systems. Methods Mol. Biol. 2020, 2059, 1. 10.1007/978-1-4939-9798-5_1

[36] H. Xin, S. Naficy. Drug delivery based on stimuli-responsive injectable hydrogels for breast cancer therapy: A review. Gels. 2022, 8, 45. https://doi.org/10.3390/gels8010045

[37] J. Shi, L. Yu, J. Ding. PEG-based thermosensitive and biodegradable hydrogels. Acta Biomater. 2021, 128, 42. 10.1016/j.actbio.2021.04.009

[38] N. U. Khaliq, J. Lee, S. Kim, D. Sung,H. Kim. Pluronic F-68 and F-127 based nanomedicines for advancing combination cancer therapy. Pharm. J. 2023, 15, 2102. https://doi.org/10.3390/pharmaceutics15082102

[39] P. Zarrintaj, J. D. Ramsey, A. Samadi, Z. Atoufi, M. K. Yazdi, M. R. Ganjali, L. M. Amirabad, E. Zangene, M. Farokhi, K. Formela, M. R. Saeb, M. Mozafari, S. Thomas. Poloxamer: A versatile tri-block copolymer for biomedical applications. Acta Biomater. 2020, 110, 37. 10.1016/j.actbio.2020.04.028

[40] N. A. Di Spirito, N. Grizzuti, M. Casalegno, F. Castiglione, R.Pasquino. Phase transitions of aqueous solutions of Pluronic F68 in the presence of Diclofenac Sodium. Int. J. Pharm. 2023, 644, 123353. 10.1016/j.ijpharm.2023.123353

[41] G.Wanka, H. Hoffmann,W. Ulbricht. Phase diagrams and aggregation behaviour of poly(exyethylene)-poly(oxypropylene)-poly(oxyethylene) triblockcopolymers in aqueous solutions. Macromolecules 1994, 27, 4145. https://doi.org/10.1021/ma00093a016

[42] D. Wei, L. Ge, R. Guo. Synthetic strategies toward DNA-coated colloids that crystallize. Colloids Surf., A 2018, 553, 1. https://doi.org/10.1021/jacs.5b06607

[43] M. S. H. Akash, K. Rehman. Recent progressin biomedical applications of Pluronic (PF127): Pharmaceutical perspectives. J. Controlled Release 2015, 209, 120. 10.1016/j.jconrel.2015.04.032

[44] C. He, S. W. Kim, D. S. Lee. In situ gelling stimuli-sensitive block copolymer hydrogels for drug delivery. J. Controlled Release 2008, 127, 189. 10.1016/j.jconrel.2008.01.005

[45] M. Bhowmik, P. Kumari, G. Sarkar, M. K. Bain, B. Bhowmick, Md. M. R. Mollick, D. Mondal, D. Maity, D. Rana, D. Bhattacharjee, D. Chattopadhyay. Effect of xanthan gum and guar gum on in situ gelling ophthalmic drug delivery system based on Poloxamer-407. Int. J. Biol. Macromol. 2013, 62, 117. 10.1016/j.ijbiomac.2013.08.024.

[46] E. Brambilla, S. Locarno, S. Gallo, F. Orsini, C. Pini, M. Farronato, D.V. Thomaz, C. Lenardi, M. Piazzoni, G. Tartaglia. Poloxamer-based hidrogel as drug delivery system: How polymeric excipients influence the chemical-physical properties. Polymers 2022, 14, 3624. https://doi.org/10.3390/polym14173624

[47] I. de Dios-Pérez, A. González-Garcinuño, A. Tabernero, M. Blanco-López, J. A. García-Esteban, V. Moreno Rodilla, B. Curto, P. Pérez-Esteban, E. M. Martín del Valle. Development of a thermosensitive hidrogel based on Poloxamer 407 and gellan gum with inclusion complexes (Sulfobutylated-β-cyclodextrin-Farnesol) as a local drug delivery system. Eur. J. Pharm. Sci. 2023, 191, 106618.

[48] M. Blanco-López, I. de Dios-Pérez, Á. González-Garcinuño, A. Tabernero, E. Martín del Valle. Innovative thermosensitive composite materials: Merging Poloxamer PF-127 and polysaccharies for enhanced functional properties. Macromol. Mater. Eng. 2025, 2400457. 10.1002/mame.202400457

[49] J. Liu, T. Tagami, T. Ozeki. Fabrication of 3d-printed fish-gelatin-based polymer hydrogel patched for local delivery of pegylated liposomal doxorubicin. Mar. Drugs. 2020, 18, 325. https://doi.org/10.1016/j.jaci.2020.05.021

[50] N. Li, J. Lin, C. Liu, Q. Zhang, R. Li, C. Wang, C. Zhao, L. Lu, C. Zhou, J. Tian. Temperature –and pH-responsive injectable chitosan hydrogels loaded with doxorubicin and curcumin as long-lasting release platforms for the treatment of solid tumors. Front. Bioeng. Biotechnol. 2022, 10, 1043939. https://doi.org/10.3389/fbioe.2022.1043939

[51] D. Chen, K. Sun, H. Mu, M. Tang, R. Liang, A. Wang, S. Zhou, H. Sun, F. Zhao, J. Yao, W. Liu. pH and temperature dual-sensitive liposome gel based on novel cleavable mPEG-Hz-CHEMS polymeric vaginal delivery system. Int. J. Nanomed. 2012, 7, 2621-2630. https://doi.org/10.2147/IJN.S31757

[52] H. Zhang. Thin-film hydration followed by extrusion method for liposome preparation. Methods Mol. Biol. 2017, 1522, 17–22. 10.1007/978-1-4939-6591-5_2

[53] M. Abrami, I. D'Agostino, G. Milcovich, S. Fiorentino, R. Farra, F. Asaro, R. Lapasin, G. Grassic, M. Grassi. Physical characterization of alginate-Pluronic F127 gel for endoluminal NABDs delivery. Soft Matter 2014, 10, 729. https://doi.org/10.1039/C3SM51873F

[54] M. Dewan, G. Sarkar, M. Bhowmik, B. Das, A. K. Chattoapadhyay, D. Rana, D. Chattopadhyay. Effect of gellan gum on the thermogelation property and drug release profile of Poloxamer 407 based ophtalmic formulation. Int. J. Biol. Macromol. 2017, 102, 258. 10.1016/j.ijbiomac.2017.03.194

[55] C. Karthika R. Sureshkumar, D.V. Sajini, G.Md. Ashraf, Md.H. Rahman. 5-fluorouacil and curcumin with pectin coatig as a treatment regimen for titanium dioxide with dimethylhydrazine-induced colon cancer model. Environ. Sci. & Pollut. Res. 2022, 29, 63202-63215. 10.1007/s11356-022-20208-y

[56] B. Shriky, A. Kelly, M. Isreb, M. Babenko, N. Mahmoudi, S. Rogers, O. Shebanova, T. Snow, T. Gough. Pluronic F127 thermosensitive injectable smart hydrogels for controlled drug delivery system development. J. Colloid Interface Sci. 2020, 565, 119. 10.1016/j.jcis.2019.12.096

[57] Y.-I. Chung, S.-Y. Lee, G. Tae. The effect of heparin on the gelation of Pluronic F-127 hydrogel. Colloids Surf., A 2006, 284, 480. https://doi.org/10.1016/j.colsurfa.2005.10.060

[58] A. P. Constantinou, V. Nele, J. J.Doutch, J. S. Correia, R. V.Moiseev,M. Cihova, D. C. A. Gaboriau, J. Krell, V. V. Khutoryanskiy,M.M. Stevens, T. K. Georgiou. Investigation of the thermogelation of a promising biocompatible ABC triblock terpolymer and its comparison with Pluronic F127. Macromolecules 2022, 55, 1783. 10.1021/acs.macromol.1c02123

[59] O. Kontogiannis, D. Selianitis, D. R. Perinelli, G. Bonacucina, N. Pippa, M. Gazouli, S. Pispas. Non-ionic surfactant effects on innate Pluronic 188 behavior: Interactions, and physicochemical and biocompatibility studies. Int. J. Mol. Sci. 2022, 23, 13814. 10.3390/ijms232213814

[60] A. Jain, S.K. Jain. In vitro release kinetics model fitting of liposomes: An insight. Chem. Phys. Lipids. 2016, 201, 58-40. 10.1016/j.chemphyslip.2016.10.005

[61] N.A. Peppas, J.J. Sahlin. A simple equation for the description of solute release. Coupling of diffusion and relaxation. Int. J. Pharm. 1989, 57, 169-172. https://doi.org/10.1016/0378-5173(89)90306-2

[62] M. Barzegar-Jalali, K. Adibkia, H. Valizadeh, M.R.S. Shadbad, A. Nokhodchi, Y. Omidi, G. Mohammadi, S.H. Nezhadi, M. Hasan. Kinetic analysis of drug release from nanoparticles. J. Pharm. Pharmaceut. Sci. 2008, 11, 167-177. 10.18433/j3d59t

[63] R.E. Duncan, M.C. Archer. Farnesol induces thyroid hormone receptor (THR) beta1 but inhibits THR-mediated signaling in MCF-7 human breast cancer cells. Biochem. Biophys. Res. Commun. 2006, 343, 239–243. https://doi.org/10.1016/j.bbrc.2006.02.145

[64] S. Peng, J-Y. Lin, M-H. Cheng, C-W. Wu, I-M. Chu. A cell-compatible PEO-PPO-PEO (Pluronic ®)-based hydrogel stabilized through secondary structures. Mater. Sci. Eng. 2016, 69, 421-428. http://dx.doi.org/10.1016/j.msec.2016.06.091

[65] C. Nieto, M.A. Vega, E. Martín del Valle. Nature-inspired nanoparticles as paclitaxel targeted carrier for the treatment of HER2-positive breast cancer. Cancers. 2021, 13, 2526. https://doi.org/10.3390/cancers13112526

[66] T. Ishida, Y. Okada, T. Kobayashi, H. Kiwada. Development of pH-sensitive liposomes that efficiently retain encapsulated doxorubicin (DXR) in blood. Int. J. Pharm. 2006, 309, 94-100. 10.1016/j.ijpharm.2005.11.010

[67] S. Nie, W.W. Hsiao, W. Pan, Z. Yang. Thermoreversible Pluronic F127-based hydrogel containing liposomes for the controlled delivery of paclitaxel: In vitro drug release, cell cytotoxicity and uptake studies. Int. J. Nanomed. 2011, 6, 151-166. 10.2147/IJN.S15057

[68] P. Crosasso, P. Brusa, F. Dosio, S. Arpicco, D. Pacchioni, F. Schuber, L. Cattel. Antitumoral activity of liposomes and immunoliposomes containing 5-fluorouridine prodrugs. J. Pharm. Sci. 1997, 86, 7. 10.1021/js9604467

[69] G. Gregoriadis. Liposomes in Drug Delivery: How It All Happened. Pharmaceutics. 2016, 8, 19. 10.3390/pharmaceutics8020019

[70] C. Caddeo, M. Gabriele, X. Fernández-Busquets, D. Valenti, A.M. Fadda, L. Pucci, M. Manconi. Antioxidant activity of quercetin in Eudragit-coated liposomes for intestinal delivery. Int. J. Pharm. 2019, 565, 64-69. 10.1016/j.ijpharm.2019.05.007

[71] M. Xu, X. Han, H. Xiong, Y. Gao, B. Xu, G. Zhu, J. Li. Cancer nanomedicine: Emerging strategies and therapeutic potentials. Molecules. 2023, 28, 5145. https://doi.org/10.3390/molecules28135145

[72] Y. Mao, X. Li, G. Chen, S. Wang. Thermosensitive hydrogel system with paclitaxel liposomes used in localized drug delivery system for in situ treatment of tumor: Better antitumor efficacy and lower toxicity. J. Pharm. Sci. 2016, 105, 194-204. http://dx.doi.org/10.1002/jps.24693

[73] S. Mourtas, S. Fotopoulou, S. Duraj, V. Sfika, C. Tsakiroglou, S.G. Antimisiaris. Liposomal drugs dispersed in hydrogels. Effect of liposome, drug and gel properties on drug release kinetics. Colloids Surf. B Biointerfaces. 2007, 55, 212-221. 10.1016/j.colsurfb.2006.12.005

[74] Y. Mou, P. Zhang, W-F. Lai, D. Zhang. Design and applications of liposome-in-gel as carriers for cancertherapy. Drug Deliv. 2022, 29, 3245-3255. 10.1080/10717544.2022.2139021.

[75] H. Daraee, A. Etemadi, M. Kouhi, S. Alimirzalu, A. Akbarzadeh. Application of liposomes in medicine drug delivery. Artif. Cells Nanomed. Biotechnol. 2016, 44, 381-391. 10.3109/21691401.2014.953633

[76] Y. Shachaf, M. Gonen-Wadmany, D. Seliktar. The biocompatibility of Pluronic F127 fibrinogen-based hydrogels. Biomaterials. 2010, 31, 2836-2847. 10.1016/j.biomaterials.2009.12.050

[77] K. Sharun, S.A. Banu, M. Mamachan, R.S. Emmanuel, R. Kumar, O.R. Vinodhkumar, K. Dhama, A.M. Pawde, S.K. Maiti, A. Pal. Thermoresponsive and injectable Pluronic F127 hydrogels for loading adipose-derived mesenchymal stem cells. Discov. Med. 2024, 36, 294-307. https://doi.org/10.24976/Discov.Med.202436181.28

[78] V. Mollo, P. Scognamiglio, A. Marino, G. Ciofani, F. Santoro. Probing the ultrastructure of spheroids and their uptake of magnetic nanoparticles by FIB-SEM. Adv. Mater. Technol. 2020, 5, 1900687. https://doi.org/10.1002/admt.201900687

[79] L-B. Weiswald, D. Bellet, V. Dangles-Marie. Spherical cancer models in tumour biology. Neoplasia 2015, 17, 1–15. https://doi.org/10.1016/j.neo.2014.12.004

[80] A. Tchoryk, V. Taresco, R.H. Argent, M. Ashford, P.R. Gellert, S. Stolnik, A. Grabowska, M.C. Garnett. Penetration and uptake of nanoparticles in 3D tumor

spheroids. Bioconjug. Chem. 2019, 30, 1371–1384. 10.1021/acs.bioconjchem.9b00136

Supporting Information

Developing an injectable thermo-responsive PF-127 hydrogel incorporating pH-responsive Eudragit®-coated liposomes for dual-stimuli controlled drug delivery in post-surgical breast cancer therapy

Marcos Blanco-López[1], Inma de Dios-Pérez[1,3], Antonio Tabernero[1,2,], Patricia Pérez-Esteban[3], Eva Martín del Valle[1,2].*

4) *Department of Chemical Engineering. University of Salamanca. Plaza Los Caídos s/n, 37008 Salamanca (Spain).*
5) *Institute for Biomedical Research in Salamanca (IBSAL), Paseo de San Vicente 87, 37007, Salamanca (Spain).*
6) *Healthcare Technologies Institute (HTI), University of Birmingham, B15 2TT, Birmingham (UK).*

**** Corresponding author at: Antonio Tabernero (antaber@usal.es)***

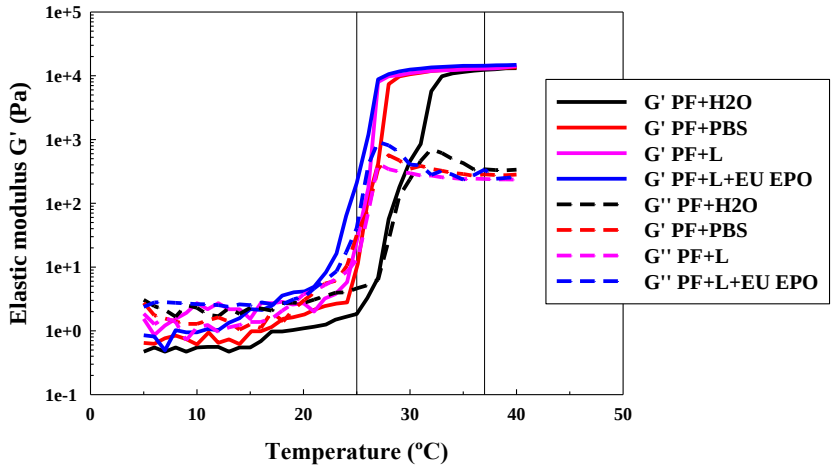

a)

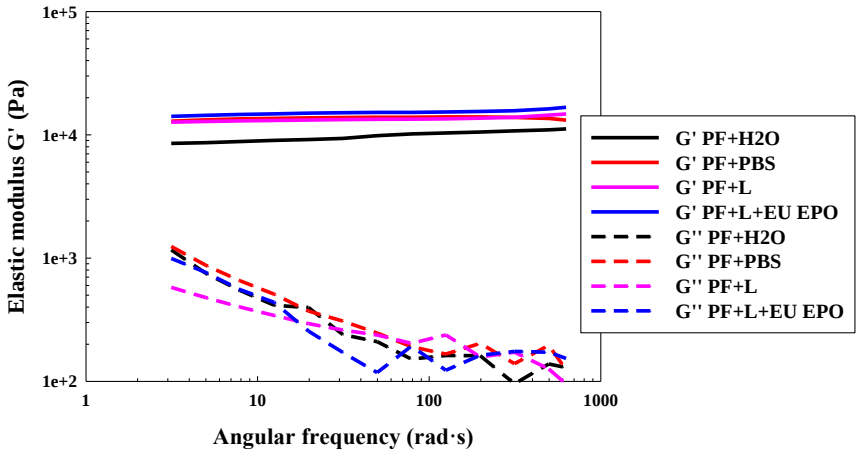

b)

Figure S1: Rheological measurements of PF-127 (PF) hydrogels dissolved in water (H2O), PBS, and with embedded conventional (L) and EU EPO coated liposomes, including viscous moduli: a) Temperature sweep oscillatory test, and b) Frequency sweep oscillatory test.

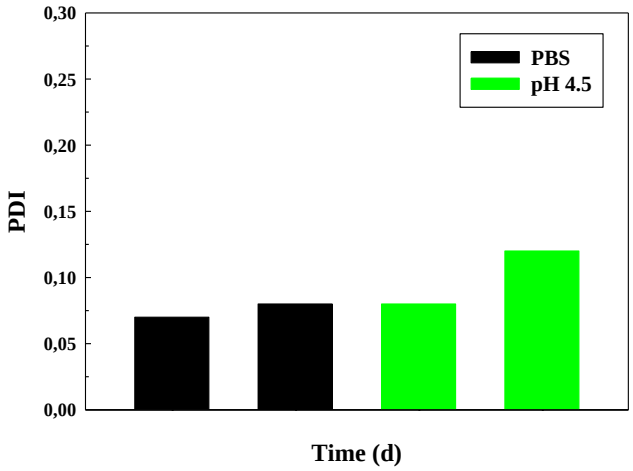

Figure S2: Conventional liposomes PDI at day 0 (left) and day 7 (right) when diluted in PBS (pH 7.4, black) and acidic PBS (4.5, green)

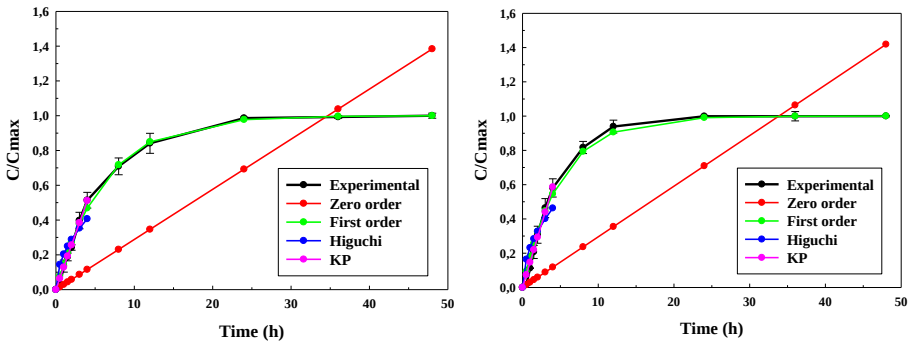

a) b)

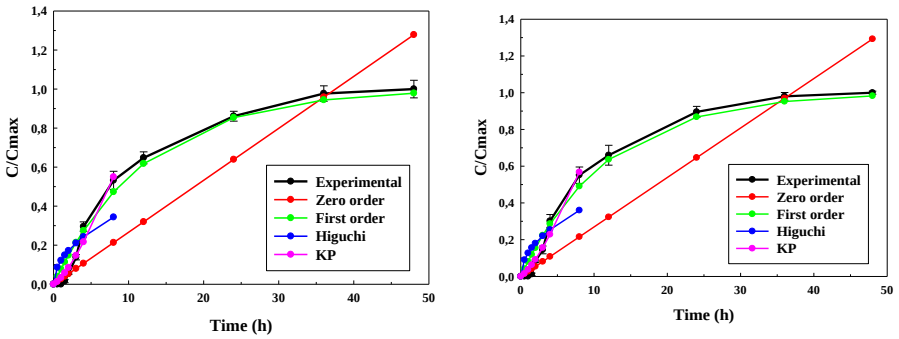

c) d)

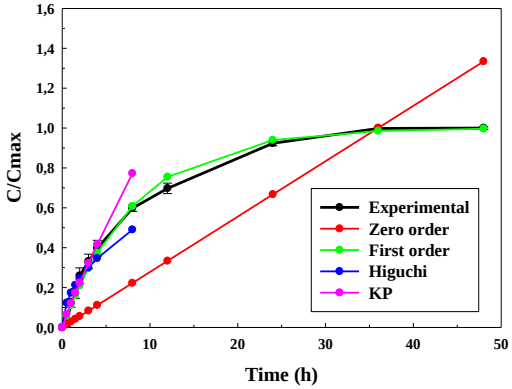

e)

Figure S3: Fitting of one-stage theoretical models (Zero order, first order, Higuchi and Korsmeyer Peppas) to experimental data of drug release tests of PF-127 hydrogels with liposomes embedded: Conventional in media a) PBS (7.4) and b) acidic PBS (4.5); and EU EPO coated liposomes in media: c) PBS (7.4), d) acidic PBS (5.5), and e) acidic PBS (4.5).

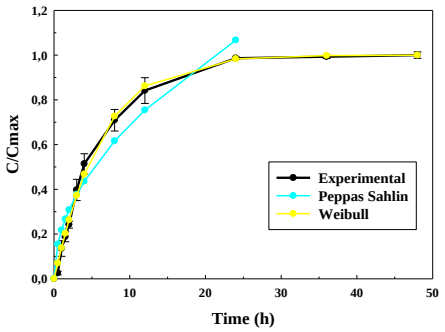

a)

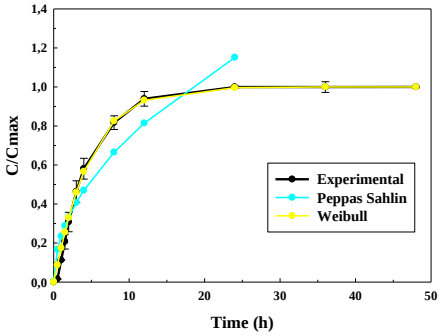

b)

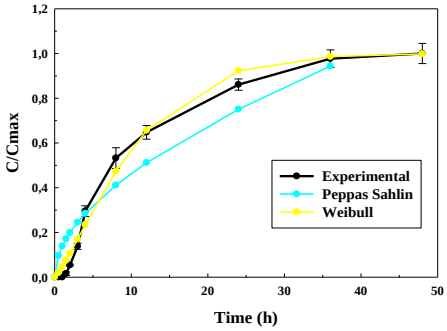

c)

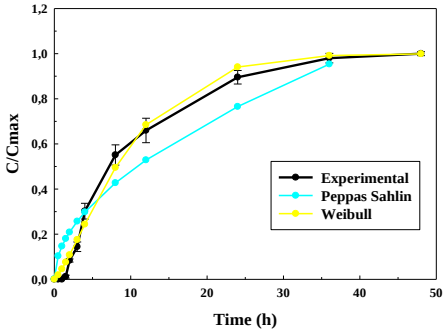

d)

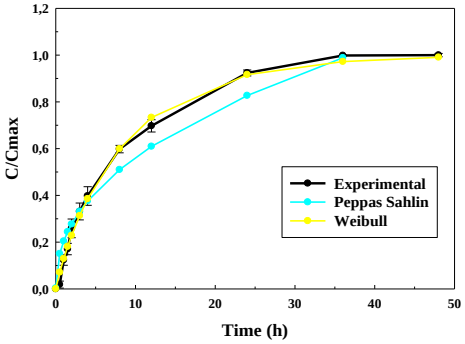

e)

Figure S4: Fitting of two-stage theoretical models (Peppas Sahlin and Weibull) to experimental data of drug release tests of PF-127 hydrogels with liposomes embedded: Conventional in media a) PBS (7.4) and b) acidic PBS (4.5); and EU EPO coated liposomes in media: c) PBS (7.4), d) acidic PBS (5.5), and e) acidic PBS (4.5).

a)

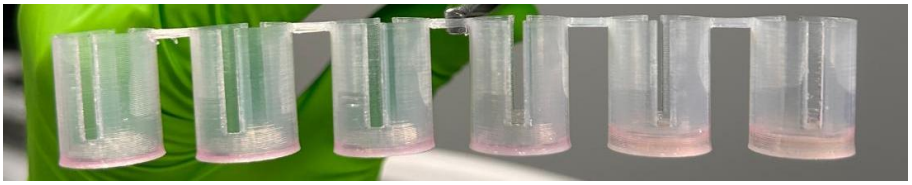

b)

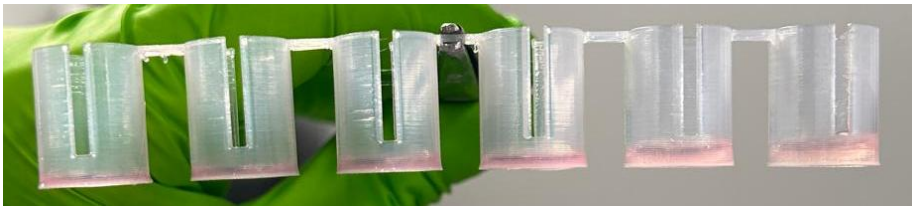

c)

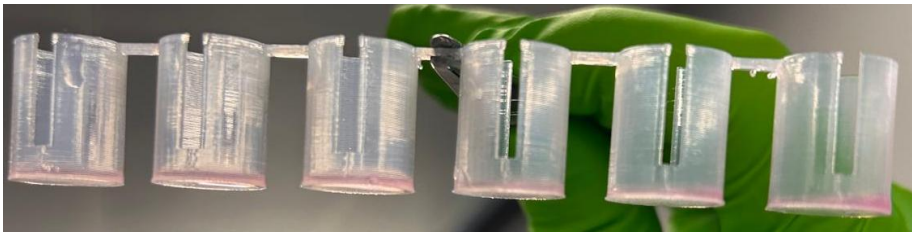

d)

Figure S5: Results of qualitative gel degradation under *in vitro* conditions for volumes of: 0.05, 0.1, 0.2, 0.3, 0.4, and 0.5 mL from left to right. a) Sol state after 30 secs under incubation, but b) Strong gel behaviour after 2 mins of incubation (t=0), c) t=4h, and d) t=8h. The observed residual pink in the bottom in this picture (d) only corresponds to gel residues in 0.5 mL support, the rest is DMEM+ that could not be properly removed.

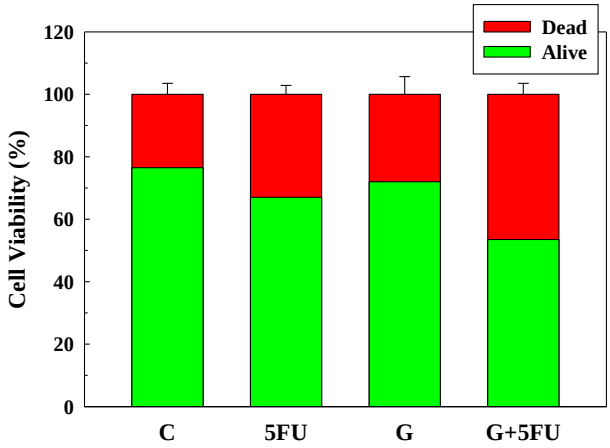

Figure S6: Cell viability in BT-474 MCTS in cell-counting assay at 24h. Treatments are: Control (C), free solution of 5-FU (5FU), dual-responsive hydrogel with EU EPO coated liposomes unloaded (G) and 5-FU loaded (G+5FU).

7.5. Conclusions

In conclusion, a dual-responsive drug delivery system combining a thermo-sensitive PF-127 hydrogel and pH-responsive Eudragit® EPO coated liposomes was successfully developed as a localized therapeutic alternative for post-surgical breast cancer treatment. Moreover, the hybrid system presented the same or improved stimuli-responses as their components did separately in previous chapters 5 and 6.

On the one hand, liposomes incorporation to the hydrogel matrix presented a similar effect to the polysaccharides implementation, improving its viscoelastic properties (G' of 15 kPa) and obtaining a more resistant network (viscosity of 6.8 Pa·s) without limiting its injectability, confirmed by rheological analyses. On the other hand, the liposomes physicochemical characteristics were not modified with their incorporation to the hydrogel matrix, confirmed by microscopy, and neither was their pH-response, confirmed by drug release tests, which additionally presented delayed releases due to the hydrogel effect. Thus, the dual-response system integrated local retention, sustained drug release, and tumour targeting effectiveness.

The synergy found in drug release tests was further confirmed in mathematical modelling. Results indicated a predominantly diffusional transport in two-stage model Peppas Sahlin, which was modulated by additional barriers, like the coating layer and the hydrogel network. The multi-resistance system provided enhanced control over drug release kinetics.

Finally, *in vitro* assays validated the therapeutic potential of the formulation. The dual-response system demonstrated again the tumour targeting in the breast cancer cells viability compared to the healthy stromal fibroblasts. Additionally, evaluation in 3D breast tumour spheroid models, which reproduce better their *in vivo* architecture, confirmed the enhanced anticancer performance of the dual-responsive system.

Overall, this work established a promising minimally invasive locally administered drug delivery system capable of combining thermo and pH-responsiveness for a sustained release and tumour targeting strategy, enhancing its anticancer activity in breast cancer post-surgical treatment for recurrence prevention. The general conditions can also be seen in Figure 7.3.

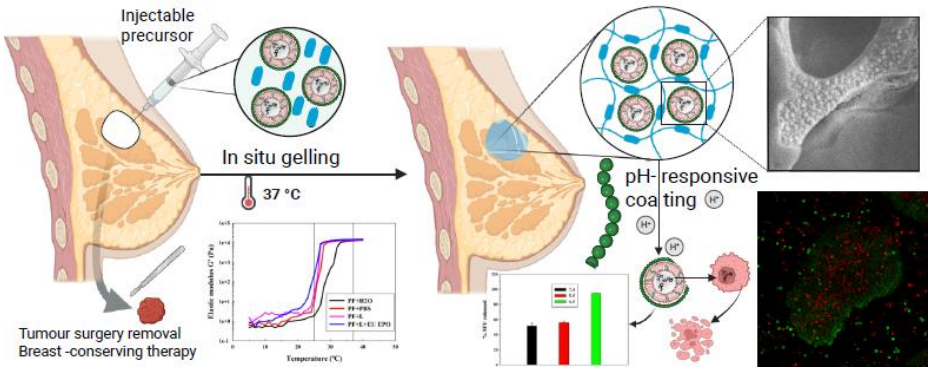

Figure 7.3. Main results obtained from the development of the dual-responsive platform for breast cancer post-surgical treatment.

7.6. References also cited

[1] Wahl AO, Rademaker A, Kiel KD, Jones EL, Marks LB, Croog V, et al. Multi-Institutional Review of Repeat Irradiation of Chest Wall and Breast for Recurrent Breast Cancer. Int J Radiat Oncol. 2008;70:477-84.

[2] Norouzi M, Nazari B, Miller DW. Injectable hydrogel-based drug delivery systems for local cancer therapy. Drug Discov Today. 2016;21:1835-49.

[3] Allen TM, Cullis PR. Liposomal drug delivery systems: From concept to clinical applications. Adv Drug Deliv Rev. 2013;65:36-48.

[4] Zuo H, Jiao Y, Chen J, Tong S, Li Y, Zhao W. Recent Advances in Smart Stimulus-Responsive Hydrogels for Precision Drug Delivery in Tumours. Gels. 2026;12:98.

[5] Mou Y, Zhang P,Lai W-F, Zhang D. Design and applications of liposome-in-gel as carriers for cancer therapy. Drug Deliv. 2022;29:3245-3255.

[6] GuhaSarkar S, More P, Banerjee R. Urothelium-adherent, ion-triggered liposome-in-gel system as a platform for intravesical drug delivery. J Control Release 2017;10:147-156.

[7] Wu W, Dai Y, Liu H. Local release of gemcitabine via in situ UV-crosslinked lipid-strengthened hydrogel for inhibiting osteosarcoma. Drug Deliv 2018;25:1642-51.

[8] Rahni S, Kazakov S. Hydrogel micro-/nanosphere coated by a lipid bilayer: preparation and microscopic probing. Gels 2017;3:7.

[9] Li T, Ci T, Chen L. Salt-induced reentrant hydrogel of poly(-ethylene glycol)-poly(lactide-*co*-glycolide) block copolymers. Polym Chem 2014;5:979-991.

[10] Mao Y, Li X, Chen G. Thermosensitive hydrogel system with paclitaxel liposomes used in localized drug delivery system for in situ treatment of tumor: better antitumor efficacy and lower toxicity. J Pharm Sci 2016;105:194-204.

[11] Fathi M, Alami-Milani M, Geranmayeh MH, Barar J, Erfan-Niya H, Omidi Y. Dual thermo-and pH-sensitive injectable hydrogels of chitosan/(poly(N-isopropylacrylamide-co-itaconic acid)) for doxorubicin delivery in breast cancer. Int J Biol Macromol. 2019;128:957-64.

[12] Mohan A, Santhamoorthy M, Phan TTV, Kim SC. pNIPAm-Based pH and Thermoresponsive Copolymer Hydrogel for Hydrophobic and Hydrophilic Drug Delivery. Gels. 2024;10:184.

[13] Ahmadi S, Olad A, Fathi M, Molavi O. An injectable chitosan based dual thermo/pH-responsive fast gelling hydrogel loaded by methotrexate/curcumin as local drug delivery system of breast cancer. J Drug Deliv Sci Technol. 2025;104:106540.

[14] Li N, Lin J, Liu C, Zhang Q, Li R, Wang C, et al. Temperature- and pH-responsive injectable chitosan hydrogels loaded with doxorubicin and curcumin as long-lasting release platforms for the treatment of solid tumors. Front Bioeng Biotechnol. 2022;10:1043939.

[15] Chen D. pH and temperature dual-sensitive liposome gel based on novel cleavable mPEG-Hz-CHEMS polymeric vaginal delivery system. Int J Nanomedicine. 2012;2621.

7.7. List of abbreviations

5-FU — 5-Fluorouracyl
BT-474 — Breast Tumour Cell Line
cgt— Completion Gelation Temperature
CHEMS — Cholesterol Hemysuccinate
CHOL — Cholesterol
CLSM — Confocal Laser Scanning Microscopy
CUR — Curcumin
DDS — Drug Delivery System
DLS — Dynamic Light Scattering
DMEM — Dulbecco's Modified Eagle Medium
DMSO — Dimethyl Sulfoxide
DOX — Doxorubicin
EDTA — Ethylenediaminetetraacetic Acid
EU — Eudragit®
FBS — Foetal Bovine Serum
FDA — Food and Drug Association
HEC — Hydroxymethyl Cellulose
HEK — Human Embryonic Kidney Cell Line
HS-5 — Human Bone Marrow Stromal Cell Line
Hz — Hydrazone
IC_{50} — Inhibitory Concentration 50
KP — Kormeyer Peppas
MAC — Micellar Aggregation Capacity
MCTS — Multicellular Tumour Spheroid

MDA-MB — MD Anderson Mammary Breass Cancer Cell Line MCF
mPEG — Methoxy-Poly(Ethylene Glycol)
MR — Molar Ratio
MTT — 3-(4,5-dimethylthiazol-2-yl)-2,5-diphenyltetrazolium Bromide
MW — Molecular Weight
NPs — Nanoparticles
PBS — Phosphate Buffer Saline
PC — 1,2-Diacyl-sn-Glycero-3-Phosphocholine (Phosphatidylcholine)
PDI — Polidispersity Index
PEG — Poly(Ethylene Glycol)
PEO — Poly(Ethylene Oxide)
PF — Pluronic in Flakes
PLGA — Poly(Lactic-co-Glycolic Acid)
PPO — Poly(Propylene Oxide)
PS — Penicillin-Streptomycin
SEM — Scanning Electron Microscopy
UV — Ultraviolet

8. Conclusions

This doctoral thesis has demonstrated the rational design and development of a dual-responsive local administered drug delivery platform for breast cancer recurrence prevention in the post-surgical stage of the treatment. The design of this system was based on the major drawbacks that current post-surgical approaches present due to their systemic administration, highlighting the low therapeutic efficiency, accumulating inefficient drug doses at tumour site, and systemic toxicity. Accordingly, this doctoral thesis proposed a novel strategy of a locally administered platform that overcomes the limitations associated with systemic administration, being directly implanted in the post-resection tumour cavity, where residual cancer cells are most likely to persist and initiate local relapse. The development of this platform presented the engineering and synthesis of two distinct stimuli-responsive drug delivery systems, subsequently incorporating the optimal one to an injectable thermo-responsive matrix.

Initially, the novel strategy focused on the development of stimuli-responsive alginate-gelatin A coacervates due to their structural versatility and biocompatibility showing a highly adaptable platform for drug encapsulation and delivery. An extensive optimization of their synthesis was expanded, taking into account each process variable to enhance their colloidal stability, through the novel incorporation of the temperature to this study, since it influenced the gelatin A structural conformation. All the parameters studied apart from temperature, like pH, polymers ratio or concentration, ionic strength, etc. showed how they influenced the electrostatic interactions between the compounds, defining the resulting coacervate physicochemical properties and stability. Ultimately, by modifying temperature and pH, optimal coacervate formulations were successfully developed with nano scale sizes (400-700 nm) and narrow size distributions (PDI <0.2). However, despite this achievement, these formulations presented a tendency towards high size and polidispersity variations when the temperature decreased from 37ºC and pH was not acidic. This finding revealed the incompatibility of the coacervates for a successful application, since their stability was strongly compromised at ambient and physiological conditions.

Therefore, an alternative nanocarrier for pH-response was explored. This time, liposomes were the preferred option since they exhibit great translational relevance, clinical use, structural resemblance to cellular membranes, and tuneable structure. Firstly, conventional liposomes based on phosphatidylcholine and cholesterol were synthesized and successfully optimized to yield a small unilamellar vesicle system (85 nm, PDI <0.1) that remained stable for at least three weeks. Although this system showed a high encapsulation efficiency of the anticancer drug 5-FU (> 90%), its drug release presented a fast (4h) and non-pH-responsive kinetic profile, lacking tumour targeting. Therefore, liposomal modification for obtaining a pH-response was required. An innovative proposed technique for this, which does not affect the vesicles stability at physiological conditions, is the coating process with a pH-responsive polymer.

For this purpose, Eudragit® polymers offer a wide range of formulations depending on the designed pH-response regarding its intended application. Liposomes were coated with two opposite functioning formulations to further expand their pH-response to various applications and enhance their performance as a drug delivery platform. Eudragit® S100 coating formulation, which is designed for alkaline releases, presented unexpected micrometric aggregates due to its high molecular weight and behaviour in aqueous solution, whilst Eudragit® EPO (for acidic releases) presented a stable liposomal system with a slight increase in size and polidispersity (114 nm, PDI <0.15). Both coatings showed encapsulation efficiencies higher than the conventional liposomal base, and provided efficient and delayed drug releases (24 h), where insoluble pH ranges prevented up to a 50% of the drug from being released. Furthermore, the coating layer and its insolubility proved to delay release kinetics and alter the release mechanism in mathematical model fittings, which esstablished diffusion as the predominant one. Importantly, these formulations exhibited selective cytotoxic effects *in vitro*, where significantly Eudragit® EPO coated liposomes enhanced anticancer activity in breast cancer cells over 30% more than the rest of formulations, whilst preserving healthy fibroblasts viability. This finding further validated the pH-sensitive tumour targeting capacity of the

developed nanocarrier for its future implementation within the dual-responsive system.

In parallel, an injectable thermo-responsive hydrogel matrix based on Pluronic F-127 (PF-127) was developed to achieve localized administration by injection and sustained drug release. For this purpose, extensive rheological characterizations were used to confirm its suitability for injection, finding liquid-like solution behaviour at room temperature, whilst solid-like strong gel behaviour at physiological temperature. In order to improve the viscoelastic properties without affecting injectability, four polysaccharides presenting different structural conformations were implemented in the hydrogel network. Their concentration and structural effects were evaluated in order to determine the optimal formulations for further drug release tests, based on injectability and improved strong gel behaviour at 37ºC. As expected, formulations incorporating polysaccharides prolonged 5-FU release up to fourfold relative to the PF-127 only hydrogel. Furthermore, mathematical modelling supported that implemented polysaccharide structures with increasing concentrations and structure complexity introduced an additional diffusional resistance, delaying the hydrogel degradation rate and presenting more resistance against water permeation and matrix erosion.

After the developed studies and optimizations of the systems separately, the integration of the pH-responsive Eudragit® EPO coated liposomes into the injectable thermo-responsive PF-127 hydrogel network was achieved. Characterization studies via rheology and cryo-SEM demonstrated a successful combination of both systems with reinforced viscoelastic properties. Moreover, the hybrid formulation preserved the independent functionality of each component, whilst generating an additional synergy in drug release, delaying times by an extra day (48h) due to the hydrogel effect and the coating layer. One and two-stage model fittings showed the decrease in every kinetic constant compared to liposomal systems, and the addition of a relaxation term when coating layers were insoluble. Therefore, the hydrogel matrix acted as an additional diffusion barrier, delaying liposomal diffusion, and subsequently, the overall drug release.

Biological validation in both 2D monolayer cultures and more physiologically relevant 3D breast tumour spheroid models confirmed the therapeutic activity of the dual-responsive system. MTT assays presented the same effects of tumour targeting as liposomal systems exhibited. However, in this case, the anticancer activity slightly decreased, due to the delayed drug delivery in the hybrid formulation. Most importantly, tumour spheroids assays exhibited promising therapeutic efficacy of the system, promoting cell death and disruption of the spheroid integrity compared with 5-FU solution. These results supported the functional benefits of combined local administration with tumoural microenvironment targeting strategy. In a more summarized manner, the whole project is illustrated in Figure 8.1.

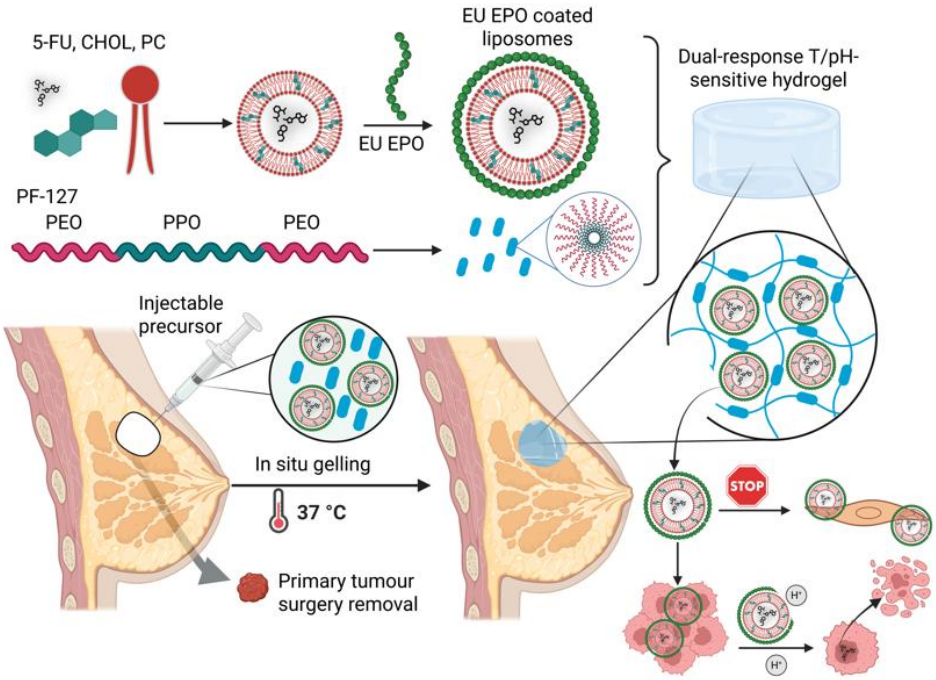

Figure 8.1. Brief scheme of conclusions developed in this doctoral thesis about the synthesis and functioning mechanism of a dual temperature and pH-responsive injectable hydrogel for local recurrences prevention in post-surgery breast cancer treatment.

To conclude, this work establishes a robust engineered local drug delivery system with significant translational potential for post-surgical breast cancer treatment. The innovative integration of both stimuli-

responses provided an enhanced performance of therapeutic efficacy whilst potentially minimizing systemic toxicity.